ARCTIC SEA ICE TRAFFICABILITY – NEW STRATEGIES FOR A CHANGING ICESCAPE

By

Dyre Oliver Dammann

A Dissertation Submitted in Partial Fulfillment of the Requirements

for the Degree of

Doctor of Philosophy

in

Geophysics

University of Alaska Fairbanks

August 2017

APPROVED:

Hajo Eicken, Committee Chair
Andrew R. Mahoney, Committee Member
Franz J. Meyer, Committee Member
Uma S. Bhatt, Committee Member
Chanda L. Meek, Committee Member
Paul McCarthy, Chair
Department of Geosciences
Paul Layer, Dean
College of Natural Science and Mathematics
Michael Castellini, *Dean of the Graduate School*

ABSTRACT

Sea ice is an important part of the Arctic social-environmental system, in part because it provides a platform for human transportation and for marine flora and fauna that use the ice as a habitat. Sea ice loss projected for coming decades is expected to change ice conditions throughout the Arctic, but little is known about the nature and extent of anticipated changes and in particular potential implications for over-ice travel and ice use as a platform. This question has been addressed here through an extensive effort to link sea ice use and key geophysical properties of sea ice, drawing upon extensive field surveys around on-ice operations and local and Indigenous knowledge for the widely different ice uses and ice regimes of *Utqiaġvik, Kotzebue, and Nome, Alaska.*

A set of nine parameters that constrain landfast sea ice use has been derived, including spatial extent, stability, and timing and persistence of landfast ice. This work lays the foundation for a framework to assess and monitor key ice-parameters relevant in the context of ice-use feasibility, safety, and efficiency, drawing on different remote-sensing techniques. The framework outlines the steps necessary to further evaluate relevant parameters in the context of user objectives and key stakeholder needs for a given ice regime and ice use scenario. I have utilized this framework in case studies for three different ice regimes, where I find uses to be constrained by ice thickness, roughness, and fracture potential and develop assessment strategies with accuracy at the relevant spatial scales.

In response to the widely reported importance of high-confidence ice thickness measurements, I have developed a new strategy to estimate appropriate thickness compensation factors. Compensation factors have the potential to reduce risk of misrepresenting areas of thin ice when using point-based in-situ assessment methods along a particular route. This approach was tested on an ice road near Kotzebue, Alaska, where substantial thickness variability results in the need to raise thickness thresholds by 50%.

If sea ice is thick enough for safe travel, then the efficiency of travel is relevant and is influenced by the roughness of the ice surface. Here, I develop a technique to derive trafficability measures from ice roughness using polarimetric and interferometric synthetic

aperture radar (SAR). Validated using Structure-from-Motion analysis of imagery obtained from an unmanned aerial system near *Utqiaġvik*, Alaska, I demonstrate the ability of these SAR techniques to map both topography and roughness with potential to guide trail construction efforts towards more trafficable ice.

Even when the ice is sufficiently thick to ensure safe travel, potential for fracturing can be a serious hazard through the ability of cracks to compromise load-bearing capacity. Therefore, I have created a state-of-the-art technique using interferometric SAR to assess ice stability with capability of assessing internal ice stress and potential for failure. In an analysis of ice deformation and potential hazards for the Northstar Island ice road near Prudhoe Bay on Alaska's North Slope I have identified a zone of high relative fracture intensity potential that conformed with road inspections and hazard assessments by the operator.

Through this work I have investigated the intersection between ice use and geophysics, demonstrating that quantitative evaluation of a given region in the ice use assessment framework developed here can aid in tactical routing of ice trails and roads as well as help inform long-term strategic decision-making regarding the future of Arctic operations on or near sea ice.

DEDICATION

I dedicate this work to my parents who despite odds traveled across the world in pursuit of a life in harmony with nature by learning the ancient ways of the Iñupiat people of northern Alaska. Their respect and admiration for the great wisdom rooted in this culture inspired me to pursue this work.

TABLE OF CONTENTS

LIST OF FIGURES

Page

LIST OF TABLES

Page

ACKNOWLEDGEMENTS

This work would not have been possible without funding by NSF through the Seasonal Ice Zone Observing Network (SIZONet2: NSF-0856867). Funding was also generously provided by Arctic Science, Engineering, and Education for Sustainability (ArcSEES: NSF-4868895) through the Sustainable Futures North Project, the North Slope Arctic Scenarios Project (NASP: NSF-1263850), and the University of Alaska Graduate School.

I want to extend my sincere thanks to my advisor Dr. Hajo Eicken who extended me the freedom to pursue my interests and guided me in a thorough yet hands-off way maximizing my learning and independence. I would also like to thank the rest of my committee. Dr. Andrew Mahoney provided extensive invaluable guidance in a role almost resembling co-advisor more than committee member. Dr. Franz Meyer served as an inspiration to pursue remote sensing, a field I previously had given little attention, but that I now greatly fancy. I am grateful to Dr. Uma Bhatt, my former advisor, who encouraged me to pursue a Ph.D. and taught me so much about both science and life, which greatly helped me through this process. I am also grateful to Dr. Chanda Meek who provided guidance on the social science piece of this thesis.

I want to express my deepest appreciation for the Iñupiat people of Alaska who have opened their homes and shared their knowledge about the sea ice system. In particular, I would like to thank Brandon Ahmasuk in Nome who opened his home and taught me how to travel on sea ice. I would like to extend a special thanks to Ross Schafer in Kotzebue who also opened his home and let me observe a seal hunt across the sea ice. I am further grateful to all the people I interviewed in Barrow, Kotzebue, and Nome, giving me valuable insight into sea ice travel and use. I acknowledge Barrow Whaling Captains Association for extending me the privilege to collect data from whaling trails over the years. I also acknowledge the help from Dr. Craig George, Harry Brower Jr., and Billy Adams with the North Slope Department of Wildlife Management and Quuniq Donovan and the Ukpeaġvik Iñupiat Corporation Science that made so much possible. I am grateful to Seth Kantner in Kotzebue who served as a guide on the sea ice and taught me about life in native Alaska communities.

I would like to thank Dr. Matthew Druckenmiller, Sarah Betcher, and Karen Brewster for teaching me first hand how to work in villages, adjusting to the different way of life, and helping me see the world from new perspectives. Many other people have generously helped me here at the university. I would like to thank Mette Kaufman and Josh Jones in the sea ice group, Max Kaufman, Peter Hickman with the Geographical Information Network of Alaska, and Bill Hauer and Jeremy Nicoll with Alaska Satellite Facility. I have thrived here during this time due to wonderful cubicle neighbors David McAlpin, Olaniyi Ajadi, Megan O'Sadnick, Alex Sacco and many other great friends.

I would like to extend both great gratitude and admiration for my wife Brittany Dammann who agreed to move back up to Alaska so I could pursue my studies. She agreed to live in the most simplistic way, in a Mongolian nomadic tent, throughout the past four years in accordance with both our ideals and fascination for native cultures. Brittany also blessed me with a wonderful son Sune during the last year here. I would like to thank my parents Heidi Dammann and Rein Dammann who inspired me to live in the Arctic and learn from the Iñupiat culture. Together with my brother Mikkel Dammann, they have provided enormous support to me and for my path.

1 GENERAL INTRODUCTION

1.1 Background

The Earth's surface is warming, with much of the observed changes since the 1950's unprecedented over recent decades to millennia [*Pachauri et al.*, 2015]. This warming is driving a decline in Arctic sea ice [*Stroeve et al.*, 2012] contributing to a further amplified warming of the Arctic [*Serreze and Francis*, 2006]. This amplification is expected to force continued decreases in summer Arctic sea ice extent, hastening a transition towards a seasonally open Arctic Ocean [*Overland and Wang*, 2013; *Wang and Overland*, 2015]

The rapidly changing Arctic sea ice cover has prompted an increase in sea ice-related research with thorough investigation of the geophysical properties leading to advances in our understanding of how sea ice impacts global climate [*Overland et al.*, 2011] and thus indirectly impacts humans through increased sensitivity to weather and climate extremes [*Meehl et al.*, 2000]. However, there is also an equally imminent direct impact on the services the sea ice provides different interest groups in the Arctic *[Eicken et al., 2009]* and consequences for ice users.

People have been living in close relationship with sea ice for millennia throughout the circumpolar North, drawing on the premise of this unique environment and its many benefits [*Krupnik et al.*, 2010]. Of all the forms that sea ice can take, perhaps most significant to coastal communities is landfast ice, which attaches to shore in often kilometer-wide belts along the Arctic coastlines. This form of sea ice, which is known as "tuvaq" among the Iñupiat population in northern Alaska, serves as a seasonal platform enabling travel and subsistence and is therefore inseparable from many northern cultures. In recent years, the private sector has also utilized the landfast sea ice to support logistics and operations associated with the industrial development of oil and gas resources.

Most coastal ice use depends first and foremost on the presence of landfast ice and is thus seasonally constrained. Figure 1.1 shows the location of the majority of Arctic communities or operations near sea ice, indicating access to landfast ice for at least a few months (e.g. January – June) during spring where some form of ice use can take place. However, landfast

sea ice has in many places undergone major reductions in recent years in terms of extent and seasonal persistence [*Mahoney et al.*, 2014; *Selyuzhenok et al.*, 2015] with potentially widespread negative consequences for ice travel (Chapter 9.4.5 in *AMAP* [2011]). For instance, through increasingly more unpredictable ice and difficult or dangerous travel conditions [*Aporta and Higgs*, 2005; *Ford et al.*, 2008] some communities are becoming more isolated [*AMAP*, 2011].

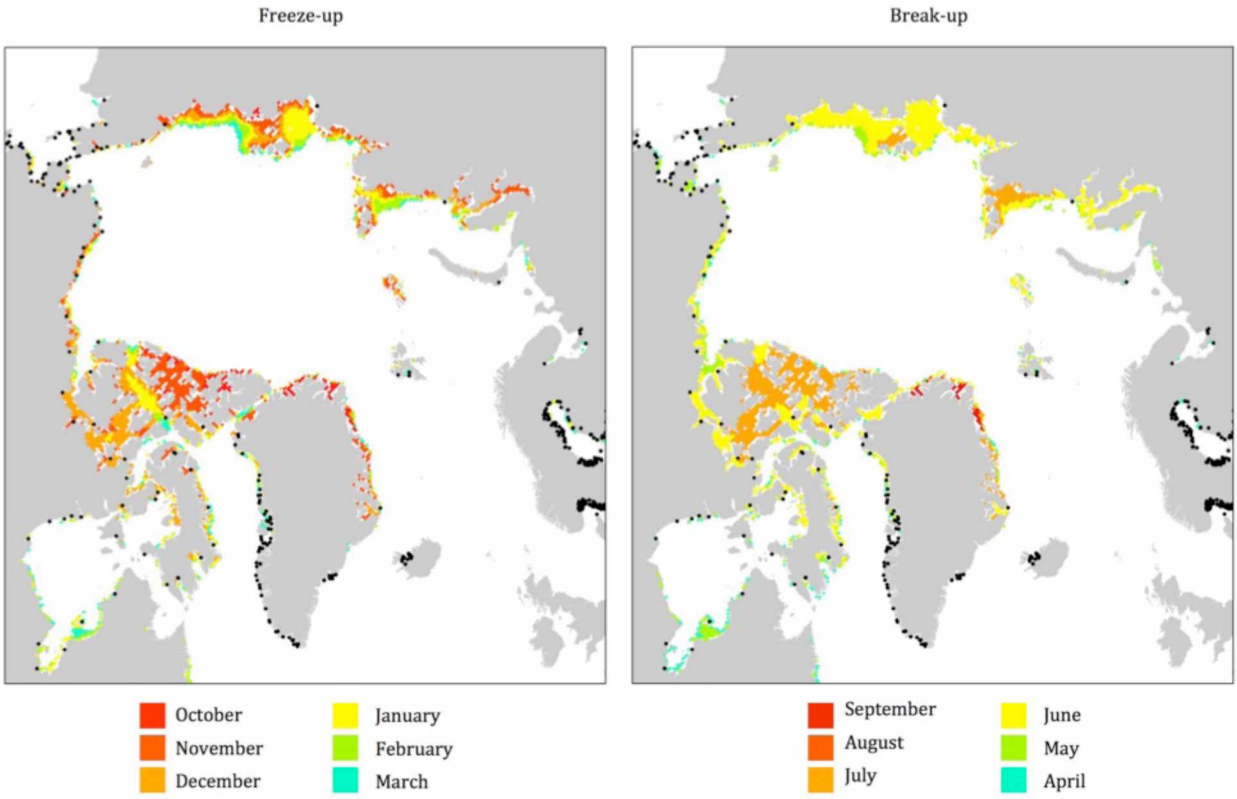

Figure 1.1 Climatological (1972-2007) mean landfast ice extent is used to display freeze-up (left) and break-up (right) of landfast ice in the Arctic. Information is gathered from National Ice Center Arctic Sea Ice Charts and Climatology (*Yu et al.* [2014]). Many of the settlements within 50km of sea ice during March 1983 (maximum ice extent on satellite record) are marked in black. Community locations are predominately obtained from the Socio Economic Data and Applications Center (SEDAC). This database is missing some communities, in particular in the Russian Arctic.

1.2 Motivation

The state and seasonality of landfast sea ice can be described through a set of parameters, which change throughout the season and vary regionally depending on the atmospheric, ocean, and ice environment. Sea ice trafficability can be defined as the ability to traverse sea ice in relation to the efficiency, cost, and safety of over-ice travel, and hence depends on a range of sea ice characteristics such as topography, surface conditions, and stability. In light of continued human reliance on landfast ice, and environmental and regulatory changes in the Arctic, there is a clear need for a comprehensive approach to define and objectively evaluate parameters critical to trafficability and to document changes and regional variations to inform continued safe use of and operations on sea ice. Some work has been done to evaluate the future accessibility of Arctic regions from the perspective of shipping and land-based ice roads through climate model simulations [*Stephenson et al.*, 2011]. However, this work by necessity had to simplify assumptions about constraints on ice access and did not include any retrospective analysis of trafficability and its variation with time due to the complexity of parameters involved.

A range of studies have explored ice use and sought to identify relevant ice characteristics [*Aporta*, 2009; *Druckenmiller et al.*, 2013; *Gearheard et al.*, 2010; *Laidler et al.*, 2010; *Tremblay et al.*, 2006] as well as the impact of recent and projected sea ice changes on coastal communities [*Aporta*, 2011; *Aporta and Higgs*, 2005; *Fienup-Riordan and Rearden*, 2010; *Ford et al.*, 2008; *Huntington and Fox*, 2005; *Laidler et al.*, 2009]. This body of work has led to new insights informing guidance to ice users [*Bell et al.*, 2014; *Druckenmiller et al.*, 2013; *Wilkinson et al.*, 2011]. However, we need formulations to link specific ice parameters to geophysical processes and quantities in order to effectively support or inform tactical and strategic decisions in the context of ice use and on-ice operations.

At present, we are lacking a framework to provide quantitative, objective guidance on ice use, e.g., in the context of short-term tactical or long-term strategic decisions. Instead, stakeholders continue to depend on semi-empirical, often qualitative methods to evaluate proxy parameters (such as ice thickness) that do not necessarily reflect the complexity of ice use and the impacts of recent environmental change. Prior work identifies and highlights

different aspects of ice use, laying the groundwork for a more comprehensive approach to defining, tracking, and predicting ice properties, processes, and parameters relevant in this context. For both local assessments and large-scale regional surveys, remote sensing approaches have great potential but are at present underutilized as a tool to support ice use and document relevant changes.

The work presented in this thesis builds on prior work by defining environmental parameters constraining ice use and creating an ice use decision support and monitoring framework that draws in particular on remote sensing data. The goal of this work is to evaluate how sea ice trafficability is changing as a result of large-scale sea ice decline.

1.3 Thesis outline

While coastal communities and industry already feel the impacts of a changing landfast ice cover, the potential consequences have yet to be understood in their entirety. Addressing this problem requires a solid grasp of those aspects of the landfast ice that are critical to stakeholders, and methodology and tools to monitor relevant sea ice and environmental variables from the local to the pan-Arctic scale through the lens of stakeholder interests. This thesis takes a two-fold approach to help close this information gap. Part 1 seeks to improve understanding of the link between ice trafficability and the geophysical constraints on this type of ice use (Chapter 2). Part 2 builds on this work to develop strategies capable of evaluating and monitoring landfast sea ice in terms of ice use (Chapters 3-5).

Chapter 2 [*Dammann et al.*, in preparation] presents a framework for new strategies to evaluate landfast sea ice in the context of sea ice use. The work involves a rigorous selection of parameters relevant to ice use, arrived at through interviews with local and regional ice users in coastal Alaska. The framework guides the development of an assessment strategy relevant to a set of stakeholder needs and resources by focusing on parameters relevant to a particular ice regime. A case study in Kotzebue, Alaska, illustrates this approach by developing a method to evaluate ice thickness safety thresholds for ice road planning,

construction and use. Chapter 2 also introduces an overview of the case studies and associated strategies developed in Chapters 3-5.

Based on an unmatched combination of spatial coverage, accuracy, and availability, synthetic aperture radar (SAR) holds considerable potential in sea ice science and is utilized in the final three chapters. Chapter 3 [*Dammann et al.*, in review-b] explores a range of different SAR techniques including interferometry, polarimetry, and single-channel SAR to quantify trafficability of landfast ice for the purposes of informing ice trail routing and construction, drawing on an example at Utqiaġvik, Alaska. For validation of the remote sensing data, a high-resolution Digital Elevation Model (DEM) was constructed by applying Structure-from-Motion analysis to imagery obtained during an Unmanned Aerial System (UAS) campaign. This approach allows for a comparison between SAR products and geophysical measures of roughness. Additionally, ice trails in Utqiaġvik were surveyed, which afforded an evaluation of trafficability based on trail routes selected by local ice experts.

Chapter 4 *[Dammann et al., 2016*] investigates the potential of SAR interferometry for evaluation of small-scale deformation within the landfast ice. Even cm-scale deformation can impact the stability of the ice and is thus relevant to a range of ice users, including in-ice installations that depend on the long-term integrity of the ice cover. Interpretation of SAR interferometry is not straightforward and an inverse model was developed to determine both deformation mode and rate over large spatial scales.

Chapter 5 [*Dammann et al.*, in review-a] builds on the modeling approach developed in Chapter 4. First, both interferometry and the model were validated by a high-precision GPS grid deployed in Elson Lagoon, Alaska, confirming accuracy in terms of deformation mode and rate. Second, ice deformation was evaluated in the vicinity of the Northstar Island ice road – a critical logistic route for an offshore oil and gas production site in the Beaufort Sea, Alaska. Understanding small-scale deformation across sea ice is particularly relevant for similar roads and other fixed in-ice installations due to the potential for fracture and reduced load bearing capacity over time. Ice stress and fracture were calculated based on a simple model of ice rheology, which led to identification of sections of the ice road potentially impacted by hazardous ice conditions and warranting thorough ground surveys.

1.4 Contributions

The majority of the content of each major chapter of this thesis (Chapter 2-5) is either published (Chapter 4), in review (Chapter 3 and 5), or intended for publication (Chapter 2). I am the lead author of all four manuscripts and have conducted the fieldwork and interviews, which from all the analysis builds. However, substantial contributions have been made by all co-authors in terms of drafting the complete manuscripts/chapters, interviews, fieldwork, and analysis. Hajo Eicken, Andrew Mahoney, and Franz Meyer are all co-authors on all four manuscripts and have made substantial contributions to the overall direction of this work as well as provided critical guidance to the entire process from planning of fieldwork to drafting of the manuscripts.

Chapter 2 was in large part built around interviews from three Alaska communities where Sarah Betcher (co-author) and Karen Brewster made substantial contributions to the interviews. Chapter 3 included operations of an unmanned aerial system (UAS) and the development of a Structure-from-Motion digital elevation model. The UAS was operated by key personnel with Alaska Center for UAS integration (ACUASI) and the raw data was processed by Eyal Saiet (co-author). The UAS operation was largely successful thanks to Craig George (co-author) through providing guidance and resources. Chapter 5 included work with high-precision GPS sensors. Here, Jeff Freymueller and Max Kaufmann processed the raw data and provided substantial guidance in terms of operation of the sensors and data analysis.

1.5 References

AMAP (2011), Snow, water, ice and permafrost in the Arctic (SWIPA): Climate Change and the Cryosphere, *Rep.*, xii + 538 pp, Oslo, Norway.

Aporta, C. (2009), The trail as home: Inuit and their pan-Arctic network of routes, *Hum Ecol*, *37*(2), 131-146.

Aporta, C. (2011), Shifting perspectives on shifting ice: documenting and representing Inuit use of the sea ice, *The Canadian Geographer/Le Géographe canadien*, *55*(1), 6-19, doi: 10.1111/J.1541-0064.2010.00340.X.

Aporta, C., and E. Higgs (2005), Satellite culture - Global positioning systems, inuit wayfinding, and the need for a new account of technology, *Curr Anthropol*, *46*(5), 729-753, doi: 10.1086/432651.

Bell, T., R. Briggs, R. Bachmayer, and S. Li (2014), Augmenting Inuit knowledge for safe sea-ice travel—The SmartICE information system, paper presented at 2014 Oceans-St. John's, IEEE.

Dammann, D. O., H. Eicken, F. Meyer, and A. Mahoney (2016), Assessing small-scale deformation and stability of landfast sea ice on seasonal timescales through L-band SAR interferometry and inverse modeling, *Remote Sens Environ*, *187*, 492-504, doi: 10.1016/j.rse.2016.10.032.

Dammann, D. O., H. Eicken, A. Mahoney, F. Meyer, and S. Betcher (in preparation), Sea ice trafficability - new strategies for a changing icescape, *Polar Geography*.

Dammann, D. O., H. Eicken, A. Mahoney, F. Meyer, J. Freymueller, and A. M. Kaufman (in review-a), Assessing landfast sea ice stability and internal ice stress around ice roads using L-band SAR interferometry and inverse modeling, *Cold Reg Sci Technol*.

Dammann, D. O., H. Eicken, E. Saiet, A. Mahoney, F. Meyer, and J. C. George (in review-b), Traversing sea ice - linking surface roughness and ice trafficability through SAR polarimetry and interferometry *IEEE Journal of Selected Topics in Applied Earth Observations and Remote Sensing*.

Druckenmiller, M. L., H. Eicken, J. C. George, and L. Brower (2013), Trails to the whale: reflections of change and choice on an Iñupiat icescape at Barrow, Alaska, *Polar Geography*, *36*(1-2), 5-29, doi: 10.1080/1088937X.2012.724459.

Eicken, H., A. L. Lovecraft, and M. L. Druckenmiller (2009), Sea-Ice System Services: A Framework to Help Identify and Meet Information Needs Relevant for Arctic Observing Networks, *Arctic*, *62*(2), 119-136.

Fienup-Riordan, A., and A. Rearden (2010), The ice is always changing: Yup'ik understandings of sea ice, past and present, in *SIKU: knowing Our Ice: Documenting Inuit*

Sea Ice knowledge and Use, Igor Krupnik, Claudio Aporta, Shari Gearheard, Gita Laidler and Lene Kielsen Holm, 295-320, Springer, New York.

Ford, J. D., T. Pearce, J. Gilligan, B. Smit, and J. Oakes (2008), Climate change and hazards associated with ice use in northern Canada, *Arctic, Antarctic, and Alpine Research*, *40*(4), 647-659.

Gearheard, S., G. Aipellee, and K. O'Keefe (2010), The Igliniit project: Combining Inuit knowledge and geomatics engineering to develop a new observation tool for hunters, in *SIKU: Knowing Our Ice*, 181-202, Springer.

Huntington, H. P., and S. Fox (2005), The changing Arctic: indigenous perspectives, in *Arctic Climate Impact Assessment*, C Symon, L Arris and B Heal, 61–98, Cambridge University Press, New York, NY.

Krupnik, I., C. Aporta, S. Gearheard, G. J. Laidler, and L. K. Holm (2010), *SIKU: knowing our ice*, Springer.

Laidler, G. J., P. Elee, T. Ikummaq, E. Joamie, and C. Aporta (2010), Mapping Inuit sea ice knowledge, use, and change in Nunavut, Canada (Cape Dorset, Igloolik, Pangnirtung), in *SIKU: knowing Our Ice: Documenting Inuit Sea Ice knowledge and Use*, Igor Krupnik, Claudio Aporta, Shari Gearheard, Gita Laidler and Lene Kielsen Holm, 45-80, Springer.

Laidler, G. J., J. D. Ford, W. A. Gough, T. Ikummaq, A. S. Gagnon, S. Kowal, K. Qrunnut, and C. Irngaut (2009), Travelling and hunting in a changing Arctic: assessing Inuit vulnerability to sea ice change in Igloolik, Nunavut, *Climatic change*, *94*(3-4), 363-397.

Mahoney, A., H. Eicken, A. G. Gaylord, and R. Gens (2014), Landfast sea ice extent in the Chukchi and Beaufort Seas: The annual cycle and decadal variability, *Cold Reg Sci Technol*, *103*, 41-56, doi: 10.1016/J.Coldregions.2014.03.003.

Meehl, G. A., T. Karl, D. R. Easterling, S. Changnon, R. Pielke Jr, D. Changnon, J. Evans, P. Y. Groisman, T. R. Knutson, and K. E. Kunkel (2000), An introduction to trends in extreme weather and climate events: observations, socioeconomic impacts, terrestrial ecological impacts, and model projections, *Bulletin of the American Meteorological Society*, *81*(3), 413-416.

Overland, J. E., and M. Wang (2013), When will the summer Arctic be nearly sea ice free?, *Geophys Res Lett*, *40*(10), 2097-2101.

Overland, J. E., K. R. Wood, and M. Wang (2011), Warm Arctic-cold continents: climate impacts of the newly open Arctic Sea, *Polar Research*, *30*.

Pachauri, R. K., L. Meyer, G.-K. Plattner, and T. Stocker (2015), *IPCC, 2014: Climate Change 2014: Synthesis Report. Contribution of Working Groups I, II and III to the Fifth Assessment Report of the Intergovernmental Panel on Climate Change*, 151 pp., IPCC, Geneva, Switzerland.

Selyuzhenok, V., T. Krumpen, A. Mahoney, M. Janout, and R. Gerdes (2015), Seasonal and interannual variability of fast ice extent in the southeastern Laptev Sea between 1999 and 2013, *Journal of Geophysical Research: Oceans*, *120*(12), 7791-7806.

Serreze, M. C., and J. A. Francis (2006), The arctic amplification debate, *Climatic Change*, *76*(3-4), 241-264, doi: Doi 10.1007/S10584-005-9017-Y.

Stephenson, S. R., L. C. Smith, and J. A. Agnew (2011), Divergent long-term trajectories of human access to the Arctic, *Nat Clim Change*, *1*(3), 156-160, doi: 10.1038/Nclimate1120.

Stroeve, J. C., M. C. Serreze, M. M. Holland, J. E. Kay, J. Malanik, and A. P. Barrett (2012), The Arctic's rapidly shrinking sea ice cover: a research synthesis, *Climatic Change*, *110*(3-4), 1005-1027, doi: 10.1007/S10584-011-0101-1.

Tremblay, M., C. Furgal, V. Lafortune, C. Larrivée, J.-P. Savard, M. Barrett, T. Annanack, N. Enish, P. Tookalook, and B. Etidloie (2006), Communities and ice: Bringing together traditional and scientific knowledge, *Climate change: linking traditional and scientific knowledge*, 289.

Wang, M., and J. E. Overland (2015), Projected future duration of the sea-ice-free season in the Alaskan Arctic, *Progress in Oceanography*, *136*, 50-59.

Wilkinson, J. P., S. Hanson, N. E. Hughes, A. James, B. Jones, R. MacKinnon, S. Rysgaard, and L. Toudal (2011), Tradition and technology: Sea ice science on Inuit sleds, *Eos, Transactions American Geophysical Union*, *92*(1), 1-4.

Yu, Y., H. Stern, C. Fowler, F. Fetterer, and J. Maslanik (2014), Interannual Variability of Arctic Landfast Ice between 1976 and 2007, J Climate, 27(1), 227-243.

2 SEA ICE TRAFFICABILITY – STRATEGIES FOR A CHANGING ICESCAPE*

2.1 Abstract

Arctic sea ice has undergone rapid changes during the last few decades with negative implications for ice travel, navigation and on-ice operations, all of which depend on services provided by the sea ice as a platform for such activities. A Parameter-based Trafficability Hierarchy (PATH) is presented here as a framework to enable the development of quantitative assessment strategies capable of providing guidance for planning and execution of operations on landfast sea ice and for quantification of impacts of recent changes on ice use. PATH outlines steps to identify key parameters relevant to evaluate feasibility (e.g. landfast ice extent), safety (e.g. ice thickness), and efficiency (e.g. ice roughness) of over-ice travel based on specific ice regimes and local and Indigenous knowledge. The number of parameters is further reduced based on specific user objectives enabling the development of assessment strategies with the necessary accuracy and spatial and temporal scales. A PATH assessment has been completed in three case studies in Arctic Alaska. These cases correspond to a range of different icescapes and ice use scenarios, with different parameters linked to trafficability and safe operations identified and quantified. PATH was first used to determine an ice thickness compensation factor to help translate sporadic auger ice thickness measurements along the Kotzebue – Kiana ice road into an envelope for safe operations. A large compensation factor of up to 1.5 is found to be necessary to ensure safety due to the high local thickness variability in some regions, currently a concern for ice road operators. PATH is further discussed in terms of its ability to support expansion of remote sensing strategies and demonstrates its ability to guide the development of trafficability assessments of ice roughness in Utqiaġvik and safety assessments based on fracture potential around Northstar Island.

* Dammann, D. O., H. Eicken, A. Mahoney, F. Meyer, and S. Betcher (in preparation). Sea ice trafficability – new strategies for a changing icescape. *Arctic*.

2.2 Introduction

2.2.1 Sea ice use and recent change

Sea ice plays a critical role in the Arctic providing a range of services in social-environmental systems, such as regulating global climate, protecting coastlines against erosion, providing habitat for marine species, and supporting ice use by humans. Such services have been referred to as Sea Ice System Services [*Eicken et al.*, 2009] and support ice use by humans, such as travel or hunting on landfast ice by coastal residents as well as the construction of ice roads for use by resource extraction industries. Sea ice services extend beyond operational or logistical benefits derived from the presence of ice and include historical, cultural, and educational components, which are critical for the wellbeing of coastal communities. Sea ice also inhibits certain activities and presents a hazard for marine craft ranging from small skin boats to cargo and cruise ships. A comprehensive overview of ice use by humans in the Arctic is provided in Table 2.1. The different uses of sea ice all depend on different ice processes or properties, which in many cases can be represented by geophysical parameters or sets of parameters that describe the state of the ice and help track relevant changes. Examples of ice users and uses (see Table 2.1) and associated parameters are displayed in Figure 2.1 in an effort to illustrate how different aspects of use take place on and around sea ice.

Arctic sea ice has undergone rapid decline during the past few decades in terms of extent [*Comiso and Nishio*, 2008; *Comiso and Hall*, 2014; *Meier et al.*, 2014; *Stroeve et al.*, 2012; *Stroeve et al.*, 2008] and thickness [*Kwok and Rothrock*, 2009; *Lindsay and Schweiger*, 2015; *Rothrock et al.*, 2008]. Summer Arctic sea ice extent is expected to continue to decrease during the 21st century and the observed decrease over the past decade suggests acceleration in the response of the Arctic sea ice cover to external forcing, hastening the ongoing transition towards a seasonally open Arctic Ocean [*Stroeve et al.*, 2008]. In light of these recent changes, it is important to evaluate the future of ice use [*Stephenson et al.*, 2011] through strategies capable of determining climatological as well as seasonal change that directly addresses stakeholder-specific needs [*Eicken et al.*, 2009; *Lovecraft et al.*, 2013]. In particular, it will be important to understand determining factors for whether ice use is

possible or safe in a specific location and also how to identify potential hazards [*Eicken and Mahoney*, 2015; *Eicken et al.*, 2011]. This is challenging for several reasons: (1) ice properties that govern ice use are relevant at the local or regional scale and are use-specific and hence depend upon individual user or stakeholder perspectives, (2) user or stakeholder information needs are not necessarily directly linked to typical geophysical properties that are assessed through ongoing Arctic scientific research or monitoring, and (3) we mostly lack quantitative information that describes a safe sea-ice operating or use space.

Table 2.1 Different types of sea ice use by humans in the Arctic

User group	**Activity associated with ice use**	**Examples of specific relevance**
Arctic communities	Hunting and fishing	Subsistence, cultural tradition, identity
	Transportation	Transporting fuel, food, goods etc.
	Travel	Travel across ice (e.g. hunting, visiting nearby communities etc.)
	Recreation	Dog mushing, exercising, snowmobile riding, competitions
	Education / cultural activities / social events	Teaching navigation, ice safety, and other skills to younger generations
	Cultural activities	Ceremonies and rituals
Industry	Natural resource development	Oil and gas exploration and production, small-scale operations such as placer gold mining
	Shipping	Trans-Arctic and destinational cargo shipping
Tourism	Cruise-ship tourism	
	Solo trips / exploration	
Science	Field work and expeditions	Use of coastal ice as a platform or natural laboratory for broader understanding of relevant sea ice processes
Defense	Naval operations and training	Concealing nuclear submarines as part of the Mutual Assured Destruction Doctrine during the Cold War

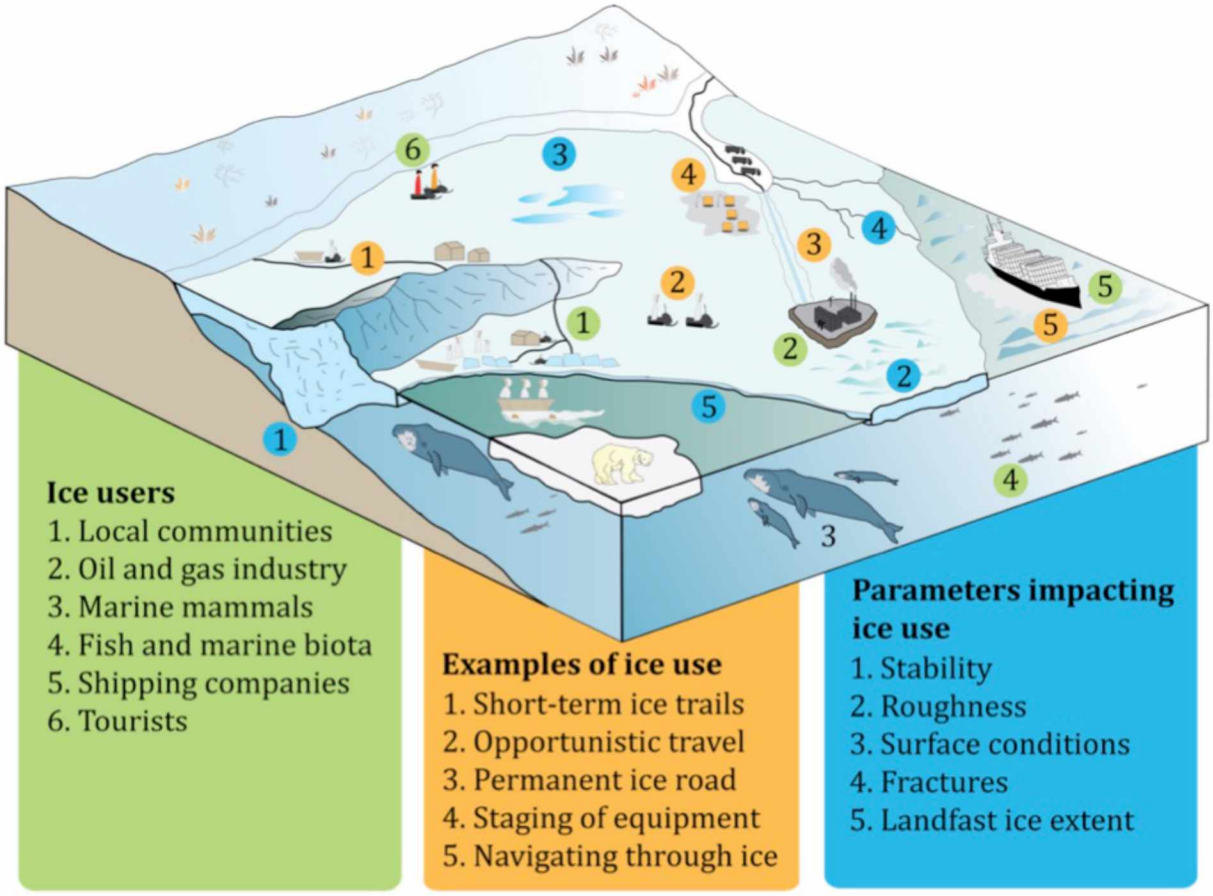

Figure 2.1 Schematic showing examples of ice users, ice use activities, and ice related parameters impacting ice users.

Some work has been done identifying ice-thickness thresholds for safe travel over ice [*Finucane and Scher*, 1983; *Gold*, 1971; *Squire et al.*, 1996; *USACE*, 2002], but this work has not related specific threshold values to different sea ice regimes or local ice conditions and associated use. Also, while the broader category of ice parameters relevant to ice use has often been identified, for ice stability [*Bashaw et al.*, 2013; *Potter et al.*, 1981] it is far from clear which specific variables or processes need to be measured and tracked over what spatio-temporal scales to support ice use and stakeholder needs. Qualitative information may be appropriate for individual Indigenous user groups, who can draw upon a vast body of traditional environmental or Indigenous knowledge and associated responses to hazards and opportunities.

However, for operators such as industry, quantitative data is superior to information gathered from qualitative assessment strategies, such as air reconnaissance. In particular for assessment of environmental changes impacting strategic decision-making and operations, qualitative methods are insufficient. Changing Arctic sea ice also impacts Indigenous and local knowledge holders' ability to rely on their body of expertise. In some locations this has been recognized [*Jolly et al.*, 2002], including recognition of a need for new, complementary assessment strategies to inform ice use.

2.2.2 Motivation for case studies on landfast sea ice

Along the Arctic coast, sea ice commonly attaches to shore as landfast ice and has been used for travel by coastal communities for millennia throughout the circumpolar North as well as by oil and gas companies in recent decades [*Masterson and Spencer*, 2001]. Landfast ice has undergone significant reductions in recent years in terms of duration [*Mahoney et al.*, 2014; *Selyuzhenok et al.*, 2015] and extent [*Yu et al.*, 2014] affecting and potentially jeopardizing the services provided by the ice cover and ice use by both industry and communities [*Eicken et al.*, 2009]. It is widely recognized that recent Arctic change has resulted in more difficult travel conditions [*Fienup-Riordan and Rearden*, 2010; *Laidler et al.*, 2010] and increasingly dangerous ice [*AMAP*, 2011; *Aporta*, 2011; *Aporta and Higgs*, 2005; *Druckenmiller et al.*, 2013; *Ford et al.*, 2008; *Huntington and Fox*, 2005].

We choose to focus on the use of landfast ice as a platform for transportation and on-ice operations due to the range of stakeholder interests and the urgency of understanding these environmental changes from an ice user's perspective. The use of landfast ice as a platform depends on the trafficability of the ice, which we define as the ability to operate on the ice within the limitations of feasibility, efficiency and safety. Trafficability thus depends on quantifiable parameters such as surface properties and composition. Here, we present a Parameter-based Trafficability Hierarchy (PATH), that can serve as a framework to develop, evaluate and synthesize new methods and techniques to help ice users and stakeholders

cope with rapidly changing ice environments and to serve the research community in guiding process studies and sustained observations (Section 2.2).

PATH was utilized in three case studies in Alaska (Kotzebue, Utqiaġvik, and Prudhoe Bay) in an effort to evaluate its utility for different ice regimes and use activities and to develop techniques relevant for multiple regions. The sites for the two first case studies were chosen in part based on vastly different ice regimes representing extreme conditions in terms of deformation and surface roughness, capturing some of the most significant ice types relevant for ice use in coastal environments. These locales therefore represent end-members of coastal ice types, but are also characterized by different types of ice use.

Kotzebue is situated on an isolated isthmus of land separating Kotzebue Sound and Hotham Inlet (known locally as Kobuk Lake). Kotzebue has served as a hub for rural communities for centuries where a significant portion of the population regularly travels on the ice for the purpose of hunting, fishing, and transporting fuel and goods to summer cabins and nearby communities, which makes the sea ice around Kotzebue one of the most significant ice use regions in the Arctic. Utqiaġvik (formerly Barrow) is an important strategic location for hunting of marine mammals from the ice and hence community members construct extensive seasonal trails on the landfast sea ice [*Druckenmiller et al.*, 2013].

Kotzebue and Utqiaġvik, like other coastal and near-coastal communities in Northwest Alaska, are facing severe challenges related to climate change through delayed freeze up and shorter landfast ice season. In Kotzebue, over-ice travel is delayed by 8 days per decade [*Uhl*, 1990-2003] and threatening continuation and safety of ice travel [Fred Smith and Seth Kantner, 2014, personal communication]. In Utqiaġvik, changing ice conditions are becoming the primary constraint on ice related travel [*Druckenmiller et al.*, 2009].

The ice road in Kotzebue (case study 1 - *Section 2.4.1*) traverses a predominately sheltered river-influenced, estuarine location dominated by smooth ice, while the ice trails in Utqiaġvik (case study 2 - *Section 2.4.2*) often cross severely deformed ice shaped by processes representative of offshore ice dynamics. The results from the two regions support the use of PATH in a third scenario, an industrial ice road near Prudhoe Bay (case study 3 – *Section*

2.4.3) traversing partly sheltered ice, but still influenced by offshore pack ice interaction. Together these studies clearly demonstrate the ability of PATH to guide the development of new quantitative assessment strategies in support of safety and continued on-ice operations.

2.3 PATH - A framework for developing new assessment strategies for ice use guided by stakeholder needs

2.3.1 Description of the Parameter-based Trafficability Hierarchy (PATH)

To be able to develop new strategies in support of ice use, it is critical to understand individual ice-user and stakeholder needs. For on-ice operations, these needs are most often driven by a combination of feasibility (i.e., is it possible to carry out an activity?), safety (i.e., is it safe to do so?), and efficiency (i.e., can it be done in an economically viable fashion or with sustainable use of community resources?) and constrained by parameters and thresholds applicable for the individual ice user or ice regime illustrated in Figure 2.2. Examples of specific ice use scenarios with associated examples of user needs are listed in Table 2.2, which are each addressed in Section 2.4. The challenge is to evaluate whether these needs can be met during a time of changing ice conditions and high year-to-year variability in critical ice-use related ice conditions. To meet this challenge we are proposing a framework that can help narrow down assessment strategies capable of evaluating and tracking landfast ice properties and processes tied to specific user needs. This framework arranges the critical trafficability parameters based on user-specific needs into a Parameter-based Trafficability Hierarchy (PATH). PATH consists of three stages, each of which is composed of separate steps (Figure 2.3).

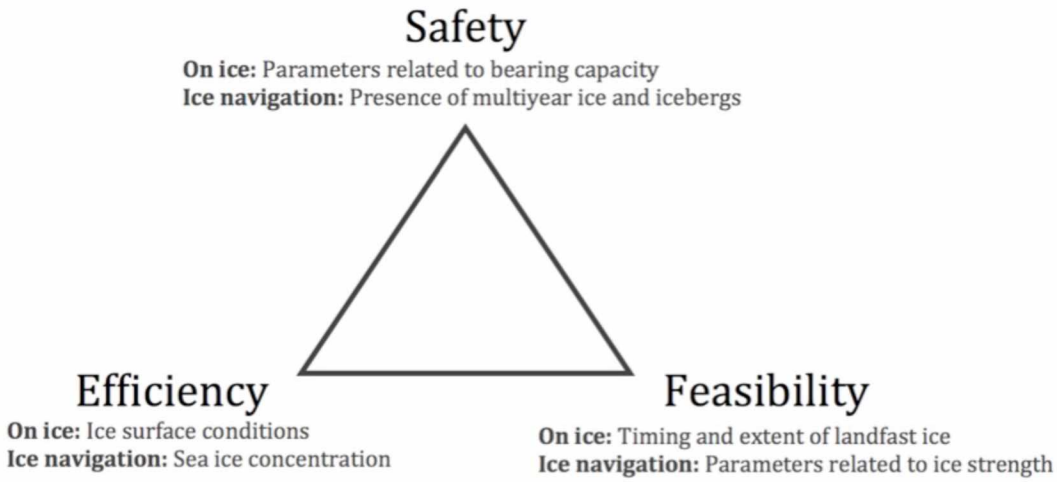

Figure 2.2 Schematic of user needs grouped into categories with associated examples of relevant parameters for on-ice operations and ice navigation for marine vessels operating in ice.

The first stage of PATH is to identify relevant ice-associated parameters for a particular ice use scenario and ice regime, and involves several steps. The initial step is to determine all potential parameters that may be relevant (Step 1a), a process where local and Indigenous knowledge can offer substantial insight (Section 2.2.2), followed by a series of steps to exclude less important variables. Parameters can be excluded based on a regional evaluation of the particular ice regime (Step 1b). This can be achieved using a variety of datasets ranging from local maps, climate data, previously acquired remote sensing data, as well as current remote sensing and weather data. The third step is to gather information from local and Indigenous knowledge (Step 1c) to evaluate relevance of parameters based on experience with regional ice use. The fourth step (Step 1d) is to identify what ice-associated parameters or constraints can easily be overcome with available resources and are thus less critical. For instance, for a community ice road with few resources, adequate ice thickness is of higher relevance than for an industry ice road, where resources exist to artificially thicken the ice.

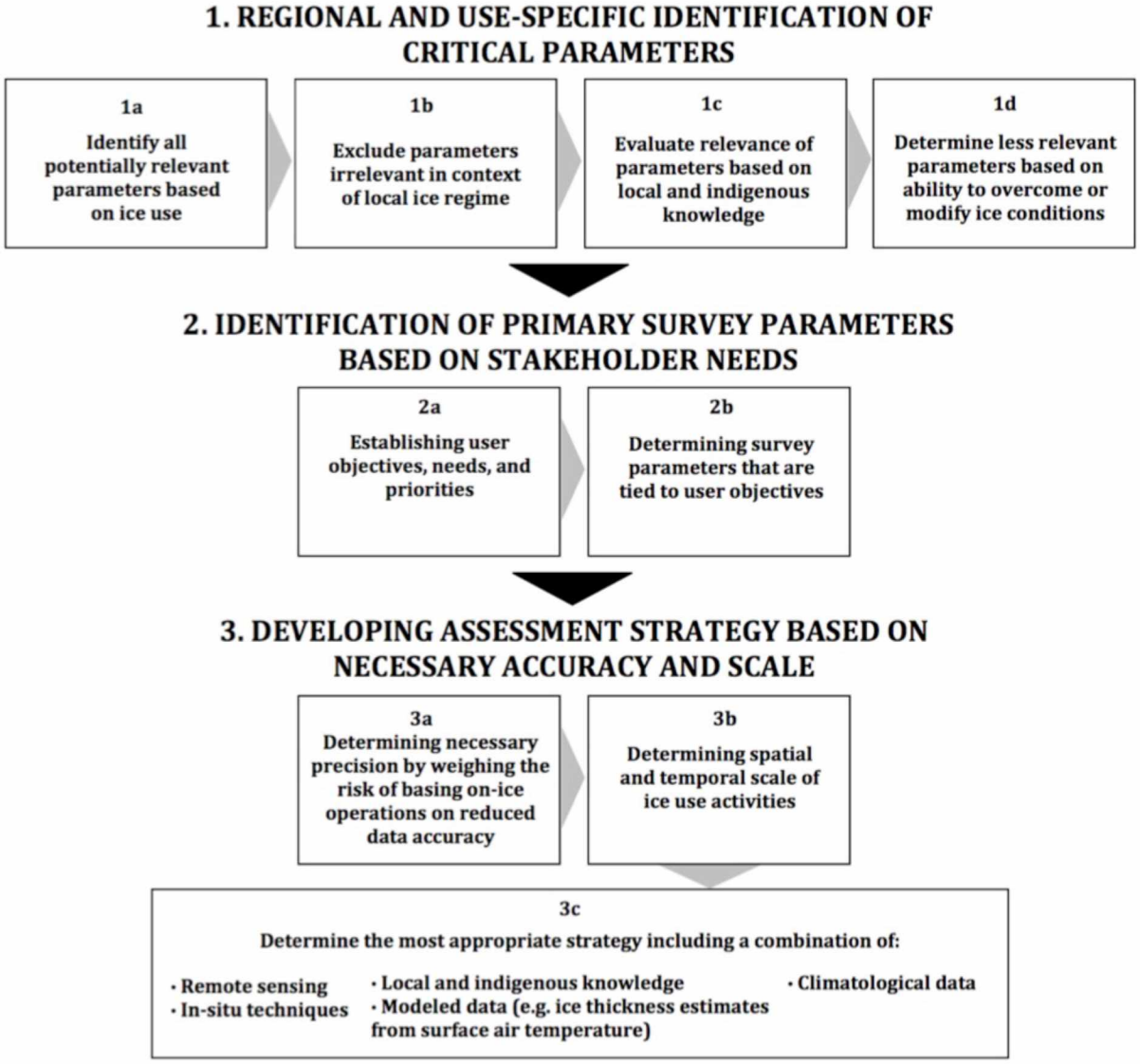

Figure 2.3 Overview of the three steps in PATH for developing assessment strategies in response to stakeholder needs.

The second stage of PATH is to thoroughly identify the users' needs and priorities (Step 2a) evaluating user objectives (see examples in Table 2.2). Subsequently, these priorities are used to determine which parameters are most important in meeting specific user objectives (Step 2b). For instance, safety is in general the highest priority; hence properties governing safety are of highest relevance. The third stage of PATH is to develop an assessment strategy

based on the relevant parameters identified in parts 1 and 2. To appropriately determine a strategy it must first be determined what accuracy is necessary (Step 3a). For instance, parameters related to safety often require far greater accuracy than parameters related to efficiency since the consequences of misinterpretation of data are far more serious. The scale at which ice is used is also a factor in determining the selection of a specific assessment tool (Step 3b). A strategy with high accuracy often fails to provide information over a large spatial extent; hence, the last step involves some degree of compromise in developing methods, often utilizing a combination of techniques, that can ensure that needs are met within the scope of available stakeholder resources (Step 3c).

Table 2.2 Examples of ice use and associated user needs

Ice use	**Example of user need**
Community ice road operated by local government (*Section 2.4.1*)	Ability to safely operate an ice road within a strict financial budget thus without possibility for modifications such as artificial thickening. Ability to operate within a time window with sufficient ice thickness to sustain required bearing capacity of road maintenance equipment.
Subsistence ice trails constructed by local community members (*Section 2.4.2*)	Ability to manually construct trails through rough ice from shore to the landfast ice edge within constraints to financial budget, construction time, and trail length.
Industry ice road (*Section 2.4.3*)	Ability to operate on ice that can hold construction vehicles and will remain immobile during the season. Ability to travel across the ice multiple times without compromising load-bearing capacity or surface conditions.

2.3.2 Gathering perspectives from over-ice travel

In the first stage of PATH it is necessary to establish all potentially relevant parameters impacting ice travel and relate these to data that may aid in providing information that meets

stakeholder needs (Step 1a). To develop a complete set of parameters impacting on-ice operations and travel, local ice experts (e.g. local hunters, ice road operators etc.) were interviewed in three communities in Alaska during winter of 2013/2014. Utqiaġvik, Kotzebue, and Nome (Figure 2.4a) were selected based on both difference in ice conditions and the different ice associated activities and together span a large range of ice use enabling the identification of a range of relevant parameters.

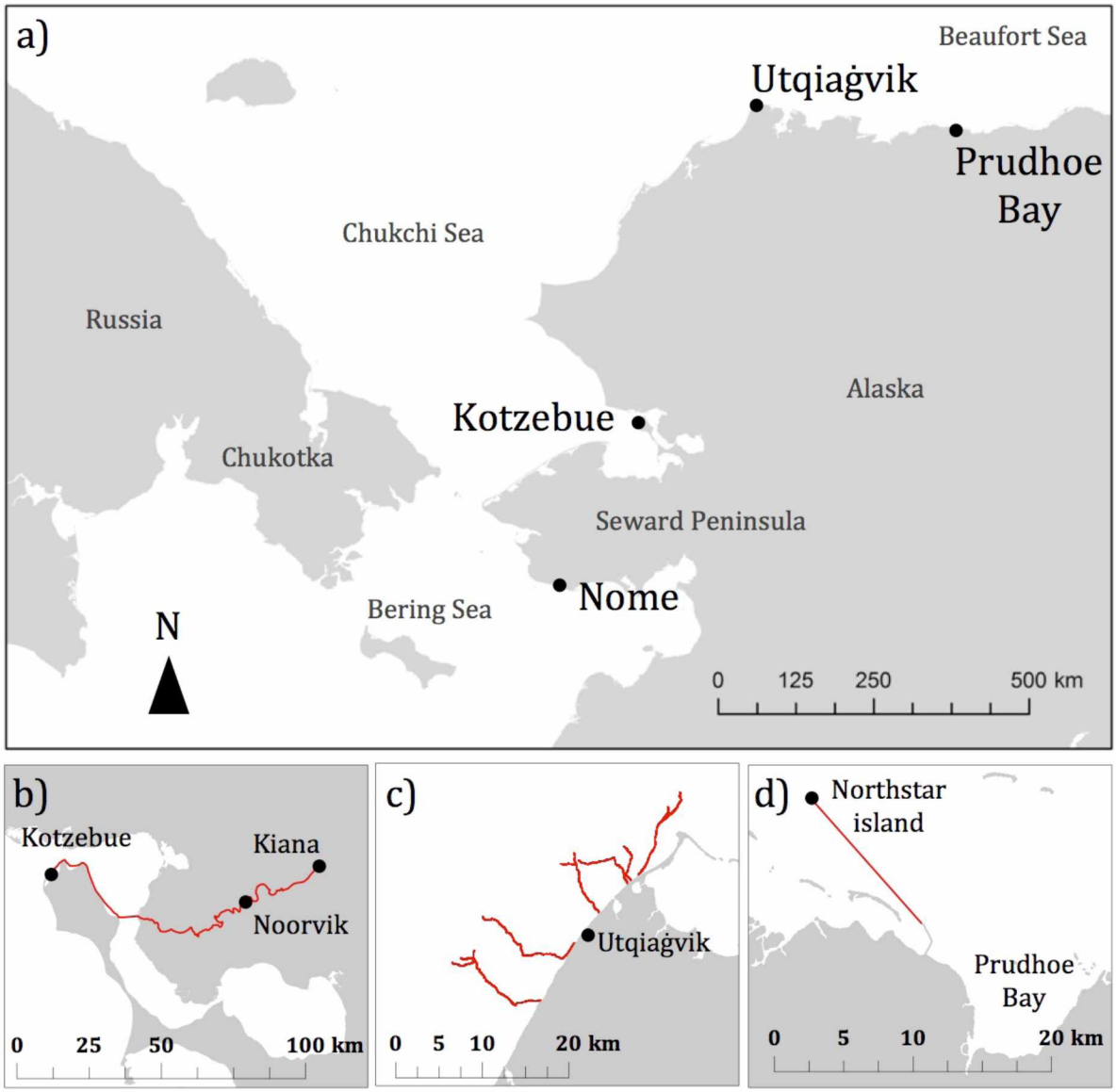

Figure 2.4 Overview of study areas (a), with close-up view of ice roads (b, d) and ice trails (c). Note that roads and trails shown in (b) and (c) represent a subset of all those studied.

Nome is situated in northwestern Norton Sound on the coast of the Bering Sea and a large part of its population spends some time on the sea ice during the winter season fishing, seal hunting, gold mining, or participating in recreational activities [*Ahmasuk*, 2014]. The landfast ice near Nome consists of mostly level to moderately rough first year sea ice and is susceptible to breakout events throughout winter. Kotzebue lies ~250 km northeast of Nome and is situated on the Baldwin Peninsula surrounded by the waters of Kotzebue Sound and Kobuk Lake. The ice around Kotzebue is more sheltered than that near Nome and features infrastructure such as marked ice trails and a fully maintained ice road used for transportation of goods. Common ice use near Kotzebue includes fishing, seal and caribou hunting, and travel to nearby communities [*Smith*, 2014]. The sea ice near Utqiaġvik is predominately first year ice often with moderate to severe roughness. The landfast ice is not sheltered like Kotzebue and is subject to wintertime breakout events. Ice-associated activities around Utqiaġvik are mostly limited to hunting of ducks, seals, and bowhead whales, the latter of which involves the construction of seasonal ice trails [*Druckenmiller et al.*, 2013].

Interviews in Utqiaġvik were conducted jointly by Karen Brewster and Dyre Dammann as part of the Sea Ice Jukebox Project [*Brewster*, 2016] and in Nome and Kotzebue jointly by Sarah Betcher and Dyre Dammann as part of the Sustainable Futures North Project [*Betcher*, 2017]. The Sea Ice Jukebox project has previously supported research such as *Druckenmiller et al.* [2013]. Both projects followed Institutional Review Board (IRB) procedures and were found to be exempt from IRB oversight. Only experienced ice travelers were interviewed in all communities: Brandon Ahmasuk and Roy Ashenfelter in Nome [*Ahmasuk*, 2014; *Ashenfelter*, 2014], Fred Smith and Ross Schaeffer in Kotzebue [*Schaeffer*, 2014; *Smith*, 2014], and Joe Leavitt, Eugene Brower, Billy Adams, Jacob Adams, Roy Nageak, and Crawford Patkotak in Utqiaġvik [*Brewster*, 2016]. All interviews were semi-directed [*Huntington*, 2000] containing questions related to sea ice and specifically covered discussion of ice features considered to be of significance for ice travel. The interview with Brandon Ahmasuk took place on the sea ice where important ice features and areas of concern were identified. The interview with Ross Schaeffer took place during a seal hunt where the use of ice was demonstrated both in the context of traveling and hunting.

The interviews from Kotzebue, Utqiaġvik, and Nome were used in conjunction with published literature to form a comprehensive set of parameters that are critical to travel on landfast sea ice. The parameters generally fit into nine categories, which are relevant on different time and spatial scales: (1) ice thickness, (2) roughness and topography, (3) stability (i.e. the ability of the ice to withstand forcing without breaking out), (4) Pre-existing defects (e.g. macro-scale fractures that may lead to reduced strength), (5) fracture potential (e.g. ability for the ice to fracture through small-scale movement), (6) microstructure and state variables (e.g. salinity, temperature), (7) snow and water covering the ice surface, (8) duration of landfast ice season and timing of freeze up and break up, and (9) shorefast ice extent. These nine categories can be arranged in a matrix configuration according to their importance and relevant spatio-temporal scale (Figure 2.5).

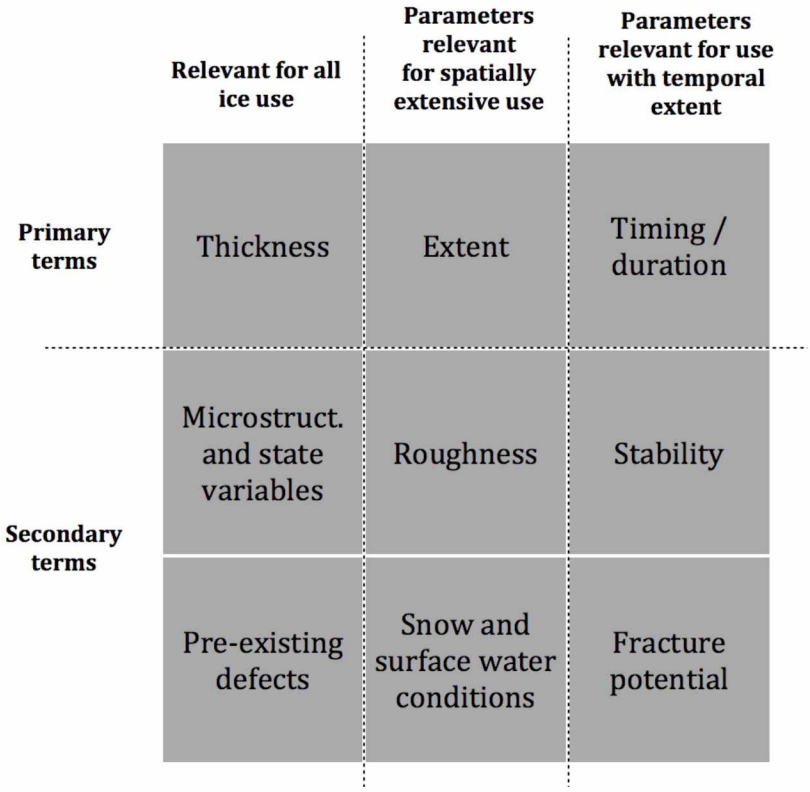

Figure 2.5 General ice use-related parameters structured in a matrix where columns contain parameters related to (1) all ice use, (2) use with a spatial extent, and (3) use with either temporal extent or constraints. Row 1 represents primary terms that govern the principal feasibility of ice use while the lower rows contain secondary terms related to safety and efficiency (relevant if primary conditions are sufficient for use).

The left column contains parameters relevant for all aspects of on-ice activities. The middle column contains additional parameters to consider for spatially extensive use such as over-ice travel. The right column contains parameters relevant for use with temporal extent such as ice roads or trails. A justification of the nine categories through a summary of the findings from interviews and literature is provided in Section 2.2.3.

2.3.3 Relevant parameters for over-ice travel on landfast sea ice

2.3.3.1 Ice thickness

Without adequate thickness to sustain the load, ice travel is impossible [*Adams*, 2013a; *Adams*, 2013b; *Ahmasuk*, 2014; *Aporta*, 2004; *Ashenfelter*, 2014; *Brower*, 2013; *Ford et al.*, 2008; *Laidler et al.*, 2010; *Leavitt*, 2013; *Nageak*, 2013; *Patkotak*, 2013; *Schaeffer*, 2014; *Smith*, 2014], or as Smith [2014] states, "*When the ice isn't thick, it isn't safe*". Sea ice thickness throughout the Arctic has been reduced significantly in recent decades. At Utqiaġvik, the ice regime has changed from containing large sections of multiyear ice with thickness 3.0 - 4.6m (10-15') to predominately first-year ice with thickness of 0.9 - 1.8m (3-6') in roughly half a century [*Adams*, 2013b; *Brower*, 2013]. Ice thickness is important for hunting on sea ice in terms of safety and ability to access hunting grounds [*Brower*, 2013; *Patkotak*, 2013; *Schaeffer*, 2014] and although the new thickness regime still allows most hunting activities it has made travel more difficult [*Nageak*, 2013; *Smith*, 2014] and hunters must act accordingly with greater caution [*Adams*, 2013b; *Nageak*, 2013]. Increasing incorporation of thin young ice into the landfast ice is often problematic [*Brower*, 2013; *Leavitt*, 2013] or potentially unsafe when harvesting marine mammals [*Adams*, 2013a; *Ashenfelter*, 2014; *Leavitt*, 2013]. "In recent years it has been open patches of thin ice you can't even traverse on foot" [*Nageak*, 2013]. The spatial distribution of thickness is particularly significant when the ice is thin. Patches of dangerously thin ice represent a hazard that Inuit try to avoid [*Nageak*, 2013; *Smith*, 2014] often causing early season trails to be more circuitous than later trails [*Aporta*, 2004]. Due to such spatial variability in ice thickness, ice roads must be

monitored carefully [*Mesher et al.*, 2008; *Smith*, 2014]. However, when the ice has adequate thickness for travel, the thickness is not directly important but will have implications for roughness and stability of the ice cover [*Druckenmiller et al.*, 2013]. Thick ice that can withstand external forcing is important [*Adams*, 2013b] since thin ice will not be able to withstand interaction with drifting pack, which then may "crumple it" [the landfast ice] or "take the whole shorefast ice out" [*Brower*, 2013]. Thin ice also may move out with the wind [*Ashenfelter*, 2014].

2.3.3.2 Roughness and topography

Increased roughness and associated implications for ice travel are already felt across the Arctic [*Fienup-Riordan and Rearden*, 2010; *Laidler et al.*, 2010], resulting in increasing risk associated with on-ice travel [*Ford et al.*, 2008]. In recent years, the process of freeze-up has often progressed inconsistently, causing the ice cover to repeatedly break up and "get blown out" as it forms, leading to rougher ice [*Laidler et al.*, 2010]. At the same time, despite increasing small-scale roughness, local experts report that the landfast ice contains fewer large ridges [*Brower*, 2013; *Leavitt*, 2013] reducing the number and size of grounded ridges, which are important for stability [*Adams*, 2013b; *Brower*, 2013; *Nageak*, 2013]. "Increased roughness means less freedom to go places" [*Adams*, 2013a] as rough areas have to be worked around [*Adams*, 2013b]. Smooth ice is advantageous for efficiency and cost when traveling and travelers often avoid rough spots even if they have to constantly turn while traveling [*Fienup-Riordan and Rearden*, 2010]. However, increasing distance traveled across ice can in of itself increase risk [*Nageak*, 2013].

Industry also recognizes that an ice road should compromise between avoiding areas of ridged ice while decreasing distance on the ice [*Potter et al.*, 1981]. Ice roughness is a key factor in transportation across ice for local communities and industry [*Haas and Druckenmiller*, 2010] and for potential emergency evacuation from industrial drilling installations and tourist vessels [*Eicken*, 2010]. For coastal residents, ice roughness is important for trail construction impacting travel time and cost [*Druckenmiller et al.*, 2010; *Druckenmiller et al.*, 2013; *Eicken and Mahoney*, 2015] and even small-scale roughness has

been shown to have implications for the use of ice as aircraft landing strips [*Haas and Druckenmiller*, 2010].

2.3.3.3 Stability

Typically, stability is defined as the ability of shorefast ice to remain largely undeformed despite atmosphere, ocean, or ice forcing acting on the ice cover; ice stability depends on the anchoring strength imparted by grounded ridges and/or topographic features such as islands or promontories, as well as on ice thickness, structure, and the presence of defects such as pre-existing cracks [*Mahoney et al.*, 2007]. The stability of the ice is complicated through the dependence on an array of key variables such as thickness, defects, ridges, and even the angle of the grounded pressure ridges [*Brower*, 2013]. Major construction projects, such as ice roads, should seek to increase use of stable ice near islands [*Potter et al.*, 1981]. A major concern for ice users from both communities and industry are hazards associated with large-scale landfast ice movement or breakout events, i.e., detachment of large portions of shorefast ice during the time period the ice cover is generally considered to be stable [*Eicken et al.*, 2011; *George et al.*, 2004]. Landfast ice stability is a critical factor governing safety of ice use for local communities [*Adams*, 2013a; *Brower*, 2013; *George et al.*, 2004; *Leavitt*, 2013; *Nageak*, 2013; *Patkotak*, 2013]. However, the stability of landfast ice in Alaska has been decreasing [*Nageak*, 2013; *Patkotak*, 2013] with the near-absence of multiyear ice [*Adams*, 2013a; *Brower*, 2013; *Leavitt*, 2013; *Nageak*, 2013; *Patkotak*, 2013] and reduction in grounded ridges [*Adams*, 2013a; *Brower*, 2013; *Leavitt*, 2013; *Nageak*, 2013; *Patkotak*, 2013].

2.3.3.4 Pre-existing defects

Cracks are considered a potential hazard by local communities [*Ford et al.*, 2008; *Schaeffer*, 2014] due to the destabilizing effect and the potential for the ice to shear off [*Brower*, 2013] and are often monitored throughout the season [*Leavitt*, 2013] or sometimes completely

avoided [*Adams*, 2013a; *Adams*, 2013b; *Nageak*, 2013]. For industry, ice structural defects are a concern due to the decreasing load-bearing capacity; hence, monitoring [*Mesher et al.*, 2008] and repair [Walton Crowell (2016), personal communication] are often required for hazardous dry cracks or wet wedges (A crack that extend throughout the ice and split into two cracks to form a wedge) [*Potter et al.*, 1981]. Even refrozen cracks are a concern due to the lower strength of the ice formed within the crack [*Petrich et al.*, 2007]. Refrozen cracks are therefore likely to break again and are monitored [*Leavitt*, 2013]. Fracturing of the ice can make it too hazardous to travel and thus limit ice use [*Patkotak*, 2013].

2.3.3.5 Fracture potential

Although anchoring points such as islands or grounded ridges might prevent the ice from undergoing large-scale deformation and breaking out, landfast ice can still experience fracture through small-scale deformation. Reduced thickness has led to a more dynamic landfast ice cover and increase of frequency in deformation [*Brower*, 2013] leading to fracturing of areas not previously known to fracture [*Nageak*, 2013]. Understanding the complex system of wind and currents is crucial for determining if ice is moving and if so, in what direction [*Adams*, 2013a; *Brower*, 2013; *Nageak*, 2013; *Patkotak*, 2013] to determine where cracks will form and the safety of crossing such openings [*Laidler*, 2006]. Ice deformation is a key concern for industry since even small-scale movement can be a sign of short-term failure or long-term creep, which is of general importance to engineering problems with large loads on the ice [*BP*, 2013; *Schwarz and Weeks*, 1977].

2.3.3.6 Microstructure and state variables

The way the ice is formed changes the microstructure. For instance, brackish or fresh estuaries consist of stronger ice due to reduced brine inclusions in the ice and can thus carry higher loads. However, thin saline ice is more ductile and can thus in certain situations support larger moving loads than possible for fresh ice under similar conditions [*Schaeffer*,

2014]. Variable salinity (e.g. around the mouth of a river) can therefore cause variable internal structure and load bearing capacity [*Smith*, 2014]. The ice has also in recent years been observed to suddenly fail unexpectedly into "pencil-like" pieces [*Smith*, 2014], which may indicate that the ice in the sound is becoming more similar to lake ice with the presence of candle ice due to a changing microstructure. Refrozen slush ice (known as agiukpak in the local Inupiaq language) is another example of a modified microstructure. Slush ice is created by grinding between ice floes (muġałłiq) and can refreeze to form a weak and hazardous surface [*Adams*, 2013a; *Leavitt*, 2013]. "It's not too safe to be on anywhere where there's slush. When it breaks up, it just disperses everywhere and there's nowhere to be safe on that kind of ice -- not even for a little fox maybe" [*Adams*, 2013a]. "It used to be more solid ice that attached to each other. But now there's more pressure ridges and thin ice that tend to press against each other resulting in ice that is not solid" [*Nageak*, 2013].

2.3.3.7 Snow and meltwater

Snow and water on the ice can greatly impact travel conditions. A thin layer of snow, as opposed to pure ice, makes the sea ice substantially easier to travel on with snowmobiles [Seth Kantner (2014), personal communication]. Snow can also make rough areas traversable that otherwise wouldn't be [*Dammann et al.*, in review-a]. However, snowfall and snowdrifts can seasonally shut down ice roads [Wendie Schaeffer (2015), personal communication]. Snow can also result in dangerous travel conditions due to the ability to cover up cracks [*Ford et al.*, 2008]. "You don't hunt after a west wind since it creates cracks. The ice is broken up and the snow covers everything" [*Schaeffer*, 2014]. Soft snow can also be difficult to navigate for ATV vehicles for instance limiting travel to nighttime and early morning, when the snow is typically firmer [*Ahmasuk*, 2014]. In late spring, warming weather can also offer substantial challenges. Flooding and soft ice can be a hazard both to local residents [*Ford et al.*, 2008] and industry [*Potter et al.*, 1981] due to rapid thinning of the ice.

2.3.3.8 *Landfast ice extent, timing, and duration*

Landfast ice has undergone reductions in extent across much of the Arctic [*Yu et al.*, 2014], consistent with local observations [*Ashenfelter*, 2014; *Smith*, 2014]. This limits how far it is possible to travel out on the ice, which can be important for some subsistence activities [*Ahmasuk*, 2014]. The timing where the landfast ice is usable is also reduced [*Adams*, 2013a; *Ahmasuk*, 2014; *Ashenfelter*, 2014; *Brower*, 2013; *Mahoney et al.*, 2014] and is generally attributed to global warming [*Ashenfelter*, 2014; *Brower*, 2013; *Nageak*, 2013]. The travel season is rapidly decreasing [*Brower*, 2013] as freeze-ups progress over longer time allowing less time for either boat or snowmobile travel during fall [*Smith*, 2014]. For instance, recorded ice crossings to the mainland from Kotzebue show a delay of 8 days per decade [*Uhl*, 1990-2003] and certain routes are no longer usable [Seth Kantner (2014), personal conversation] or associated with increased risk [*Smith*, 2014].

2.4 Methods

2.4.1 *Assessing ice thickness variability with ground penetrating radar*

Radio echo sounding (RES), also referred to as ground penetrating radar (GPR), can be used to derive the thickness of floating ice [*Haas and Druckenmiller*, 2010; *Holt et al.*, 2009; *Kanagaratnam et al.*, 2007]. The ice thickness (h) is calculated from the return time (t) of an emitted electromagnetic signal traveling with speed (v) reflecting back from the underside of the ice due to the strong dielectric contrast at the ice/water interface:

$$h = \frac{vt}{2} \qquad (2.1)$$

The speed of light in fresh ice is roughly 0.17 m ns^{-1}, but is reduced depending on salinity down to roughly 0.10 m ns^{-1} for sea ice [*Liu et al.*, 2014].

We surveyed the Kotzebue – Kiana ice road using a GPR, which provided continuous ice thickness measurements from Kotzebue to the Kobuk River Delta (Figure 2.6a). The GPR unit

was a 1GHz pulseEKKO-Pro system mounted in a plastic sled and towed on the ice road behind a snowmobile from Kotzebue to the mouth of the Kobuk River. The unit was towed at a speed of roughly 8 m s^{-1} (30 km h^{-1}), which was slow enough for the sled not to bounce on the ice surface. GPR is susceptible to a significant loss of signal strength in sea ice due to impurities in the ice (e.g. brine channels, air bubbles, fractures) hence is most reliable on fresh, thin, and undeformed ice. Ice salinity ranged between 0 and 1 ppt (Dammann, 2014, unpublished data) by Lockhart Point indicating predominance of fresh ice across most of the road resulting in sufficient signal for accurate ice thickness measurements.

Low ice salinity (<1 ppt) along most of the road also results in a near-zero bias in the derived thickness data due to changing signal velocity. Examples of raw datasets from the GPR survey are displayed in Figure 2.6b-d. GPR can only resolve the snow layer separately if the snow depth exceeds a certain depth. For the particular system used, snow depth would have to exceed roughly 1 m, which is not typical on landfast sea ice in Alaska. However, the ice road was cleared, eliminating the potential for biased thickness readings due to snow. To validate the GPR measurements, eight auger holes were drilled along the survey.

2.4.2 Ice thickness compensation factor

Ice thickness is relevant in terms of its bearing capacity, which can in an idealized case be calculated for a continuous sheet of ice using the formula:

$$h_0 = \sqrt{\frac{P}{A}} \qquad (2.2)$$

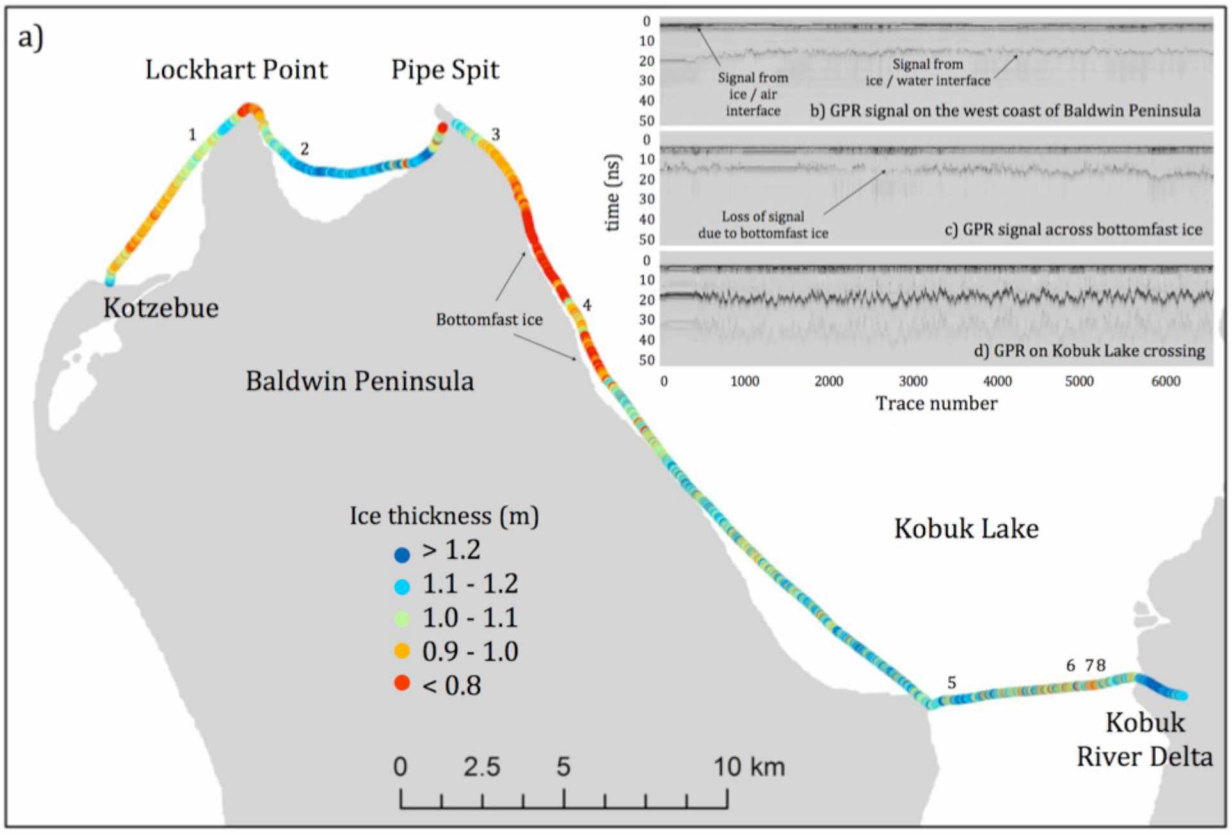

Figure 2.6 a) Ice thickness along the Kotzebue - Kiana ice road from Kotzebue and into the Kobuk River Delta. The area of thin ice (red) close to shore near Lockhart Point, Pipe Spit, and south of Pipe Spit is thin ice due to bottomfast ice. Numbers indicate auger validation points. Unprocessed GPR data from three sections of the ice road are displayed in the top right corner. b) Signal from most saline ice close to Kotzebue. The radar return signal is apparent, but weak predominately due to brine inclusions. c) Signal with reduced strength across bottomfast ice. d) Signal showing full strength in fresh water and high thickness variability on Kobuk Lake crossing. Top and bottom lines represent ice/air and ice/water interface respectively. The y-axis is in time units, which is used to derive depth and the x-axis is individual trace numbers. The length of these segments is roughly 3km.

where h_0 is minimum ice thickness in m, P is the required load bearing capacity in kg, and A is a constant, which can range up to $1.75 \cdot 10^5$ kg m^{-2} for strong ice [*Gold*, 1971]. For ice use purposes, ice thickness is predominately measured using augers due to the unmatched mm-scale accuracy of the direct measuring method. However, although this approach is accurate, it results in a point measure and hence is subject to uncertainties over larger scales where thickness may vary substantially between auger holes. Different guidelines exist for the

frequency at which measurements should be made. The U. S. Army Corps of Engineers (USACE) Ice Engineering guidelines [*USACE*, 2002] advise drilling holes at least every 45 meters. The Northwest Territories Department of Transportation (NWT DOT) advise measuring as often as every 30 m close to shore [*NWTDOT*, 2007]. However, such guidelines present a challenge for longer ice roads [*Mesher et al.*, 2008] such as the one considered here. It is expensive and logistically not feasible to achieve the measurement intervals recommended by USACE and NWT DOT and instead auger hole spacings of 3-4 km are common along the Kotzebue – Kiana ice road. However, such auger hole spacings may overlook significant thickness variability and areas of thin ice.

A common practice has been to apply a 'compensation factor', Γ, in such cases raising the minimum thickness, from h_0 to h, to account for thickness variability and factors that may reduce the bearing capacity of ice below its calculated measure:

$$h = \left(\sqrt{\frac{P}{A}}\right)\Gamma \qquad (2.3)$$

Γ typically ranges between 1.15 [Walton Crowell 2016, personal communication] and 2-2.25 [*USAAF*, 1968] depending on the constant A, temperature, salinity, and ice conditions, but does not take into account substantial thickness variability between auger holes in cases of large auger-hole spacing. Here we calculate Γ from a thickness compensation offset Z:

$$Z \equiv h_0(\Gamma - 1) \qquad (2.4)$$

Z represents the difference between minimum thickness measured in an auger survey and the actual minimum thickness measured along the same survey stretch. Continuous (1 m interval) thickness data from GPR allows for simulated surveys where the minimum thickness that would be sampled with auger holes can be estimated based on hypothetical auger-hole spacings and survey starting points. Each simulated survey results in an offset between the actual minimum thickness and the sampled minimum. Multiple simulated surveys were generated for auger-hole spacings ranging from 1 m – 3 km, but with the starting position incrementally offset by one meter. One thousand different starting points

were used resulting in one hundred unique surveys with 100 m spacing and one thousand unique surveys with 3 km spacing. This approach provides similar results as a periodogram approach, except duplicate surveys are introduced for auger-holes spacing < 1 km and not all combinations are sampled with spacing > 1 km. However, the distribution of the set of offset values (from every auger-hole spacing) will be similar. Assuming a normal distribution of offset values, Z is found as two standard deviations away from the mean. This ensures that when Z is subtracted from the minimum value in an auger survey, this new lower value falls below the actual minimum ice thickness value in 97.5% of surveys.

2.4.3 Assessing trafficability based on ice roughness

Synthetic aperture radar (SAR) is a valuable tool for assessing trafficability due to the sensitivity of the signal to surface roughness, unmatched large-scale coverage and data availability, independence of weather conditions, and m-scale resolution. Different SAR-derived products can provide unique insight into the type of roughness; the radar backscatter cross section can indicate the roughness of the terrain, SAR polarimetry (PolSAR) to some extent what type of roughness features are present, and SAR interferometry (InSAR) how high the elevation of the rough features is [*Dammann et al.*, in review-a].

Each remote sensing product (PALSAR L-band and TanDEM-X/TerraSAR-X X-band) was utilized in combination with GPS surveys of Utqiaġvik ice trails during spring 2015 to determine to what extent individual trails favor different values/classes of each SAR product. A trafficability index ranging from zero (large ridges not crossed by trails) to ~0.5 (smooth ice crossed extensively by trails) was created based on how frequently trails crossed different roughness types in an approach outlined in *Dammann et al.* [in review-a].

Based on the trafficability index, a cost factor conversion was applied to represent relative differences in the cost equivalent of trail construction between roughness types (i.e., extent of unfavorable conditions in relation to stakeholder needs and resources including financial cost, time, safety etc.). The cost conversion differs depending on the particular use case. For

instance, roughness features have a high cost for the Utqiaġvik ice trails since the work to level the ice or cut trail through such ice with pick axes is substantial. The same roughness features would have a lower cost for an industry ice road due to availability of heavy equipment to level the ice. In essence, the relative cost between rough and smooth ice is lower for industry ice roads due to high baseline costs of necessary road maintenance such as artificial thickening and extensive use of the road throughout the season making a straight path more economical. The cost conversion allows for the derivation of optimal trail routes and is described in detail in *Dammann et al.* [in review-a].

2.4.4 Determining fracture potential based on sea ice deformation

SAR interferometry (InSAR) is a technique that is gaining traction in sea ice research and is capable of determining small-scale deformation in the landfast sea ice cover down to the mm-scale based on phase displacement in the SAR signal. Interpretation of raw InSAR data is not straightforward since displacement is only determined in the line of sight direction of the SAR antenna. However, through the development of an inverse model we are now able to reconstruct the deformation mode and magnitude [*Dammann et al.*, 2016]. This enables an assessment of the internal stress buildup and especially the primary tensile stress as the key driver of fracturing within sea ice. The stress and associated fracture potential can be derived from the deformation rate assuming an elasto-brittle rheology for the ice, which can lead to identification of areas particularly prone to fracturing and failure. More details on this approach can be found in *Dammann et al.* [in review-b]. Here, we have evaluated PALSAR L-band interferometric data in the vicinity of Northstar Island, an offshore oil production platform, and an associated ice road near Prudhoe Bay, Alaska.

2.5 Results

2.5.1 Applying PATH for the Kotzebue ice road

2.5.1.1 Identifying ice thickness as the critical ice parameter for the Kotzebue ice road

The Kotzebue – Kiana ice road is a seasonal ice road extending roughly 100 km connecting Kotzebue with two communities, Noorvik and Kiana, on the Kobuk River (Figure 2.4b). The road has been constructed annually over the last several years by the Northwest Arctic Borough (NAB) and remains open for periods between February and May depending on ice and snow conditions in a given year. The road extends across brackish ice at Kotzebue into fresh ice across the estuary known locally as Kobuk Lake (Hotham Inlet) before continuing on river ice on the Kobuk River.

Here, the Kotzebue – Kiana ice road serves as one end member of three cases studies illustrating the application of the PATH framework (*Section 2.2.1*). The suite of parameters relevant for over-ice travel has already been identified (step 1a) in *Section 2.2.2* and will be narrowed down further to a small set of critical parameters. In this process, information from NAB personnel and in particular Fred Smith and Wendie Schaeffer was critical. The inner Kotzebue Sound and Kobuk Lake are sheltered and ice forms relatively early and persists around the Baldwin Peninsula throughout winter ruling out landfast ice extent and stability as relevant parameters. The ice road is not constructed until spring when small-scale deformation is minimal in this region of stable ice. This reduces the relevance of the fracture potential (step 1b). A salinity core we extracted by the ice road on the western side of Lockhart Point (on the first stretch of the ice road) in April 2014 revealed low salinity (maximum 1.0 ppt). Little ocean water influx into the estuary may indicate low salinity variability along most of the ice road eliminating the potential significance of altered bearing capacity as a result of variable salinity and microstructure (*Section 2.3.1*), but this needs to be addressed more closely. Roughness is also often less of a concern along the ice road as a result of the typically calm fall freeze-up of the Kobuk Lake region resulting in mostly smooth, level ice surfaces (step 1c). Pre-existing defects can be mitigated through reinforcement of the ice by road construction staff and snow can be plowed away from the

road within a set financial budget (Wendie Schaeffer, 2015, personal communication) (step 1d).

Based on this evaluation, only two relevant ice parameters remain. Thickness is critical and one of the 0th order ice trafficability terms (Figure 2.5). The ice road is also sensitive to timing and duration of the landfast ice season since there is often a very short timespan when the ice is thick enough (76 cm) for road construction [Wendie Schaeffer, 2015, personal communication]. Reduced freezing-degree days [*Hori et al.*, 2016; *Petrich and Eicken*, 2010] through delayed freeze-up or warmer-than-average temperatures may therefore preclude ice road construction altogether. The ice road is used for transportation of goods and construction materials, lowering the price of products in rural communities. A further key purpose of the road is to increase the connectivity of rural communities within the Northwest Arctic Borough [*NAB*, 2011]. Since these aims and services are not considered critical from an operations perspective, NAB's focus is on road safety if an ice road is constructed at all. With safety being the primary concern [Wendie Schaeffer, 2015, personal communication] ice thickness is the most critical parameter to consider (Figure 2.7). Currently, the borough assesses ice thickness about every 3 km (based on 2013-2014 NAB survey data) to determine adequate ice thickness. However, it is uncertain whether this large auger-hole spacing may overlook thinner sections resulting in a potential safety hazard [*Smith*, 2014].

In the context of recent Arctic changes, ice thickness is particularly relevant having been reduced in the Kotzebue region from historically 1.5 - 1.8 m (5 – 6 ft) to now 0.8 - 0.9 m (2.5 – 3 ft) [*Schaeffer*, 2014], emphasizing the need for better thickness assessment strategies, which became clear in interviews: 'We need to invest in equipment that can measure continuous ice thickness along a particular path, enabling us to make accurate decisions for where to put ice roads and staked trails. Such equipment can improve safety for our people' [*Smith*, 2014]. The benefits of a system capable of continuously assessing ice thickness along the ice road capable of identifying sections subject to subsurface thinning due to strong currents associated with the nearby river channels was brought up.

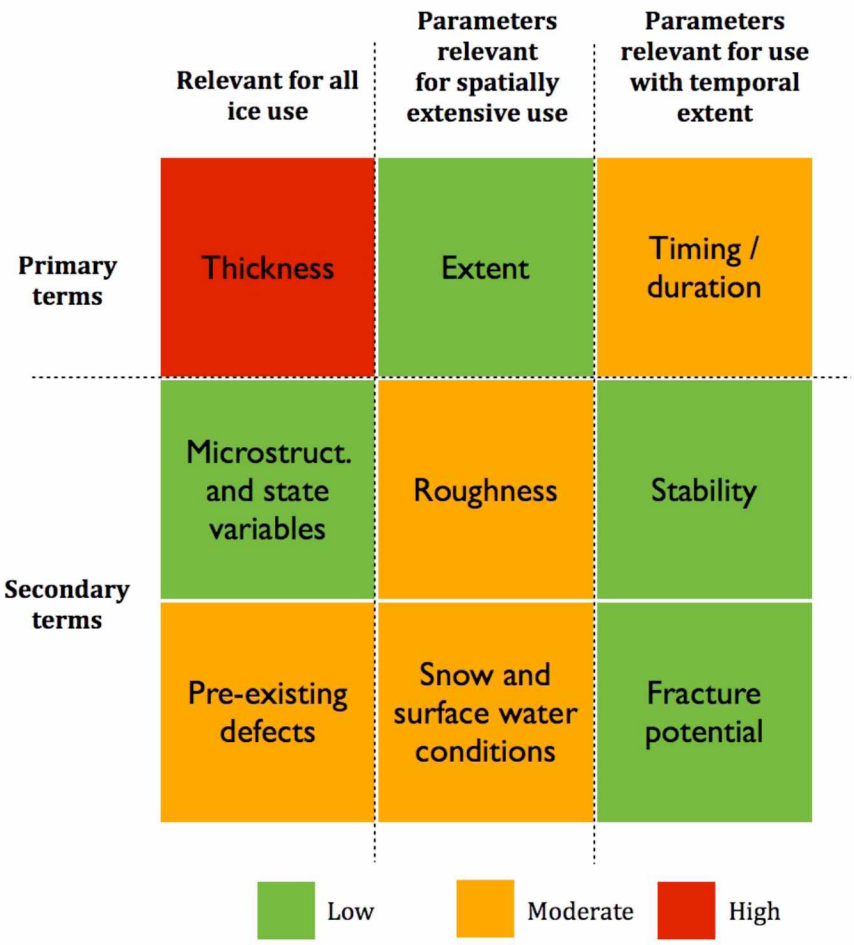

Figure 2.7 The nine ice use parameters arranged as columns in a matrix associated with the relevant scale. Colors indicate level of sensitivity to particular parameters determined by PATH for the Kotzebue-Kiana ice road.

The most promising technique is ground penetrating radar (GPR), employed in this work, but it is both expensive and can be difficult to operate and interpret without proper training. Taking into account the currently modest road construction budget [*NAB*, 2011] we sought to develop an assessment strategy based on continuous thickness data without the need for yearly repeated continuous measurements. This can be achieved by implementing a compensation factor solely corresponding to the expected thickness variability. The ice on the Kobuk Lake region is expected to possess significant thickness variability from subsurface thinning due to inflow from nearby large rivers (Noatak and Kobuk), but the

severity is not established. Therefore, deriving an applicable compensation factor requires further analysis.

2.5.1.2 Developing an assessment strategy for the Kotzebue ice road using ice thickness compensation factors

The Kotzebue - Kiana ice road crosses smooth ice interrupted only by small cm-scale roughness along Baldwin Peninsula before crossing Kobuk Lake towards the Kobuk River Delta (Figure 2.6a). The collected GPR data closely match the auger hole measurements collected for validation (red dots in Figure 2.8a) and areas of thin ice and large thickness variability are apparent (Figure 2.8b). Areas of bottomfast ice were identified through weak signal return (Figure 2.6c) in sections featuring substantially thinner ice (Figure 2.6a and 2.9a), reduced backscatter signal return in SAR imagery (not shown) and were confirmed through auger assessment. In the last segment, the crossing of Kobuk Lake, the data exhibits particularly high thickness variability featuring differences of 40 cm in as little as 20 m intervals confirmed by auger holes (Figure 2.8b). This significant thickness variability indicates that auger holes cannot be expected to yield a representative thickness within the limitations of a practical sampling interval. It can therefore be concluded that it is critical to apply a compensation factor in nearly all cases where local ice thickness variability is not known.

The GPR data, excluding areas of bottomfast ice, were analyzed to determine Z as the discrepancy between auger hole measurements and actual ice thickness (*Section 2.3.2*). The non-linear relationship between Z and the sampling intervals from 0 to 3 km is illustrated in Figure 2.9. For sampling intervals of 0 to 50 m Z increases rapidly to 10 cm. Z increases to roughly 30 cm at a sampling interval of 500 m after which the relationship is approximately linear with Z close to 40 cm at sampling interval of 3 km – a typical sampling interval for this ice road.

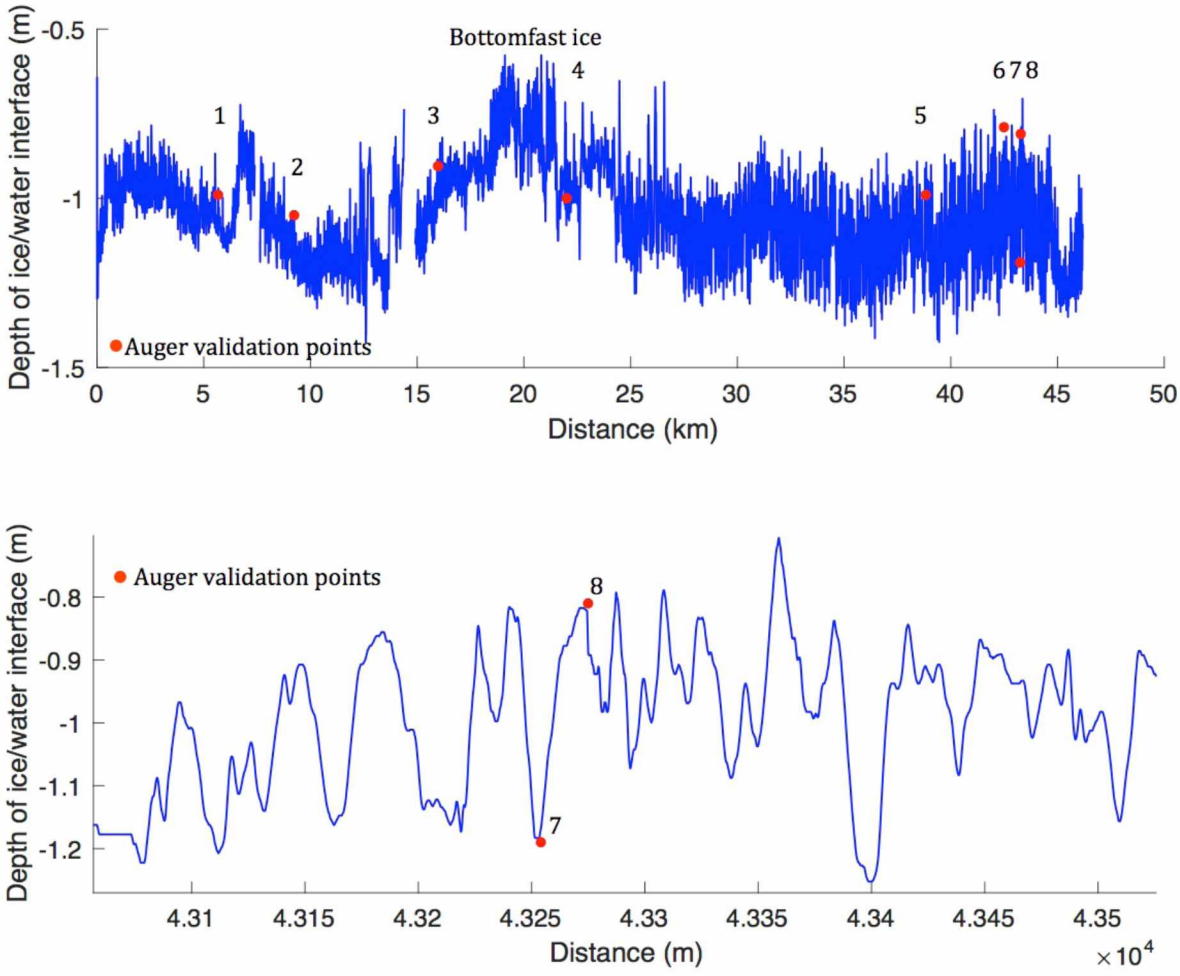

Figure 2.8 Ice thickness across the Kotzebue ice road from Kotzebue to Kobuk Delta (top). High-frequency thickness variability on the Kobuk Lake crossing around validation points 7 and 8 (bottom).

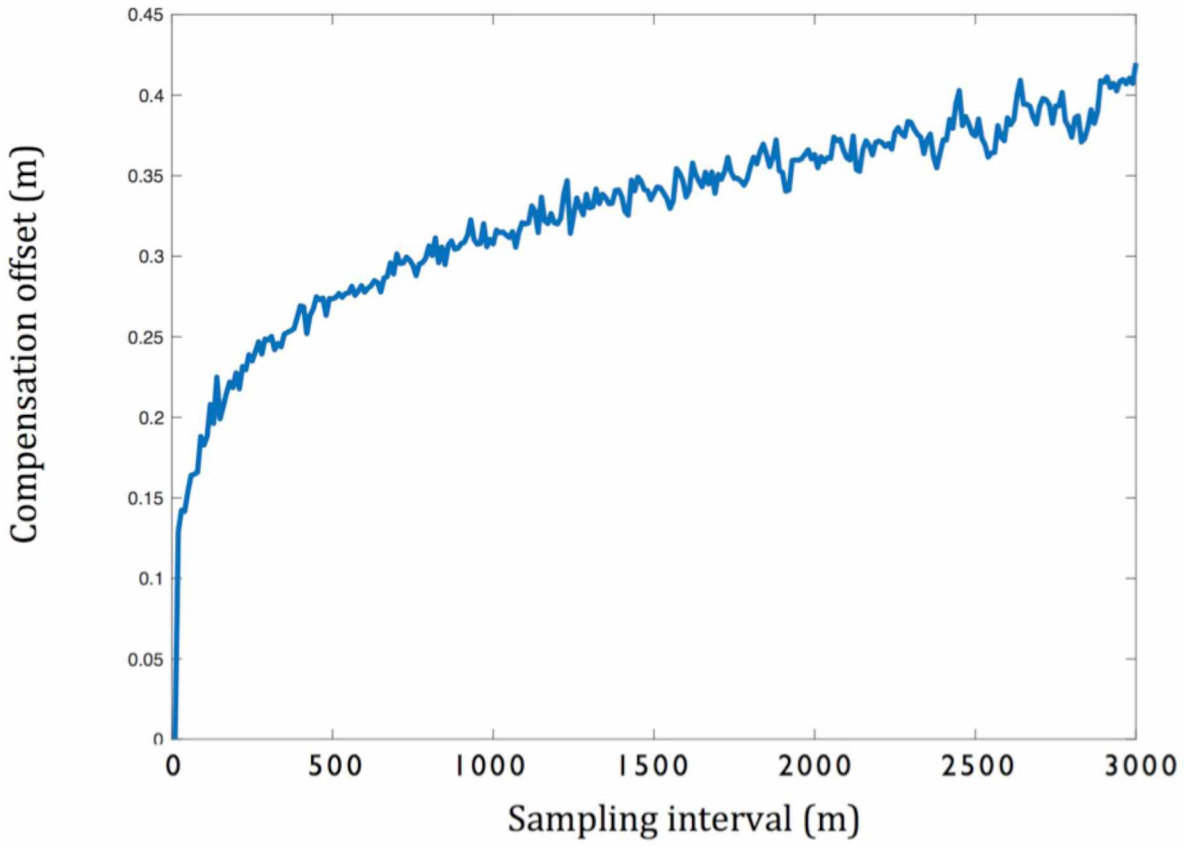

Figure 2.9 Compensation offset for different sampling intervals.

Thickness thresholds for operations on ice vary by region and depending on required load bearing requirements. The Northwest Arctic Borough typically seeks a minimum ice thickness, h_0, in excess of at least 76 cm [Wendie Schaeffer, 2015, personal communication] based on the maximum estimated load of equipment transported across the road. According to this analysis, measurements every 3 km should therefore exceed 116 cm ($h_0 + Z$) to ensure that the entire ice road meets adequate thickness requirements with 97.5% confidence. Adding Z to the minimum thickness corresponds to $\Gamma = 1.5$, which is higher than the compensation factors typically used by Hilcorp for the Northstar ice road (1.15) and would result in a substantial increase of the compensation factor suggested by the US Army (2.0-2.25), which does not account for thickness variability (described in *Section 2.3.2*).

2.5.2 *Applying PATH for seasonal ice trails near Utqiaġvik, AK*

After demonstrating how the PATH framework can be applied in the specific case of the Kotzebue ice road (*Section 2.4.1*), we now explore how PATH can be applied in an entirely different ice use scenario and ice regime at Utqiaġvik, Alaska. The landfast ice near Utqiaġvik is subject to significant pack ice interaction throughout the season, often leading to rough ice conditions. A large fraction of the Iñupiat population takes part in constructing trails extending from shore to the landfast ice edge that serve as access and transportation routes for annual spring hunting activities [*Druckenmiller et al.*, 2013].

Following through step 1 of PATH, ice roughness is a key parameter of concern since rough ice can make trail construction time consuming and expensive to the point of almost impossible to traverse certain regions (related to efficiency in Figure 2.2). Ice roughness also impacts the safety of the trails since trails meandering around in rubble fields will take longer time to evacuate in case of emergency such as a breakout event (detachment of landfast ice) [*Druckenmiller et al.*, 2013]. Roughness can also impact stability, which itself is a key parameter in large part impacting the safety of the trails. Timing and duration are also relevant, but impact trail construction itself to a lesser degree. Snow conditions also dramatically impact travel conditions by smoothing over and reducing the severity of roughness elements. Bearing capacity (left column in Figure 2.5) is generally less of a concern due to thicker ice at Utqiaġvik than in the Kotzebue region. However, it is worth noting that ice thickness does play an important role when it comes to subsistence whaling activities that take place at the landfast ice edge where ice of sufficient bearing capacity is needed for hauling a whale onto the ice for butchering (not considered in this analysis). The relevance of different ice parameters for ice trail use at Utqiaġvik is summarized in Figure 2.10.

Applying step 2 of PATH we define one stakeholder need as the ability to travel from a point on the coast to a point at the ice edge following a route with minimal trail construction effort without compromising safety. Based upon this need, we single out ice roughness as a key parameter. As part of step 3, we determine that large spatial coverage is necessary for an assessment strategy to be able to guide ice use over the several tens of square kilometers

used for trail construction near Utqiaġvik. SAR is a good candidate for obtaining relevant information on ice roughness due to its ability to provide sufficient spatial coverage at the relevant spatial resolution. Also, in this particular case, there is a reduced need for in-situ surveys since there is less concern with accuracy for a strategy assessing efficiency rather than safety.

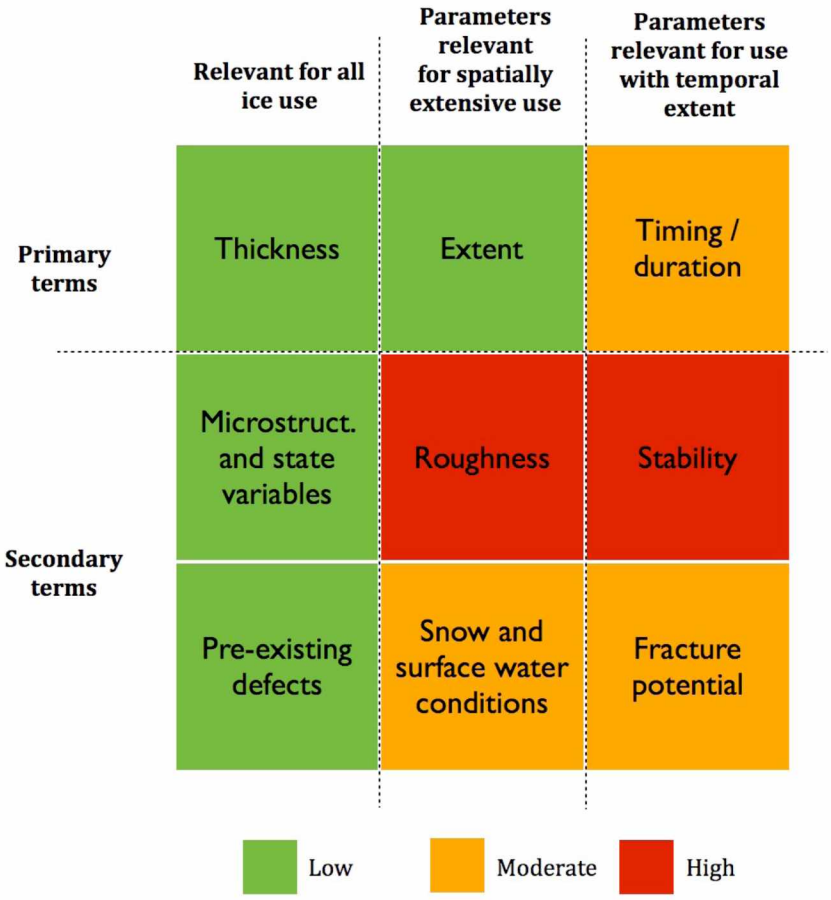

Figure 2.10 The nine ice use parameters arranged as columns in a matrix associated with the relevant scale. Colors indicate level of sensitivity to particular parameters determined by PATH for Utqiaġvik ice trails.

Little effort has been made to develop techniques to assess ice roughness from a trafficability perspective and hence we explored several different promising SAR techniques, which

formed the basis for a combined trafficability index (*Section 2.3.3*). The trafficability index ranges between 0 (very difficult to pass and hence almost never crossed by trails) and up to roughly 0.5 (smooth ice and hence crossed extensively by trails). The trafficability index is displayed in Figure 2.11a around two trails (A and B) shown as black lines. It is clear that these trails favor areas of high trafficability and are attempting to minimize use of low-trafficability areas. Trail A followed a smooth refrozen lead with high trafficability before heading into less trafficable ridged ice. Trail B was heading almost straight out from the coast, crossing a large ridge (dashed line in Figure 2.11a) before following a refrozen lead on the other side with high trafficability.

By assigning a cost function to the trafficability index, taking into account cost of trail construction, time, effort etc., it is possible to calculate a normalized cost from the starting point of trail A (close to the starting point of trail B as well) to all other pixels (Figure 2.11b). This map aids identification of preferred routes and further enables the determination of lowest-cost paths from the starting point to where the trail stops or leaves the study area. The lowest-cost trails (green) follow the actual trails (black) with impressive accuracy taking advantage of multiple highly trafficable areas (Figure 2.11 a and b). Some discrepancies exist and may be due to insufficient information from SAR data or inaccurate cost functions. Another possibility is that under the conditions, the trail crews were not able to assess the ice conditions that might have led to less cost-effective trails. Details on how trafficability and cost indices were developed along with a broader discussion can be found in *Dammann et al.* [in review-a].

Utilizing multiple SAR-derived data products (including gray values derived from backscatter coefficients, InSAR-derived ridge topography, and PolSAR-derived roughness classes) has allowed us to develop an assessment strategy for the determination of optimal travel paths based on ice roughness. The low-cost strategy can also be utilized for different types of transportation, such as ice roads used by trucks or heavy equipment, by applying alternate trafficability-to-cost conversion schemes [*Dammann et al.*, in review-a]. Roughness is only one of two primary concerns for trail construction at Utqiaġvik (Figure 2.10). The other key parameter is stability, which is in large part based on grounded ridges ensuring

stability through sufficient anchoring strength [*Jones et al.*, 2016]. Preliminary results indicate that the location of grounded ridges can be estimated based on TanDEM-X DEM and bathymetric data to calculate weight above hydrostatic equilibrium, grounding strength, and stability. However, due to uncertainties with respect to the composition and structure of individual ridges stability is difficult to assess without direct measurements of ice motion [*Jones et al.*, 2016; *Mahoney et al.*, 2007; *Meyer et al.*, 2011]. Next, we explore the potential for detecting small-scale landfast ice motion, which may eventually be used in combination with assessments of grounding strength to evaluate ice stability.

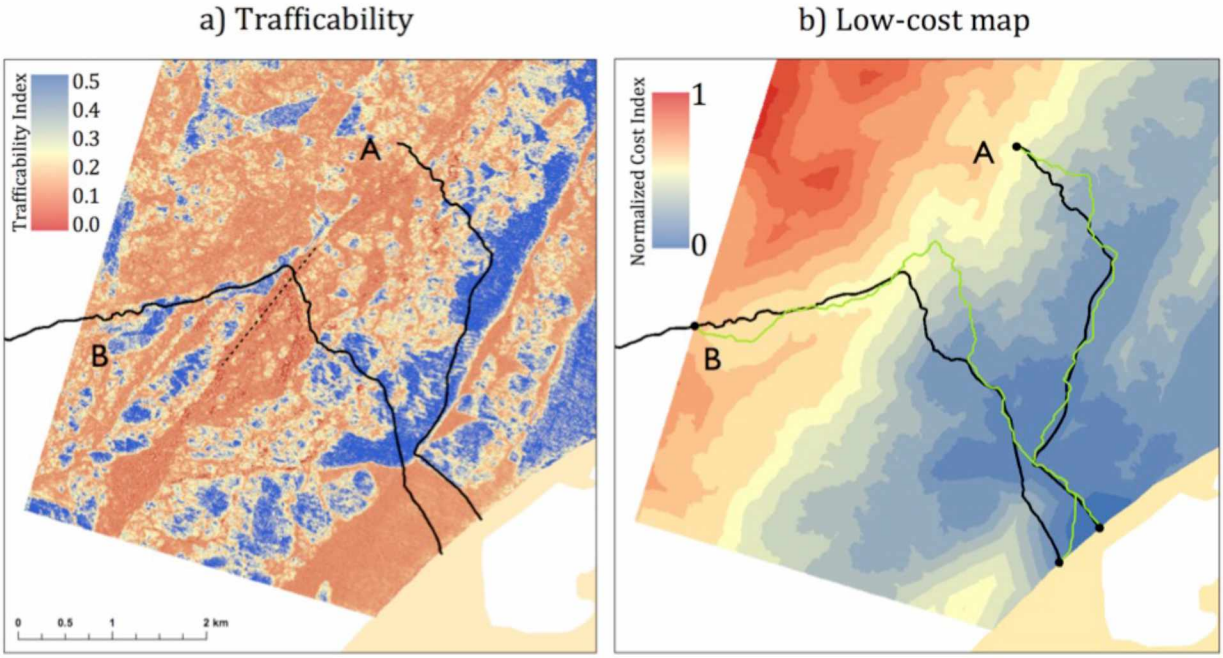

Figure 2.11 a) Trafficability index calculated for the sea ice surrounding two ice trails (black) extending out from Utqiaġvik. Dashed line represents location of large ridge. b) Normalized cost of ice trail construction from starting point of trail A to any other location on the map. Green lines represent optimal trails. Trails were mapped in April-May 2015.

2.5.3 Building on PATH in support of industrial operations on Alaska's North Slope

The Kotzebue ice road case study covers a region with smooth and stable landfast ice, where ice use is largely limited by small-scale properties governing bearing strength. The Utqiaġvik ice trail case study comprises rough unstable landfast ice where ice use is governed in large part by ice roughness. Kotzebue and Utqiaġvik are end members that delimit a wide span of ice conditions (insofar as they limit ice use) and types of ice use (professionally surveyed ice road to connect settlements vs. local ice trails to access hunting sites). The information collected from these two communities may therefore help in identifying critical properties for other areas and ice use scenarios where less local information is available. As an example, we will consider the Prudhoe Bay region that is important to the oil and gas industry - a major stakeholder that has yet to be discussed in the context of this paper. Similar to other regions of strategic importance, the landfast sea ice around Prudhoe Bay is important for economical transport of equipment across ice roads [*Bashaw et al.*, 2013; *Potter et al.*, 1981; *Sooäär and Jaagus*, 2007]. An ice road leading to an offshore drilling operation is illustrated in Figure 2.1. An example of such a setting is Northstar Island west of Prudhoe Bay [*Krieger et al.*, 2003], which is discussed here.

The nine parameters identified in *Section 2.2.2* can be combined across scales into three general categories: surface (roughness and other surface conditions), motion (stability and fracture potential), and bearing capacity (thickness, defects, and composition). Each region or ice use scenario is plotted qualitatively in Figure 2.12 as an area displaying its sensitivity to each category (each category with its own axis). This 3-d data is shown in 2-d cross sections indicating the sensitivity of ice use to the three prime parameters for Utqiaġvik (solid line) and Kotzebue (dotted line). Use of Utqiaġvik ice trails is sensitive to ice stability and surface roughness, yet much less so to bearing capacity (with the exception of the lead edge). Kotzebue ice use is mostly sensitive to bearing capacity as outlined above. We assume these two regions to be end members of the Arctic sea-ice parameter space, occupying corners or sides of the diagram.

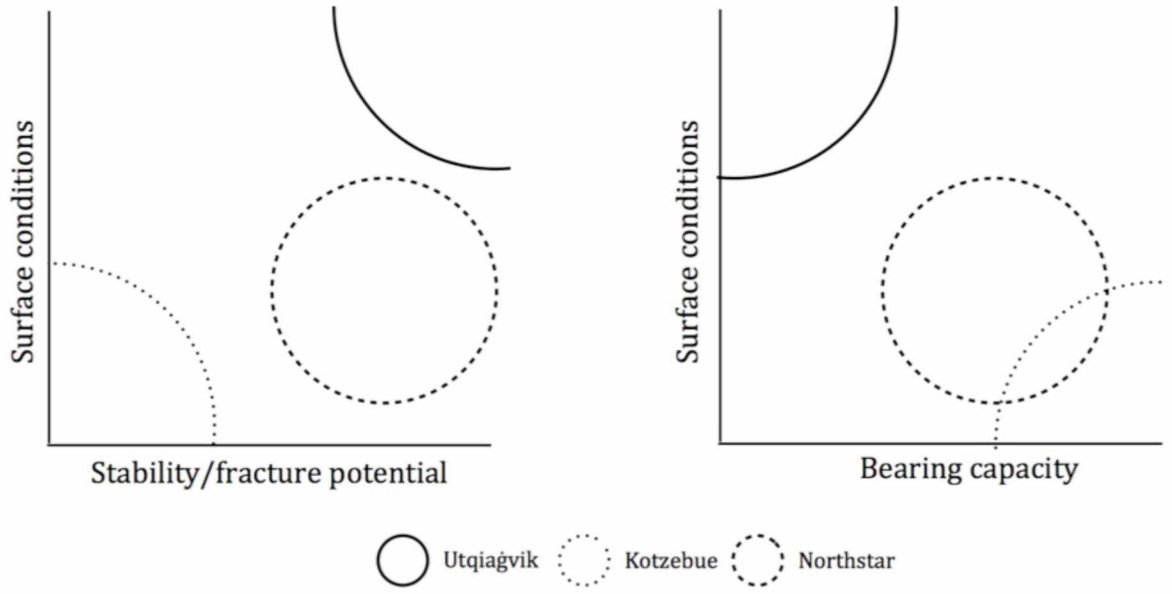

Figure 2.12 Ice use parameters displayed as sections of 3-d parameter space with axes indicating sensitivity of ice use to ice deformation (stability and fracture potential), bearing capacity (e.g. thickness, defects, composition and surface conditions (e.g. roughness / snow and water conditions). The sensitivity of ice use to these parameters is indicated qualitatively for Utqiaġvik, Kotzebue, and Northstar Island."

We can now evaluate and plot the sensitivity of ice operations around Northstar Island to key ice parameters (Figure 2.12), drawing upon ancillary information from Utqiaġvik and Kotzebue. In contrast with the operating environment and available resources at Kotzebue, planning, construction, and maintenance of the Northstar ice road is less dependent on the ice cover's initial bearing capacity. Industry resources in the form of heavy equipment and personnel are such that ice thickness can be sufficiently monitored and artificially increased through sequential flooding of the road early in the season (Walton Crowell, personal communication, 2016). At the same time, the Northstar ice road is much more impacted by detection and management of surface roughness features and fracture potential than the Kotzebue ice road since it traverses an area more exposed to ice deformation (Figure 2.12).

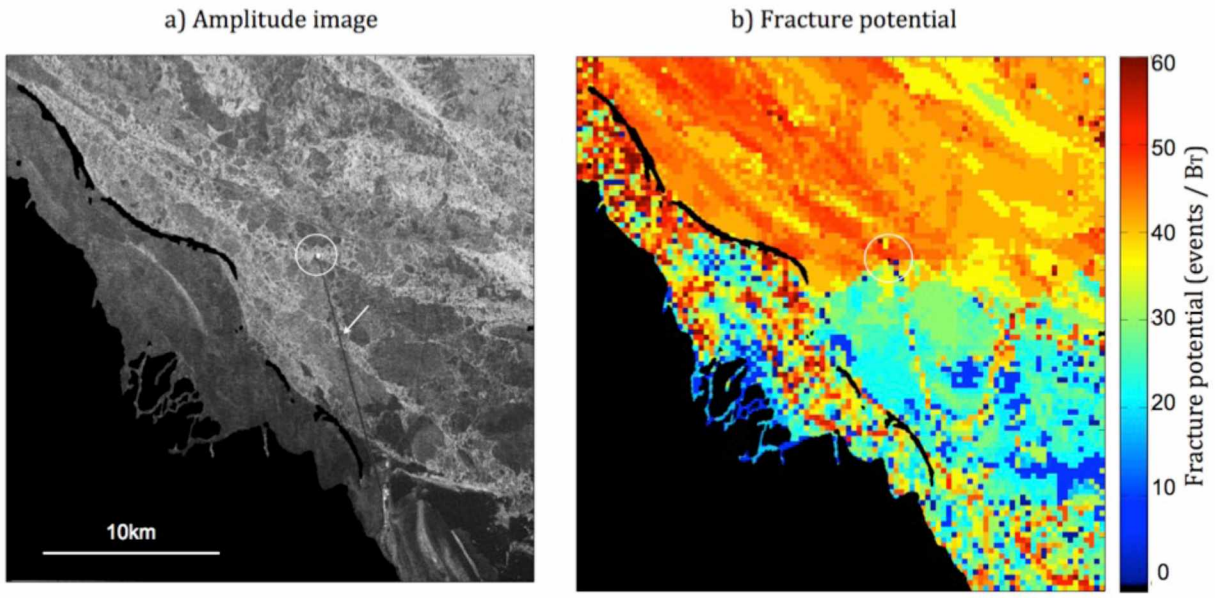

Figure 2.13 Fracture potential. (a) ALOS-1 PALSAR amplitude image for the Northstar Island (circled) and Prudhoe Bay region, Alaska (21 Mar 2010). The arrow is pointing to the ice road connecting the island to the mainland. (b) Apparent fracture potential for the time period 21 Mar – 6 May 2010 using an elasto-brittle rheology.

SAR was again utilized due to cost-effectiveness and ability to survey large areas. Deformation mode and rate were evaluated based on inverse modeling of InSAR data and used to derive fracture potential using an elasto-brittle rheology (*Section 2.3.4*). The backscatter image is displayed in Figure 2.13a with the associated fracture potential illustrated in Figure 2.13b, clearly indicating less severe fracturing shoreward of Northstar Island due to the stabilizing effect of the island. Also, we identify an increase in fracture potential (up to roughly 40 fracture events per 300 m x 300 m pixel during 1.5 months) in the vicinity of the ice road and in particular in areas prone to fracturing according to field observations by ice road engineers (Walton Crowell, personal communication, 2016), validating the approach taken here [Dammann et al., in review-b].

Even when ice thickness is close to its seasonal maximum of more than 1.5 m, the landfast ice cover is not immune to cm- to m-scale deformation, which can be a concern for ice road engineers [*Bashaw et al.*, 2013; *BP*, 2013; *Potter et al.*, 1981]. Displacements may lead to

cracks impacting load bearing capacity or lead to wider openings or foster development of hazardous features such as strudel scour later in the spring melt season, with surface water draining through cracks and posing a threat to subsurface pipelines [*Dickins et al.*, 2011]. It is therefore recognized that ice roads should try to avoid areas of ice movement and rely on routes across stable ice [*Bashaw et al.*, 2013; *Potter et al.*, 1981] with reduced fracture potential. However, information on the extent and distribution of small-scale movement and defects is often difficult to acquire due to the comparatively small magnitude of the movement and the long timescale over which the deformation takes place.

A key stakeholder need identified for the Northstar site is for continuous and extensive use of the ice road (identified by an arrow in Figure 2.13a) throughout the 2.5-month operating season [*Krieger et al.*, 2003] with minimal exposure to fractures or cracks impacting load-bearing capacity. This aim can be achieved by either routing the road through ice that has minimal occurrence of cracks and limited exposure to processes generating cracks, or by placing the road on ice with confined occurrences of cracks that can be closely monitored and repaired as needed. The development of fractures is largely driven by small-scale deformation driven by wind, ocean, and pack ice forcing as well as thermal processes. Therefore, the challenge is to obtain accurate measurements of ice movement over a large area in a cost-effective and timely manner [*Mesher et al.*, 2008].

By utilizing the PATH framework to determine critical parameters for ice use, we have identified the relevance of critical parameters and in particular the fracture potential (Figure 2.14) based on the location of the ice road, partly exposed to pack ice forcing. The approach outlined here can potentially be used as a monitoring tool throughout the season, but also as a planning tool, informing the routing of ice roads through areas less prone to deformation by creating a climatology of deformation based on past interferograms. More details and a broader discussion can be found in *Dammann et al.* [in review-b].

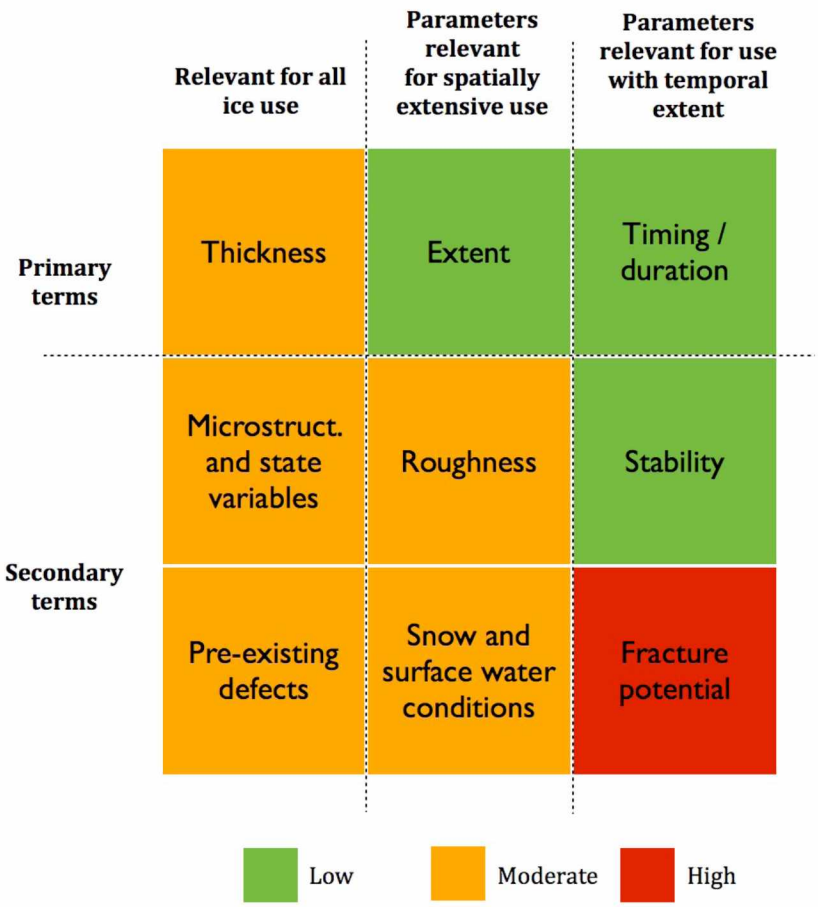

Figure 2.14 The nine ice use parameters arranged as columns in a matrix associated with the relevant scale. Colors indicate level of sensitivity to particular parameters determined using PATH for the Northstar Island ice road.

2.6 Discussion – steps for implementation in decision making

Through three case studies, PATH helped guide the process of translating specific user-defined needs into quantitative assessment strategies. However, for these and future expanded strategies to effectively be utilized by decision makers, additional steps are needed. First, decision makers such as ice-road engineers and local and regional governments need to implement quantitative guidelines for ice use based on the newly developed metrics. In this process, thresholds for operation need to be determined, requiring a new understanding of ice use and relevant ice properties and processes, such as

(1) what thickness variability can significantly alter ice thickness assessments to the point where it has to be separately assessed and accounted for, (2) what roughness scales are traversable with different modes of transportation, and (3) what level of fracturing will critically compromise the bearing capacity of the ice by a local ice trail vs. an industry ice road. These and similar questions are also critical for entities such as funding agencies to be able to adequately distribute resources and help determine future steps to secure sustainable and continued ice use. More research is therefore required to fully take advantage of the strategies developed here.

Second, there is a need for increasing data accessibility. Techniques commonly used to assess sea ice on scales relevant to use depend heavily on satellite remote sensing such as SAR, altimetry, SSM/I, and optical sensors. However, in this work on landfast sea ice we identify high spatial variability of sea ice parameters and the need for cm-scale accuracy resulting in more stringent requirements than what can be accommodated by some of these techniques. For instance, altimetry such as ICESat-1 and 2 can be used to estimate ice thickness and roughness, but with incomplete coverage at scales larger than the swath width of 3km and with uncertainties reaching up to around 50cm [*Kwok and Cunningham*, 2008]. The Special Sensor Microwave Imager (SSM/I) and the Advanced Microwave Scanning Radiometer – EOS (AMSR-E) sensors can be used to estimate ice thickness of thin ice (<20 cm) with high accuracy (~5 cm) [*Nihashi et al.*, 2009; *Tamura et al.*, 2007] or for thicker ice (< 50 cm) using a lower frequency product from ESA's Soil Moisture and Ocean Salinity (SMOS) with dm-scale accuracy [*Tian-Kunze et al.*, 2014] but both with spatial resolution in tens of km. Our work has focused predominately on SAR, due to the unmatched combination of m-scale resolution and repeat-pass cycles on the order of days to weeks. However, SAR coverage and availability is still sparse and particularly in terms of single pass bi-static interferometric products. The recent launch of Sentinel-1 and ALOS-2 in 2014 and planned launch of NISAR in 2020 is expected to greatly increase data availability enabling detailed analysis for both tactical and strategic decisions.

Third, the processes to develop data products such as fracture potential and trafficability need to be automated so they can be implemented by personnel with only limited remote

sensing experience since some of the products developed here require a thorough understanding of SAR interferometry and polarimetry. Additionally, for these techniques to have optimal potential, they need to be adaptable to different ice regimes throughout the Arctic. This is possible for the strategies developed here, but will require some more work described below.

In the case of ice thickness compensation factors (*Section 2.4.1*), the thickness variability will be different depending on region, hence new GPR surveys may have to be conducted for any new location. In areas of saline ice, GPR signals can be compromised, but an electromagnetic conductivity meter (EM) could be used instead of a GPR, unless variable water salinity (limiting EM measurements) is present. However, the region studied here is expected to have relatively high thickness variability compared to other sheltered ice regimes due to the many river channel outlets resulting in subsurface currents and advection of water with above-freezing temperatures, which was also observed along the profile obtained here (Figure 2.8). These results and the function illustrated in Figure 2.9 may therefore be of use in other areas as an upper compensation factor limit for thickness variability. However, there is no guarantee that variability will remain similar from year to year in Kotzebue or any other location, which is subject to further research.

The trafficability index (*Section 2.4.2*) is based exclusively on data from ice trails in Utqiaġvik and therefore has limitations in terms of determining trafficability for other modes of transportation. The SAR products are also based upon roughness predominately, while the trail routes are based upon multiple factors including considerations of hunting preferences and safety. More ice use data should be included so that trail routes that follow other considerations will average out, resulting in a more accurate index. Additionally, polarimetric classifications need to be standardized. In this work, the classes are developed through maximum likelihood, based on the individual image. However, the classes need to be defined so that future polarimetric decompositions classify similar roughness regimes equally.

We have already applied the model to determine fracture potential (*Section 2.4.3*) in multiple locations in Alaska, including Elson Lagoon, Prudhoe Bay, and Foggy Island Bay. We

therefore expect this approach to work well in several ice regimes. However, InSAR has limited success in areas of very smooth ice due to a low signal to noise ratio reducing coherence. In addition, other conditions such as higher tidal displacement than those in our study regions may also reduce accuracy. Here, more work is required to understand the robustness of this approach.

2.7 Conclusion

Throughout the Arctic, there is a diverse set of ice users and stakeholders depending on services provided by the landfast sea ice. Arctic sea ice is undergoing rapid changes that may jeopardize or severely impact the benefits derived from the ice cover by these users. In the context of such changes, it is necessary to fully understand and quantify the links between sea ice and its use based on key geophysical parameters and monitor changing ice conditions through the lens of individual ice users or stakeholders. Here we identify nine largely independent geophysical parameters that govern the feasibility, safety, and efficiency of landfast sea ice travel and related uses. These nine can be constrained further into three independent categories of ice motion, bearing capacity, and surface conditions. We present the PATH framework as a means to link geophysical measurements and ice user and stakeholder information needs based on the relevance of different parameters in relation to ice use.

As outlined in *Section 2.5*, some more work is needed to fully develop these methods into products that can be applied across all sea ice regimes. With fully standardized products, it will be possible to apply each method in combination, something that was not attempted here. For instance, combining the roughness analysis (*Section 2.4.2*) with the estimation of fracture potential (*Section 2.4.3*) for the same area would enable a much broader trafficability assessment taking into account not only efficiency, but also safety. In such combined analysis, multiple existing assessment strategies could also be integrated such as optical sensors for detection of surface melt and flooding [*Webster et al.*, 2015] as well as presence of snow [*Gesell*, 1989]. This process would greatly benefit from better accessibility

to ice use data either through interviews or surveys of ice trails and roads. In particular, more access to ice use information from industry would be beneficial in terms of determining consequences of different fracture levels.

As demonstrated in *Section 2.4.2*, ice use data resulting from expert local and Indigenous knowledge can help develop a strategy by linking geophysical parameters with user needs. In such locations, it is also often expected that ice users already construct trails along favorable routes. However, calculated optimal trail routes may still differ from actual trails where trail crews did not have access to information obtained using remote sensing or when having additional priorities than what is considered in the trafficability analysis. Discrepancies between calculated and actual routes can therefore further be used to inform and optimize a trafficability analysis by identifying additional ice user considerations. Also, trafficability analysis and maps developed will be particularly valuable in areas of limited access to local and Indigenous knowledge, such as in scenarios of escape, evacuation, and rescue. Also, in certain regions, elements of local and Indigenous knowledge do no longer apply due to rapid sea ice change [*AMAP*, 2011], which may even be more prevalent in the future. In such cases, similar assessments as presented here can provide insight aiding in adaptation to such change.

The approaches to assess ice use related parameters using remote sensing enable the use of archived SAR data to assess past changes in trafficability on a decadal scale, information relevant to stakeholders and decision makers. Model results have been used to predict the future accessibility of the Arctic by land based ice roads and shipping [*Stephenson et al.*, 2011]. By identifying the relationship between ice use and geophysical parameters of sea ice, similar to what is presented here, it would also be feasible to develop predictions of future landfast sea ice trafficability based on model results. This would depend on a landfast ice model that is able to capture the relevant parameters presented in this work. Landfast sea ice models are under development [*Hopkins*, 2008], a process in which the deformation and roughness analysis presented here can potentially provide substantial new insight for model validation.

Although this work is focused around landfast ice use through the development of PATH, the approach itself does not limit itself to the trafficability realm alone. We argue that addressing geophysical properties through the lens of specific ice users can offer substantial benefits to stakeholders depending on sea ice in a broader sense such as shipping. Here, new ice-associated parameters would have to be included in a PATH framework, such as ice strength, drift velocity etc. The strategy presented here can also be applied to the use of sea ice by marine mammals that depend on different ice-associated parameters for travel, shelter, or denning. This approach may also have potential for the implementation of temporary logistical infrastructure far outside sea ice science such as mining and logging roads, military operations, and supply routes to disaster areas where existing infrastructure is compromised.

2.8 Acknowledgements

This project was supported in part by the National Science Foundation through the Seasonal Ice Zone Observing Network (NSF-0856867) and Arctic Science, Engineering, and Education for Sustainability (NSF-4868895). Additional funding was provided by the Northwest Arctic Borough. ALOS PALSAR data were made available through a data grant by the Japan Aerospace Exploration Agency (JAXA, Project ID 1493). We thank the communities of Kotzebue, Nome, and Utqiaġvik and in particular the interviewees who generously shared their knowledge. We thank Seth Kantner and Karen Brewster for valuable guidance.

2.9 References

Adams, B. (2013a). Oral history Interview with Karen Brewster and Dyre Oliver Dammann on November 12, 2013 in Barrow, Alaska. ORAL HISTORY 2013-25-02, Oral History Collection, University of Alaska Fairbanks. http://jukebox.uaf.edu/site7/p/2059

Adams, J. (2013b). Oral history Interview with Karen Brewster on November 15, 2013 in Barrow, Alaska. 2013-25-07, Parts 1 and 2, Oral History Collection, University of Alaska Fairbanks. http://jukebox.uaf.edu/site7/p/2098

Ahmasuk, B. (2014). Oral history Interview with Sarah Betcher and Dyre Oliver Dammann on March 29 in Nome, Alaska. Project film transcript, Arctic Science, Engineering, and Education for Sustainability Project.

AMAP (2011), Snow, water, ice and permafrost in the Arctic (SWIPA): Climate Change and the Cryosphere*, Rep.*, xii + 538 pp, Oslo, Norway.

Aporta, C. (2004), Routes, trails and tracks: Trail breaking among the Inuit of Igloolik, *Études/Inuit/Studies*, *28*(2), 9-38.

Aporta, C. (2011), Shifting perspectives on shifting ice: documenting and representing Inuit use of the sea ice, *The Canadian Geographer/Le Géographe canadien*, *55*(1), 6-19, doi: 10.1111/J.1541-0064.2010.00340.X.

Aporta, C., and E. Higgs (2005), Satellite culture - Global positioning systems, inuit wayfinding, and the need for a new account of technology, *Curr Anthropol*, *46*(5), 729-753, doi: 10.1086/432651.

Ashenfelter, R. (2014). Oral history Interview with Sarah Betcher and Dyre Oliver Dammann on March 29 in Nome, Alaska. Arctic Science, Engineering, and Education for Sustainability Project,

Bashaw, E. K., J. Drage, S. K. Lewis, and C. Billings (2013), Applied Ice Engineering for Exploring Arctic Natural Resources, paper presented at ISCORD 2013@ sPlanning for Sustainable Cold Regions, ASCE.

Betcher, S. (2017), Sustainable Futures North interviews, edited by S. Betcher, International Arctic Research Center, University of Alaska Fairbanks.

BP (2013), BPXA Winter Geotechnical Ancillary Activity Notification 2013*, Rep.*, 22 pp.

Brewster, K. (2016), Northern Alaska Sea Ice Project Jukebox, edited by K. Brewster, University of Alaska Fairbanks Oral History Program.

Brower, E. (2013). Oral history Interview with Karen Brewster and Dyre Oliver Dammann on November 12, 2013 in Barrow, Alaska. ORAL HISTORY 2013-25-03, Oral History Collection, University of Alaska Fairbanks. http://jukebox.uaf.edu/site7/p/2062

Comiso, J. C., and F. Nishio (2008), Trends in the sea ice cover using enhanced and compatible AMSR-E, SSM/I, and SMMR data, *J Geophys Res-Oceans*, *113*(C2), doi: 10.1029/2007jc004257.

Comiso, J. C., and D. K. Hall (2014), Climate trends in the Arctic as observed from space, *Wiley Interdisciplinary Reviews: Climate Change*, *5*(3), 389-409.

Dammann, D. O., H. Eicken, F. Meyer, and A. Mahoney (2016), Assessing small-scale deformation and stability of landfast sea ice on seasonal timescales through L-band SAR interferometry and inverse modeling, *Remote Sens Environ*, *187*, 492-504, doi: 10.1016/j.rse.2016.10.032.

Dammann, D. O., H. Eicken, E. Saiet, A. Mahoney, F. Meyer, and J. C. George (in review-a), Traversing sea ice - linking surface roughness and ice trafficability through SAR polarimetry and interferometry *IEEE Journal of Selected Topics in Applied Earth Observations and Remote Sensing*.

Dammann, D. O., H. Eicken, A. Mahoney, F. Meyer, J. Freymueller, and A. M. Kaufman (in review-b), Assessing landfast sea ice stability and internal ice stress around ice roads using L-band SAR interferometry and inverse modeling, *Cold Reg Sci Technol*.

Dickins, D., G. Hearon, K. Morris, K. Ambrosius, and W. Horowitz (2011), Mapping sea ice overflood using remote sensing: Alaskan Beaufort Sea, *Cold Reg Sci Technol*, *65*(3), 275-285.

Druckenmiller, M. L., H. Eicken, J. C. George, and L. Brower (2010), Assessing the shorefast ice: Iñupiat whaling trails off Barrow, Alaska, in *SIKU: Knowing our ice*, 203-228, Springer.

Druckenmiller, M. L., H. Eicken, J. C. George, and L. Brower (2013), Trails to the whale: reflections of change and choice on an Iñupiat icescape at Barrow, Alaska, *Polar Geography*, *36*(1-2), 5-29, doi: 10.1080/1088937X.2012.724459.

Druckenmiller, M. L., H. Eicken, M. A. Johnson, D. J. Pringle, and C. C. Williams (2009), Toward an integrated coastal sea-ice observatory: System components and a case study at Barrow, Alaska, *Cold Reg Sci Technol*, *56*(2-3), 61-72, doi: 10.1016/J.Coldregions.2008.12.003.

Eicken, H. (2010), Indigenous knowledge and sea ice science: What can we learn from indigenous ice users?, in *SIKU: Knowing Our Ice*, 357-376, Springer.

Eicken, H., and A. R. Mahoney (2015), Sea Ice: Hazards, Risks, and Implications for Disasters, in *Coastal and Marine Hazards, Risks, and Disasters*, Jean T. Ellis, Douglas J. Sherman and John F. Shroder, 381-399, Elsevier Inc., Amsterdam, Netherlands.

Eicken, H., A. L. Lovecraft, and M. L. Druckenmiller (2009), Sea-Ice System Services: A Framework to Help Identify and Meet Information Needs Relevant for Arctic Observing Networks, *Arctic*, *62*(2), 119-136.

Eicken, H., J. Jones, F. Meyer, A. Mahoney, M. L. Druckenmiller, M. Rohith, and C. Kambhamettu (2011), Environmental security in Arctic ice-covered seas: from strategy to tactics of hazard identification and emergency response, *Mar Technol Soc J*, *45*(3), 37-48, doi: doi.org/10.4031/MTSJ.45.3.1.

Fienup-Riordan, A., and A. Rearden (2010), The ice is always changing: Yup'ik understandings of sea ice, past and present, in *SIKU: knowing Our Ice: Documenting Inuit Sea Ice knowledge and Use*, Igor Krupnik, Claudio Aporta, Shari Gearheard, Gita Laidler and Lene Kielsen Holm, 295-320, Springer, New York.

Finucane, R., and R. Scher (1983), Floating Ice Road Construction, *Journal of Energy Resources Technology*, *105*(1), 26-29.

Ford, J. D., T. Pearce, J. Gilligan, B. Smit, and J. Oakes (2008), Climate change and hazards associated with ice use in northern Canada, *Arctic, Antarctic, and Alpine Research*, *40*(4), 647-659.

George, J. C., H. P. Huntington, K. Brewster, H. Eicken, D. W. Norton, and R. Glenn (2004), Observations on shorefast ice dynamics in Arctic Alaska and the responses of the Iñupiat hunting community, *Arctic*, *57*(4), 363-374.

Gesell, G. (1989), An algorithm for snow and ice detection using AVHRR data An extension to the APOLLO software package, *Int J Remote Sens*, *10*(4-5), 897-905.

Gold, L. W. (1971), Use of ice covers for transportation, *Canadian Geotechnical Journal*, *8*(2), 170-181.

Haas, C., and M. Druckenmiller (2010), Ice thickness and roughness measurements, in *Field Techniques for Sea Ice Research*, Hajo Eicken and Maya Salganek, 49-116, University of Alaska Press, Fairbanks, Alaska.

Holt, B., P. Kanagaratnam, S. P. Gogineni, V. C. Ramasami, A. Mahoney, and V. Lytle (2009), Sea ice thickness measurements by ultrawideband penetrating radar: First results, *Cold Reg Sci Technol*, *55*(1), 33-46.

Hopkins, M. A. (2008), *Simulation of Landfast Ice Along the Alaskan Coast*, 15 pp., US Army Cold Regions Research and Engineering Laboratory, US Department of the Interior, Minerals Management Service, Alaska OCS Region., Hanover, New Hampshire.

Hori, Y., W. A. Gough, K. Butler, and L. J. Tsuji (2016), Trends in the seasonal length and opening dates of a winter road in the western James Bay region, Ontario, Canada, *Theoretical and Applied Climatology*, 1-12.

Huntington, H. P. (2000), Using traditional ecological knowledge in science: methods and applications, *Ecological applications*, *10*(5), 1270-1274.

Huntington, H. P., and S. Fox (2005), The changing Arctic: indigenous perspectives, in *Arctic Climate Impact Assessment*, C Symon, L Arris and B Heal, 61–98, Cambridge University Press, New York, NY.

Jolly, D., F. Berkes, J. Castleden, and T. Nichols (2002), We can't predict the weather like we used to: Inuvialuit observations of climate change, Sachs Harbour, Western Canadian Arctic, in *The earth is faster now: Indigenous observations of Arctic environmental change*, Igor Krupnik and Dyanna Jolly, 93-125, Arctic Research Consortium of the United States, Fairbanks, Alaska.

Jones, J. M., H. Eicken, A. R. Mahoney, M. V. Rohith, C. Kambhamettu, Y. Fukamachi, K. I. Ohshima, and J. C. George (2016), Landfast sea ice breakouts: Stabilizing ice features, oceanic and atmospheric forcing at Barrow, Alaska, *Continental Shelf Research*, *126*(50-63), doi: 10.1016/j.csr.2016.07.015.

Kanagaratnam, P., T. Markus, V. Lytle, B. Heavey, P. Jansen, G. Prescott, and S. P. Gogineni (2007), Ultrawideband radar measurements of thickness of snow over sea ice, *Geoscience and Remote Sensing, IEEE Transactions on*, *45*(9), 2715-2724.

Krieger, A. G., G. N. Kidd, and D. A. Cocking (2003), Northstar Drilling-Delivering the First Arctic Offshore Development, *SPE drilling & completion*, *18*(02), 188-193.

Kwok, R., and G. Cunningham (2008), ICESat over Arctic sea ice: Estimation of snow depth and ice thickness, *Journal of Geophysical Research: Oceans (1978–2012)*, *113*(C8).

Kwok, R., and D. A. Rothrock (2009), Decline in Arctic sea ice thickness from submarine and ICESat records: 1958-2008, *Geophys Res Lett*, *36*, doi: 10.1029/2009gl039035.

Laidler, G. J. (2006), Inuit and scientific perspectives on the relationship between sea ice and climate change: The ideal complement?, *Climatic Change*, *78*(2-4), 407-444, doi: Doi 10.1007/S10584-006-9064-Z.

Laidler, G. J., P. Elee, T. Ikummaq, E. Joamie, and C. Aporta (2010), Mapping Inuit sea ice knowledge, use, and change in Nunavut, Canada (Cape Dorset, Igloolik, Pangnirtung), in *SIKU: knowing Our Ice: Documenting Inuit Sea Ice knowledge and Use*, Igor Krupnik, Claudio Aporta, Shari Gearheard, Gita Laidler and Lene Kielsen Holm, 45-80, Springer.

Leavitt, J. (2013). Oral history Interview with Karen Brewster and Dyre Oliver Dammann on November 13, 2013 in Barrow, Alaska. ORAL HISTORY 2013-25-04, Parts 1 and 2, Oral History Collection, University of Alaska Fairbanks. http://jukebox.uaf.edu/site7/p/2064

Lindsay, R., and A. Schweiger (2015), Arctic sea ice thickness loss determined using subsurface, aircraft, and satellite observations, *The Cryosphere*, *9*(1), 269-283, doi: 10.5194/tc-9-269-2015.

Liu, H., K. Takahashi, and M. Sato (2014), Measurement of dielectric permittivity and thickness of snow and ice on a brackish lagoon using GPR, *IEEE Journal of Selected Topics in Applied Earth Observations and Remote Sensing*, *7*(3), 820-827.

Lovecraft, A. L., C. Meek, and H. Eicken (2013), Connecting scientific observations to stakeholder needs in sea ice social–environmental systems: the institutional geography of northern Alaska, *Polar Geography*, *36*(1-2), 105-125, doi: 10.1080/1088937X.2012.733893.

Mahoney, A., H. Eicken, and L. Shapiro (2007), How fast is landfast sea ice? A study of the attachment and detachment of nearshore ice at Barrow, Alaska, *Cold Reg Sci Technol*, *47*(3), 233-255, doi: 10.1016/J.Coldregions.2006.09.005.

Mahoney, A., H. Eicken, A. G. Gaylord, and R. Gens (2014), Landfast sea ice extent in the Chukchi and Beaufort Seas: The annual cycle and decadal variability, *Cold Reg Sci Technol*, *103*, 41-56, doi: 10.1016/J.Coldregions.2014.03.003.

Masterson, D., and P. Spencer (2001), The Northstar on-ice operation, paper presented at Proceedings of the International Conference on Port and Ocean Engineering Under Arctic Conditions, Paper no. 105, Ottawa, ON, August, 2001.

Meier, W. N., G. K. Hovelsrud, B. E. Oort, J. R. Key, K. M. Kovacs, C. Michel, C. Haas, M. A. Granskog, S. Gerland, and D. K. Perovich (2014), Arctic sea ice in transformation: A review of recent observed changes and impacts on biology and human activity, *Reviews of Geophysics*, *52*(3), 185-217.

Mesher, D., S. Proskin, and E. Madsen (2008), Ice road assessment, modeling and management, paper presented at 7th International Conference on Managing Pavement Assets, Calgary, AB, June, 2008.

Meyer, F. J., A. R. Mahoney, H. Eicken, C. L. Denny, H. C. Druckenmiller, and S. Hendricks (2011), Mapping arctic landfast ice extent using L-band synthetic aperture radar interferometry, *Remote Sens Environ*, *115*(12), 3029-3043, doi: 10.1016/J.Rse.2011.06.006.

NAB (2011), Northwest Arctic Borough - Ice Road Construction, edited, Commerce, Community and Economic Development, Kotzebue, Alaska.

Nageak, R. (2013). Oral history Interview with Karen Brewster and Dyre Oliver Dammann on November 13, 2013 in Barrow, Alaska ORAL HISTORY 2013-25-05, Parts 1 and 2, Oral History Collection, University of Alaska Fairbanks. http://jukebox.uaf.edu/site7/p/2072

Nihashi, S., K. I. Ohshima, T. Tamura, Y. Fukamachi, and S. i. Saitoh (2009), Thickness and production of sea ice in the Okhotsk Sea coastal polynyas from AMSR-E, *Journal of Geophysical Research: Oceans*, *114*(C10), doi: 10.1029/2008JC005222.

NWTDOT (2007), *A field guide to ice construction safety*, 37 pp., Northwest Territories Department of Transportation.

Patkotak, C. (2013). Oral history Interview with Karen Brewster and Dyre Oliver Dammann on November 13, 2013 in ORAL HISTORY 2013-25-01, Parts 1 and 2, Oral History Collection, University of Alaska Fairbanks. http://jukebox.uaf.edu/site7/p/2104

Petrich, C., and H. Eicken (2010), Growth, structure and properties of sea ice, in *Sea Ice*, Thomas DN and Dieckmann GS, 23-77, Wiley-Blackwell, Oxford, U. K.

Petrich, C., P. J. Langhorne, and T. G. Haskell (2007), Formation and structure of refrozen cracks in land-fast first-year sea, *J Geophys Res-Oceans*, *112*(C4), doi: 10.1029/2006jc003466.

Potter, R., J. Walden, and R. Haspel (1981), Design and construction of sea ice roads in the Alaskan Beaufort Sea, paper presented at Offshore Technology Conference, Offshore Technology Conference, Houston, Texas.

Rothrock, D. A., D. B. Percival, and M. Wensnahan (2008), The decline in arctic sea-ice thickness: Separating the spatial, annual, and interannual variability in a quarter century of submarine data, *J Geophys Res-Oceans*, *113*(C5), doi: 10.1029/2007jc004252.

Schaeffer, R. (2014). Oral history interview with Sarah Betcher and D.O. Dammann on April 3 in Kotzebue, Alaska. Project film transcript, Arctic Science, Engineering, and Education for Sustainability Project.

Schwarz, J., and W. Weeks (1977), Engineering properties of sea ice, *Journal of Glaciology*, *19*(81).

Selyuzhenok, V., T. Krumpen, A. Mahoney, M. Janout, and R. Gerdes (2015), Seasonal and interannual variability of fast ice extent in the southeastern Laptev Sea between 1999 and 2013, *Journal of Geophysical Research: Oceans*, *120*(12), 7791-7806.

Smith, F. (2014). Oral history interview with April 2 in Kotzebue, Alaska. Project film transcript, Arctic Science, Engineering, and Education for Sustainability Project.

Sooäär, J., and J. Jaagus (2007), Long-term changes in the sea ice regime in the Baltic Sea near the Estonian coast, *Proc Estonian Acad Sci Eng*, *13*(3), 189-200.

Squire, V., R. J. Hosking, A. D. Kerr, and P. Langhorne (1996), *Moving loads on ice plates*, Kluwer Academic Publishers, Dordrecht, The Netherlands.

Stephenson, S. R., L. C. Smith, and J. A. Agnew (2011), Divergent long-term trajectories of human access to the Arctic, *Nat Clim Change*, *1*(3), 156-160, doi: 10.1038/Nclimate1120.

Stroeve, J. C., M. C. Serreze, M. M. Holland, J. E. Kay, J. Malanik, and A. P. Barrett (2012), The Arctic's rapidly shrinking sea ice cover: a research synthesis, *Climatic Change*, *110*(3-4), 1005-1027, doi: 10.1007/S10584-011-0101-1.

Stroeve, J. C., M. Serreze, S. Drobot, S. Gearheard, M. Holland, J. Maslanik, W. Meier, and T. Scambos (2008), Arctic sea ice extent plummets in 2007, *Eos, Transactions American Geophysical Union*, *89*(2), 13-14.

Tamura, T., K. I. Ohshima, T. Markus, D. J. Cavalieri, S. Nihashi, and N. Hirasawa (2007), Estimation of thin ice thickness and detection of fast ice from SSM/I data in the Antarctic Ocean, *Journal of Atmospheric and Oceanic Technology*, *24*(10), 1757-1772.

Tian-Kunze, X., L. Kaleschke, N. Maaß, M. Mäkynen, N. Serra, M. Drusch, and T. Krumpen (2014), SMOS-derived thin sea ice thickness: algorithm baseline, product specifications and initial verification, *The Cryosphere*, *8*(3), 997-1018.

Uhl, William R. (1990-2003), "Daily observations from Sisualik, Cape Krusenstern National Monument, Northwest Alaska," last accessed Apr 2014, https://www.nps.gov/cakr/learn/historyculture/bob-uhl-journals.htm

USAAF (1968), *Planning and design of roads, airbases, and heliports in the theater of operations*, 5-330 pp., Departments of the army and the air force, Washington DC.

USACE (2002), *Ice Engineering*, 475 pp., Department of the Army, US Army Corps of Engineers Washington DC.

Webster, M. A., I. G. Rigor, D. K. Perovich, J. A. Richter-Menge, C. M. Polashenski, and B. Light (2015), Seasonal evolution of melt ponds on Arctic sea ice, *Journal of Geophysical Research: Oceans*, *120*(9), 5968-5982.

Yu, Y., H. Stern, C. Fowler, F. Fetterer, and J. Maslanik (2014), Interannual Variability of Arctic Landfast Ice between 1976 and 2007, *J Climate*, *27*(1), 227-243.

3 TRAVERSING SEA ICE – LINKING SURFACE ROUGHNESS AND ICE TRAFFICABILITY THROUGH SAR POLARIMETRY AND INTERFEROMETRY*

3.1 Abstract

Arctic landfast sea ice is widely utilized for transportation by local communities and industry, with trafficability largely governed by ice roughness. Here, we introduce an approach to evaluate ice roughness that can aid in routing of ice roads and assessment of spatial variability and long-term changes in trafficability. Drawing on Synthetic Aperture Radar (SAR) polarimetry (PolSAR), SAR interferometry (InSAR), and other remote sensing techniques, we integrated approaches into the trafficability assessment that had rarely been applied over sea ice in the past. Analysis of aerial photogrammetry obtained through Structure-from-Motion helped verify cm-scale accuracy of X-band InSAR-derived ridge height and link L-band polarimetric classification to specific roughness regimes. Jointly, these approaches enable a km-scale evaluation of ridge topography and cm- to m-scale roughness - both critical for the assessment of trafficability. A trafficability index was derived from such SAR data in conjunction with analysis of ice trail routing and ice use near Utqiaġvik, Alaska. The index identifies areas of reduced trafficability, associated with pressure ridges or rubble ice, and served to delineate favorable trail routes for different modes of transportation, with potential uses ranging from ice road routing to emergency evacuation. Community outreach is needed to explore how this approach could assist different ice users in reducing risk, minimizing trail or ice construction efforts and improving safety.

* Dammann, D. O., H. Eicken, E. Saiet, A. Mahoney, F. Meyer, and J. C. George (in review). Traversing sea ice – linking surface roughness and ice trafficability through SAR polarimetry and interferometry. *IEEE journal of selected topics in applied earth observations and remote sensing*.

3.2 Introduction

3.2.1 Sea ice roughness and implications for sea ice travel and on-ice operations

Landfast sea ice provides a range of services to people, marine mammals, and the broader ecosystem around the circumpolar North [*Eicken et al.*, 2009]. This relatively narrow belt of ice is attached to the coast and serves as an extension of the land used for community travel and subsistence activities [*Aporta*, 2004; *Druckenmiller et al.*, 2013; *Jaervik*, 2006; *Laidler et al.*, 2009; *Nuttall et al.*, 2005]. Landfast ice also serves as a platform for ice road construction by industry [*Bashaw et al.*, 2013; *Krieger et al.*, 2003; *Mesher et al.*, 2008; *Potter et al.*, 1981]. Over the past few decades, landfast sea ice has undergone rapid decline in extent and seasonal persistence [*Mahoney et al.*, 2014; *Selyuzhenok et al.*, 2015] associated with Arctic-wide sea ice retreat [*Comiso and Hall*, 2014; *Meier et al.*, 2014; *Stroeve et al.*, 2012]. At the same time, coastal community dependence on ice-based transportation has increased due to higher alternate transportation costs, greater removal of subsistence resources, and a growing industrial presence (9.4.5 in *AMAP* [2011]). The potential socio-economic implications of these developments [*Eicken and Lovecraft*, 2011] require research progress to aid in adaptation or mitigation of change [*Eicken et al.*, 2011a].

Mapping of local ice use [*Aporta*, 2009; *Druckenmiller et al.*, 2013; *Gearheard et al.*, 2010; *Laidler et al.*, 2010; *Tremblay et al.*, 2006] and studies of environmental change impacts on coastal communities have progressed significantly [*Aporta*, 2011; *Aporta and Higgs*, 2005; *Fienup-Riordan and Rearden*, 2010; *Ford et al.*, 2008; *Huntington and Fox.*, 2005; *Laidler et al.*, 2009]. Such progress includes new methods to monitor ice conditions relevant to ice use and to provide guidance to ice users [*Bell et al.*, 2014; *Druckenmiller et al.*, 2013; *Wilkinson et al.*, 2011]. However, so far, quantitative approaches to analysis and hazard assessment of ice conditions relevant to ice road and trail use, applicable over larger scales and across seasons have been lacking.

This work focuses on ice roughness at scales of 0.1 – 10 m, which is a key factor determining the use of landfast ice for transportation by local residents [*Aporta*, 2004; *Fienup-Riordan and Rearden*, 2010; *Laidler et al.*, 2010], industry [*Haas and Druckenmiller*, 2010], and in the

context of potential emergency evacuation from industrial installations and winter vessel traffic [*Barker et al.*, 2006; *Eicken et al.*, 2011b; *Spencer et al.*, 2007]. Ice roughness is relevant in routing and construction of ice trails and roads due to the negative impacts of rough ice on travel time and cost through increased road length by avoiding rough areas, surface preparation cost, equipment wear etc. However, grounded pressure ridges, typically the largest roughness elements in the landfast ice cover, help stabilize the ice, thereby potentially reducing the hazards of ice travel [*Druckenmiller et al.*, 2010; *Jones et al.*, 2016; *Mahoney et al.*, 2007].

Landfast ice can form through in situ freezing in the coastal zone, the advection of ice formed offshore, or a combination of these two processes. Landfast ice formed through in situ freezing typically will be smooth, though wind and ocean stress or interaction with drifting pack ice may increase its roughness. Landfast ice advected from offshore may be deformed already, or deform during the attachment process. In addition to amplitude, ranging up to the m-scale, roughness can be identified by the wavelength of the roughness features. We define short-wave roughness (SW), where the ratio of amplitude to wavelength is close to one, and long-wave roughness (LW) where amplitude is much smaller than the wavelength.

Small-scale roughness of sea ice can be determined by the sea state during the early stages of freeze-up. Initial freezing during calm conditions will result in smooth nilas, while a choppy sea will result in cm-scale SW roughness (e.g. pancake ice). Potentially small-scale roughness inherent in the ice since freeze-up will remain as the ice grows thicker. While the ice is still thin, it is subject to cm-scale roughness features due to rafting and buckling. Rafting will result in roughness in the form of a step in the leading edges of the rafting floes [*Hopkins et al.*, 1999] while buckling will often impart LW roughness features to ice smooth on shorter length scales. As the ice approaches meter-scale thickness, it is strong enough to resist moderate forces, but is still subject to deformation under substantial forcing events such as pack ice interaction.

Such events can result in grinding of ice in the shear zone between pack ice and the landfast ice edge or coastline [*Bell et al.*, 2014], resulting in rough ice. Forces can also propagate further into the landfast ice, leading to aggregation of ice fragments into rubble and

potentially ridges. Here, the ice bottom, in combination with the sea floor can channel currents beneath the ice, which may play an important role weakening ice and predisposing it to deformation [*Jones et al.*, 2016; *Ohshima*, 2000]. During spring and summer, melt pond formation will result in cm-scale LW roughness features, which if surviving multiple summers will turn into multiyear ice with potential m-scale roughness with longer wavelength as melt ponds deepen leading to increased relief of adjacent bare ice [*Eicken et al.*, 2004]. The different surface roughening processes and the associated scales and types of roughness are listed in Table 3.1.

Throughout the Arctic, sea ice roughness has increased in recent years as a result of (i) increased deformation due to thinner ice [*Rothrock et al.*, 2008] and higher ice drift speeds [*Kwok et al.*, 2013; *Spreen et al.*, 2011], (ii) increasing ice strain and fracture [*Rampal et al.*, 2009], (iii) increasing storm activity [*Zhang et al.*, 2004], and (iv) later formation of landfast sea ice [*Mahoney et al.*, 2014] when storms are strongest [*Zhang et al.*, 2004]. The effects of increased roughness on ice travel, including associated hazards [*Ford et al.*, 2008], are already felt in some regions [*Fienup-Riordan and Rearden*, 2010; *Laidler et al.*, 2010]. A particular concern is inconsistent freezing progression; instead of forming once, the ice continues to melt, break apart, and drift out during fall leading to rougher ice [*Laidler et al.*, 2010].

To date, quantitative assessments or projections of Arctic sea-ice trafficability are mostly lacking. *Stephenson et al.* [2011] used modeling to understand how accessibility may change for shipping and ice roads on land. Due to increasing dependence on sea ice travel in combination with landfast sea ice change it has become important to be able to evaluate changes in trafficability across sea ice and in particular sea ice roughness on scales critical to ice users. Here, we focus strictly on traveling over ice and hence define trafficability as the ability to travel on the sea ice surface in terms of efficiency and required effort. Factors impacting safety such as ice thickness or fractures are not considered here; trafficability is strictly dependent on surface conditions, in particular, roughness. This paper aims to classify and quantify ice roughness, yielding data products in support of tactical and long-term strategic decisions for on-ice operations and travel.

Table 3.1 Thermal and dynamic processes and resulting roughness types and scales

	Process	Roughness
Thermal	Ice freezing in-place during calm conditions	Smooth ice or cm-scale LW roughness
	Ice freezing in-place during rough ocean conditions resulting in consolidation of slush or pancake ice	cm-scale SW roughness
	End-of-season surface melt processes and melt pond formation	cm-scale LW roughness
	Multiyear forming in place	cm or m-scale LW roughness with potential large vertical relief between regions of multiyear and first-year ice
Dynamic	Displacement of thinner ice (<<1 m) resulting in fractures, moderate buckling and rafting	cm-scale LW roughness in the form of sporadic features of cm-scale vertical extent
	Thicker ice (~ 1 m) yielding under severe forcing conditions resulting in rearranging orientation of floes into the vertical	m-scale continuous or non-continuous areas of SW roughness in the form of rubble fields or ridges
	Advection of first year or multiyear pack ice into the region and freezing into landfast ice	Roughness depends on conditions under initial formation and transport

3.2.2 Remote sensing strategies to assess sea ice roughness

Ice users in coastal communities typically assess ice roughness visually at ground level. Maps delineating areas of rough ice based on radar satellite imagery have proven useful as qualitative supplemental information in several communities [*Bell et al.*, 2014; *Druckenmiller et al.*, 2010; *Laidler et al.*, 2011]. The oil and gas industry also commonly evaluates roughness strictly qualitatively through aerial reconnaissance [*Potter et al.*, 1981]. However, tactical decisions on timescales from days to weeks (e.g. ice road routing, evacuation route planning), require quantitative roughness assessments [*Barker et al.*, 2006] obtained in a cost effective and timely manner [*Mesher et al.*, 2008]. To date, ice roughness

and trafficability assessments predominately comprise in-situ observations with limited spatial and temporal coverage [*Bell et al.*, 2014; *Haas and Druckenmiller*, 2010; *Potter et al.*, 1981]. Recent advances in satellite remote sensing set the stage for more comprehensive, efficient trafficability assessments compared to aerial reconnaissance (incl. human image interpretation [*Wang et al.*, 2014]) or groundtruth [*Bell et al.*, 2014].

Seasonal planning and tactics of on-ice operations require repeat surveys with m- to dm-scale resolution at intervals of days to weeks covering the entire area of interest. Ice roughness information can be obtained through several methods, including LIDAR, stereo-photogrammetry, and synthetic aperture radar (SAR). However, only SAR meets all the requirements of operational planning and tactics. The narrow swath width and long repeat intervals of spaceborne Lidar instruments [*Abdalati et al.*, 2010], and the poor spatial overlap of high-resolution imagery from e.g., WorldView/Digital Globe [*Shean et al.*, 2016], and their dependence on clear-sky conditions render both of these approaches unsuitable for operational and many ice roughness research applications.

SAR signals are sensitive to surface roughness: Rough surfaces contain more scattering elements than smooth ice, resulting in a larger radar backscatter cross-section. With resolution on the order of 1-10 m, wide coverage from multiple platforms, independence of weather conditions, and repeat cycles of days to weeks, SAR is well-suited for operational use. Over some sea ice types, some of the microwave energy penetrates below the surface and is subject to volume backscatter from internal structural elements that does not necessarily indicate roughness. Here, SAR polarimetry (*Section 3.2.4*) and interferometry (*Section 3.2.5*) may help in further discriminating between different backscatter mechansisms and type and size of roughness features. We validate these two techniques over sea ice, employing ground truth observations to evaluate the accuracy of the polarimetric classification [*Moen et al.*, 2013; *Scheuchl et al.*, 2001b] and the interferometric digital elevation model (DEM) (*Section 3.3.1 and 3.3.2*).

For the purpose of validation, we acquired images with an unmanned aerial system (UAS) to construct a high-resolution image and a DEM using Structure-from-Motion photogrammetry (SfM) (*Section 3.2.6*). SfM has shown promise in geoscience applications [*Fonstad et al.*, 2013;

Koenderink and Van Doorn, 1991; *Westoby et al.*, 2012], including cm-resolution reconstruction of snow surface features [*Nolan et al.*, 2015]. This study focuses on the landfast sea ice near Utqiaġvik, Alaska (formerly known as Barrow, Figure 3.1) as a test region. Landfast ice at Utqiaġvik typically spans a range of roughness types, from large grounded ridges to smooth ice. Utqiaġvik is the site of extensive ice use, with construction of a network of seasonal ice trails that occupy areas of higher trafficability [*Druckenmiller et al.*, 2013]. Drawing upon GPS surveys of these trails, combinations of SAR techniques are used to develop a large-scale ice roughness and trafficability assessment strategy (*Section 3.3.3* – *Section 3.3.5*).

3.3 Data and methods

The study focus is on landfast ice near Utqiaġvik, Alaska, and both in-situ and space borne data acquisition occurred in April-May 2015 (Figure 3.1). Satellite products from three different SAR systems were utilized: TerraSAR-X and TanDEM-X operated by the German Aerospace Center (DLR) since 2008 and 2010, respectively, with a repeat pass cycle of 11 days, and Japanese Advanced Land Observing Satellite (ALOS-2) PALSAR-2 operating since 2014, with a repeat pass cycle of 14 days. UAS SfM data were acquired in collaboration with the Alaska Center for UAS integration (ACUASI). Remote sensing data sets acquired are listed in Table 3.2 and discussed further below.

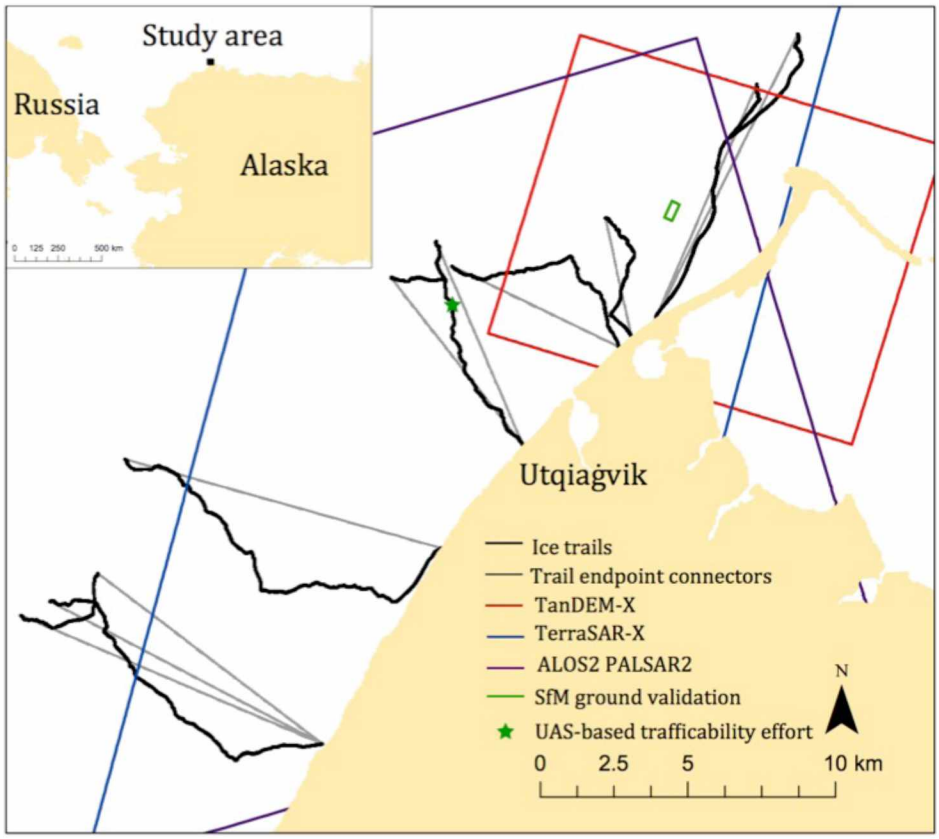

Figure 3.1 Map of ice trails (black) close to Utqiaġvik, Alaska during spring 2015 as well as trail endpoint connectors (gray). The colored rectangles show the coverage of SfM (green), TanDEM-X (red), TerraSAR-X (blue) and PALSAR (purple).

Table 3.2 List of remote sensing datasets analyzed. Here GSI refer to the ground sampling interval (GSI).

Product	Platform	Sensor	Date	GSI (m)	Dir./mode	Additional info
Structure from Motion	Ptarmigan UAS	DSLR	03/21/ 2015	0.11	-	Optical
Polarimetry	ALOS-2 PALSAR-2	SAR	04/02/ 2015	10 m	Ascend / Stripmap	Polarizations HH,HV,VH,VV
Interferometry	TanDEM-X	SAR	04/10/ 2015	2.35	Descend / Stripmap	Baseline 477m
Backscatter	TerraSAR-X	SAR	03/15/ 2015	2.75	Descend / Stripmap	

3.3.1 In-situ data

Every spring, members of the community of Utqiaġvik construct trails leveling several mile-long corridors through the rugged landscape of the landfast ice using only hand tools [*Druckenmiller et al.*, 2010]. These trails are essential to the community, providing subsistence hunters access to marine mammals and birds. Trail construction and use are also an important part of Iñupiaq traditional instruction and subsistence culture [*Eicken et al.*, 2009]. University of Alaska Fairbanks sea ice researchers have collaborated with Iñupiaq sea-ice experts and hunters and local organizations, including the Barrow Whaling Captains Association and the North Slope Borough Department of Wildlife Management, in mapping these community ice trails starting in spring 2000 and consistently every spring starting in 2007. Iñupiaq ice observers and hunters have also shared Indigenous and local knowledge in regards to ice properties that are directly relevant or even critical for the construction and safety of operations on the ice trails during spring [*Brewster*, 2016; *Dammann et al.*, in preparation ; *Druckenmiller et al.*, 2013; *Eicken et al.*, 2014; *George et al.*, 2004].

The trail data used here includes trail location and continuous ice thickness measurements along the trails. The latter were collected with an EM-31 electromagnetic conductivity meter linked with a GPS pulled by a snowmobile, described in detail by *Druckenmiller* [2011]. The trail data was collected in April and May of 2015, extending out along the coast within approximately 15 km from Utqiaġvik (black lines shown in Figure 3.1). The trail crews draw on Indigenous knowledge to construct the trails [*Druckenmiller et al.*, 2013]. The trail path is carefully selected and often routed through stretches of level ice reducing the trail making effort in terms of time and financial costs. However, trails also favor areas of grounded ridges, which help anchor the landfast ice, in order to reduce the risk of break-out events (i.e. detachment of large pieces of ice from the landfast ice). More details of ice properties impacting trail locations can be found in *Druckenmiller et al.* [2013].

For our analysis, we investigated all ten trails constructed for the 2015 spring season. Trail location and ice thickness were sampled by GPS and EM every second along the trails, hence point spacing is dependent on the speed of the snowmobile (roughly every 5 m). The trail is oversampled to construct equal sampling intervals (1 m) for every trail. Ten endpoint

connectors (gray lines in Figure 3.1) are constructed in a straight line from start to end of each trail (1 m sampling interval). These connectors are constructed as an estimate of hypothetical trail location independent of ice conditions impacting trail construction.

Additional in-situ measurements include laser surveying of transects [*Haas and Druckenmiller*, 2010] as well as operation of a survey grade GPS system (Trimble 5700) to assess the quality of the SfM data. 15 ground control points were also included to aid identification of important features such as ridge summit, transect boundaries, and roughness features with significance for trafficability. Two transects were created to evaluate the SfM performance, one across the ridge summit and one over barely navigable rubble-ice.

3.3.2 Classifying sea ice roughness from a trafficability perspective

In the introduction, we identified thermal and dynamic processes that govern surface roughness regimes on landfast ice. Here, we focus on those roughness types found at our study site, which are all associated with dynamic deformation of first-year sea ice. The roughness regime is similar to that described by *Barker et al.* [2006] and hence we are applying a similar categorization of smooth, rubble (light, medium, and rough), and ridges, encompassing the roughness types found in our SfM data (Figure 3.2). Rubble is defined as an area of extremely deformed sea ice of unusual thickness formed during the winter by the motion of drift ice against, or around a protruding rock, islet or other obstruction [*WMO*, 2014]. Here, we define smooth ice as exhibiting roughness features (H_t) 5 cm high or less (#1 in Figure 3.2). Light rubble has a roughness of vertical relief of up to roughly 10 cm and can consist of scattered fragments of thinner ice (#2). We define medium rubble as scattered larger block sizes with a vertical relief on the order of tens of cm (#3). Rough rubble (#4) we identify as continuous rubble with large vertical relief approaching maximum ice thickness (H_i). Ridges are roughness features exceeding ice thickness consisting of stacks of ice blocks. Roughness categories and their impact on trafficability are listed in Table 3.3.

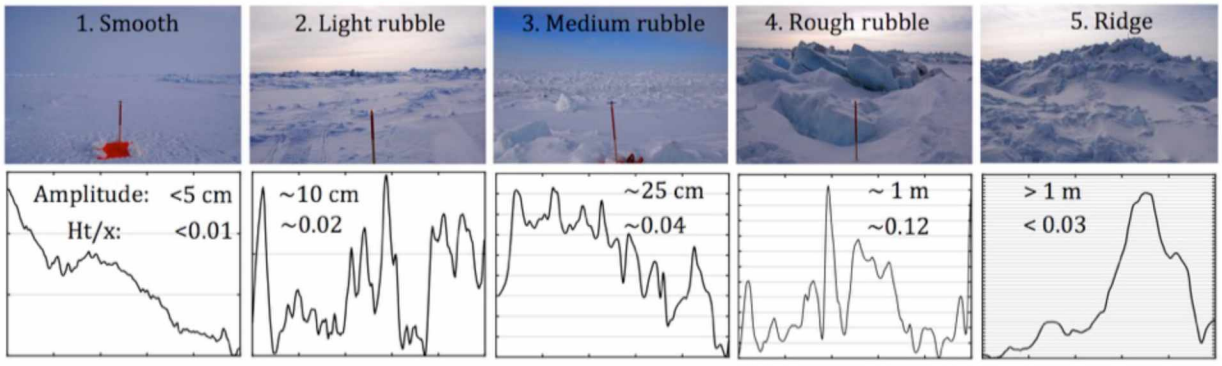

Figure 3.2 Images of the five roughness categories encountered during ground validation with 50 m long height transects from the individual locations obtained from SfM DEM. Vertical axis tick mark spacing and separation of horizontal grid lines is 10 cm. Approximate values for roughness amplitudes and the ratio of feature height (Ht) vs. feature spacing (x) are listed for each roughness class.

The roughness of multiyear sea ice is different from that of first-year sea ice, typically comprising roughness elements of longer wavelength roughness, with high freeboard further limiting trafficability. However, due to the regional decline in multiyear ice and its absence in the 2015 landfast ice, it is not included as a separate category in this study.

Snow plays an important role in terms of the surface roughness of the ice and hence for trafficability at least in winter and early spring before snow-melt. Snowfall on smooth ice will under calm wind conditions result in a smooth snow surface substantially improving conditions for snowmobile travel. However, under strong winds, roughness can increase through wind redistribution of accumulated snow ranging from cm-scale ripple marks to dm-scale sastrugi. Through sintering, snow dunes can harden and become permanent roughness features [*Bell et al.*, 2014; *Filhol and Sturm*, 2015] inhibiting surface travel. On the other hand, over rough ice, snow generally reduces roughness by filling cavities between larger roughness features, hence increasing trafficability.

Table 3.3 Types of ice roughness and impact on trafficability

Class **(see Figure 3.2 for details)**	**Impact on trafficability**	**Typical scale of roughness features**
Smooth ice	Favorable for all transportation	< 5 cm
Light rubble	Unproblematic for snowmobiles with thin snow layer, but impacts speed of cars on cleared ice roads	< 10 cm
Moderate rubble	Slows down transportation or requiring circumnavigation of features in ATV use, and can be a direct obstacle for cars.	Tens of cm
Rough rubble	Resulting in obstructed travel with ice modification necessary for all modes of transportation	~ 1 m
Ridges	Large ridges can result in obstructed travel and significant ice modification is needed	> 1m

When considering trafficability, the height of features (H_t) is not the only important factor, but also their wavelength (x). 50 m H_t transects are created across each roughness type roughly indicating amplitude and H_t/x ratio (Figure 3.2). These values are strictly approximations due to the inevitable impact of the snow cover, which ranged from roughly 5 to 40 cm in depth within the sampled area. We further used these values to construct a schematic linking the feature spacing and feature size to trafficability in a qualitative manner (Figure 3.3).

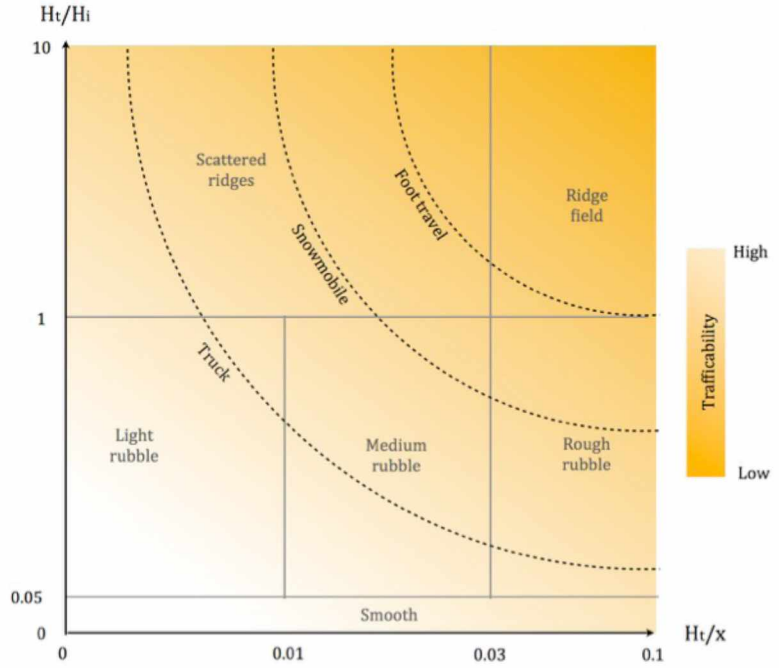

Figure 3.3 Feature height and spacing shown as a parameter plane with different roughness categories occupying different sections of the plot (boundaries shown as schematic approximations). H_t is the topographic relief of ice features, H_i is the ice thickness (proxy for block size), and x is the wavelength (distance between features). Level of trafficability is roughly indicated in color shading as well as the approximate area, which can be traversed using different modes of transportation.

3.3.3 Quantifying sea ice roughness

We utilize two established techniques to quantify sea-ice roughness: standard deviation (σ), and autocorrelation [*Liu et al.*, 2014; *Manninen*, 1997; *Rivas et al.*, 2006]. σ calculates the terrain's deviation from a level surface:

$$\sigma = \sum_{i=1}^{N}\sum_{j=1}^{N}\sqrt{\frac{\left(h_{i,j}-\bar{h}\right)^2}{N^2}} \qquad (3.1)$$

where $h_{i,j}$ is the height in a particular pixel within a patch of NxN pixels with a mean height ($\bar{h}$). Since this metric does not determine the roughness length-scale such that different

structures yield the same σ, we also compute Moran's I [*Moran*, 1950], as a commonly used measure of spatial autocorrelation [*Chen*, 2013; *Lee and Li*, 2016]:

$$I = \frac{N^2}{\sum_i \sum_j d_{ij}} \frac{\sum_i \sum_j d_{ij} (h_i - \bar{h})(h_j - \bar{h})}{\sum_i (h_i - \bar{h})^2} \qquad (3.2)$$

where d_{ij} is a spatial weight set to one when i and j are separated by a desired length scale and otherwise set to zero. Moran's I ranges between -1 (inversely correlated) and 1 (perfectly correlated) with 0 being completely uncorrelated. The autocorrelation length scale (L) is defined by the distance over which I drops to 1/e. Both σ and L were calculated for a standard patch size of 10 m (N=100) corresponding to the multi-look PALSAR resolution cells. I is calculated every 0.5 m (shorter intervals did not result in improved results) up to 8 m. Features generally did not correlate with a spacing approaching 8 m. Using 8 m as a cutoff allowed for several correlation estimates to calculate I within the 10 m patch size.

3.3.4 Polarimetric H/α-decomposition analysis

For radar signals transmitted in two polarimetric orientations, horizontal and vertical relative to the antenna (H and V), polarimetric SAR evaluates backscatter in the four resultant independent datasets (HH, HV, VH, and VV) [*Lee and Pottier*, 2009; *Ulaby and Elachi*, 1990]. Backscatter strength provides information on the surface type [*Lee and Pottier*, 2009]. Polarimetry has previously been shown to be able to indicate different age classes of sea ice, which can be used to estimate ice thickness [*Dierking et al.*, 2003; *Eltoft et al.*, 2013; *Kim et al.*, 2012; *Moen et al.*, 2013; *Nakamura et al.*, 2005; *Wakabayashi et al.*, 2004]. However, to the best of our knowledge, polarimetry has not been applied yet to the derivation of different ice-roughness types. Here, we applied a common classification scheme based on the Wishart distribution [*Lee et al.*, 1994; *Pottier and Lee*, 2000; *Scheuchl et al.*, 2001b], an approach that has shown promise over sea ice [*Scheuchl et al.*, 2001b] .

We have used PolSARpro 5.0.4 to process fully polarimetric PALSAR datasets. We assumed

a linear relationship between the polarimetric channels, allowing for a principal component analysis (PCA) on the four channels HH, HV, VH and VV. The following approach was introduced by *Cloude and Pottier* [1996]. Each pixel can be represented by a scattering matrix:

$$S = \begin{bmatrix} S_{HH} & S_{HV} \\ S_{VH} & S_{VV} \end{bmatrix} \qquad (3.3)$$

where H and V represent horizontal and vertical polarization respectively. Since the acquisition is monostatic, S_{VH} is equal to S_{HV} [*Lee and Pottier*, 2009]. The scattering is used to construct the Pauli vector, which is advantageous due to its independence of the rotation of the SAR system:

$$K_p = \frac{1}{\sqrt{2}} \begin{bmatrix} S_{HH} + S_{VV} \\ S_{HH} - S_{VV} \\ 2S_{HV} \end{bmatrix} \qquad (3.4)$$

from which we obtain the coherency matrix:

$$[T_p] = K_p K_p^T \qquad (3.5).$$

Multi-look polarimetric SAR processing requires averaging n 1-look independent covariance matrices (in this case L=3x3 neighboring pixels):

$$[\langle T \rangle] = \frac{1}{n} \sum_{p=1}^{n} [T_p] \qquad (3.6).$$

A Refined Lee Filter [*Lee et al.*, 1999a] was used with a 7x7 pixel window and an approximated Gaussian distribution. To be able to discriminate between different scattering mechanisms from the covariance matrix, the signal was decomposed using principal component analysis. A 3x3 pixel window is used across $[\langle T \rangle]$:

$$[\langle T \rangle] = [U][\Sigma][U]^{-1} \qquad (3.7)$$

where

$$[\Sigma] = \begin{bmatrix} \lambda_1 & 0 & 0 \\ 0 & \lambda_2 & 0 \\ 0 & 0 & \lambda_3 \end{bmatrix} \qquad (3.8)$$

and

$$[U] = \begin{bmatrix} cos\alpha_1 & cos\alpha_2 & cos\alpha_3 \\ sin\alpha_1 cos\beta_1 e^{i\delta_1} & sin\alpha_2 cos\beta_2 e^{i\delta_2} & sin\alpha_3 cos\beta_3 e^{i\delta_3} \\ sin\alpha_1 sin\beta_1 e^{i\gamma_1} & sin\alpha_2 sin\beta_2 e^{i\gamma_2} & sin\alpha_2 sin\beta_3 e^{i\gamma_2} \end{bmatrix} \qquad (3.9)$$

Rotation angle (α), entropy (H) and anisotropy (A) of the signal can now be calculated:

$$\alpha = \sum_{i=1}^{3} P_i \alpha_i \qquad (3.10)$$

where P_i are probabilities obtained from the eigenvalues:

$$0 \leq P_i = \frac{\lambda_i}{\sum_{i=1}^{3} \lambda_i} \leq 1 \qquad (3.11)$$

$$H = -\sum_{i=1}^{3} P_i log_3(P_i) \qquad (3.12)$$

$$A = \frac{\lambda_2 - \lambda_3}{\lambda_2 + \lambda_3} \qquad (3.13)$$

The entropy, α, and anisotropy, A, jointly indicate what kind of scattering mechanism is present. The initial part of the classification effort is based on the assumption that there are three distinctively different scattering mechanisms [*Freeman and Durden*, 1998]: Double bounce scattering, Bragg scattering, and volume scattering. The rotation angle provides insight into the predominant scattering mechanisms.

Pure double bounce scattering is associated with a rotation of 90°, whereas perfect Bragg scattering will have a rotation of 0°. Volume scattering, which is a result of multiple scattering

mechanisms, will likely cause a rotation closer to 45°. The other component of the classification scheme is entropy. Low entropy is indicative of a single predominant scattering mechanism, whereas high entropy indicates a combination of scattering mechanisms. It is worth mentioning that α has very little physical meaning for high entropy values, restricting the range of interpretable α angles. For an in-depth analysis of complex scattering mechanisms in high H regimes, anisotropy will have to be evaluated. Here, anisotropy did not appear to add value to the analysis and is therefore left out of the H/α decomposition. *Cloude and Pottier* [1996] proposed 8 classes in the H/α that generally can be used to describe different scattering mechanisms. Based on low success of using these predefined classes by much of the ice being classified by a single class, we applied a subsequent Wishart classification, which uses the predefined classes as training classes.

The Complex Wishart Classification has shown promise as a tool to map different types of sea ice, but there is a need for ground truth to properly evaluate the potential of the method [*Scheuchl et al.*, 2001a]. Therefore, we choose to apply a Complex Wishart Classification and collect the necessary data to evaluate the approach (see *Section 3.2.6*). From the Gaussian assumption it follows that the covariance matrix $\langle T_i \rangle$ of a pixel, i, in the image has a complex Wishart distribution [*Lee and Grunes*, 1992]:

$$P([\langle T \rangle]/[T_m]) = \frac{L^{Lp}|\langle [T] \rangle|^{L-p} exp\left(-LTr([T_m]^{-1}\langle [T] \rangle)\right)}{\pi^{\frac{p(p-1)}{2}} \prod_{i=1}^{p} \Gamma(L-i+1)[T_m]^L} \qquad (3.14)$$

for $L \geq p$, where L is number of looks, p is polarimetric dimension (3 for reciprocal and 4 for bistatic case), $\Gamma(\cdot)$ is the Euler gamma function, and *Tr* is trace of a matrix. From the Wishart distribution, pixels were classified based on the Bayes Maximum Likelihood Classification Procedure where a probabilistic measurement of the distance between the matrix of coherence of an unspecified pixel $\langle [T] \rangle$, and the average matrix of coherence $\langle [T_m] \rangle$ of the class candidate ω_m, was obtained using:

$$\langle [T] \rangle \in [T_m] \quad if \quad d_m(\langle [T] \rangle) < d_j(\langle [T] \rangle) \quad \forall \quad j \neq m \qquad (3.15)$$

and

$$d_m(\langle[T]\rangle) = Tr([T_m]^{-1}\langle[T]\rangle) + ln(T_m) \qquad (3.16)$$

$$[T_m] = \frac{1}{L_m}\sum_{i=1}^{L_m}\langle T\rangle \qquad (3.17)$$

where $[T_m]$ is the cluster center of the class m and $P([T_m])$ is the a priori probability of the class m [*Lee et al.*, 1998; *Lee et al.*, 1999b]. The first iteration was used to train the preceding iterations until a consistent result was obtained. Combining H/α – decomposition with a Wishart classification yields more detailed information than the H/α – decomposition on its own [*Ouarzeddine et al.*, 2007].

3.3.5 DEM generation from interferometric SAR

InSAR is a technique that measures phase differences between two SAR scenes acquired from two coherent viewing geometries ([*Bamler and Hartl*, 1998; *Ferretti et al.*, 2007]). The observed phase difference originates from displacement of the scattering surface if measurements were acquired at different times (non-zero temporal baselines) and/or from surface topography if measurements originate from slightly different vantage points (zero spatial baselines) [*Bamler and Hartl*, 1998]. A number of studies have applied long-temporal baseline (> 1 day) InSAR to explore deformation of landfast ice [*Dammann et al.*, 2016; *Dammert et al.*, 1998; *Li et al.*, 1996; *Meyer et al.*, 2011; *Morris et al.*, 1999] and fewer studies have explored the potential for short-temporal baseline (< 1 m) InSAR to investigate more rapid deformation [*Mahoney et al.*, 2016; *Scheiber et al.*, 2011; *Wegmüller et al.*, 2009]. However, we are not aware of any studies that used bistatic interferometry to calculate topography of sea ice by constructing a digital elevation model (DEM) [*Lang et al.*, 2013].

This study utilizes an X-band SAR bistatic image pair acquired by the TanDEM-X satellite constellation operated by the German Aerospace Center (DLR). The images were acquired on April 10, 2015 at identical times, but from different geometric vantage points. The interferograms were constructed using the Sentinel Toolbox (S1TBX), which is used to

derive the interferometric signal from the complex conjugate multiplication of the two image signals:

$$\gamma = |u_1||u_2|e^{i(\psi_1 - \psi_2)} \qquad (3.18)$$

where u_1 and u_2 are returned signals from image 1 and 2 with respective phase values ψ_1 and ψ_2. The interferogram is the spatial distribution of the calculated phase difference Φ:

$$\Phi = arctan\left[\frac{Im(\gamma)}{Re(\gamma)}\right] \qquad (3.19)$$

Due to the image pair being acquired at identical times, the main contributor for a bistatic phase signal is the topographic phase component Φ_{topo} that can be written as:

$$\Phi_{topo} = \frac{4\pi}{\lambda}\frac{B_\perp}{R}\frac{h}{sin\theta} \qquad (3.20)$$

where R is slant range distance to the target, λ is the sensor wavelength, $B_\perp$ is the perpendicular baseline, h is the topographic relief of a feature, and θ is the radar's off-nadir look angle (see *Dammann et al.* [2016] for details). The topographic height difference causing a full phase cycle between two points in a neighborhood can be described as the ambiguity height, h_a:

$$h_a = \frac{\lambda R_s sin\theta}{2B_\perp} \qquad (3.21)$$

[*Bamler and Hartl*, 1998]. For the image pair used here, h_a is close to 14 m due to a $B_\perp$ of 477 m resulting in large ridges being represented by roughly one half fringe. Since the phase information is directly related to height, it can therefore be used to create a DEM (referred to from here as IDEM).

3.3.6 Structure-from-Motion

High resolution aerial imagery was acquired using a camera mounted on a hexacopter UAS carrying a downward looking digital mirror-less camera (Sony NEX-7) and a Novatel survey grade Global Navigation Satellite System (GNSS). Using this system, we surveyed an area of roughly 200 m x 600 m (green area centered in the red rectangle in Figure 3.1) from an altitude of roughly 100 m. The Novatel GNSS recorded the ephemeris data from both GPS and GLONASS satellites. An Arduino processor was used to orchestrate simultaneous acquisitions of data from both the camera and GPS. Data acquisition and processing workflows are outlined in Figure 3.4. Two data products were generated: (i) a high-resolution orthorectified image mosaic (Figure 3.5a) and (ii) a digital elevation model (referred to from here as SDEM, Figure 3.5b) each with 11 cm ground sampling interval. The GNSS Ephemeris data was post processed (differential correction) using Novatel GrafNAV software (with Barrow airport as the a base station) to achieve a DEM with high localization accuracy. The SfM processing was performed using Agisoft Photo Scan software.

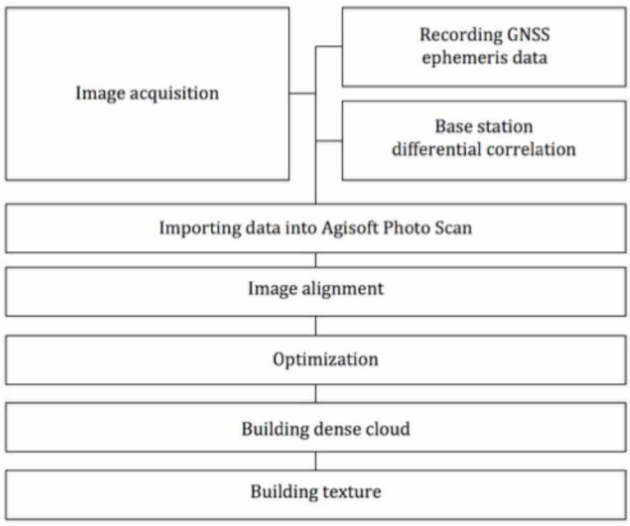

Figure 3.4 Structure-from-motion processing workflow

3.4 Results

3.4.1 Evaluating SAR interferometry as a tool to assess ice topography

The UAS-acquired image mosaic is used to visually interpret the type of roughness on the ground aided by ground control points (colored rectangles in Figure 3.5a and b). The numbered triangles and intersecting lines in Figure 3.5b correspond to the location of individual numbered images and transects in Figure 3.2. Superimposing the IDEM on the UAS-acquired image mosaic confirms high spatial correlation between the two data products (Figure 3.6). The height of the SDEM was evaluated along two transects. Transect 1 traversed the ridge while Transect 2 extended across a section of continuous medium rubble (see lines in Figure 3.6). The IDEM was only evaluated across Transect 1 due to resolution constraints making it incapable of capturing cm-scale roughness of the medium rubble field. Both transects were surveyed in-situ with laser leveling equipment for quality analysis. The height of the ridge in the IDEM agrees well with both the SDEM and in-situ survey across Transect 1 (Figure 3.7a), confirming the ability for InSAR to accurately estimate ridge height and thus its potential ability to be used in trafficability analysis.

The ability to use SfM to assess ice roughness for further evaluation of datasets (e.g. PolSAR) requires the ability to capture both low-frequency roughness (confirmed along Transect 1) as well as high-frequency roughness. The SDEM was therefore further evaluated along Transect 2 (Figure 3.7b). The in-situ roughness measurements were conducted with a 10 cm sampling interval, close to the SfM sampling interval (11 cm). There is a close match between features in the two datasets indicating the potential for SfM dataset to provide ice roughness data with enough detail for roughness validation and comparison (*Section 3.3.2*). Despite the close match between the two datasets, some of the peaks are underestimated in the SDEM. This is due to the high frequency roughness (low L) resulting in some roughness features potentially being reduced by even a slight coregistration offset between the two transects. While the SDEM captures the full roughness frequency spectrum, relative to laser surveying some of the extreme values of individual roughness features are underestimated. As discussed below, this does not affect the findings from broader, classification- or index-based trafficability assessments.

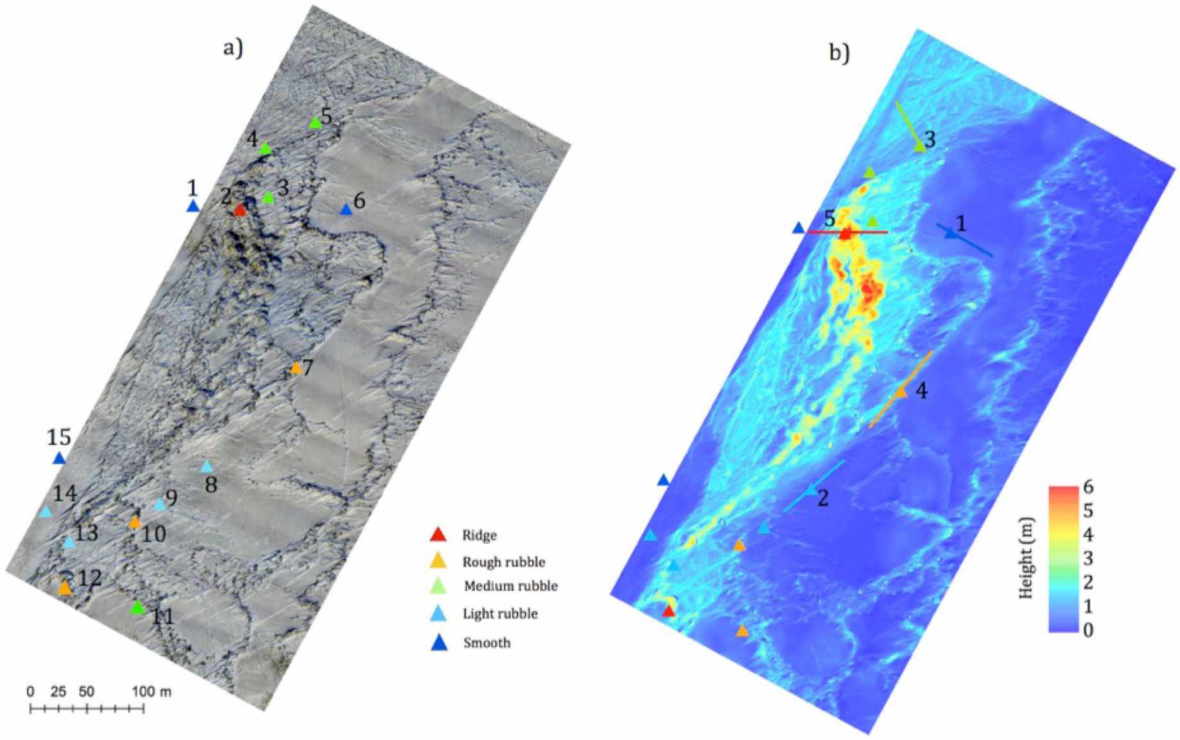

Figure 3.5 a) UAS-acquired image mosaic illustrates several different roughness regimes from a large ridge to level smooth ice. Triangles show locations of ground control points indicating type of roughness on the ground (warm colors represent rougher and cool represent smoother ice). Subtle shadow lines extend across the width of the image, which is an unresolved artifact from the SfM processing. b) SDEM with lines indicating location of transects shown in Figure 3.2.

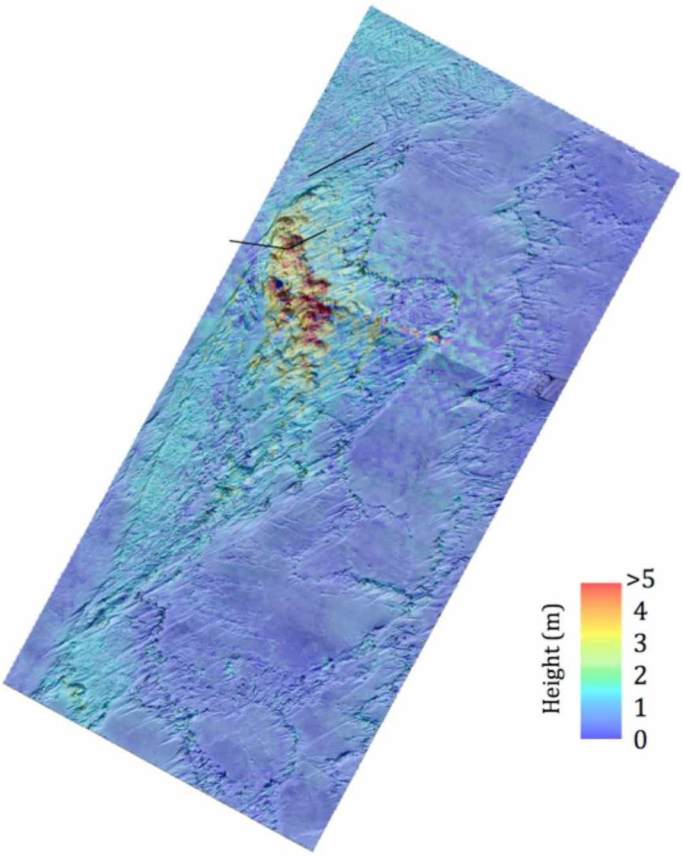

Figure 3.6 UAS-acquired image mosaicsuperimposed on IDEM (April 10, 2015) indicating good spatial correlation of the ridge. The black lines indicate location of transects validated using laser survey.

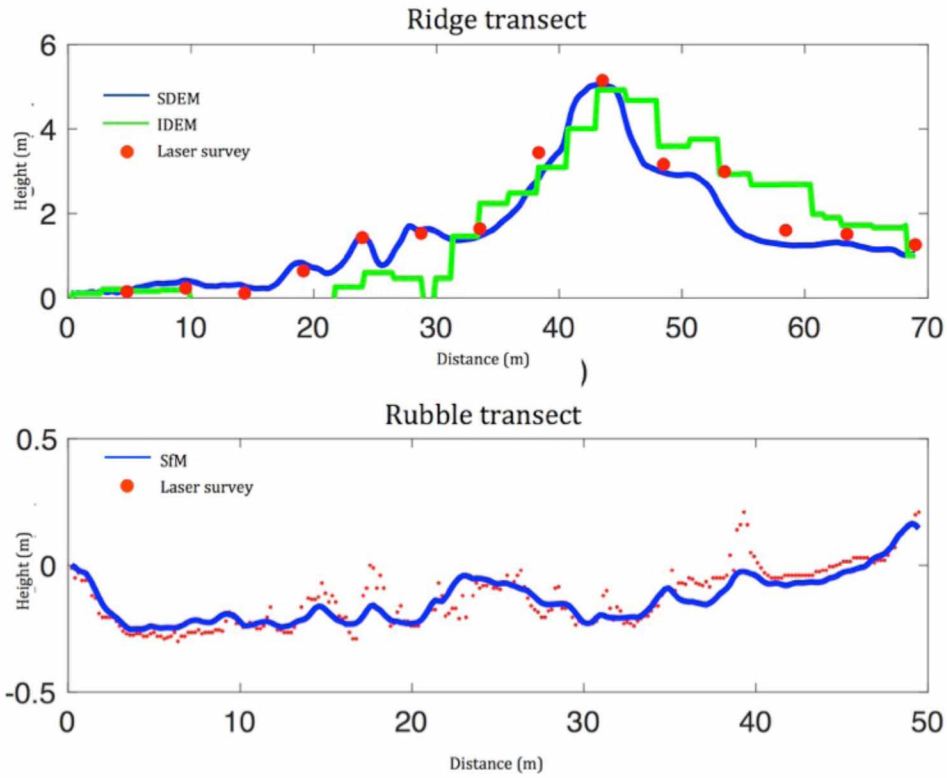

Figure 3.7 Transects from ground-laser survey systemcompared with the SDEM and IDEM over the ridge (a) and compared with only SDEM in an area of medium rubble (b). The graphs indicate good correlation between both DEMs and ground survey.

3.4.2 Assessing ice roughness through polarimetric classification

An initial PolSAR H/α-decomposition (not shown here), based on the derivation of entropy H and rotation angle α indicates that (i) smooth areas are dominated by volume scattering, (ii) some ridged areas exhibit strong Bragg (roughness) scattering, and (iii) the majority of the study area is classified by a combination of backscatter mechanisms with Bragg scattering dominant. This finding, with much of the study area falling into a single class, makes it clear that the outcome of a H/α-decomposition is not suited for an in-depth analysis of ice roughness and trafficability. Hence, we applied a Complex Wishart Classification as described in *Section 3.2.4* to arrive at an optimal segmentation based on data clusters identified through maximum likelihood classification. The Wishart scheme applied here groups an image into 8 classes, based on the original H/α classes (see *Section 3.2.4*). Of these,

6 classes are within the area covered by the SfM DEM (class 1 and 2 were only found outside of this area). Classes 6 and 7 correspond to the central, highly deformed part of the ridge or continuous rubble, classes 3 and 4 correspond to the outer margins of the ridge/rubble field, class 5 covers areas of light rubble, and class 8 corresponds to wide stretches of smooth ice (Figure 3.8). This preliminary analysis suggests that polarimetric classification holds promise as a source of supporting information to guide trafficability assessments and aid route selection. However, the classification does not provide quantitative information on actual ice roughness, required for an in-depth assessment.

To address this problem, we derived quantitative information on ice roughness from the SDEM, slightly over-sampled to a resolution of 10 cm, i.e., 1/100 of the polarimetric SAR resolution cell size (10 m). For every SAR resolution cell, we calculated the standard deviation (σ) from the SDEM and superimposed on the same dataset. The spatial distribution of σ is structured as expected, with low values over smooth ice and higher values for rough ice (Figure 3.9a). However, σ by itself is not sufficient to distinguish between different spatial roughness scales. Hence L was derived to enhance trafficability assessments. By dividing L by σ (Figure 3.9b), areas of high L associated with smooth ice will have a high L/σ ratio, whereas high L in conjunction with rough or ridged ice (in the case of correlation between large roughness features) will result in lower L/σ ratios. L/σ is low for both ridges and rubble and thus a good discriminator between consistently smooth ice (high L/σ – see regions marked A in Figure 3.9b) and smooth ice with interspersed roughness features (lower L/σ – see regions marked B in Figure 3.9b). PDFs of σ and L/σ are plotted for all six Wishart classes in Figure 3.10a and b. With the exception of the classes 3 and 4 at the margins of deformed ice it is clear that each class represents a unique surface type based on a distinctively different PDF of L/σ values. Class 8 favors high L/σ values, while class 5 contains some higher L/σ values as well. Classes 3 and 4, corresponding to the margins of deformed areas, mostly lack low and high L/σ ratios. Ridged ice (classes 6 and 7) is represented by the lowest values in the study area.

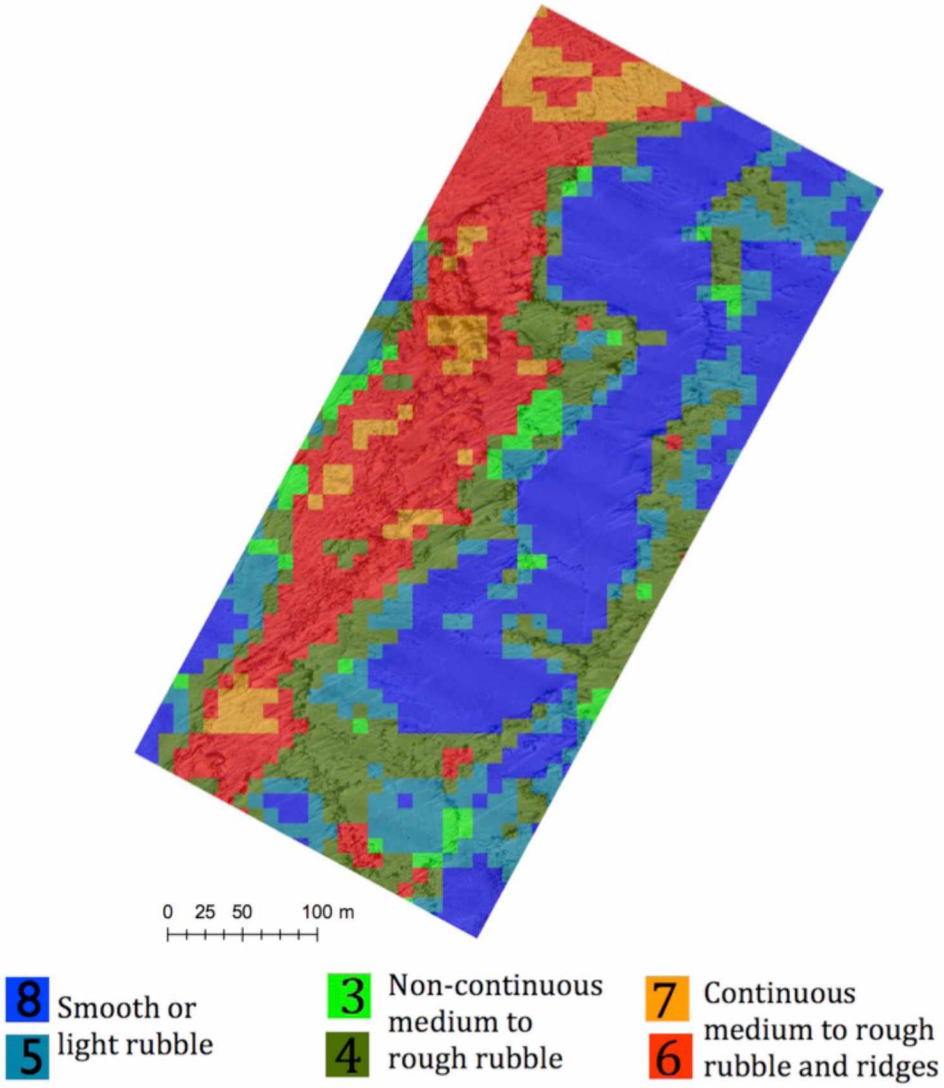

Figure 3.8 UAS-acquired image mosaicsuperimposed on Complex Wishart Classification, where 6 out of 8 classes appear in the study area. The ridge and areas of continuous rubble is dominated by class 6 and 7. Regions of rubble adjacent to smoother ice is dominated by class 3 and 4. Smooth ice and light rubble is dominated by class 5 and 8.

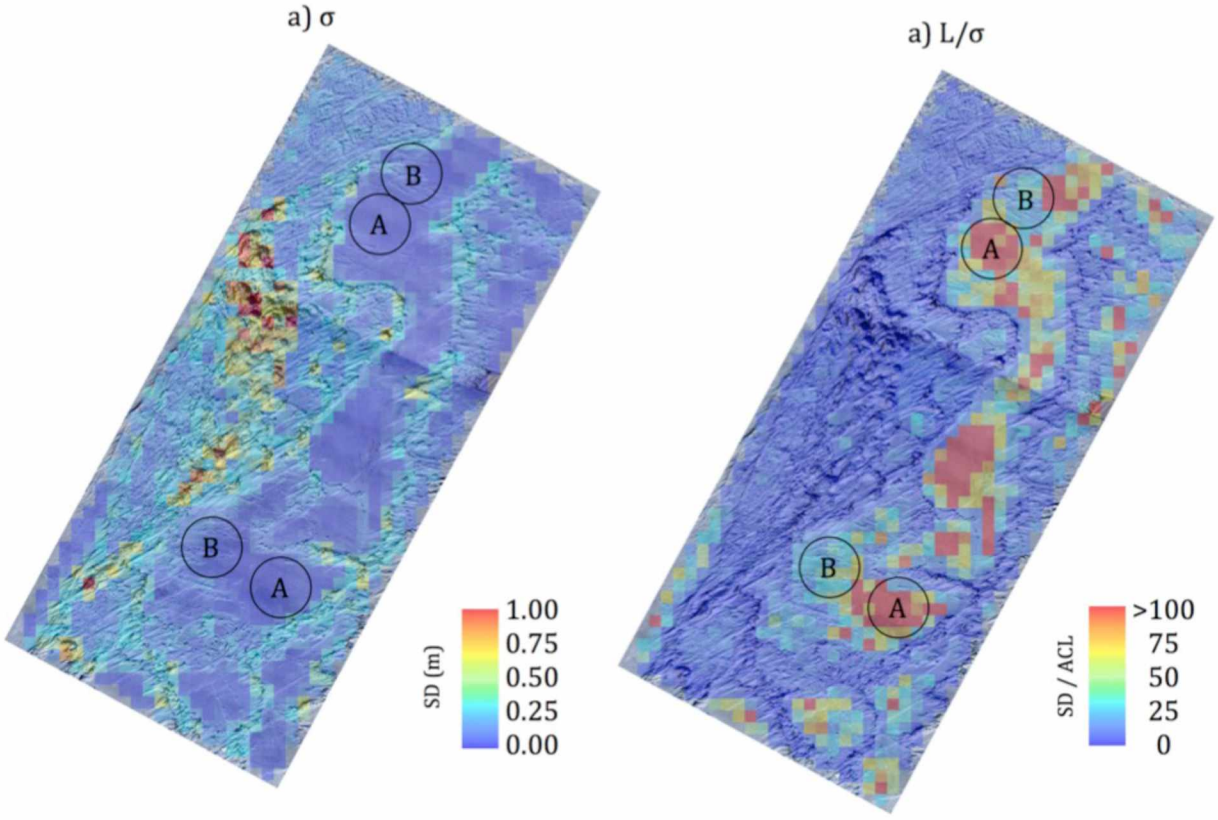

Figure 3.9 Standard deviation (σ) of SDEM (a), and autocorrelation length scaledivided by standard deviation (L/σ) (b), calculated over 100x100 pixels. The UAS-acquired image mosaic is superimposed on each plot. Circles indicate areas of similar σ-values, but with different roughness and L/σ-values between A and B.

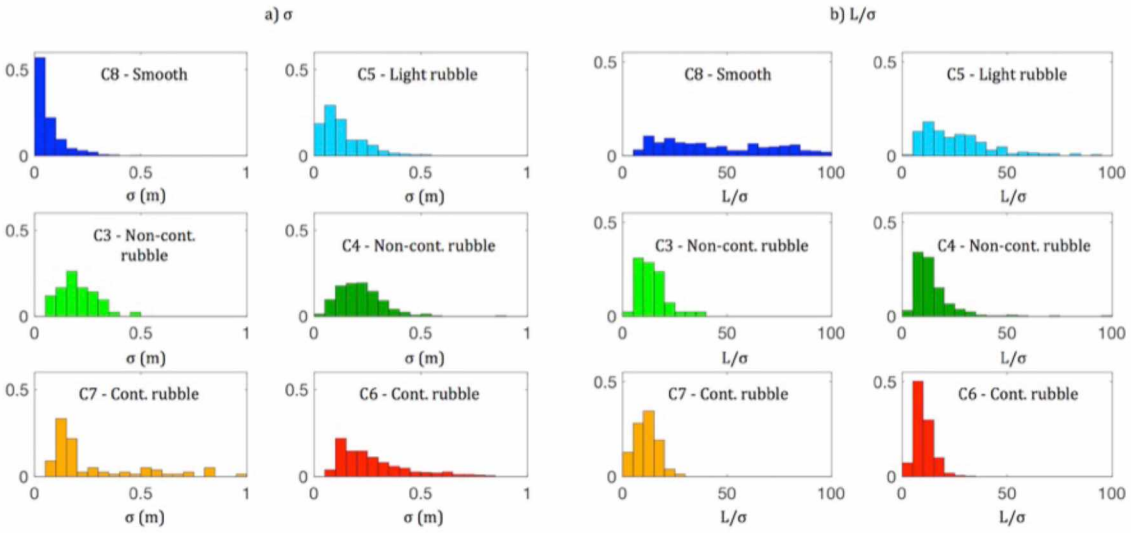

Figure 3.10 PDF of σ (a) and L/σ (b) within their respective polarimetric class. L/σ for class 8 is cut off by 100, but includes values above 200 indicated in Figure 3.9b.

3.4.3 Assessing ice trafficability for community ice trail areas

Based on the results of the Complex Wishart classification and other standard measures of ice roughness, we can now evaluate the relative roughness and hence trafficability of different subregions of our study area. To achieve this, we utilize trails as placed by Iñupiaq ice experts at Utqiaġvik (Figure 3.1). SAR products are sampled every meter along the trail and the linear endpoint connectors. Resulting Probability Density Functions are displayed in Figure 3.11 of X-band SAR 8-bit gray-level values converted from the backscatter coefficient (a), X-band InSAR-derived relative height (b), and L-band Complex Wishart classification (c). From the comparison, it is clear that the trails as placed by Iñupiaq ice experts (red) favor both lower SAR backscatter values and lower height values compared to the endpoint connectors (blue). In addition, class 8 and less so class 5 from the Complex Wishart Classification appear to be favored for trail routing. This is to be expected from the analysis in *Section 3.3.1* and *3.3.2* indicating that these classes correspond to smooth ice or light rubble.

Using information from the PDFs shown in Figure 3.11, we calculate the relative likelihood of a particular pixel value representing a preferred surface type for ice trail construction. For every pixel [i,k] and SAR-based product (i.e, interferometric height, polarimetric class, or X-band amplitude values) we calculate $T_n[i,k]$, a measure describing whether the pixel is favored ($T_n > 0.5$) or not ($T_n < 0.5$) in terms of trafficability:

$$T_n[i,k] = \frac{p_t}{p_e + p_t} \qquad (3.22)$$

Every pixel belongs to a single bin in all three PDFs where p_t and p_e is the probability of a trail and endpoint connector occupying the same bin respectively. Tn is the trafficability determined by a specific SAR-based method, with n = I, P, or X indicating use of interferometric height, polarimetric classes, or X-band gray-level values. T_n ranges from 0 (no trail segment falls in the respective bin, hence low trafficability) to roughly 0.8 (trail segments falls in the respective bin four times as frequent as endpoint connectors), with a hypothetical limit of 1. It is worth noting that this range is subject to change with different roughness regimes. For instance, for smoother ice, endpoint connectors will more frequently occupy bins similar to trails narrowing the range of T_n values. Trafficability for bins on the left side of the histograms in Figure 3.11a and b is set to 1 and on the right side set to 0. We define the trafficability, T_{IPX} utilizing interferometric (T_I), polarimetric (T_P) and X-band gray-level values (T_X) as:

$$T_{IPX} = T_I \cdot T_P \cdot T_X \qquad (3.23)$$

T_{IPX} is assessed for both the trails and the endpoint connectors in a similar manner using PDFs and is displayed in Figure 3.11d. The distribution shows, as expected, that trail routing favors areas of higher trafficability. The combination of T-values obtained through three different methods amplifies the spread of values, and hence likely increases accuracy of the compound trafficability estimate T_{IPX} compared to individual T values.

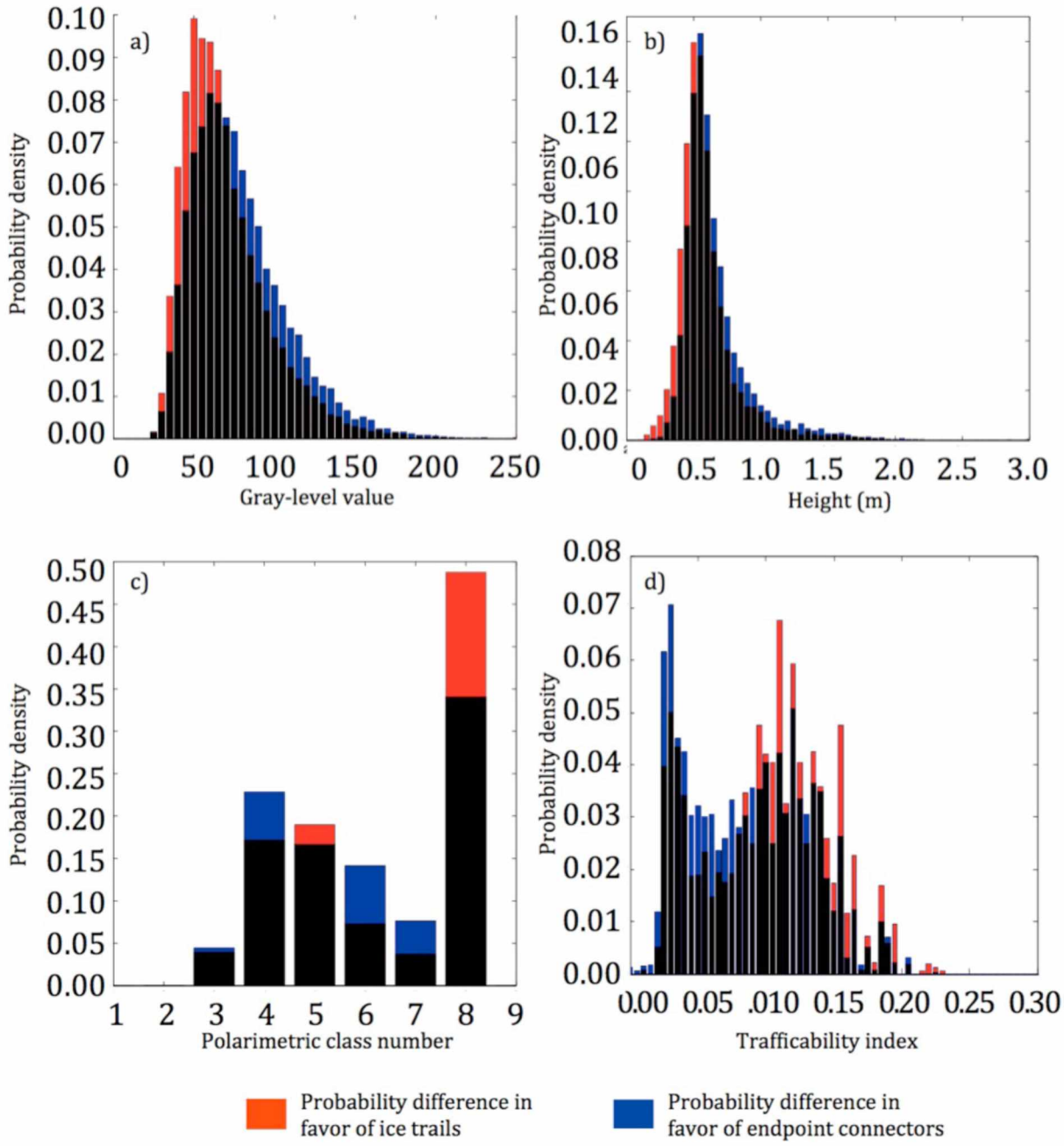

Figure 3.11 PDF of values under ice trails (shown in red) superimposed on PDFs of endpoint connectors (blue) with overlapping bars in black for X-band gray-level image values (a), X-band interferometric height (b), Complex Wishart Classification (c). The calculated trafficability PDF utilizing PDF a-c is displayed as Figure d (T_{IPX}).

The trafficability index T_{IPX} retains the resolution of the highest-resolution SAR product, in this case 2.35 m, which is the multilook resolution of T_I. Over the extent of the SfM scene, the magnitude of T_{IPX} anti-correlates highly with the ridge (Figure 3.12). Low values are shown in red, which cover the ridge and the areas difficult or impossible to traverse. High values shown as blue and green over smooth or light rubble areas classify these as trafficable. Yellow, mid-range values cover border regions between smooth and rough ice.

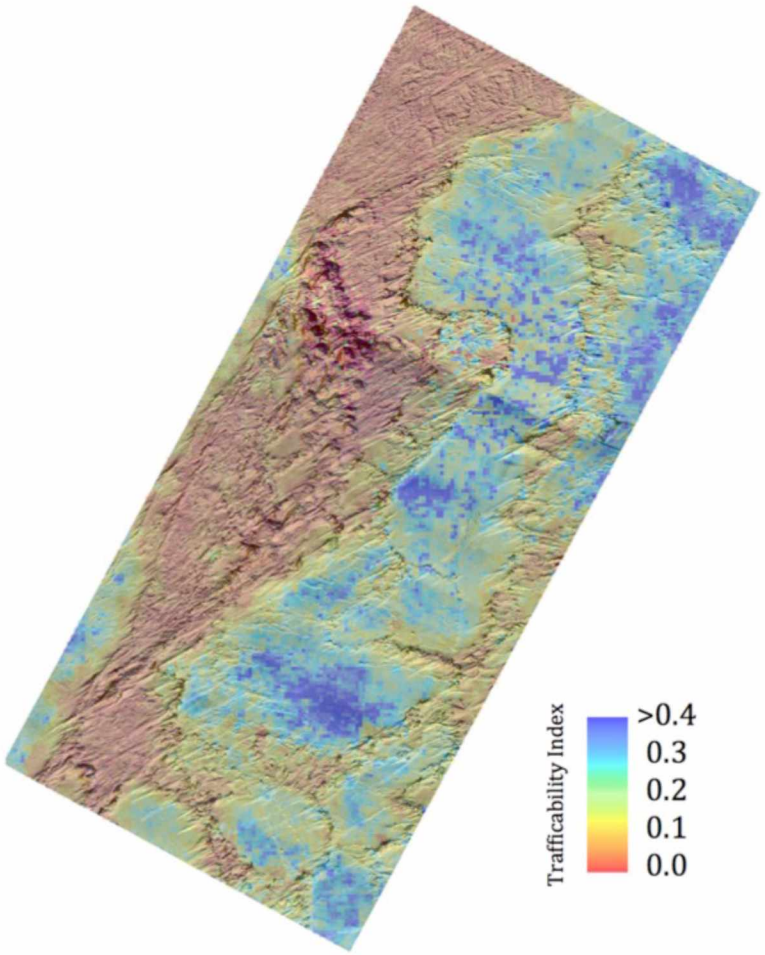

Figure 3.12 Trafficability index superimposed on the UAS-acquired image mosaic.

3.4.4 Route selection based on cost-index estimates

Utilizing multiple SAR products, it is possible to create a large-scale trafficability assessment that can help guide decision making for ice road or trail development. An important question to explore is whether data such as those analyzed here allow for the determination of an optimal trail route. Such an evaluation requires a measure of relevance of different roughness categories for the specific trail or ice user, which will largely depend on the mode of transportation, level of ice construction or modification needed, crew size and related factors.

The trafficability assessment (*Section 3.3.3*) is used to determine an idealized route and to identify optimal data combinations for routing purposes. T_{IPX} values for 5 control points spanning all five roughness classes (point 15, 8, 11, 12, and 2 in Figure 3.5a) are listed in the last column of Table 3.4. Depending on the mode of transportation, these different roughness classes are associated with different costs or penalty values, which can be estimated in both workload, price of construction, or time and will depend on available resources and the trail surface end state needed (e.g., level of smoothness). An example of how this can be calculated can be found in *Spencer et al.* [2007]. Here, we demonstrate the general approach for arbitrary cost values (Table 3.2), focusing on relative, not absolute magnitudes.

Table 3.4 Costs of different transportation/construction purposes and ice roughness types

Ice roughness type	**Cost of ice trail (IT)**	**Cost of ice road (IR)**	**Cost of ice scouting (IS)**	**Trafficability at control points**
Smooth	0.2	4	0.01	0.231
Light rubble	1	5	0.01	0.183
Medium rubble	2	6	0.01	0.162
Rough rubble	4	9	10	0.056
Ridge	6	10	10	0

Every derived trafficability value is linearly interpolated to a cost value for three different use scenarios: (a) ice trail construction (IT) by local communities utilizing snowmobiles, (b) construction of an ice road (IR) by a local government or industry capable of supporting construction vehicle and car traffic, and (c) ice scouting (IS) with snowmobiles without any ice modification or construction. The relative cost values between roughness classes are different for the three use scenarios (Table 3.4). The cost associated with each use scenario depends on a number of factors relevant along the optimum path, such as height thresholds that determine whether a ridge can be traversed. Mostly, the routing will be constrained by the cost/benefit ratio associated with traversing rough areas for the benefit of a short path. Following is a justification for the assigned cost values.

For ice trails (IT) such as those created at Utqiaġvik by the local population, rougher stretches frequently involve cutting of paths and infilling with ice blocks cut and shaped to smooth out the trail, so as to allow towing of large sleds and boats through the ice by snowmobile. Several crews may choose to collaborate on breaking through the roughest sections. Since all labor is by hand, it is critical for existing smooth areas to be utilized wherever possible. At the same time, the trail should not be too long, allowing for quick evacuation in a case of emergency. Smooth ice is therefore given a small cost (0.2), but not zero ensuring a small penalty for a long trail. From smooth ice, cost is set to increase up to 6 for ice difficult or impossible to navigate where substantial construction is needed. For an ice road (IR), we place a substantially larger penalty on smooth ice. For intensive road use during the season, reducing distance traveled via road becomes important. Also, in case of an industry ice road, substantial work is associated with road construction (e.g. artificial thickening of the ice) across even smooth areas reducing differences in cost for different ice types (roughest ice is set to only 2.5 times the penalty of smooth ice for IR versus 30 times for IT). For over-ice travel by snowmobile for the purposes of ice scouting (IS) in search of a navigable path, i.e., not associated with repeated use of trails and without any ice modification, we are selecting a near binary cost assignment. For ice that is fairly easily traversable, the cost is set to near zero and for ice that can be difficult or potentially impossible to navigate, the cost is set to ten. This will allow for a long travel route circumnavigating areas of rough ice.

To evaluate the proposed approach, we compared the most cost-effective routes based on the conversion outlined above with constructed trails. Two trail segments (of the three enclosed in the red rectangle in Figure 3.1) were assessed, with the eastern trail (A) considered in its entirety and the western trail (B) considered from the start at the shore to the edge of the TanDEM-X scene. The trafficability index validated in Figure 3.12 is displayed for the area in Figure 3.13a with ice trails indicated in black. Using the cost assignments from Table 3.4, lowest cost paths are calculated for IT (red), IR (cyan), and IS (blue). The expectation is that the trails created by local experts after considerable scouting and tracking of ice conditions over the course of the season are close to optimal, with some dependence on the experience of the crew [*Druckenmiller et al.*, 2013]. Hence any method that is able to closely match actual trail routing holds promise to help determine trail or ice road construction in operational settings.

For trail, A (eastern trail in Figure 3.11a), the trail (black) follows the edge of an area of rubble ice to the west and through a small ridge (indicated by "1" in Figure 3.13a) of lower trafficability. From there, the trail stays on a stretch of newer ice outside of the deformed shear zone ("2"). The trail follows this low-resistance route and makes a turn ("3") heading almost perpendicular to the ridges to minimize the distance traversed in the ridged areas. The IT (red) follows the general path of the actual trail and makes the two major turns ("1" and "2") at the same locations. Only towards the end there is a small deviation. The IR prediction (cyan) takes a straighter route through a passage of high trafficability (but lower than the path of the actual trail) to reduce cost of added distance. The IR continues up the same smooth refrozen lead ("2") and makes a less sharp turn to save on distance for the second turn. IS (blue), the smoothest route, hugs the shore, part of it likely on bottomfast ice, before looping around in a detour avoiding some of the light to medium rubble and continuing up the smooth frozen lead. For the last section IS and IT follow the same path.

Trail B (eastern trail in Figure 3.11a), does not take advantage of the smooth frozen lead, but tracks a straighter path out from the coast. The trail finds a relatively efficient route through the extensively ridged area. This trail was particularly difficult to construct through this area and the trail work ceased for some time before it was completed (Unpublished trail surveys,

2015). On the other side of the rough ice ("4") the trail follows a refrozen lead taking advantage of the smooth ice in this passage. IS and IT are following similar paths attempting to avoid as much of the rubble ice in the beginning of the trail and are passing through "1". This is different from the actual trail and is linked to the presence of snow at the time of trail building further discussed in *Section 3.4.4*. IT and IS deviate approaching the severely ridged area and choosing to enter the refrozen lead further up than "4". This passage crosses lower elevation ridges in an area of higher trafficability (T_{IPX}). The IR follows a relatively straight path (passing just north of the narrowest part of the ridge "5") with small deviations to take advantage of smoother areas.

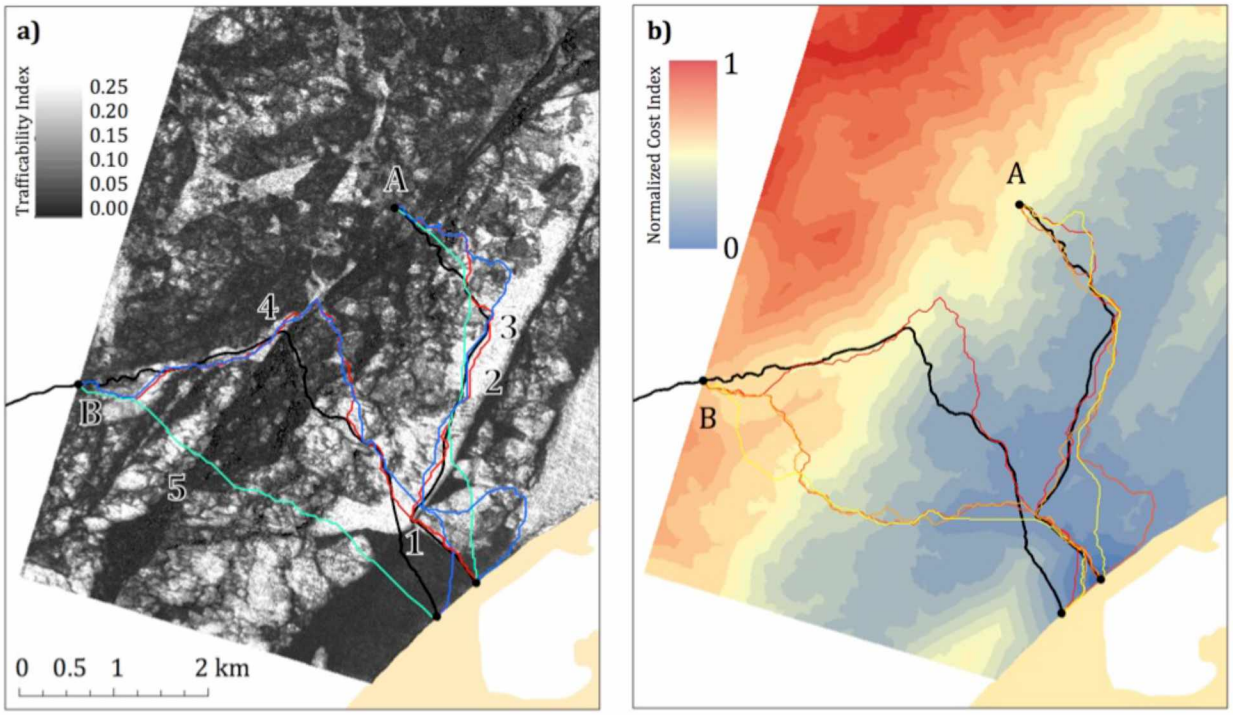

Figure 3.13 (a) Trafficability index (T_{IPX}) surrounding two ice trails (black lines) near Utqiaġvik. Colored lines represent lowest cost paths for construction of an ice trail (red) and an ice road (cyan) and ice scouting (blue). (b) Normalized cost of ice trail construction from starting point of trail A to any other location on the map. Colored lines represent optimal trails calculated using a combination of SAR products: IT_{IPX} (red), IT_{PX} (dark orange), IT_X (light orange), and IT_L (yellow).

3.4.5 Optimal path routes and sensitivity to different SAR-derived data products

By utilizing the trafficability index T_{IPX} to cost conversion for ice trails (IT) outlined in *Section 3.3.4* we can calculate the cost from a given starting point to any other location. Here, we perform this calculation from the starting point of trail A. The resulting normalized cost index map (Figure 3.13b) allows us to identify different directions of low cost, which may help guide routing of trails. The starting point of Trail B is close to that of Trail A, hence the cost index maps for the two starting points are nearly identical (not shown). To address the relevance of each individual SAR product in the calculation of an optimal trail we repeated the steps outlined in *Section 3.3.3 – 3.3.4* for (IT) (Figure 3.13b) based on X-band SAR backscatter and PolSAR (excluding InSAR) (T_{PX}), and only X-band backscatter (T_X). We also tested the dependence on wavelength frequency by applying L-band backscatter (T_L). All products were resampled to the lowest resolution of L-band SAR (multilooked to 10x10m).

The calculated optimal trails are again compared to trails A and B. The trail calculated using T_{IPX} (IT_{TPX}) is displayed in red, IT_{PX} in dark orange, IT_X in light orange, and IT_L in yellow. For trail A, all calculated IT follows the general path, with an exception of the starting direction in IT_{PX} and IT_L. These two products are not sensitive to elevation and are either exclusively based on or more strongly impacted by L-band than IT_{IPX} (IT_L and IT_{PX} respectively). As L-band, compared to X-band, is less sensitive to small-scale roughness features, it is possible that these routes cross light rubble features while the other approaches choose alternate paths.

There is a larger difference between the trail products for trail B. Initially the optimum trails take the same path, but here, IT_{IPX} is the only trail that follows the general path of trail B by crossing the ridge close to "4" and utilizing the refrozen lead. By not utilizing InSAR-derived height, the trails take a more direct path crossing what is likely more topographically challenging terrain. Towards the end IT_L deviates, choosing a path through an area of likely small-scale roughness that is underrepresented in the L-band signal, but shows up more clearly in X-band.

3.5 Discussion

Our analysis demonstrates that the remote sensing tools employed here, specifically SAR polarimetry, backscatter amplitude analysis, and InSAR-derived DEM, support detailed evaluation of sea-ice trafficability for different applications. The approach developed here can help determine favorable paths, in particular if combined with application-specific parameterization of trail cost. Cost maps, such as featured in Figure 3.13b, can be used to identify least costly options, but also identify several possible options for ice travel. The latter are particularly relevant in the following contexts:

1) Routing of seasonal ice trails by coastal communities for hunting and travel. This approach may help improve safety and efficiency of trail construction. For instance, Figure 3.13b demonstrates that trail A, where rough ice led to termination of trail breaking before the ice edge was reached, would have resulted in high costs to complete.
2) Determine optimal travel paths for a range of uses such as scientific research and, military operations.
3) Routing of ice roads through roughness types compatible with a specific trail construction method.
4) Delineation of evacuation routes away from offshore infrastructure and installations.
5) Temporary logistical operations such as stretching of fuel lines across landfast ice between refueling barges and coastal communities.
6) Identification of potential on-ice aircraft landing strips.

3.5.1 Benefits of InSAR-derived height in trafficability analysis

We need to consider the relevance of the source data used to calculate roughness and trafficability for ice trail or road routing assessments – in particular, whether DEM products require use of InSAR data for sufficient accuracy. Polarimetric and backscatter amplitude data have the advantage that they do not need to be acquired by twin constellations such as TanDEM-X. Unless requested specifically, single-pass interferometric products are rarely

acquired routinely and should be obtained in bi-static mode since even a few seconds of temporal baseline can result in vertical shifts through ocean interaction to produce a phase signal interfering with the height analysis [*Mahoney et al.*, 2016]. A more effective way of acquiring bi-static data is from airborne platforms. Interferometry provides important, non-redundant information in the context of trafficability assessments, yielding a predicted trail route most closely tracking that of the actual trail (Figure 3.13b). However, with a non-restrictive path length and only high costs for severe roughness (IS), the predicted travel path based on L-band data alone closely captures the actual ice trail route (not shown). The larger wavelength of L-band (24 cm), compared to X-band (3 cm), makes it less sensitive to small-scale roughness, with little impact on assessments for most modes of transportation. The L-band data captures and integrates both the smooth refrozen lead and the severe ridging into an optimal trail route. Hence, out of all factors considered, accurate representation of differential trail costs is most critical for optimal trail route prediction. Furthermore, trafficability is significantly constrained by ridge height [*Dammann et al.*, in preparation] such that the promising results obtained from InSAR highlight the need for better coverage by twin constellation InSAR systems in the future.

3.5.2 Sensitivity to radar wavelength and resolution

Throughout this work we have identified different classes and types of roughness, each associated with different features and length scales. Hence, sensor resolution and wavelength play an important role in the detection of surface obstacles, with little contribution to backscatter by feature sizes well below sensor wavelength. Trail routes obtained from X-band and L-band data differ mostly only in areas of small-scale roughness. Community ice trails are largely insensitive to roughness scales smaller than L-band wavelengths, making sensors like ALOS PALSAR more valuable SAR tools for such applications. X-band may be more appropriate for identification of potential aircraft landing strips where even cm-scale roughness can be critical unless smoothed by snow [*Haas and Druckenmiller*, 2010]. An added benefit of X-band is its higher spatial resolution, enabling identification of narrow passageways between ridged areas. X-band backscatter is also able

to better distinguish between roughness such as rubble close to shore (lower backscatter) versus ridges further offshore (higher backscatter).

SAR product grid size may impact the extent of multi-look acquisition and processing of scenes at full resolution. For the comparison in *Section 3.3.5* we undersampled all X-band data to the coarser 10 m x 10 m grid. Low-cost paths calculated for X-band on this coarse grid differ little from routes derived for a 2.75 m x 2.75 m grid, suggesting low sensitivity of this approach to grid size.

3.5.3 Cost assignment

It is apparent that calculations of optimal ice trails depend heavily on the cost assigned to individual ice types. Costs estimated in this study are based on a heuristic approach that takes into consideration differences between ice road or trail uses and is informed by cost assessments in other settings. Cost elements such as construction effort, time, workload, and safety were considered. More accurate cost estimates reflecting local conditions could be obtained through Monte Carlo simulations. Routes predicted for a large ensemble of trails with slightly altered cost values will provide estimates of the sensitivity of trail routing on cost models and help arrive at appropriate cost functions that reflect the full set of constraints governing trail or ice road construction and use. For such an approach, a larger validation dataset can help identify biases in road or trail routes based on factors other than roughness.

We have compared calculated low-cost trails with actual trails to evaluate the methodology, assuming that the actual trail is an efficient route. However, more efficient routes may exist. This could be due to (1) routing priorities other than roughness avoidance, such as ice stability, proximity to town etc., and (2) the trail building crew not being able to fully assess the roughness in alternate areas. Ideally, different trail priorities should be separated to enable trail optimization for different cost combinations, such as cost effectiveness or safety. Separating the cost functions would also allow for considering only relevant costs in a

specific scenario, which is important when expanding this approach to different modes of transportation or ice use scenarios.

3.5.4 Additional trafficability analysis constraints

As outlined in *Section 3.3.3*, trafficability has been calculated utilizing a set amount of existing ice trails that are located within the area covered by remote sensing data. For the interferometric data and analysis in particular, this corresponds to a small number of trail segments. Consequently, trafficability calculations drawing on the PDFs shown in Figure 3.11 are constrained by a comparatively small set of source data. Nevertheless, even for a low number of trail segments, the method appears to perform well, capturing actual trafficability as well as predicting optimal trails (Figure 3.13 a and b). This statistical approach to calculate trafficability will be further improved as more remote sensing datasets become available and future trails are mapped.

Sea ice travel greatly depends on the presence of snow and in some communities, ice travel often has to wait until after snowfall [*Fienup-Riordan and Rearden*, 2010]. Snow greatly affects the trafficability of rubble and ridged ice leading to some of the discrepancies between actual and predicted optimal trails in this analysis. For instance, for the first section of trail B, none of the IT or IS followed the actual trail, but chose the shortest path out of this area of low trafficability. This area was close to non-trafficable early in the season, but by the time the trail was made, snow covered the rubble to such a degree as to allow effortless traversing. SAR signals are not significantly affected by the presence of snow, such that the impact of snow cover on changing inherent ice roughness and trafficability is more difficult to estimate in regions where this is of relevance.

There are, however, methods that can help account for snow cover in the T_{IPX} estimates. The rubble field at the start of trail B appears with variable height in the IDEM (not shown) resulting in lower than 0.5 trafficability calculated from the interferometric height (Figure 3.11b), but if the relative elevation were reduced by 20 cm (approximate snow depth) the majority of the area would exhibit a trafficability above 0.5 and hence contribute to higher

rather than lower trafficability scores. With evidence for substantial snowfall, e.g., from time series of automated snow depth measurements (such as available at Utqiaġvik), one possibility is to classify heights below a snow-depth dependent threshold as trafficable. Snow cover also inevitably impacts the roughness calculations in Figure 3.10a and b since SfM does not penetrate the snow like SAR does.

3.5.5 Potential for UAS-based trafficability analysis

In addition to acquiring a UAS-based SfM-derived DEM for SAR validation purposes, we also explored the possibility for UAS surveys in support of ice use. Leading up to the trail construction season in Utqiaġvik, we communicated with community leaders and members of the Barrow Whaling Captains Association to determine what scientific efforts could aid trail construction and safety on the ice. We found a general community interest in products that could determine ice roughness and associated support for surveying a relevant section of very rough sea ice around trail construction efforts. On 11 April 2015, we set up a UAS launch site on the side of a trail (Figure 3.1) by what was at the time the current trail endpoint. We then launched (Figure 3.14a) and surveyed the ice immediately ahead of the construction crews (Figure 3.14b). Within 24 hours, we returned to the trail and presented crewmembers with a digital elevation model and orthorectified image mosaic processed in the field (Figure 3.14c). The map highlighted large ridges in red and allowed for identification of important features for crewmembers to avoid such as a refrozen lead (Figure 14d), where fractures may occur (Eugene Brower, 2015, personal communication). The final trail ended up steering clear of some of the most severe roughness and the refrozen lead (purple dots in Figure 3.14d).

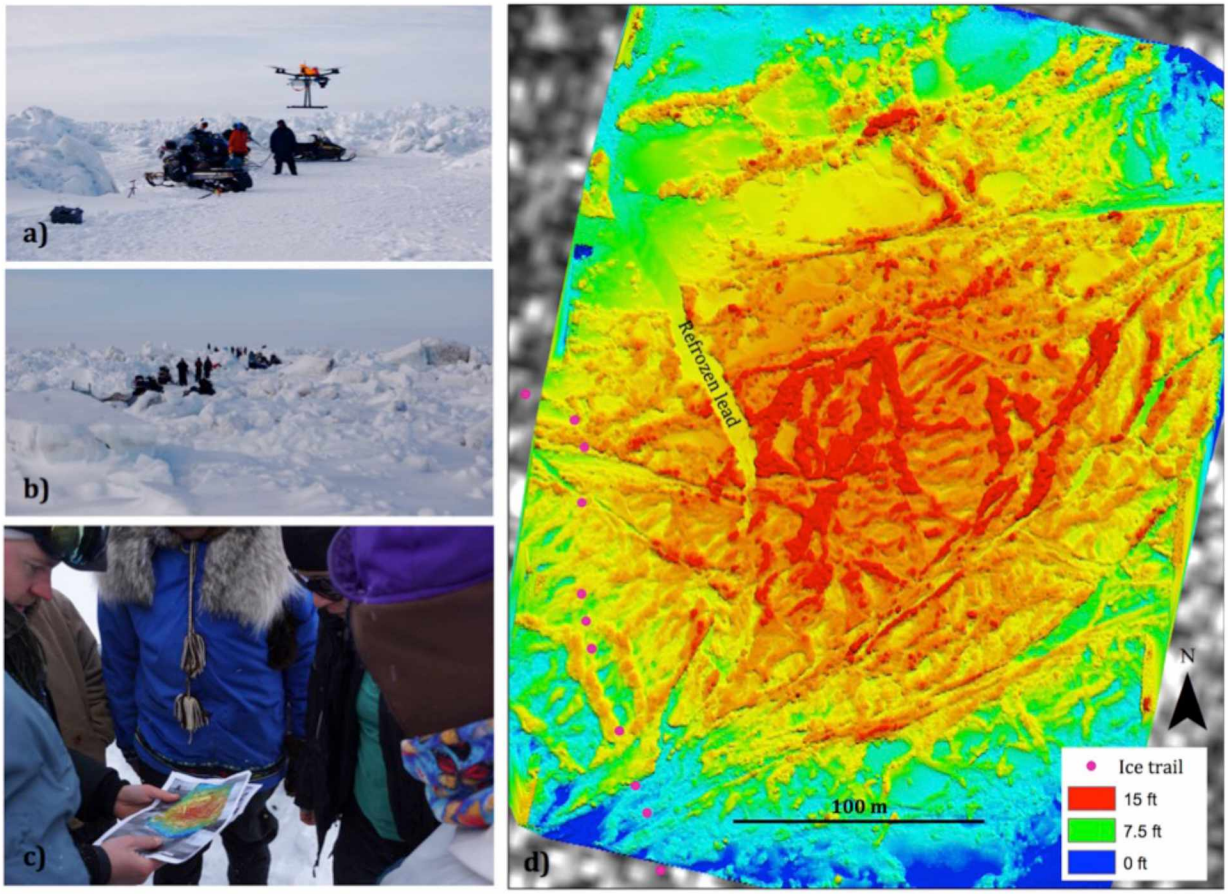

Figure 3.14 (a) Launching hexacopter UAS next to trail surveying crews 11 April 2015. (b) Crew members on the ice trail observing the UAS flying overhead. (c) Discussion of data products out on the trail with crewmembers. (d) DEM product shared with community members working on ice trail on 12 April 2015. Green colors represent medium topography (roughly 2 m) while red indicates topography up to roughly 5 m. Scale bar is in feet to conform with local use.

The potential of UAS-based tactical surveying and trafficability analysis through SfM became clear through this work. Following is a selection of some of the findings arrived at throughout the survey effort:

1) UAS-based systems, such as the hexacopter used here have a lower impact visually and in terms of noise than airplanes, hence result in reduce disturbance of marine mammals and subsistence activities.

2) Extreme Arctic conditions can create narrow operating windows for operations posing a challenge to operational use. We found it difficult to operate UASs at temperatures below roughly –20 ˚C at which point finger dexterity for the controller becomes reduced. Also, the hexacopter with its full payload was only able to operate up to roughly 5 m s^{-1} winds, reducing the operating window.
3) By using the described hexacopter we were able to demonstrate the potential of using a UAS-based surveying approach, but a fixed-wing UAS is needed to survey the roughly 30 km coastline used for trail construction. A fixed-wing system may also reduce the concerns in (2).
4) The way we displayed the DEM (Figure 3.14d) was not optimal for effectively communicating ice topography to the local population and more work needs to be done to explore best practices for visualizations presented to community members.
5) Long-term impacts of use of UAS in subsistence areas needs to be considered such as direct and indirect consequences on subsistence activities including its cultural and educational components.

3.6 Conclusions

This work represents one of the first studies of sea ice trafficability using remotely sensed data drawing upon multiple methods developed within the last decade or two decades, but which have not been applied to sea ice. The acquisition of high resolution imagery using UAS allowed us to both evaluate Structure-from-Motion (SfM) over sea ice and validate other approaches such as SAR polarimetry and interferometry. We demonstrate here that cm-scale SfM is capable of distinguishing between different types of roughness relating to ice trafficability. Also, SfM has provided a deeper understanding of relevant polarimetric scattering mechanisms and improved discrimination between different roughness classes that are unique in the classification scheme. We have demonstrated that roughness, from a trafficability perspective, can be assessed from SAR data alone. A combination of interferometry, polarimetry, and the backscatter coefficient provides an optimal assessment

of trafficability through an evaluation of both scattering mechanisms and surface height of the scattering medium.

The combination of remote sensing data and ice trail surveys supported the development of a trafficability index and calculation of optimal travel routes. This method is most accurate when including bistatic interferometry to assess ridge heights. However, backscatter data alone has shown promise as a tool to assess trafficability. These findings suggest that large-scale assessments of landfast ice trafficability at pan-Arctic scales are possible due to the wide availability of SAR backscatter cross-section data. A large-scale or pan-Arctic assessment of trafficability and analysis of how trafficability has changed over the last decade can potentially lead to important new insight into the effects of climate change on both communities and industry. Large-scale assessments may improve ice route selection making ice travel more cost effective and possibly counter negative effects of rougher ice and a shorter landfast ice season.

In this study, we defined trafficability as the efficiency and required resources of traveling across ice, which mostly depends on surface conditions. However, trafficability can also be defined more broadly incorporating elements related to safety as well as a larger set of objectives for travel. It is likely that applying an additional set of remote sensing techniques to construct a trafficability assessment could accommodate a broader trafficability definition. Also, it is clear here that an important aspect of trafficability is not only the general roughness of the ice cover, but perhaps more importantly the presence and connectivity of smooth trafficable areas. An important next step will be to develop a metric for this connectivity and determine how it links to overall trafficability.

Optimal travel routes depend on the mode of transportation and priorities with respect to path length versus roughness types. More work needs to be done to understand the exact specifications of different modes of transportation and their limitations in terms of ice roughness. The strategy outlined in this paper, utilizing multiple remote sensing products to approach a trafficability assessment, does not limit itself to sea ice, but can potentially be utilized on any surface and mode of transportation.

3.7 Acknowledgements

This work was supported by the National Science Foundation (Seasonal Ice Zone Observing Network, NSF-0856867) and the Alaska Center for UAS Integration (ACUASI). We would like to thank the community of Utqiaġvik and the Barrow Whaling Captains Association for their generosity allowing UAS flights in subsistence hunting areas. A special thanks to whaling captain Harry Brower Jr. who provided valuable guidance during planning and execution of the UAS mission surveying his crew's trail. We thank the North Slope Borough Department of Wildlife Management for guidance and in-kind support and acknowledge UIC Science for providing logistic support making this project possible. We would like to thank Peter Hickman at the Geographical Network Of Alaska for programming support. A great thank you to Jeremy Nicoll at the Alaska Satellite Facility for guidance relating to polarimetric analysis. Satellite data was generously provided by the Japanese Space Agency JAXA through a data grant (ALOS PI 1493), the Alaska Satellite Facility, and by the German Aerospace Center (DLR) (TanDEM-X and TerraSAR-X) through science proposals (COA_1987 and XTI_GLAC6921).

3.8 References

Abdalati, W., H. J. Zwally, R. Bindschadler, B. Csatho, S. L. Farrell, H. A. Fricker, D. Harding, R. Kwok, M. Lefsky, and T. Markus (2010), The ICESat-2 laser altimetry mission, *Proceedings of the IEEE*, *98*(5), 735-751.

AMAP (2011), Snow, water, ice and permafrost in the Arctic (SWIPA): Climate Change and the Cryosphere, *Rep.*, xii + 538 pp, Oslo, Norway.

Aporta, C. (2004), Routes, trails and tracks: Trail breaking among the Inuit of Igloolik, *Études/Inuit/Studies*, *28*(2), 9-38.

Aporta, C. (2009), The trail as home: Inuit and their pan-Arctic network of routes, *Hum Ecol*, *37*(2), 131-146.

Aporta, C. (2011), Shifting perspectives on shifting ice: documenting and representing Inuit use of the sea ice, *The Canadian Geographer/Le Géographe canadien*, *55*(1), 6-19, doi: 10.1111/J.1541-0064.2010.00340.X.

Aporta, C., and E. Higgs (2005), Satellite culture - Global positioning systems, inuit wayfinding, and the need for a new account of technology, *Curr Anthropol*, *46*(5), 729-753, doi: 10.1086/432651.

Bamler, R., and P. Hartl (1998), Synthetic aperture radar interferometry, *Inverse problems*, *14*(4), R1.

Barker, A., G. Timco, and B. Wright (2006), Traversing grounded rubble fields by foot—Implications for evacuation, *Cold Reg Sci Technol*, *46*(2), 79-99.

Bashaw, E. K., J. Drage, S. K. Lewis, and C. Billings (2013), Applied Ice Engineering for Exploring Arctic Natural Resources, paper presented at ISCORD 2013@ sPlanning for Sustainable Cold Regions, ASCE.

Bell, T., R. Briggs, R. Bachmayer, and S. Li (2014), Augmenting Inuit knowledge for safe sea-ice travel—The SmartICE information system, paper presented at 2014 Oceans-St. John's, IEEE.

Brewster, K. (2016), Northern Alaska Sea Ice Project Jukebox, edited by K. Brewster, University of Alaska Fairbanks Oral History Program.

Chen, Y. (2013), New approaches for calculating Moran's index of spatial autocorrelation, *Plos One*, *8*(7), e68336.

Cloude, S. R., and E. Pottier (1996), A review of target decomposition theorems in radar polarimetry, *Geoscience and Remote Sensing, IEEE Transactions on*, *34*(2), 498-518.

Comiso, J. C., and D. K. Hall (2014), Climate trends in the Arctic as observed from space, *Wiley Interdisciplinary Reviews: Climate Change*, *5*(3), 389-409.

Dammann, D. O., H. Eicken, F. Meyer, and A. Mahoney (2016), Assessing small-scale deformation and stability of landfast sea ice on seasonal timescales through L-band SAR interferometry and inverse modeling, *Remote Sens Environ*, *187*, 492-504, doi: 10.1016/j.rse.2016.10.032.

Dammann, D. O., H. Eicken, A. Mahoney, F. Meyer, and S. Betcher (in preparation), Sea ice trafficability - new strategies for a changing icescape, *Polar Geography*.

Dammert, P. B. G., M. Lepparanta, and J. Askne (1998), SAR interferometry over Baltic Sea ice, *Int J Remote Sens*, *19*(16), 3019-3037, doi: Doi 10.1080/014311698214163.

Dierking, W., H. Skriver, and P. Gudmandsen (2003), SAR polarimetry for sea ice classification, paper presented at Applications of SAR Polarimetry and Polarimetric Interferometry.

Druckenmiller, M. L. (2011), *Alaska shorefast ice: interfacing geophysics with local sea ice knowledge and use, Doctoral thesis*, 210 pp., University of Alaska Fairbanks, Fairbanks, Alaska.

Druckenmiller, M. L., H. Eicken, J. C. George, and L. Brower (2010), Assessing the shorefast ice: Iñupiat whaling trails off Barrow, Alaska, in *SIKU: Knowing our ice*, 203-228, Springer.

Druckenmiller, M. L., H. Eicken, J. C. George, and L. Brower (2013), Trails to the whale: reflections of change and choice on an Iñupiat icescape at Barrow, Alaska, *Polar Geography*, *36*(1-2), 5-29, doi: 10.1080/1088937X.2012.724459.

Eicken, H., and A. Lovecraft (2011), Planning for northern futures: Lessons from socialecological change in the Alaska Region, edited, pp. 681Á700 (Fairbanks: University of Alaska Press).

Eicken, H., A. L. Lovecraft, and M. L. Druckenmiller (2009), Sea-Ice System Services: A Framework to Help Identify and Meet Information Needs Relevant for Arctic Observing Networks, *Arctic*, *62*(2), 119-136.

Eicken, H., B. Forbes, and H. Wiggins (2011a), State of the Arctic conference 2010: international perspectives on progress of research responsive to decision-makers' information needs, *Ambio*, *40*(7), 824-827.

Eicken, H., T. Grenfell, D. Perovich, J. Richter-Menge, and K. Frey (2004), Hydraulic controls of summer Arctic pack ice albedo, *Journal of Geophysical Research: Oceans*, *109*(C8).

Eicken, H., J. Jones, F. Meyer, A. Mahoney, M. L. Druckenmiller, M. Rohith, and C. Kambhamettu (2011b), Environmental security in Arctic ice-covered seas: from strategy to tactics of hazard identification and emergency response, *Mar Technol Soc J*, *45*(3), 37-48, doi: doi.org/10.4031/MTSJ.45.3.1.

Eicken, H., M. Kaufman, I. Krupnik, P. Pulsifer, L. Apangalook, P. Apangalook, W. Weyapuk JR, and J. Leavitt (2014), A framework and database for community sea ice observations in

a changing Arctic: An Alaskan prototype for multiple users, *Polar Geography*, *37*(1), 5-27, doi: 10.1080/1088937X.2013.873090.

Eltoft, T., J. Grahn, A. Doulgeris, C. Brekke, L. Ferro-Famil, and B. Holt (2013), Multi-frequency polarimetric analysis of sea ice, paper presented at Synthetic Aperture Radar (APSAR), 2013 Asia-Pacific Conference on, IEEE.

Ferretti, A., A. Monti-Guarnieri, C. Prati, F. Rocca, and D. Massonet (2007), InSAR Principles-Guidelines for SAR Interferometry Processing and Interpretation, *ESA Publications*, *TM-19*.

Fienup-Riordan, A., and A. Rearden (2010), The ice is always changing: Yup'ik understandings of sea ice, past and present, in *SIKU: knowing Our Ice: Documenting Inuit Sea Ice knowledge and Use*, Igor Krupnik, Claudio Aporta, Shari Gearheard, Gita Laidler and Lene Kielsen Holm, 295-320, Springer, New York.

Filhol, S., and M. Sturm (2015), Snow bedforms: A review, new data, and a formation model, *Journal of Geophysical Research: Earth Surface*, *120*(9), 1645-1669.

Fonstad, M. A., J. T. Dietrich, B. C. Courville, J. L. Jensen, and P. E. Carbonneau (2013), Topographic structure from motion: a new development in photogrammetric measurement, *Earth Surface Processes and Landforms*, *38*(4), 421-430.

Ford, J. D., T. Pearce, J. Gilligan, B. Smit, and J. Oakes (2008), Climate change and hazards associated with ice use in northern Canada, *Arctic, Antarctic, and Alpine Research*, *40*(4), 647-659.

Freeman, A., and S. L. Durden (1998), A three-component scattering model for polarimetric SAR data, *Geoscience and Remote Sensing, IEEE Transactions on*, *36*(3), 963-973.

Gearheard, S., G. Aipellee, and K. O'Keefe (2010), The Igliniit project: Combining Inuit knowledge and geomatics engineering to develop a new observation tool for hunters, in *SIKU: Knowing Our Ice*, 181-202, Springer.

George, J. C., H. P. Huntington, K. Brewster, H. Eicken, D. W. Norton, and R. Glenn (2004), Observations on shorefast ice dynamics in Arctic Alaska and the responses of the Iñupiat hunting community, *Arctic*, *57*(4), 363-374.

Haas, C., and M. Druckenmiller (2010), Ice thickness and roughness measurements, in *Field Techniques for Sea Ice Research*, Hajo Eicken and Maya Salganek, 49-116, University of Alaska Press, Fairbanks, Alaska.

Hopkins, M. A., J. Tuhkuri, and M. Lensu (1999), Rafting and ridging of thin ice sheets, *Journal of Geophysical Research: Oceans*, *104*(C6), 13605-13613.

Huntington, H. P., and S. Fox (2005), The changing Arctic: indigenous perspectives, in *Arctic Climate Impact Assessment*, C Symon, L Arris and B Heal, 61–98, Cambridge University Press, New York, NY.

Jaervik, M. (2006), Road on the sea, paper presented at PIARC XII INTERNATIONAL WINTER ROADS CONGRESS, TORINO-SESTRIERE, ITALY, 2006.

Jones, J. M., H. Eicken, A. R. Mahoney, M. V. Rohith, C. Kambhamettu, Y. Fukamachi, K. I. Ohshima, and J. C. George (2016), Landfast sea ice breakouts: Stabilizing ice features, oceanic and atmospheric forcing at Barrow, Alaska, *Continental Shelf Research*, *126*(50-63), doi: 10.1016/j.csr.2016.07.015.

Kim, J.-W., D.-j. Kim, and B. J. Hwang (2012), Characterization of Arctic Sea ice thickness using high-resolution spaceborne polarimetric SAR data, *Geoscience and Remote Sensing, IEEE Transactions on*, *50*(1), 13-22.

Koenderink, J. J., and A. J. Van Doorn (1991), Affine structure from motion, *JOSA A*, *8*(2), 377-385.

Krieger, A. G., G. N. Kidd, and D. A. Cocking (2003), Northstar Drilling-Delivering the First Arctic Offshore Development, *SPE drilling & completion*, *18*(02), 188-193.

Kwok, R., G. Spreen, and S. Pang (2013), Arctic sea ice circulation and drift speed: Decadal trends and ocean currents, *Journal of Geophysical Research: Oceans*, *118*(5), 2408-2425.

Laidler, G. J., P. Elee, T. Ikummaq, E. Joamie, and C. Aporta (2010), Mapping Inuit sea ice knowledge, use, and change in Nunavut, Canada (Cape Dorset, Igloolik, Pangnirtung), in *SIKU: knowing Our Ice: Documenting Inuit Sea Ice knowledge and Use*, Igor Krupnik, Claudio Aporta, Shari Gearheard, Gita Laidler and Lene Kielsen Holm, 45-80, Springer.

Laidler, G. J., T. Hirose, M. Kapfer, T. Ikummaq, E. Joamie, and P. Elee (2011), Evaluating the Floe Edge Service: how well can SAR imagery address Inuit community concerns around sea ice change and travel safety?, *The Canadian Geographer/Le Géographe canadien*, *55*(1), 91-107.

Laidler, G. J., J. D. Ford, W. A. Gough, T. Ikummaq, A. S. Gagnon, S. Kowal, K. Qrunnut, and C. Irngaut (2009), Travelling and hunting in a changing Arctic: assessing Inuit vulnerability to sea ice change in Igloolik, Nunavut, *Climatic change*, *94*(3-4), 363-397.

Lang, O., J. Anderssohn, P. Lumsdon, and K. Partington (2013), Single pass bistatic interferometry for sea ice build-up around offshore structures, paper presented at 4th TanDEM-X Science Team Meeting, Oberpfaffenhofen, Germany.

Lee, J., and S. Li (2016), Extending Moran's Index for Measuring Spatiotemporal Clustering of Geographic Events, *Geographical Analysis*.

Lee, J.-S., and M. R. Grunes (1992), Classification of multi-look polarimetric SAR data based on complex Wishart distribution, paper presented at Telesystems Conference, 1992. NTC-92., National, IEEE.

Lee, J.-S., and E. Pottier (2009), *Polarimetric radar imaging: from basics to applications*, CRC press.

Lee, J.-S., M. R. Grunes, and R. Kwok (1994), Classification of multi-look polarimetric SAR imagery based on complex Wishart distribution, *Int J Remote Sens*, *15*(11), 2299-2311.

Lee, J.-S., M. R. Grunes, and G. De Grandi (1999a), Polarimetric SAR speckle filtering and its implication for classification, *Geoscience and Remote Sensing, IEEE Transactions on*, *37*(5), 2363-2373.

Lee, J.-S., M. Grunes, T. Ainsworth, L. Du, D. Schuler, and S. Cloude (1998), Unsupervised classification using polarimetric decomposition and complex Wishart classifier, paper presented at Geoscience and Remote Sensing Symposium Proceedings, 1998. IGARSS'98. 1998 IEEE International, IEEE.

Lee, J.-S., M. R. Grunes, T. L. Ainsworth, L.-J. Du, D. L. Schuler, and S. R. Cloude (1999b), Unsupervised classification using polarimetric decomposition and the complex Wishart classifier, *Geoscience and Remote Sensing, IEEE Transactions on*, *37*(5), 2249-2258.

Li, S., L. Shapiro, L. McNutt, and A. Feffers (1996), Application of Satellite Radar Interferometry to the Detection of Sea Ice Deformation, *Journal of the Remote Sensing Society of Japan*, *16*(2), 67-77.

Liu, C., J. Chao, W. Gu, L. Li, and Y. Xu (2014), On the surface roughness characteristics of the land fast sea-ice in the Bohai Sea, *Acta Oceanologica Sinica*, *33*(7), 97-106.

Mahoney, A., H. Eicken, and L. Shapiro (2007), How fast is landfast sea ice? A study of the attachment and detachment of nearshore ice at Barrow, Alaska, *Cold Reg Sci Technol*, *47*(3), 233-255, doi: 10.1016/J.Coldregions.2006.09.005.

Mahoney, A., H. Eicken, A. G. Gaylord, and R. Gens (2014), Landfast sea ice extent in the Chukchi and Beaufort Seas: The annual cycle and decadal variability, *Cold Reg Sci Technol*, *103*, 41-56, doi: 10.1016/J.Coldregions.2014.03.003.

Mahoney, A., D. O. Dammann, M. A. Johnson, H. Eicken, and F. J. Meyer (2016), Measurement and imaging of infragravity waves in sea ice using InSAR, *Geophys Res Lett*, *43*, 6383–6392.

Manninen, A. (1997), Surface roughness of Baltic sea ice, *Journal of Geophysical Research: Oceans*, *102*(C1), 1119-1139.

Meier, W. N., G. K. Hovelsrud, B. E. Oort, J. R. Key, K. M. Kovacs, C. Michel, C. Haas, M. A. Granskog, S. Gerland, and D. K. Perovich (2014), Arctic sea ice in transformation: A review of recent observed changes and impacts on biology and human activity, *Reviews of Geophysics*, *52*(3), 185-217.

Mesher, D., S. Proskin, and E. Madsen (2008), Ice road assessment, modeling and management, paper presented at 7th International Conference on Managing Pavement Assets, Calgary, AB, June, 2008.

Meyer, F. J., A. R. Mahoney, H. Eicken, C. L. Denny, H. C. Druckenmiller, and S. Hendricks (2011), Mapping arctic landfast ice extent using L-band synthetic aperture radar interferometry, *Remote Sens Environ*, *115*(12), 3029-3043, doi: 10.1016/J.Rse.2011.06.006.

Moen, M., A. Doulgeris, S. Anfinsen, A. Renner, N. Hughes, S. Gerland, and T. Eltoft (2013), Comparison of automatic segmentation of full polarimetric SAR sea ice images with manually drawn ice charts, *Cryosphere Discuss*, *7*(3), 2595-2634.

Moran, P. A. (1950), Notes on continuous stochastic phenomena, *Biometrika*, *37*(1/2), 17-23.

Morris, K., S. Li, and M. Jeffries (1999), Meso-and microscale sea-ice motion in the East Siberian Sea as determined from ERS-I SAR data, *Journal of Glaciology*, *45*(150), 370-383.

Nakamura, K., H. Wakabayashi, K. Naoki, F. Nishio, T. Moriyama, and S. Uratsuka (2005), Observation of sea-ice thickness in the Sea of Okhotsk by using dual-frequency and fully polarimetric airborne SAR (Pi-SAR) data, *Geoscience and Remote Sensing, IEEE Transactions on*, *43*(11), 2460-2469.

Nolan, M., C. Larsen, and M. Sturm (2015), Mapping snow-depth from manned-aircraft on landscape scales at centimeter resolution using Structure-from-Motion photogrammetry, *The Cryosphere Discussions*, *9*, 333-381.

Nuttall, M., F. Berkes, B. Forbes, G. Kofinas, T. Vlassova, and G. Wenzel (2005), Hunting, herding, fishing and gathering: indigenous peoples and renewable resource use in the Arctic, *Arctic climate impact assessment*, 649-690.

Ohshima, K. I. (2000), Effect of landfast sea ice on coastal currents driven by the wind, *Journal of Geophysical Research: Oceans*, *105*(C7), 17133-17141.

Ouarzeddine, M., B. Souissi, and A. Belhadj-Aissa (2007), Unsupervised classification using Wishart classifier, paper presented at Frascati: Proceedings of PolInSAR Workshop.

Potter, R., J. Walden, and R. Haspel (1981), Design and construction of sea ice roads in the Alaskan Beaufort Sea, paper presented at Offshore Technology Conference, Offshore Technology Conference, Houston, Texas.

Pottier, E., and J.-S. Lee (2000), Application of the «H/A/alpha» polarimetric decomposition theorem for unsupervised classification of fully polarimetric SAR data based on the wishart distribution, paper presented at SAR workshop: CEOS Committee on Earth Observation Satellites.

Rampal, P., J. Weiss, and D. Marsan (2009), Positive trend in the mean speed and deformation rate of Arctic sea ice, 1979–2007, *Journal of Geophysical Research: Oceans*, *114*(C5).

Rivas, M. B., J. A. Maslanik, J. G. Sonntag, and P. Axelrad (2006), Sea ice roughness from airborne LIDAR profiles, *IEEE Transactions on Geoscience and Remote Sensing*, *44*(11), 3032-3037.

Rothrock, D. A., D. B. Percival, and M. Wensnahan (2008), The decline in arctic sea-ice thickness: Separating the spatial, annual, and interannual variability in a quarter century of submarine data, *J Geophys Res-Oceans*, *113*(C5), doi: 10.1029/2007jc004252.

Scheiber, R., F. De Zan, P. Prats, L. S. A. Araújo, M. Künemund, and L. Marotti (2011), Interferometric sea ice mapping with TanDEM-X: First experiments, paper presented at Geoscience and Remote Sensing Symposium (IGARSS), 2011 IEEE International, IEEE.

Scheuchl, B., R. Caves, I. Cumming, and G. Staples (2001a), H/A/α-based classification of sea ice using SAR polarimetry, paper presented at Proceedings of the 23rd Canadian Symposium on Remote Sensing.

Scheuchl, B., R. Caves, I. Cumming, and G. Staples (2001b), Automated sea ice classification using spaceborne polarimetric SAR data, paper presented at Geoscience and Remote Sensing Symposium, 2001. IGARSS'01. IEEE 2001 International, IEEE.

Selyuzhenok, V., T. Krumpen, A. Mahoney, M. Janout, and R. Gerdes (2015), Seasonal and interannual variability of fast ice extent in the southeastern Laptev Sea between 1999 and 2013, *Journal of Geophysical Research: Oceans*, *120*(12), 7791-7806.

Shean, D. E., O. Alexandrov, Z. M. Moratto, B. E. Smith, I. R. Joughin, C. Porter, and P. Morin (2016), An automated, open-source pipeline for mass production of digital elevation models (DEMs) from very-high-resolution commercial stereo satellite imagery, *ISPRS Journal of Photogrammetry and Remote Sensing*, *116*, 101-117.

Spencer, P., B. Graham, A. Barker, G. Timco, and B. Wright (2007), Construction aspects of building an evacuation route through rubble surrounding Beaufort Sea structures, *Recent Development of Offshore Engineering in Cold Regions, Yue (ed.)*, *2*, 823-832.

Spreen, G., R. Kwok, and D. Menemenlis (2011), Trends in Arctic sea ice drift and role of wind forcing: 1992–2009, *Geophys Res Lett*, *38*(19).

Stephenson, S. R., L. C. Smith, and J. A. Agnew (2011), Divergent long-term trajectories of human access to the Arctic, *Nat Clim Change*, *1*(3), 156-160, doi: 10.1038/Nclimate1120.

Stroeve, J. C., M. C. Serreze, M. M. Holland, J. E. Kay, J. Malanik, and A. P. Barrett (2012), The Arctic's rapidly shrinking sea ice cover: a research synthesis, *Climatic Change*, *110*(3-4), 1005-1027, doi: 10.1007/S10584-011-0101-1.

Tremblay, M., C. Furgal, V. Lafortune, C. Larrivée, J.-P. Savard, M. Barrett, T. Annanack, N. Enish, P. Tookalook, and B. Etidloie (2006), Communities and ice: Bringing together traditional and scientific knowledge, *Climate change: linking traditional and scientific knowledge*, 289.

Ulaby, F. T., and C. Elachi (1990), Radar polarimetry for geoscience applications, *Norwood, MA, Artech House, Inc., 1990, 376 p. No individual items are abstracted in this volume.*, *1*.

Wakabayashi, H., T. Matsuoka, K. Nakamura, and F. Nishio (2004), Polarimetric characteristics of sea ice in the Sea of Okhotsk observed by airborne L-band SAR, *Geoscience and Remote Sensing, IEEE Transactions on*, *42*(11), 2412-2425.

Wang, X., X. Cheng, F. Hui, C. Cheng, H. Fok, and Y. Liu (2014), Xuelong Navigation in Fast Ice Near the Zhongshan Station, Antarctica, *Mar Technol Soc J*, *48*(1), 84-91.

Wegmüller, U., C. Werner, M. Santoro, T. Strozzi, and A. Wiesmann (2009), ERS–ENVISAT TanDEM data over sea and shelf ice, paper presented at FRINGE2009 Workshop.

Westoby, M., J. Brasington, N. Glasser, M. Hambrey, and J. Reynolds (2012), 'Structure-from-Motion'photogrammetry: A low-cost, effective tool for geoscience applications, *Geomorphology*, *179*, 300-314.

Wilkinson, J. P., S. Hanson, N. E. Hughes, A. James, B. Jones, R. MacKinnon, S. Rysgaard, and L. Toudal (2011), Tradition and technology: Sea ice science on Inuit sleds, *Eos, Transactions American Geophysical Union*, *92*(1), 1-4.

WMO (2014), World Meteorological Organization Sea Ice Nomenclature in *No. 259 Volume 1 - Terminology and Codes*, edited by 5th Session of JCOMM Expert Team on Sea Ice.

Zhang, X., J. E. Walsh, J. Zhang, U. S. Bhatt, and M. Ikeda (2004), Climatology and interannual variability of Arctic cyclone activity: 1948-2002, *J Climate*, *17*(12), 2300-2317.

4 ASSESSING SMALL-SCALE DEFORMATION AND STABILITY OF LANDFAST ICE ON SEASONAL TIMESCALES THROUGH L-BAND SAR INTERFEROMETRY AND INVERSE MODELING*

4.1 Abstract

Rapid environmental change and increases in use of shorefast ice by industry and coastal communities highlight the need for an approach to accurately assess landfast sea-ice stability on seasonal timescales. While stability can sometimes be inferred from field measurements, current methods are lacking robustness and the ability to be automated and applied over large areas and long time scales to ensure safety and document change in the context of transportation, Indigenous ice uses and industrial development. This paper introduces an inverse model capable of reconstructing three-dimensional deformation fields from one-dimensional interferometric L-band Synthetic Aperture Radar (SAR) phase patterns. We apply this method at three landfast ice locations on the Alaska Beaufort Sea coast near Barrow and Prudhoe Bay. We find the small-scale displacements estimated from the model consistent with regional patterns of ice motion. Our study suggests that interferometry can provide planning and decision-support information for ice road development and structures operating within ice. Moreover, InSAR can potentially increase our understanding of sea ice on a fundamental level in terms of large-scale stability and long-term changes in ice dynamics.

* Dammann, D. O., H. Eicken, F. Meyer, and A. Mahoney (2016). Assessing small-scale deformation and stability of landfast sea ice on seasonal timescales through L-band SAR interferometry and inverse modeling. *Remote Sens Environ*, *187*, 492-504, doi: 10.1016/j.rse.2016.10.032.

4.2 Introduction

Arctic sea ice has undergone major rapid change in recent decades [*Comiso and Hall*, 2014; *Meier et al.*, 2014; *Stroeve et al.*, 2012] with potentially widespread, global consequences. Direct impacts of a changing sea-ice cover are expected along circumpolar coastlines where both communities and industry depend on coastal and landfast sea ice as a platform vital to Indigenous cultures, subsistence, transportation, and industrial development [*Eicken et al.*, 2009]. In Alaska, much of the landfast ice extent has also rapidly declined during the past decades [*Fienup-Riordan and Rearden*, 2010; *Mahoney et al.*, 2014].

A major concern for ice users from both communities and industry is ice movement, which can eventually lead to reduced load bearing capacity through fracturing or even destabilization of landfast ice [*BP*, 2013; *Eicken et al.*, 2011; *George et al.*, 2004; *Potter et al.*, 1981]. The use of ice by the oil and gas industry for transportation and as a platform for exploration and staging of equipment requires clear identification of potential hazards [*Eicken and Mahoney*, 2015; *Eicken et al.*, 2011] derived from small-scale displacements that may lead to cracks, wider openings or foster development of hazardous features such as strudel scour through later drainage through cracks [*Dickins et al.*, 2011].

Evaluations of ice safety based on simple threshold criteria, e.g., with respect to minimum thickness [*Finucane and Scher*, 1983; *USACE*, 2002] are not applicable with respect to ice stability. However, it is clearly recognized that ice roads should try to avoid areas of ice movement and rely on routes over stable ice [*Bashaw et al.*, 2013; *Potter et al.*, 1981]. The challenge for industrial use of sea ice as a platform is to make accurate measurements evaluating suitability and safety of the ice in a cost-effective and timely manner [*Mesher et al.*, 2008]. Moreover, information related to stability is often difficult to acquire and, due to the many factors that govern ice stability, typically requires measurements of the actual movement and deformation of the ice. Recent technological advances in satellite remote sensing set the stage for more thorough, quantitative and cost-effective alternatives to aerial reconnaissance often used to detect critical ice features [*Potter et al.*, 1981].

Synthetic aperture radar interferometry (InSAR) has shown promise as a technique to detect differential displacement in the landfast sea ice [*Dammert et al.*, 1998; *Meyer et al.*, 2011; *Morris et al.*, 1999; *Vincent et al.*, 2004] down to the millimeter-scale in areas with small-scale deformation (mm- to m-scale) and no active ridging deformation, wet precipitation, or significant melt or desalination processes, which will change the scattering processes. These prior InSAR studies over sea ice have all demonstrated the potential value of SAR interferometry in understanding ice dynamics with potential implications for stakeholders. However, there are clear limitations to interpreting the exact 3-d deformation due to preexisting ambiguities resulting from the 1-d phase information [*Li et al.*, 1996]. This study – to our knowledge the first to analyze interferogram fringe patterns over sea ice in a rigorous manner – aims to develop a method drawing on InSAR data that can be used to evaluate large-scale deformation patterns of the landfast ice and the source of the deformation. Although the application of InSAR may eventually be used to study deformation of mobile pack ice (e.g. *Mahoney et al.* [2016]) or identify precursors to hazardous events such as ice pile-ups or breakouts, we will here focus on long temporal baseline InSAR to identify regionally persistent deformation processes in landfast ice related to thermal changes, due to ice growth, and external factors such as regional sustained pack ice forcing.

The goal is to develop an approach that can be used to establish a climatology of ice deformation that can be used during planning and execution of on-ice operations, capable of providing guidance on (i) the type of deformation occurring in different regions, (ii) the point in time when the ice is sufficiently stable to significantly reduce risk, and (iii) areas experiencing deformation large enough for substantial cracking and requiring thorough risk assessment on the ground. This method would also create the foundation for a large-scale comparison between models and observations of landfast ice dynamics, a crucial step in validating landfast ice numerical models.

The ice regime evaluated in this study ranges from smooth to severely deformed during early to mid spring before the onset of melt. The absence of both melt and widespread severe deformation events (ridging or lateral deformation >10m) enables scatterers to stay intact enabling coherent interferogram formation. InSAR is first validated over sea ice as a

technique capable of identifying small-scale displacement within the landfast ice (*Section 4.2*). Then, a two-dimensional deformation field is produced from the one-dimensional phase measurements using an inverse model constrained to a canonical set of realistic strain mechanisms (*Section 4.3*), a technique that is then tested and validated in northern Alaska (*Section 4.4*). Model ambiguities and limitations are further discussed in *Section 4.5*.

4.3 L-band InSAR data for landfast ice analysis

4.3.1 Data

Synthetic aperture radar interferometry (InSAR) is a technique that measures phase differences between two SAR scenes acquired from two coherent viewing geometries [*Bamler and Hartl*, 1998; *Ferretti et al.*, 2007]. The observed phase difference can originate from displacement of the scattering surface if measurements were acquired at different times (non-zero temporal baselines) and/or from surface topography if measurements originate from slightly different vantage points (non-zero spatial baselines).

This study utilizes L-band PALSAR-1 Synthetic Aperture Radar (SAR) images acquired by the Japanese Advanced Land Observing Satellite-1 (ALOS-1). PALSAR-1 operated from 2006 – 2011 with a 46-day repeat cycle and in a typical year provided almost complete coverage of the northern Alaska coastline in a four-month period during the landfast ice season (Figure 4.1). Obtaining coherent interferograms is most likely during this time of year, when the surface of landfast ice is most stable and least affected by thermodynamic and dynamic processes. Interferograms can also often be obtained over landfast ice earlier and later in the spring as well, provided the ice remains stationary and there is no melting, flooding or other significant change at the surface. From all available data, this study selected a series of three interferograms for three areas along the North American Arctic coast including (1) the Alaska Beaufort Sea coast near Barrow, (2) Prudhoe Bay, and (3) Foggy Island Bay (Figure 4.1). Information about the SAR data used in this study is summarized in Table 4.1.

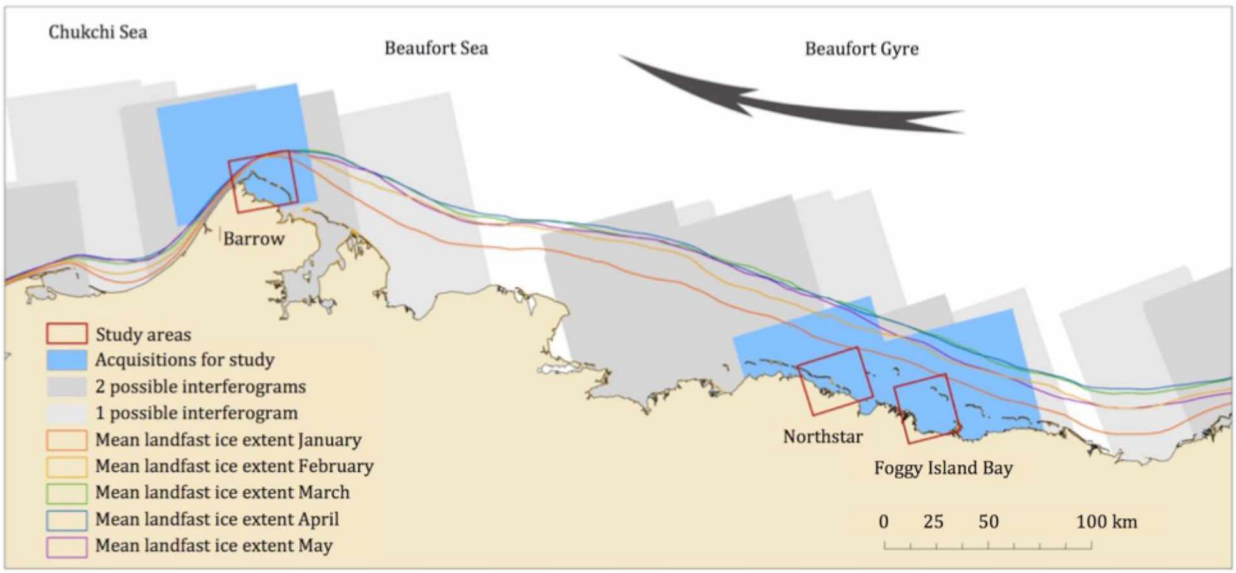

Figure 4.1 The areas covered by the three interferograms used in this study are shown in blue shading with the specific study areas outlined in red. The regional data availability of ALOS-I PALSAR-I in the middle of the landfast ice season (strictly within January–April 2010) is shown in gray. The spring monthly mean (1996-2008) landfast sea ice extent is indicated with colored lines [*Mahoney et al.*, 2014].

Table 4.1 Orbit and image data for the three interferograms used

Orbit #	**Frame**	**Dates**	**Resolution (m)**	**Perp. baseline (m)**	**Temporal baseline (d)**	**Location**
22132 22803	1410	03/21/2010 05/06/2010	Ra: 7.495 Az: 3.915	269	46	Prudhoe Bay
20907 21578	1430	12/27/2009 02/11/2010	Ra: 7.495 Az: 3.930	754	46	Barrow
22278 22949	1400	03/31/2010 05/16/2010	Ra: 7.495 Az: 4.385	325	46	Foggy Island Bay

All three acquisitions are covering areas within the landfast sea ice regime (outlined with colored lines in Figure 4.1). The likelihood of substantial movement (i.e., on the order of a few decimeters to several meters) leading to defects, destabilization or full-scale breakouts, depends on the overall stability of the ice cover. Typically, stability is defined as the ability

of shorefast ice to remain immobile and undeformed under the action of atmosphere, ocean, or ice forcing. Depending on the region, ice stability depends on a combination of the anchoring strength imparted by grounded ridges and/or topographic features such as islands or promontories, as well as on ice thickness, structure, and the presence of defects such as pre-existing cracks [*Mahoney et al.*, 2007].

A typical landfast sea ice regime is illustrated in Figure 4.2 where the stability decreases going from left to right. The most stable ice is the ice frozen to the ground (bottomfast), which is nearly completely stationary. Small-scale non-elastic deformation of lagoon ice or ice sheltered by islands from dynamic forcing is dominated by thermal creep and cracking. Shoreward of grounded ridges, deformation is also governed largely by thermal forcing, but can also be impacted by ice dynamics. Oceanward of any grounding points, the ice is more susceptible to dynamic forcing and the propagating forces from pack ice interaction and is hence less stable (especially younger and thinner ice). Except for the bottomfast ice, even sheltered ice can move several centimeters during a month and therefore exhibits interferometric fringes.

This study focuses on deformation processes in the stable landfast ice zone, which are largely driven by thermal processes (e.g., ice growth, thermal contraction) or moderate dynamic deformation (e.g., wind-generated deformation behind grounding points, internal ice stress generated by pack ice interaction propagating into the stable ice zone) occurring over long time-scales and benefit from a large temporal InSAR baseline. By applying a shorter temporal baseline, the methods used in this study can potentially be extended to the pack ice, where the ice is susceptible to dynamic ridging and rafting events and wave propagation [*Mahoney et al.*, 2016], but such analysis is beyond the scope of this study.

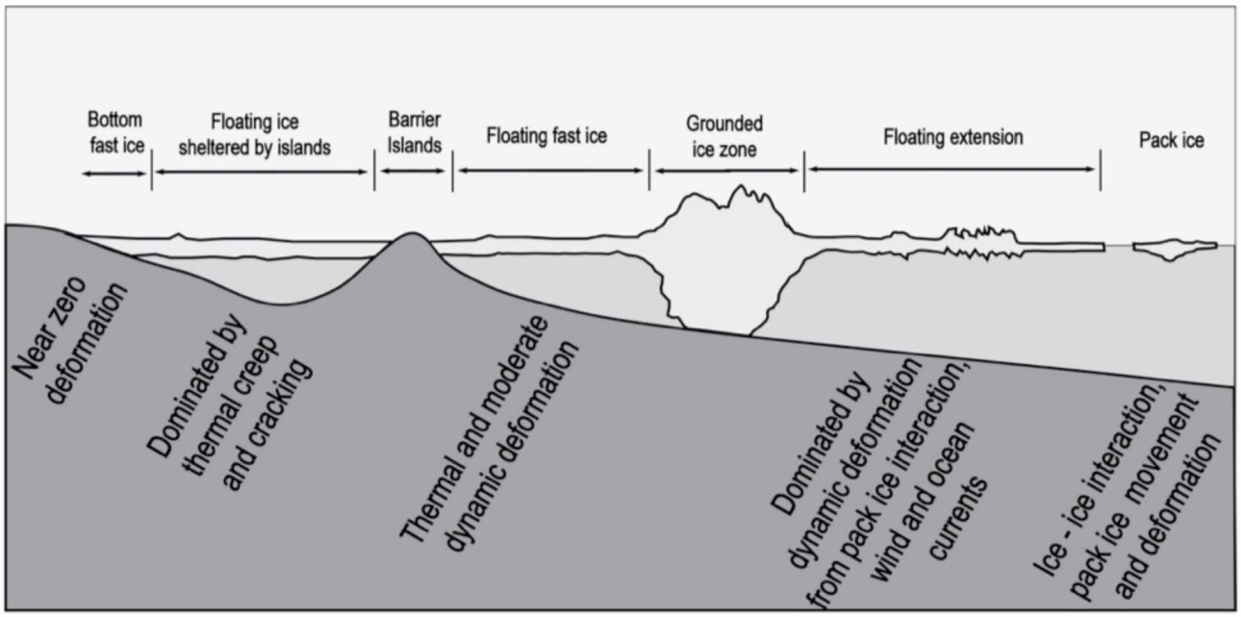

Figure 4.2 Example of landfast sea ice where different regimes possess different levels of stability.

4.3.2 InSAR processing

Interferograms in this study are constructed using a general processing workflow outlined in Figure 4.3. The multi-looked interferograms are sampled 2 and 4 pixels in slant range and azimuth respectively. Multi-looking results in pixel spacings of ~15.2m and ~ 12.5m in ground range and azimuth, respectively. All acquisitions are from ascending passes. Sea ice interferograms are complicated to interpret due to the many discrete floes that can move in multiple directions. This is also true for landfast ice where the floes are frozen together, but can still behave as mechanically discrete units. The spatial discontinuities occurring between acquisitions as well as noise can make phase unwrapping of sea ice difficult [*Morris et al.*, 1999] and we choose to not focus on this processing step since we are mostly interested in the identification of relative displacement in this study. Terrain correction is typically superfluous since the highest ridge features rarely exceed 10m. For example, for PALSAR to receive a phase signal larger than the expected phase noise from a large ridge, the perpendicular baseline would have to be close to 2km, far greater than the baselines that are

used in this study and are listed in Table 4.1 (see *Section 4.2.4* for more detailed information regarding topographic influence on fringes).

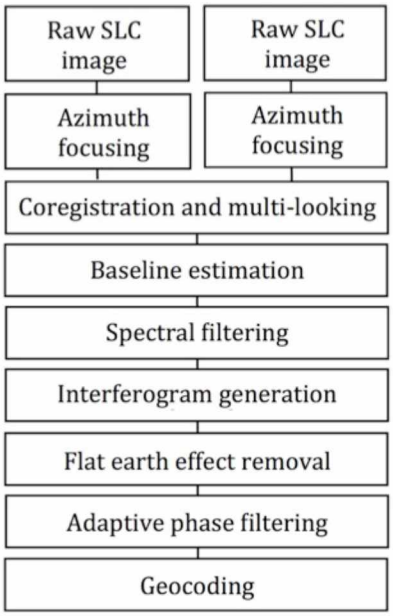

Figure 4.3 Interferogram workflow outlining steps from two raw single-look complex (SLC) images to a geocoded interferogram.

4.3.3 L-band SAR interferometry and coherence over sea ice

Derivation of image-pair coherence is an integral part of the InSAR processing flow and can provide valuable information about changes on the Earth surface such as those related to ice dynamics. An interferogram can be constructed successfully only if scattering between areas in the InSAR partners remains coherent. Complex coherence $|\gamma|$ for two co-registered SAR images u_1 and u_2 can be estimated from uniform patches, W, around pixels [j,k] using Equation 4.1.

$$|\hat{\gamma}[i,k]| = \frac{|\sum_W u_1[i,k] \cdot u_2{}^*[i,k]|}{\sqrt{\sum_W |u_1[i,k]|^2 \cdot |u_2{}^*[i,k]|^2}} \qquad (4.1)$$

According to Equation 4.1, the absolute value of the coherence estimate $|\hat{\gamma}[i,k]|$ can range between 0 (complete decorrelation) and 1 (complete coherence). The coherence between

images can be reduced by *spatial decorrelation* due to a large perpendicular baseline causing differences in incidence angle, *thermal decorrelation* due to low signal to noise ratio, *process decorrelation* due to errors in image or interferogram processing, or *temporal decorrelation* due to a change in the scattering medium [*Meyer et al.*, 2011]:

$$|\hat{\gamma}| = \gamma_{spatial} \cdot \gamma_{temporal} \cdot \gamma_{thermal} \cdot \gamma_{process} \qquad (4.2)$$

Temporal coherence decreases as the scattering surfaces either deform or move. From our experience, the most likely contribution to coherence loss in our long-temporal baseline L-band interferograms is related to lateral motion of a sea ice patch. Coherence depends on the magnitude of a deformation shift in relation to the size of the original resolution cell. If uncorrected, this motion displaces scatterers out of a given image resolution cell and introduces new ones, thereby reducing the contribution of overlapping information in the overall scattering response. As both the loss of scatterers and the introduction of new scattering elements contribute to decorrelation, surface motion larger than the size of one resolution cell leads to the complete loss of coherence. The interferometric coherence of ice therefore implies a dislocation of less than one resolution cell between satellite passes (one and a half months in the case of PALSAR) and is thus a more reliable and accurate means of identifying landfast ice [*Meyer et al.*, 2011] as compared to methods relying on SAR magnitude data alone to confirm stationarity [*Mahoney et al.*, 2007].

Prior to a study by *Meyer et al.* [2011], InSAR usage over sea ice had been predominantly limited to C-band (λ=6 cm) data. Meyer *et al.* showed that the reduced sensitivity of L-band (λ=23 cm) SAR to environmental changes affecting the dielectric properties of sea ice made it suitable for detecting and mapping landfast sea ice. In their study of Alaska landfast ice they employed PALSAR-1 data with a 46-day repeat interval. Processes such as mechanical deformation (e.g. fracturing and tilting) and thermal processes (e.g. brine wicking and drainage, frost flowers and sublimation, recrystallization) will change the scattering properties and reduce coherence, but will rarely result in complete loss of coherence over large areas. The similarity in dielectric properties between air and dry snow results in little backscattering from the snow cover itself. This insensitivity to snow cover is particularly true for L-band with wavelengths substantially larger than snow grains or grain aggregates.

Therefore, deposition and wind redistribution of snow will likely not change coherence in winter when the snow is dry. During late spring, snow and ice surface melt, desalination processes, and wet precipitation could result in substantial coherence loss over large areas.

Due to the length of the temporal baseline, we expect the temperature of the ice to change between SAR acquisitions. Based on in-situ data collected at a mass balance station installed in the landfast ice near Barrow [*Eicken et al.*, 2012], we estimate ice surface temperature at Elson Lagoon varied between approximately –15 ˚C in late December to -10 ˚C in mid-March. For the Prudhoe Bay and Foggy Island Bay interferograms, we expect the ice surface temperature varied approximately between –7 ˚C in late March and –5 ˚C in mid-May. These temperature changes will lead to changes in the penetration depth of the microwave energy due to the resulting changes in brine volume. L-band SAR, with a frequency of 1.2GHz, is expected to have a penetration depth in first-year sea ice of between approximately 1 m and 0.3 m over this temperature range.

Penetration of the microwave energy into the ice introduces volumetric decorrelation as a result of the different scattering paths caused by differences in incidence angle due to the non-zero perpendicular baseline. Volumetric decorrelation and variation in incidence angle both affect spatial coherence. The relatively large penetration depth of L-band may suggest significant scattering within the ice volume rather than strictly from the surface, which results in enhanced spatial decorrelation.

Thermal coherence depends on the signal-to-noise ratio (SNR) [*Weber Hoen and Zebker*, 2000]. Over first-year sea ice the SNR of a SAR acquisition largely depends on the morphology of the ice relative to the wavelength. Deformed sea ice, such as pressure ridges and rubble fields, typically has a high backscatter coefficient due to the roughness of the ice surface. However, first-year sea ice that has not undergone mechanical deformation is typically smooth when compared to the large (0.23m) L-band wavelength, causing specular reflection and low backscatter under the oblique observation geometries that are typical for SAR. Hence, undeformed first-year sea ice such as that found in lagoons and sheltered embayments will often have a low SNR in L-band SAR data and can be affected by thermal

decorrelation [*Meyer et al.*, 2011]. However, most of the sea ice in our study areas shows sufficient backscatter to avoid complete loss of coherence across smooth areas.

4.3.4 Fringe patterns

The other main source of information in interferometry is the fringe pattern. The interferometric signal is derived from the complex conjugate multiplication of the two image signals:

$$I = |u_1||u_2|e^{i(\psi_1 - \psi_2)} \qquad (4.3)$$

where u_1 and u_2 are returned signals from image 1 and 2 with respective phase values ψ_1 and ψ_2. The interferogram is the spatial distribution of the calculated phase difference Φ:

$$\Phi = arctan\left[\frac{Im(I)}{Re(I)}\right] \qquad (4.4)$$

In order to extract ice motion from interferograms, it is essential to understand the potential causes of phase changes over landfast sea ice. Generally, the phase change has five main contributors [*Weber Hoen and Zebker*, 2000]:

$$\Phi = \Phi_{motion} + \Phi_{topo} + \Phi_{prop} + \Phi_{noise} + \Phi_{error} \qquad (4.5)$$

Most of the phase contribution to an interferogram originates in deformation processes caused mainly by lateral or vertical deformation of the ice:

$$\Phi_{motion} = \frac{4\pi}{\lambda} d \qquad (4.6)$$

where d is the change in slant range. Φ_{motion} is a direct measurement of deformation and lateral displacement with range components of only half the sensor wavelength is sufficient to cause a phase shift of 2π (one fringe). It is therefore expected that sea ice interferograms can be useful in studying landfast sea ice dynamics.

With a non-zero perpendicular spatial baseline static, pre-existing topography may also affect Φ. The topographic phase component Φ_{topo} can be written as

$$\Phi_{topo} = \frac{4\pi}{\lambda}\frac{B_{\perp}}{R}\frac{h}{sin\theta} \qquad (4.7)$$

where R is slant range distance to the target, λ is the sensor wavelength, $B_{\perp}$ is the perpendicular baseline, h is the topographic relief of a feature, and θ is the radar's off-nadir look angle. The topographic height difference causing a full phase cycle change between two points in a neighborhood can be described as the ambiguity height, h_a:

$$h_a = \frac{\lambda R_s sin\theta}{2B_{\perp}} \qquad (4.8)$$

[*Bamler and Hartl*, 1998]. For PALSAR (λ = 0.25m, θ = 34.3, and R_s = 840km) and a large $B_{\perp}$ of 1km, a 2π phase change in the interferometric phase will require an altitude difference of 59m. The $B_{\perp}$ used here are much smaller (Table 4.1) resulting in even larger heights of ambiguity and, hence, reduced height sensitivity. Ridge heights in landfast sea ice typically do not exceed 10m [*Weeks*, 2010]. Thus, static topography (i.e. pre-existing ridges) can result in only a minor contribution to the interferometric phase Φ, ruling out topography as a main phase contributor.

Φ_{prop} is the phase difference due to different path lengths caused by spatio-temporal variations of the tropospheric or ionospheric refractive index. Φ_{noise} is the random component of the phase that is relevant in areas of low SNR. Orbit errors or coregistration errors can cause significant phase signatures Φ_{error} in InSAR data over sea ice. However, the phase contribution from these sources are usually either negligible or can be identified (over areas of flat terrain on land where phase contribution should be close to zero) and corrected [*Scharroo and Visser*, 1998].

Since the phase contribution to an interferogram mainly originates in deformation processes we will show that interferograms have the potential to reveal the complex small-scale deformation patterns within the landfast sea ice regime. However, interpretation of such interferograms is not straightforward since landfast sea ice can undergo multiple modes of

3-dimensional deformation, whereas the interferometric phase measurement only quantifies motion in the slant-range direction between the satellite and the ice surface. To overcome this challenge, we have identified a canonical set of strain processes (e.g., shear, rotation, divergence) that represent the primary modes of sea ice deformation, which can be used to model the interferometric response of sea ice undergoing strain. With these constraints, we can derive most-likely quantifications of the displacement patterns that give rise to the observed interferograms.

4.4 Interferometric inverse model to detect and map sea ice displacement

4.4.1 Model structure

Landfast sea ice can move and deform in several different ways. Hence, our sea ice model needs to encompass a wide range of motion modes in order to enable a realistic physical interpretation of the InSAR data. The canonical motion modes included in our model are (left column in Figure 4.4): (1) radial divergence as a result of temperature changes causing the landfast ice to compress or expand; (2) rotational motion as a result of shear forces acting on the less laterally constrained parts of the landfast ice far from shore; (3) uni-axial divergence due to external compressional normal forces (such as onshore wind) causing convergence or tensile forces (such as offshore wind) causing larger displacements where the ice is less constrained; (4) shear motion as a result of shear forcing from less stationary landfast ice or pack ice translating motion into adjacent fast ice; and (5) Surface tilting due to tidal or ocean surge displacement or large-scale buckling of the ice. Note that a solid non-fractured piece of ice moving isotropically in a lateral or vertical direction will result in a uniform phase shift that cannot be observed by the interferometric phase (due to the relative nature of InSAR measurements). In our mode, these five canonical displacement modes can be combined to simulate any relative local displacement on the ground.

The model uses known satellite altitude and look angle information to calculate the geometric slant ranges to pixels of an image patch of pre-defined size. The respective phase

returns, ψ, from the slant ranges, R, are calculated before and after the displacement (Equation 4.9) according to:

$$\psi = \frac{-4\pi}{\lambda} R + \psi_{scatt}. \qquad (4.9)$$

Interferograms are calculated by multiplying the pre-motion phase pattern with the complex conjugate of the post-motion signal (Equation 4.3). The model assumes that the scattering properties of the surface remained stable between acquisitions, corresponding to a coherence of 1. The model also assumes that phase contributions related to topography, atmospheric disturbance, or noise, are negligible. This approach results in a set of simulated interferograms with linear fringes with orientation dependent on a combination of look angle and direction of deformation (right column in Figure 4.4). If landfast sea ice motion is represented by a combination of different motion modes, the model will only provide the solution of the most dominant of these modes that is driving most of the simulated solution.

As the interferometric phase is only sensitive to the projection of a 3-d motion into the line-of-sight direction, different deformation modes may result in similar phase patterns, leading to potential covariance between model realizations. Uni-axial divergence, shear, and surface tilt are all dependent on the viewing geometry and, hence, must be modeled from multiple directions. The goal was to develop canonical model databases with enough viewing angles to resolve local changes in the direction of deformation while still maintaining distinctly different uncorrelated phase structures. Initially 8 angles were simulated, but an increase to 16 angles (every 22.5°) provided better results (only the orientation of the axis of uni-axial divergence can be modeled since reversed directions cannot be distinguished).

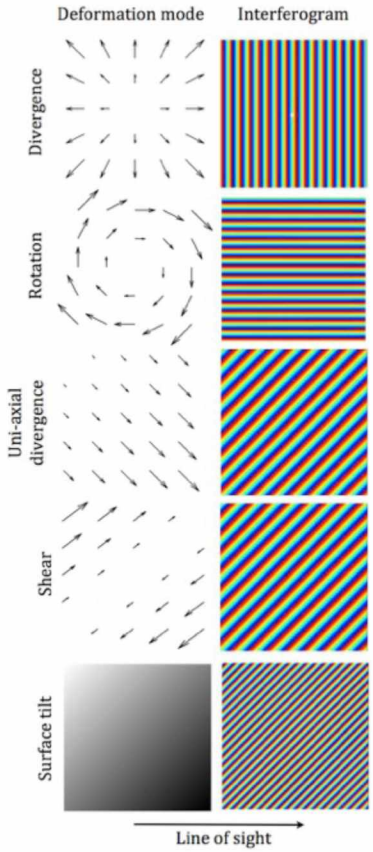

Figure 4.4 Modes of deformations modeled are displayed in the left column. Modes include divergence, rotation, shear, uni-axial divergence, and surface tilt. These displacements are modeled for 16 look angles varying at 22.5-degree intervals. Rotation and radial convergence are directionally independent. Uni-axial divergence is correlated with reversed directions. Shear and uni-axial divergence in cross-track direction is completely correlated with rotation and radial divergence respectively. Surface tilt is indicated by gray-level shading (brighter shading representing higher elevation). The corresponding modeled interferograms are displayed in the right column

The result is a total of 44 different modes (including viewing angles) modeled and the correlation between the model databases are calculated in a correlation matrix using Equation 4.1 (Figure 4.5). It is apparent that not all model databases display uncorrelated phase structures. Especially, there is high correlation between certain uni-axial divergence and shear modes as well as vertical displacement. Three scenarios exist that are associated with ambiguities, specifically between (1) radial and uni-axial divergence and surface tilt, (2) rotation, shear, and surface tilt, and (3) uni-axial divergence, shear, and surface tilt.

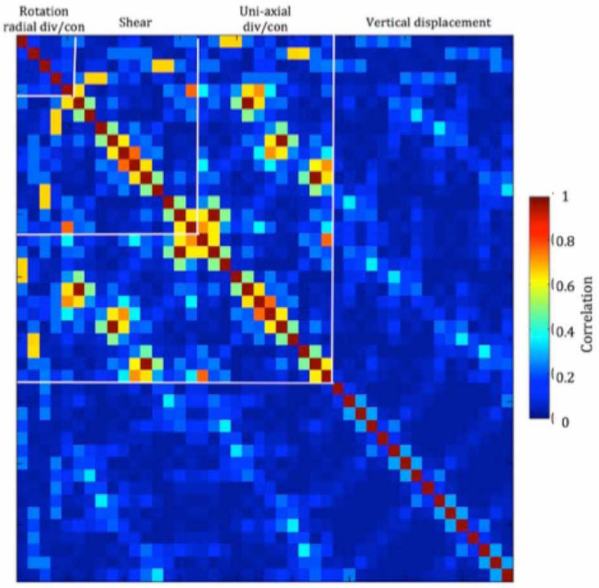

Figure 4.5 Correlation matrix between the 44 deformation modes (including different angles unless not unique). White lines distinguish between different modes of deformation. Some of the deformation modes produce highly correlated interferograms in particular between shear and uni-axial divergence.

4.4.2 Model inversion

To analyze observed interferograms and determine correct deformation modes we divide each interferogram into square patches whose size matches the size of the model outputs generated at three different resolutions (50x50, 100x100, and 200x200 pixels). The coherence between the data and the modeled patches is calculated for different deformation modes, magnitudes of deformation, and resolution levels and converted to the finest 50x50 grid:

$$|\hat{\gamma}|_{n,m,r} = \frac{\left|\sum_W u_o \cdot {u_{n,m}}^*\right|}{\sqrt{\sum_W |u_o|^2 \cdot \left|{u_{n,m}}^*\right|^2}} \quad n \in \{1 \dots N\}, m \in \{1 \dots M\}, r \in \{1 \dots R\} \qquad (4.10)$$

$|\hat{\gamma}|_{n,m,r}$ is the coherence between the observed (u_o) and modeled ($u_{m,n}$) patches for M deformation modes, N magnitudes of deformation, and R number of resolution levels. The coherence determines the consistency in the phase value between measured and modeled

patches and ranges from 1 (completely consistent) to 0 meaning the phase values are completely uncorrelated. Coherence therefore is well suited to identify the most likely deformation mode.

Figure 4.6 shows a map of coherence values between an example patch u_o and the 44x20 model patches $u_{n,m}$. This map illustrates three significant features of a typical model result: (1) Most solutions can be discarded due to low coherence. (2) There is often minor correlation between neighboring cells (as opposed to only one strong peak) due to a slight oversampling, indicating that the correct solution has been identified. (3) The model options with high coherence values are few and not more than three (e.g. certain orientation of shear, uni-axial divergence and surface tilt) are so similar the mode cannot be determined using coherence alone. In many cases this ambiguity between multiple solutions can be addressed through realistic constraints on the resulting strain magnitude or cumulative motion. For example, it is not realistic for surface tilt to continue over great distance without a reversal or discontinuity.

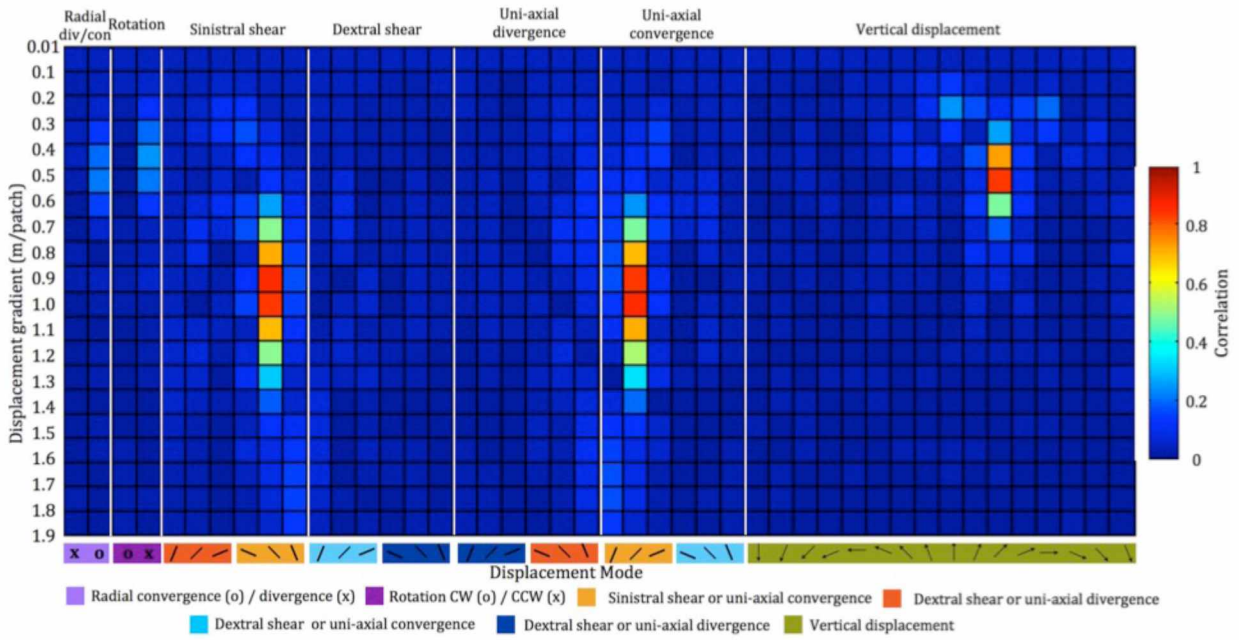

Figure 4.6 Correlation between an example patch of an observed interferogram and all 44 modeled interferograms (indicated mode above and direction of motion below the correlation map along with the color used to display the particular mode combination) and for 20 displacement gradients. In this case, 45 degree angled sinistral shear with a displacement gradient of ~1m (from center to corner of a 50x50-pixel patch) is the most

likely possibility (due to geophysical constraints – see *Section 4.4.2*). Uni-axial convergence and vertical incline towards the upper right corner is also a possibility with almost equal correlation.

The energy E_r of the solution for all resolution levels is calculated to determine the confidence that can be placed on the model result. The Energy parameter in Equation 4.11 is convenient because it conveys in one number whether the model has found a set of distinct solutions such as in Figure 4.6. The energy is calculated in the original grid and based on the ratio of the mean coherence in the entire map (Figure 4.6) over a Gaussian approximation, $|\hat{\gamma}|'$, of the largest peak integrated within one standard deviation of the peak amplitude value:

$$E_r = 1 - \frac{\overline{|\hat{\gamma}|_{n,m,r}}}{\int_{n=-\sigma}^{n=\sigma} |\hat{\gamma}|'_{n,m',r'}} \qquad r \in \{1 \dots R\} \qquad (4.11)$$

E_r will range between 1 for a strong (and unique) peak and 0 for the case where no peak could be identified at all. At the end of the process, the lower resolution peak estimates E_{100} and E_{200} are resampled to the denser E_{50} grid and the final combined deformation mode m' is found belonging to the highest coherence of the resolution possessing the highest energy:

$$|\hat{\gamma}|_{n',m',r'} = \max_{n,m} |\hat{\gamma}|_{n,m,r'} \; where \; E_{r'} = \max_{r} E_r \qquad (4.12)$$

4.4.3 Model ambiguities and constraints

Ambiguities (see Figure 4.6) between modes of displacement frequently occur between vertical tilt and the lateral displacement modes and the model results may favor one or the other solution based on slight differences in the observed fringe pattern, sometimes resulting in motion mode estimates that do not make physical sense. Often the interferogram itself provides guidance on whether fringes are due to vertical or horizontal displacements. For example, while surface tilt (vertical motion) might result in a fringe pattern that

resembles that of shear or rotation (horizontal motion) for a single tile, it is not realistic to expect surface tilt to remain constant over significant distances since the cumulative vertical displacement would become unrealistically large. At some point the tilt must reverse, which will lead to concentric elliptical fringe patterns in the interferogram. Therefore, we decided to add region-specific conditions to our geophysical model. Where interferograms lack significant elliptical fringe patterns, the model is conditioned to only simulate horizontal motion (*Section 4.4.1*, and 4.*4.2*). However, in areas where the interferogram indicates significant vertical motion the model is constrained to only simulate vertical deformation (*Section 4.4.3*) to resolve the vertical deformation of these areas specifically.

Ambiguities between shear and uni-axial divergence (both horizontal modes) can often be visually eliminated based on a combination of geographical constraints such as coastline orientation, predominant forcing patterns, and speckle tracking of less constrained landfast ice. Ambiguities can also occur (1) when the ice experiences multiple different modes of deformation within a modeled patch, (2) if there is sufficient coherence loss in the interferogram, or (3) if the deformation is so low that there is not sufficient phase gradient within a model patch. The three different resolutions were chosen based on experimentation to minimize these ambiguities. The high resolution is effective in capturing small areas with uniform deformation, but is limited by the need to achieve sufficient phase gradient to minimize ambiguities and the influence of noise. The low resolution is chosen to be able to capture most of the larger features apparent in the interferograms with high energy and provide results of sufficient phase gradient during slow deformation and in areas of low interferogram coherence, but is limited by often multiple different deformation modes within a patch.

4.5 Model results and interpretation

4.5.1 Validating the model over Elson Lagoon, Alaska

This section aims to validate the model by first explaining the model results before analyzing whether the results are geophysically plausible. The area to validate the model is Elson Lagoon close to Barrow, Alaska.

This location features first-year sea ice varying in roughness from smooth ice inside the lagoon to heavily deformed rubble and ridge fields outside the lagoon. Based on nearby sea ice mass balance research site data the ice thickness can be estimated to have grown from roughly 0.5 m to 1.0 m in the time between acquisitions. This area was chosen as a model test site primarily for two reasons. First, the University of Alaska Geophysical Institute sea ice research group and the Seasonal Ice Zone Observing Network (SIZONet) have focused their fieldwork on Barrow and the surrounding areas for more than a decade, including annual studies of sea ice thermal and dynamic development, large-scale morphology and microstructure [*Druckenmiller et al.*, 2009]. Our group therefore has knowledge of the ice environment in Elson Lagoon as well as real-time thermal and mass balance data collected nearby, which helps constrain physical properties of the landfast ice and greatly benefits the analysis and evaluation of the model. Second, the barrier islands semi-enclosing the lagoon reduce the number of deformation modes and the severity of deformation, and hence narrow down the expected solutions of the model.

An amplitude image from 27 Dec. 2009 is examined (Figure 4.7a) followed by a series of three consecutive interferograms from 27 Dec 2009 – 14 May 2010 (Figure 4.7b-d). The ice in the lagoon exhibits low backscatter characteristic of smooth first-year ice that dominates the lagoon (Figure 4.7a). A few linear, high backscatter features most likely representing low-elevation pressure ridges and rough ice formed during the first few weeks of ice growth can also be identified (most notable one marked with an arrow in Figure 4.7a).

The interferograms (Figure 4.7b-d) exhibit fringes both inside and outside the lagoon, but lose coherence a few kilometers off shore from the barrier islands. The interferogram in Figure 4.7c exhibits partial coherence loss inside and outside the lagoon possibly in part due

to ice growth extending the ice-water interface beyond the penetration depth of the radar leading to an altered backscatter signal. The density of fringes is an indication of the rate of deformation with a higher fringe density indicating a higher rate of deformation. The thicker the ice gets the less freely the ice can deform due to its increased strength. Early in the winter (Figure 4.7b), the landfast ice is still fairly thin explaining the high fringe density. Outside the lagoon, the landfast ice furthest offshore (that still exhibits coherence) deforms more rapidly due to the reduced lateral constraints. Later in the season (Figure 4.7c) the predominant fringe patterns remain mostly consistent but with reduced fringe density due to the increased stability resulting from thicker ice. By spring (Figure 4.7d) the lagoon ice has stabilized to the point where lateral deformation is almost non-existent. Even outside of the lagoon, the ice exhibits substantially reduced motion. The continued increase in stability within the lagoon is due to ice growth, while outside the lagoon can also be attributed in large part to the formation of grounded ridges sheltering the landfast ice from further deformation.

Particularly early in the season (Figure 4.7b), the fringe overall pattern shows localized distinctively different regions of internally uniform deformation behavior. The sharp boundaries between these regions (indicated by discontinuous fringes) likely represent a dislocation allowing discontinuous ice to deform more independently. Similar thermally induced dislocations have been observed in Elson Lagoon as cracks extending for several kilometers with a width of less than half a meter. The cracks are associated with only small cm-scale change in elevation as well as moderate altered roughness making them difficult to recognize with L-band SAR, but can be identified in X-band amplitude images. As the season progresses it is clear that the number of active dislocation cracks declines (due to fewer severe cold spells fostering thermal cracks and increasing ice thickness reducing overall stress) while the general deformation patterns persist under increasingly stabilized ice conditions. The interferograms provide valuable information indicating the difference in deformation gradient across these lines.

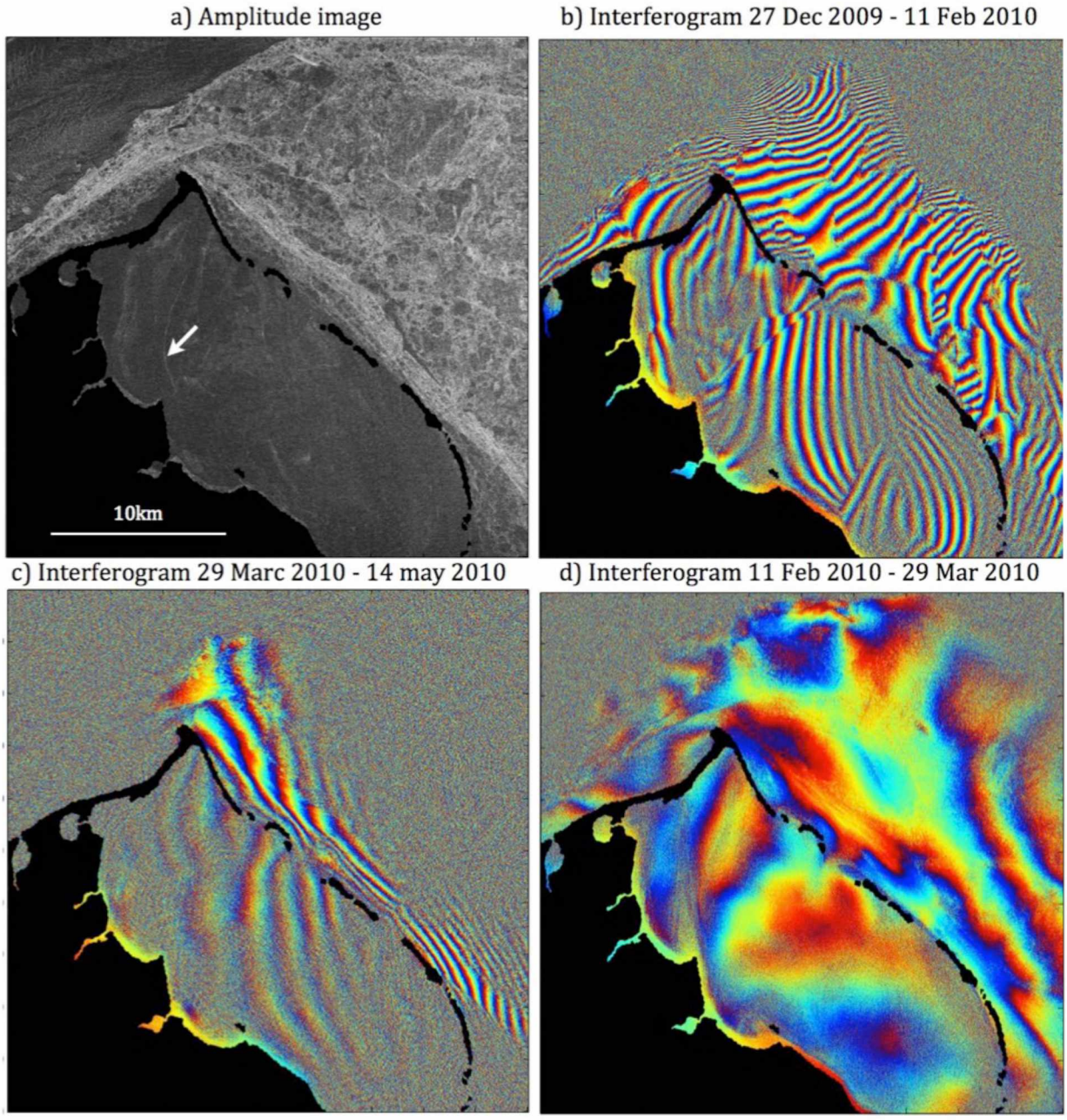

Figure 4.7 Interferograms over Elson Lagoon. (a) Amplitude image over Elson Lagoon, Alaska (27 Dec 2009). The land is masked out in black. (b-d) Interferograms created from the consecutive acquisition pairs identified in the image labels.

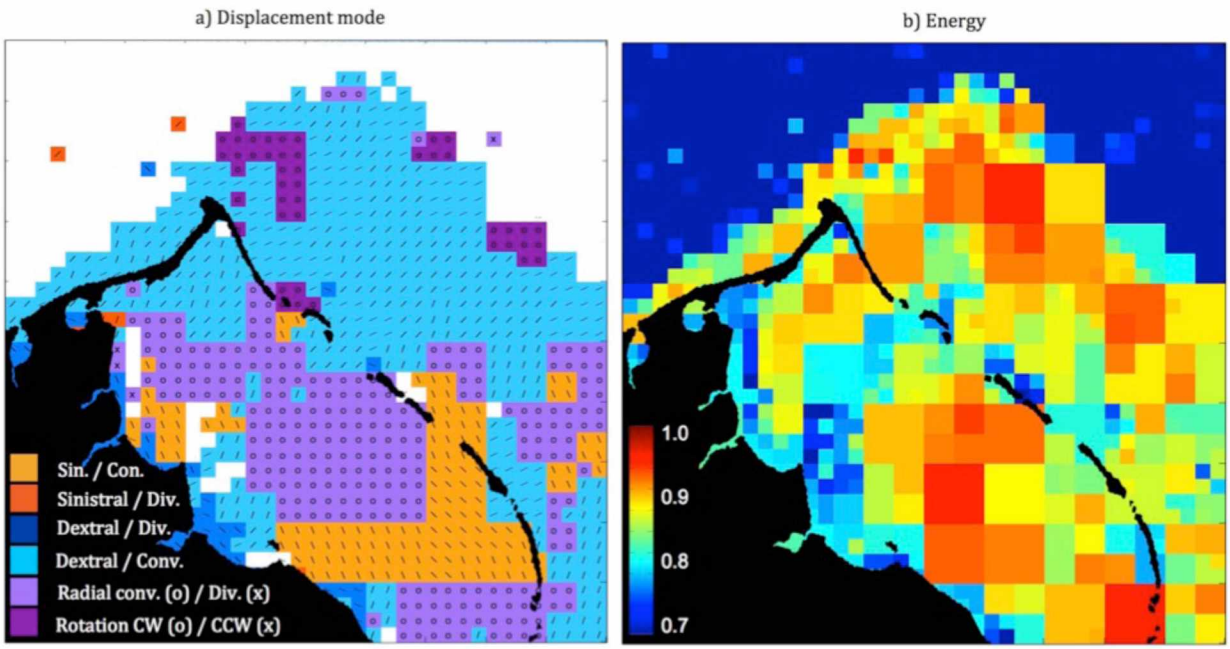

Figure 4.8 Model results over Elson Lagoon. (a) Model results display deformation mode with colors corresponding to the specific combinations of deformation mode. Light and dark purple correspond to modes that are independent of the viewing angle, including radial divergence and rotation, respectively. Yellow and orange colors indicate left-handed (sinistral) shear and uni-axial convergence or divergence, respectively. Blue and cyan indicate right-handed (dextral) shear and uni-axial divergence or convergence, respectively. The lines indicate lines of equal deformation (parallel to shear and perpendicular to uni-axial divergence) and "x" and "o" correspond to divergence / counter clockwise rotation and convergence / clockwise rotation respectively. (b) Energy of the model results indicating certainty of the model (see *Section 4.3.2* for details). White colors in Figure c correspond to where energy did not exceed 0.7.

The model is applied to the first interferogram (27 Dec 2009 – 11 Feb 2010) when the lagoon is most dynamic and was confined to using horizontal modes of displacement only (top four modes in Figure 4.4). Constraining model output to lateral motion is justified due to the lack of closed circular features in the interferogram often indicating buckling (See *Section 4.3.3*). The result of the model inversion is displayed in Figure 4.8a, in which grid cell colors correspond to at most two possible deformation modes.

The plot of energy (Figure 4.8b; Equation 4.11) is a measure of model output confidence. Overall, the model results indicate that the mode of ice deformation was homogenous over

length scales of up to 10 km, as illustrated by the spatial extent of contiguous cells of the same color. The spatial homogeneity of model solutions is a good validation of the model in itself and indicates that the model can delineate smoothly varying physical processes. The majority of Elson Lagoon is dominated by radial convergence (light purple) as indicated by the "o" symbols. The ice surrounding the central convergence in the lagoon is dominated by either sinistral (left-handed) shear (yellow) and dextral (right-handed) shear (cyan) parallel to the coastline or uni-axial convergence perpendicular to the coastline. The ice seaward of the barrier islands is almost exclusively dominated by either dextral (right-handed) shear perpendicular to the coastline or uni-axial convergence (cyan) with motion direction parallel to the coastline.

The lagoon is semi-enclosed, reducing the amount of stress from pack ice interaction. Hence ice deformation in the lagoon is expected to be primarily due to thermal stresses during this 46-day repeat pass period. The discontinuities between regions of consistent fringe patterns are likely to have experienced thermal stresses exceeding tensional yield stress resulting in formation of thermal cracks. On each side of the central radial convergence zone the model suggests either shear deformation parallel or uni-axial convergence perpendicular to the coastline. Here, uni-axial convergence is the most likely scenario where the uni-axial convergence region is separated from the radial convergence zone through discontinuities apparent in Figure 4.7b (most likely thermal cracks which have been observed in the area during previous field seasons). Shear deformation – in particular un-interrupted sinistral shear extending from one side of the lagoon to the other (Figure 4.8a) – is a less plausible explanation of the observed interferometric patterns. In contrast, the model solutions corresponding to radial and uni-axial convergence are geophysically plausible for the lagoon site in mid-winter.

Outside of the lagoon, the model indicates possible uni-axial convergence parallel to the barrier islands, which would be consistent with westward displacement of offshore pack ice translating forces onto the landfast ice kept in place by the barrier islands and Point Barrow. The other model solution corresponds to dextral shear perpendicular to the barrier islands, which is geophysically less plausible in the absence of associated near-coast convergence.

The results obtained in the Elson Lagoon area were consistent with local knowledge of the region and lend confidence to the performance of the model. The goal of this model evaluation was to test the model and learn how to interpret results so that the model can be utilized without further prior local knowledge of the individual location. The next sections will explore model output in a region with significant interaction of landfast ice with offshore pack ice and where the approach outlined above can address stakeholder information needs. For instance, how does the landfast ice deform around the Northstar Island ice road and drilling operation in the Beaufort Sea and what is the driver of the observed deformation (*Section 4.4.2*)? Also, what is the dominant deformation around the proposed Liberty prospect where ice motion is currently a concern for planned drilling activities (*Section 4.4.3*)?

4.5.2 Model results near Northstar Island, Prudhoe Bay, Alaska

Northstar Island [*Krieger et al.*, 2003] is a man-made gravel island located near the center of the Northstar oil and gas prospect in the Beaufort Sea near Prudhoe Bay (circled in Figure 4.9a). The island is connected to land with an ice road during winter months (arrow in Figure 4.9a) and transportation of supplies using heavy trucks and reinforcement of the ice road using construction machinery are both critically dependent on the stability of the ice [*Bashaw et al.*, 2013; *Potter et al.*, 1981]. The sea ice around Northstar is first-year sea ice that is generally smooth shoreward of barrier islands and shoreward of Northstar Island, with certain areas prone to cracking and ridging. Oceanward of Northstar, the ice is more heavily deformed as seen in the amplitude image. Based on airborne EM surveys, the landfast sea ice conditions in the western Beaufort Sea are comparable to Barrow (Mahoney, unpublished data), hence we can estimate that ice thickness grows from roughly 1.1 m to 1.3 m between acquisitions.

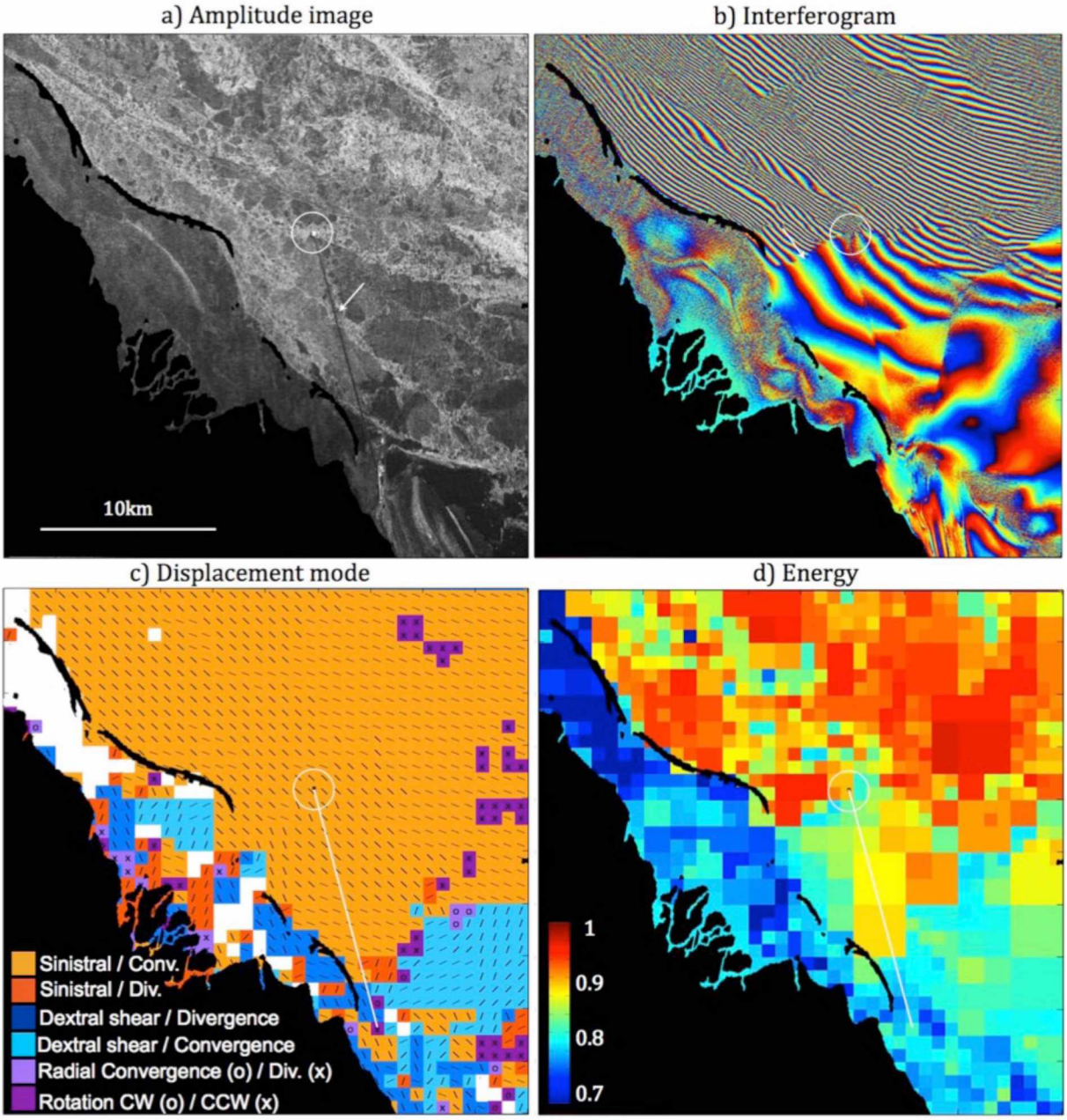

Figure 4.9 Model result over Northstar Island. (a) Amplitude image for the Northstar Island (circled) and Prudhoe Bay region, Alaska (21 Mar 2010) (arrow pointing to the ice road connecting the island to the mainland) and (b) the interferogram created from this and the following acquisition (6 May 2010) (arrow pointing to boundary between high and low fringe density at Northstar Island). (c) The model results display deformation mode with colors corresponding to the specific combination of deformation modes. The lines indicate lines of equal deformation (parallel to shear and perpendicular to uni-axial divergence) and "x" and "o" correspond to divergence / counter clockwise rotation and convergence / clockwise rotation respectively. (d) Energy of the model results indicating certainty of the

model (see *Section 4.3.2* for details). White colors in figure c correspond to where energy did not exceed 0.7.

The interferogram produced from an image pair for March 21 and May 6, 2010 is chosen due to the stark contrast between the higher fringe density oceanward and lower fringe density shoreward of Northstar Island, suggesting that potential anchor support by the island contributes to the local stabilization of shorefast ice (arrow in Figure 4.9b). The ice road is associated with a noteworthy displacement of interferogram fringes suggesting that road construction or maintenance impacts the dynamics of the underlying ice. The inverse displacement model results (Figure 4.9c) indicate large areas of either uni-axial convergence perpendicular to the coastline or sinistral shear deformation with northwesterly ice movement increasing with distance to the coast (Figure 4.9c).

The shear field is consistent with an ocean current and pack ice interaction parallel to the coast from east to west. This pattern is expected due to the consistency with the general velocity field of the Beaufort Gyre – a persistent wind driven ocean current in the Arctic Ocean illustrated in Figure 4.1 – and is the most plausible model solution.

For most areas, model solution energy is high as a proxy for model confidence (Figure 4.9d). The energy is larger northeast of Northstar due to a combination of coherent signal and homogenous fringe orientation and fringe spacing enabling the model to more accurately identify the most plausible solution. Due to low coherence inside the barrier islands, model output confidence is not high enough to be included in the analysis.

As an independent verification and to potentially narrow down solutions, we also calculated landfast ice displacements through non-coherent cross correlation, also known as speckle tracking (Figure 4.10). This technique determines sub-pixel surface displacements without considering phase information [*Bamler and Eineder*, 2005], requires large displacements and is not nearly as accurate as interferometric approaches. Cross correlation displays absolute movement and is therefore more sensitive to coregistration and orbit errors than the relative motion from interferometry. Nevertheless, the speckle tracking validates the sinistral shear

model result displaying an increase in displacement ocean-ward of Northstar Island with similar orientation as indicated by the model (Figure 4.9).

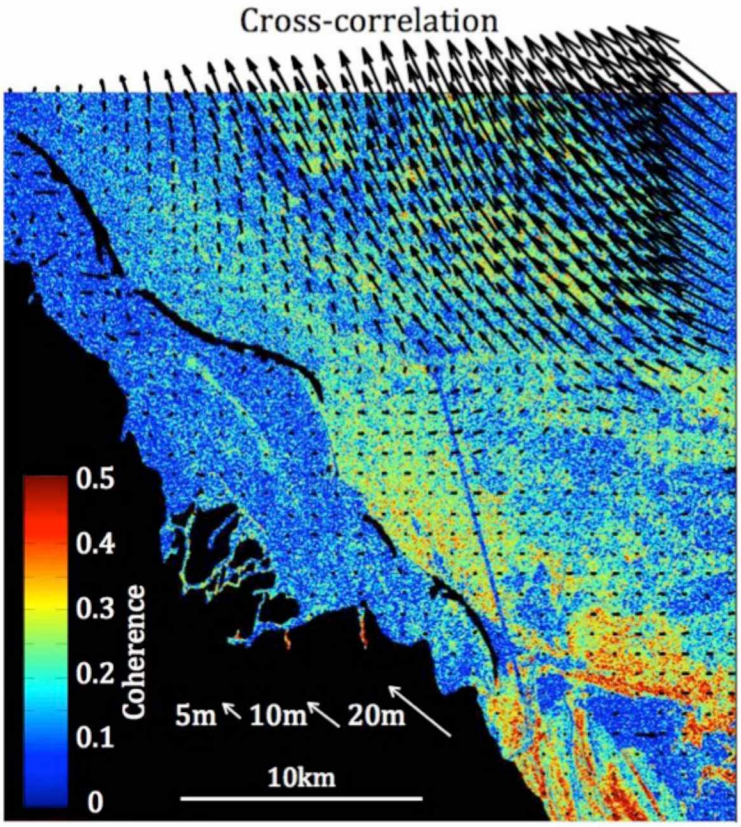

Figure 4.10 Incoherent cross-correlation displacement vectors superimposed on the interferogram coherence over Northstar (21 Mar 2010 – 6 May 2010). The ice road is apparent as an area of reduced coherence due to ongoing road construction (snow removal and thickening of the ice through pumping of water onto the ice surface). The vectors indicate a large area of uniform left-handed (sinistral) shear motion.

4.5.3 Assessing vertical displacement at Foggy Island Bay, Alaska

So far we have used the model to derive horizontal motion only and excluded vertical displacements. It is important to identify and model displacement in the vertical direction that is substantial enough to invalidate a strict lateral solution. A vertical ice displacement of d_v will produce an interferometric phase:

$$\Phi = \frac{4\pi}{\lambda} d_v sin\theta \qquad (4.13)$$

A region with a phase ramp will therefore correspond to a tilted surface, such as might be caused by depression under a heavy load, buckling under lateral stress or doming due to excess pressure under the ice between confining areas of bottomfast ice. In most cases, coherent ice surfaces cannot support significant vertical displacements across multiple model tiles (since non-realistic vertical displacement would be reached) and so any surface tilt as well as the fringes will have to reverse within relatively few fringes. This will result in elliptical features in the interferogram. A plausible maximum vertical displacement of 2m (1m of freeboard and 1m sea level displacement) would result in 9 circular fringes. An example is the interferogram over Foggy Island Bay, where vertical displacement has to be considered. This locale is of interest because it is the target of planned exploration drilling (Liberty prospect) associated with the need for (temporary) infrastructure development that utilizes the ice as a platform and may be impacted negatively by movement or loss of stability of the shorefast ice [*Hilcorp*, 2015]. According to British Petroleum, the operator of Liberty until 2014, ice movement was noted during the 2013 Liberty Geotechnical Program [*BP*, 2013], creating the need for GPS deployment to track ice motion at specific points, an approach that has proven useful, though with limitations [*Tucker et al.*, 1980; *Weeks*, 1977].

Foggy Island Bay is located about 25 km east of Prudhoe Bay and east of Endicott Island. The near-shore landfast ice consists of relatively level first-year sea ice with more heavily deformed ice further offshore in areas where the coastal morphology is not offering protection from pack ice interactions from the Beaufort Gyre (can be seen from Figure 4.11a). The interferogram is formed late in the season (ice thickness estimated to grow from roughly 1.2 m to 1.4 m between acquisitions) and was chosen due to the noteworthy circular features (Figure 11b) that we interpret as regions of vertical displacement. In the westernmost part of the bay is a depression of about four fringes, which corresponds to a peak vertical displacement of about 90cm. East of this depression (north of Liberty) is a ridge of about 2 fringes indicating near half-meter displacement.

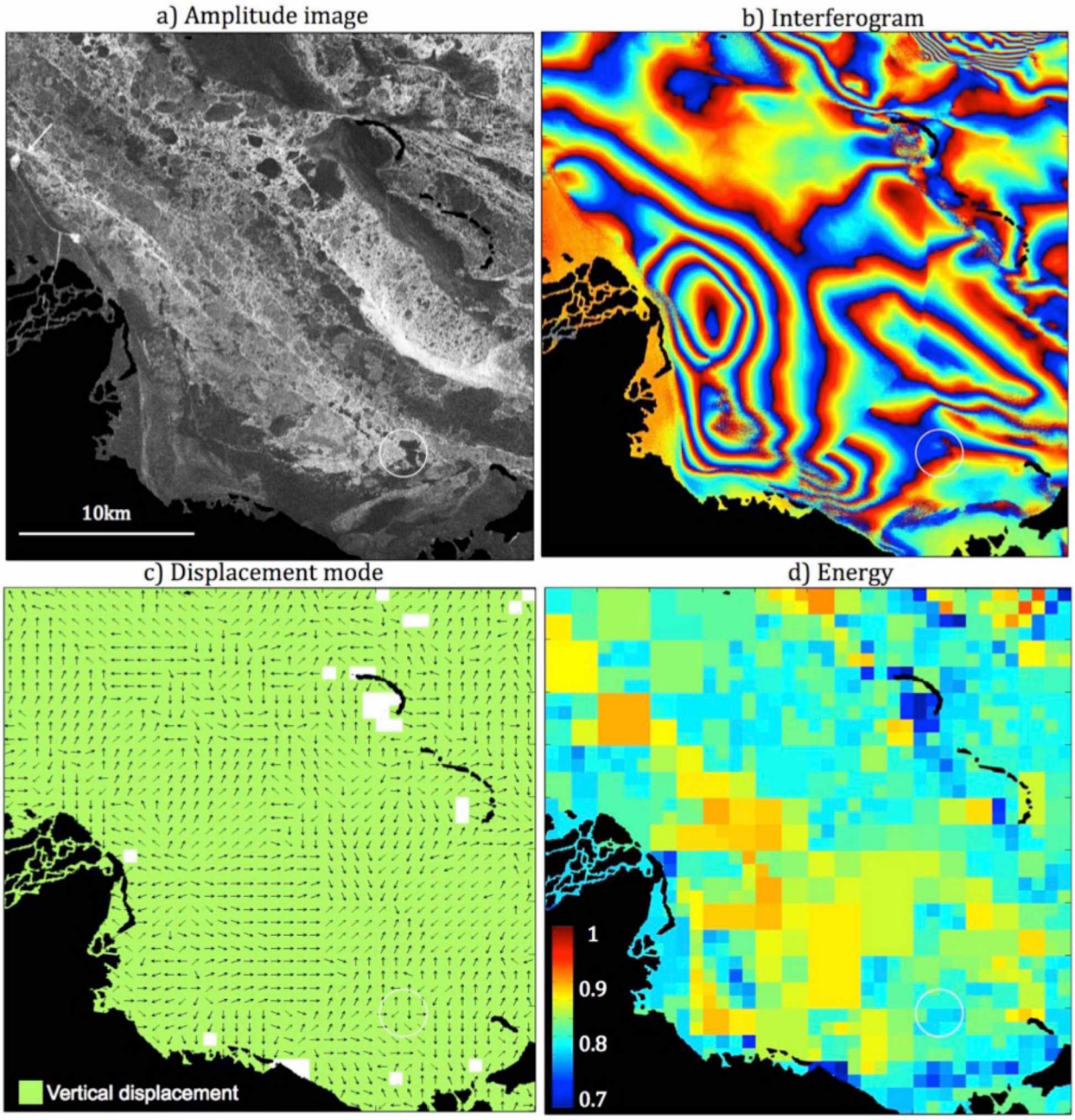

Figure 4.11 Model result over Foggy Island Bay. (a) Amplitude image over Foggy Island Bay and the Liberty prospect (Liberty is roughly indicated with a circle and Endicott is marked with an arrow) near Prudhoe Bay, Alaska (3/31/2010) and (b) the interferogram created from this and the following acquisition (5/16/2010). (c) The model results display direction of surface tilt with arrows pointing towards higher elevation. The model is set to only match vertical displacement. (d) Energy of the model results. White cells in Figure c correspond to an energy of 0.7 or less.

If running the model with both horizontal and vertical modes, some of the tiles as part of the circular features are derived as uni-axial divergence perpendicular to the center of the circular features (not shown). However, with no discontinuities and likely homogeneous forcing of the ice it is unlikely that the features correspond to uni-axial divergence. The two main circular features account for most of the significant deformation in the interferogram, hence the model can easily be stabilized by running only vertical displacements. However, if there were other non-circular features that needed to be captured, the model would have to be run in horizontal mode to understand the remaining features. The vertical result is plotted in Figure 4.11c as arrows pointing towards higher ground. The model correctly identifies tilting towards the direction of the center on all sides of the depression and ridge. The energy (Figure 4.11d) is reduced as compared to the lateral results partially due to low fringe density and higher mean coherence (Equation 4.11) when considering fewer deformation modes.

4.6 Discussion

The inverse model has been shown to identify different modes and gradients of deformation with reasonable confidence, consistent with recurring local-scale ice dynamics patterns and quantitative information obtained from cross correlation analysis of SAR amplitude images. The most important model uncertainty is associated with picking the best solution in case of ambiguities. These ambiguities are likely inherent in the InSAR method based on the one-dimensional nature of the phase values. For other media experiencing more consistent deformation (e.g., glaciers) some ambiguities can be resolved using both ascending and descending passes acquiring model results from different angles [*Lang,* 2003]. This can be achieved since (1) radial divergence and rotation is independent of look direction, hence fringe orientation will change dependent of the viewing geometry, (2) fringes as a result of shear displacement will remain constant regardless of viewing geometry, and (3) fringes as a result of uni-axial divergence will either remain constant or exhibit reversed phase gradient depending on viewing geometry. Acquiring two interferograms with separate viewing geometry is rarely possible over sea ice since both interferograms would have to be

acquired close in time due to the frequently changing sea ice dynamics. However, even with only one interferogram, wrong solutions can often be ruled out or identified as unlikely based on surrounding ice displacement, a restricting coastline, cross correlation validation, or non-isotropic solution. If obtaining shorter temporal baseline pairs, such as rapid repeat pursuit mode interferometry using TanDEM-X [e.g., *Mahoney et al., 2016*], it may be possible to utilize this model approach on pack ice with little to no access to prior local knowledge about the current ice dynamics. The model solutions would in such case be constrained either using large-scale velocity fields such as derived from Special Sensor Microwave Imager (SSMI) or directly from the SAR dataset through cross correlation analysis as described in *Section 4.4.2.*

As discussed in *Section 4.2.4*, interferometric fringes over landfast sea ice will be caused almost exclusively by small-scale deformation of the sea ice. However, it is important to consider the impact of tidal action or the effect of an ocean surge on this analysis (not leading to permanent vertical change). In the Beaufort Sea, the tidal range is about 20cm (roughly one fringe using Equation 4.13), but can be much larger (~1m) in other areas such as Norton Sound [*Huang et al.*, 2011]. In the Beaufort Sea, larger sea level changes (up to 2.5m [*Weingartner et al.*, 2009]) can occur due to altered surface pressure, ocean currents, and gravity waves, but are uncommon. Over an area of high ice deformation, the effect on the model output from such events still would be negligible. However, in areas of low ice deformation, this effect could be substantial, unless the ice in the entire scene is elevated by the same amount, in which case there would be no relative change and associated phase response.

It is possible to retrieve sea level data from buoys or reanalysis data, which could be used to estimate surface lift due to tides and ocean surges, but will otherwise slightly reduce the model accuracy unless the pattern of a continuous lift can be recognized.

The model resolution is a limitation with respect to the spatial scale of features that can be resolved. For PALSAR-1, a resolution much higher than 50x50 pixels (~750x750m) would increase ambiguities of the model (along with sensitivity to noise) too much to get accurate results. Note, however, that the resolution could potentially be improved with higher

resolution C- or X-band systems. Being able to take advantage of multiple systems for increased coverage and resolution would also be beneficial for operational use.

The long repeat-pass time limits the interpretations to deformation accumulated over 46 days. In this study, the model can therefore not resolve short-term deformation events that occur on time scales on the order of hours to a few days. However, much of the deformation within the landfast ice is thermally driven and can therefore occur over days to weeks. Also, as a tool to evaluate whether a section of ice is landfast, it can be beneficial with longer temporal baselines to avoid mischaracterization of stationary pack ice [*Mahoney et al.*, 2006]. PALSAR-2 became operational as of fall of 2014 with improved capabilities such as a shorter repeat cycle (14 days). However, suitable repeat pass Stripmap data have not yet been acquired with ALOS-2. The shorter temporal baseline of ALOS-2 has the potential for a higher temporal resolution of ice deformation and the coherence will likely be improved since surface deformation will be reduced over the shorter time period.

4.7 Conclusions

We have demonstrated that L-band PALSAR, with a 46-day temporal baseline, is capable of mapping small-scale deformation in three locations of the Alaska Beaufort Sea coast through the development of an inverse model. The displacements estimated from the model are consistent with known regional patterns of ice motion. This inverse modeling approach of InSAR outlined above provides an opportunity to study the interaction of stationary and near-stationary ice as a result of wind, ocean, and thermodynamic forcing at a level of detail and for a spatial coverage difficult to achieve in the past. The technique may furthermore be able to provide indirect insight into the sea-ice stress state as a result of such external forcing.

We have shown that the limitations of the modeling approach discussed can most often be overcome, retaining confidence in the model results, but we point out that ground validation would provide an additional tool to evaluate not only the model, but InSAR as a technique to

monitor sea ice in general. Ground validation may also help understand the nature of higher-frequency displacements contributing to the interferograms.

This study demonstrates how InSAR can potentially increase understanding of sea ice on a fundamental level in terms of large-scale stability and long-term ice dynamics. Landfast ice is a critical resource and more information is needed to understand landfast ice formation and how it is impacted by changes in the environment such as by surrounding pack ice. To understand the future of the landfast ice and how large-scale sea ice changes may impact landfast ice properties important for stakeholders, landfast ice needs to be properly integrated into regional sea ice models currently depending on laboratory experiments [*Hopkins*, 2008]. However, higher-resolution datasets are needed for validation and ultimately improvement of landfast ice models [*König Beatty*, 2007]. This study demonstrates that InSAR opens up for a large-scale comparison between model and observations of landfast ice, a crucial step in validating landfast ice models.

Landfast ice stability is not only important for industrial operations, but also for Indigenous populations [*Druckenmiller et al.*, 2013] and marine mammals [*Smith*, 1980]. This research explores InSAR as it provides valuable information to stakeholders, regulators and other decision-makers tracking the value of landfast ice as a hunting ground or as a habitat. To increase the value of InSAR in the context of sea ice use it will be important to further understand the rheology and yield stress on the scale of the landfast ice, and the temporal resolution needed to capture failure processes. An important next step will be to utilize the model developed here to quantify strain and internal ice stress and explore how the measured strains relate to destabilization of landfast ice and acting as potential precursor events for larger-scale failure and break-out [*Dammann et al.*, in review].

4.8 Acknowledgements

Part of this work was supported by the National Science Foundation as part of the Seasonal Ice Zone Observing Network (NSF-0856867). We would like to thank Peter Hickman at the Geographical Information Network of Alaska for programming support and Dr. Wenyu Gong

at the Geophysical Institute, University of Alaska Fairbanks. Satellite data and guidance was provided by the Alaska Satellite Facility. Comments by three anonymous reviewers helped to substantially improve the manuscript.

4.9 References

Bamler, R., and P. Hartl (1998), Synthetic aperture radar interferometry, *Inverse problems*, *14*(4), R1.

Bamler, R., and M. Eineder (2005), Accuracy of differential shift estimation by correlation and split-bandwidth interferometry for wideband and delta-k SAR systems, *Geoscience and Remote Sensing Letters, IEEE*, *2*(2), 151-155.

Bashaw, E. K., J. Drage, S. K. Lewis, and C. Billings (2013), Applied Ice Engineering for Exploring Arctic Natural Resources, paper presented at ISCORD 2013@ sPlanning for Sustainable Cold Regions, ASCE.

BP (2013), BPXA Winter Geotechnical Ancillary Activity Notification 2013*, Rep.*, 22 pp.

Comiso, J. C., and D. K. Hall (2014), Climate trends in the Arctic as observed from space, *Wiley Interdisciplinary Reviews: Climate Change*, *5*(3), 389-409.

Dammann, D. O., H. Eicken, A. Mahoney, F. Meyer, J. Freymueller, and A. M. Kaufman (in review), Assessing landfast sea ice stability and internal ice stress around ice roads using L-band SAR interferometry and inverse modeling, *Cold Reg Sci Technol*.

Dammert, P. B. G., M. Lepparanta, and J. Askne (1998), SAR interferometry over Baltic Sea ice, *Int J Remote Sens*, *19*(16), 3019-3037, doi: Doi 10.1080/014311698214163.

Dickins, D., G. Hearon, K. Morris, K. Ambrosius, and W. Horowitz (2011), Mapping sea ice overflood using remote sensing: Alaskan Beaufort Sea, *Cold Reg Sci Technol*, *65*(3), 275-285.

Druckenmiller, M. L., H. Eicken, J. C. George, and L. Brower (2013), Trails to the whale: reflections of change and choice on an Iñupiat icescape at Barrow, Alaska, *Polar Geography*, *36*(1-2), 5-29, doi: 10.1080/1088937X.2012.724459.

Druckenmiller, M. L., H. Eicken, M. A. Johnson, D. J. Pringle, and C. C. Williams (2009), Toward an integrated coastal sea-ice observatory: System components and a case study at

Barrow, Alaska, *Cold Reg Sci Technol*, *56*(2-3), 61-72, doi: 10.1016/J.Coldregions.2008.12.003.

Eicken, H., and A. R. Mahoney (2015), Sea Ice: Hazards, Risks, and Implications for Disasters, in *Coastal and Marine Hazards, Risks, and Disasters*, Jean T. Ellis, Douglas J. Sherman and John F. Shroder, 381-399, Elsevier Inc., Amsterdam, Netherlands.

Eicken, H., A. L. Lovecraft, and M. L. Druckenmiller (2009), Sea-Ice System Services: A Framework to Help Identify and Meet Information Needs Relevant for Arctic Observing Networks, *Arctic*, *62*(2), 119-136.

Eicken, H., R. Gradinger., T. Heinrichs, M. A. Johnson, A. L. Lovecraft, and M. Kaufman (2012), Automated ice mass balance site (SIZONET),edited, UCAR/NCAR - CISL - ACADIS http://dx.doi.org/10.5065/D6MW2F2H.

Eicken, H., J. Jones, F. Meyer, A. Mahoney, M. L. Druckenmiller, M. Rohith, and C. Kambhamettu (2011), Environmental security in Arctic ice-covered seas: from strategy to tactics of hazard identification and emergency response, *Mar Technol Soc J*, *45*(3), 37-48, doi: doi.org/10.4031/MTSJ.45.3.1.

Ferretti, A., A. Monti-Guarnieri, C. Prati, F. Rocca, and D. Massonet (2007), InSAR Principles-Guidelines for SAR Interferometry Processing and Interpretation, *ESA Publications*, *TM-19*.

Fienup-Riordan, A., and A. Rearden (2010), The ice is always changing: Yup'ik understandings of sea ice, past and present, in *SIKU: knowing Our Ice: Documenting Inuit Sea Ice knowledge and Use*, Igor Krupnik, Claudio Aporta, Shari Gearheard, Gita Laidler and Lene Kielsen Holm, 295-320, Springer, New York.

Finucane, R., and R. Scher (1983), Floating Ice Road Construction, *Journal of Energy Resources Technology*, *105*(1), 26-29.

George, J. C., H. P. Huntington, K. Brewster, H. Eicken, D. W. Norton, and R. Glenn (2004), Observations on shorefast ice dynamics in Arctic Alaska and the responses of the Iñupiat hunting community, *Arctic*, *57*(4), 363-374.

Hilcorp (2015), Development and Production Plan, *Liberty Development Project*, *Revision 1*, 266.

Hopkins, M. A. (2008), *Simulation of Landfast Ice Along the Alaskan Coast*, 15 pp., US Army Cold Regions Research and Engineering Laboratory, US Department of the Interior, Minerals Management Service, Alaska OCS Region., Hanover, New Hampshire

Huang, L., D. Wolcott, and H. Yang (2011), Tidal Characteristics Along the Western and Northern Coasts of Alaska, paper presented at U.S. Hydro 2011 Conference, Florida.

König Beatty, C. (2007), *Arctic landfast sea ice, Ph.D. thesis*, 110 pp., New York University, New York, NY.

Krieger, A. G., G. N. Kidd, and D. A. Cocking (2003), Northstar Drilling-Delivering the First Arctic Offshore Development, *SPE drilling & completion*, *18*(02), 188-193.

Lang, O. (2003), *Radar remote sensing in Western Antarctica with special emphasis on differential interferometry*, *Doctoral thesis*, 127 pp., Julius-Maximilians-Universitaet, Wuerzburg, Germany.

Li, S., L. Shapiro, L. McNutt, and A. Feffers (1996), Application of Satellite Radar Interferometry to the Detection of Sea Ice Deformation, *Journal of the Remote Sensing Society of Japan*, *16*(2), 67-77.

Mahoney, A., H. Eicken, and L. Shapiro (2007), How fast is landfast sea ice? A study of the attachment and detachment of nearshore ice at Barrow, Alaska, *Cold Reg Sci Technol*, *47*(3), 233-255, doi: 10.1016/J.Coldregions.2006.09.005.

Mahoney, A., H. Eicken, L. Shapiro, and A. Graves (2006), Defining and locating the seaward landfast ice edge in northern Alaska, paper presented at 18th International Conference on Port and Ocean Engineering under Arctic Conditions (POAC'05), Potsdam, NY.

Mahoney, A., H. Eicken, A. G. Gaylord, and R. Gens (2014), Landfast sea ice extent in the Chukchi and Beaufort Seas: The annual cycle and decadal variability, *Cold Reg Sci Technol*, *103*, 41-56, doi: 10.1016/J.Coldregions.2014.03.003.

Mahoney, A., D. O. Dammann, M. A. Johnson, H. Eicken, and F. J. Meyer (2016), Measurement and imaging of infragravity waves in sea ice using InSAR, *Geophys Res Lett*, *43*, 6383–6392.

Meier, W. N., G. K. Hovelsrud, B. E. Oort, J. R. Key, K. M. Kovacs, C. Michel, C. Haas, M. A. Granskog, S. Gerland, and D. K. Perovich (2014), Arctic sea ice in transformation: A review of recent observed changes and impacts on biology and human activity, *Reviews of Geophysics*, *52*(3), 185-217.

Mesher, D., S. Proskin, and E. Madsen (2008), Ice road assessment, modeling and management, paper presented at 7th International Conference on Managing Pavement Assets, Calgary, AB, June, 2008.

Meyer, F. J., A. R. Mahoney, H. Eicken, C. L. Denny, H. C. Druckenmiller, and S. Hendricks (2011), Mapping arctic landfast ice extent using L-band synthetic aperture radar interferometry, *Remote Sens Environ*, *115*(12), 3029-3043, doi: 10.1016/J.Rse.2011.06.006.

Morris, K., S. Li, and M. Jeffries (1999), Meso-and microscale sea-ice motion in the East Siberian Sea as determined from ERS-I SAR data, *Journal of Glaciology*, *45*(150), 370-383.

Potter, R., J. Walden, and R. Haspel (1981), Design and construction of sea ice roads in the Alaskan Beaufort Sea, paper presented at Offshore Technology Conference, Offshore Technology Conference, Houston, Texas.

Scharroo, R., and P. Visser (1998), Precise orbit determination and gravity field improvement, *Journal of Geophysical Research*, *103*(C4), 8113-8127.

Smith, T. G. (1980), Polar bear predation of ringed and bearded seals in the land-fast sea ice habitat, *Canadian Journal of Zoology*, *58*(12), 2201-2209.

Stroeve, J. C., M. C. Serreze, M. M. Holland, J. E. Kay, J. Malanik, and A. P. Barrett (2012), The Arctic's rapidly shrinking sea ice cover: a research synthesis, *Climatic Change*, *110*(3-4), 1005-1027, doi: 10.1007/S10584-011-0101-1.

Tucker, W., W. Weeks, A. Kovacs, and A. Gow (1980), Nearshore ice motion at Prudhoe Bay, Alaska, in *Sea ice processes and models: proceedings of the Arctic Ice Dynamics Joint Experiment International Commission of Snow and Ice symposium* Pritchard RS, 261-272, University of Washington Press, Seattle, Washington.

USACE (2002), *Ice Engineering*, 475 pp., Department of the Army, US Army Corps of Engineers Washington DC.

Vincent, F., D. Raucoules, T. Degroeve, G. Edwards, and M. Abolfazl Mostafavi (2004), Detection of river/sea ice deformation using satellite interferometry: limits and potential, *Int J Remote Sens*, *25*(18), 3555-3571.

Weber Hoen, E., and H. A. Zebker (2000), Penetration depths inferred from interferometric volume decorrelation observed over the Greenland ice sheet, *IEEE Transactions on Geoscience and Remote Sensing 38*(6), 2571-2583.

Weeks, W. (1977), Studies of the movement of coastal sea ice near Prudhoe Bay, Alaska, USA, *Journal of Glaciology*, *19*(81), 533-546.

Weeks, W. (2010), *On sea ice*, University of Alaska Press, Fairbanks, Alaska, 664 pp.

Weingartner, T. J., S. L. Danielson, J. L. Kasper, and S. R. Okkonen (2009), *Circulation and Water Property Variations in the Nearshore Alaskan Beaufort Sea (1999–2007)*, 168 pp., US Dept. of Interior, Minerals Management Service, Alaska Outer Continental Shelf Region, Anchorage, Alaska.

5 EVALUATING LANDFAST SEA ICE STRESS AND FRACTURE IN SUPPORT OF OPERATIONS ON SEA ICE USING SAR INTERFEROMETRY*

5.1 Abstract

Recent Arctic warming has led to reduced sea-ice thickness and a more dynamic landfast ice cover with potential widespread consequences for ice users. Here, we develop an approach to assess the small-scale deformation of landfast ice critical to on-ice operations using synthetic aperture radar interferometry (InSAR). InSAR has previously proven successful in determining long-term qualitative climatology of ice deformation around on-ice operations, but is now used to explore its potential for providing quantitative guidance for ice road planning, construction, and maintenance. A validation effort using X-band SAR and high-precision GPS data over Elson Lagoon, Alaska, confirms the ability of InSAR to accurately estimate 3-dimensional sea ice strain values accumulated between SAR image acquisitions, using an inverse model. The inverse model was further applied to L-band InSAR data over the Northstar Island ice road near Prudhoe Bay, Alaska. Assuming an elasto-brittle rheology, the derived strain values yielded a spatial distribution of internal stress consistent with preexisting ice defects and morphology. In several localized regions of the study area, stress values exceeded expected yield stress. Resulting relative fracture intensity potential was shown to conform with local knowledge based on road inspections by engineers, and may be used to guide ice road planning, construction and maintenance efforts. The results presented here demonstrate that InSAR is an accurate tool for estimating landfast ice deformation and stability in support of ice use. The findings may also provide substantial new insights into the mechanics of landfast ice.

* Dammann, D. O., H. Eicken, A. Mahoney, F. Meyer, J. Freymueller, and A. M. Kaufman (in review). Assessing landfast sea ice stability and internal ice stress around ice roads using L-band SAR interferometry and inverse modeling. *Cold Reg Sci Technol.*

5.2 Introduction

5.2.1 Background and motivation

Along Arctic coastlines during winter, landfast sea ice forms and is attached to land through a combination of processes, including freezing down to the surface of the shallow sea floor (bottomfast ice), stabilization through grounded ridges, and confinement by a convoluted coastline or barrier islands. Landfast sea ice is an essential part of the Arctic system, serving as a seasonally stable platform used extensively over millennia by people, marine mammals and other ice-associated species. Arctic coastal communities are relying on landfast sea ice to gain access to hunting grounds, resources, and neighboring settlements. During the past century, advances in transportation have led to a further diversification of landfast ice stakeholders [*Eicken et al.*, 2009], in particular through construction of sea ice roads and use of landfast ice for operation of heavy equipment [*Masterson and Spencer*, 2001]. Compared to other man-made infrastructure, sea ice roads provide for lower-cost and more effective means of transportation for much of the year [*Sooäär and Jaagus*, 2007]. Ice roads are critical as a means of access to rural communities [*NAB*, 2011] as well as oil and gas drilling and production sites [*Krieger et al.*, 2003] illustrated in Figure 5.1.

The many services the landfast ice provides to a range of different stakeholders are currently in jeopardy due to widespread Arctic change. Over the last few decades, Arctic sea ice has been declining at a rapid rate [*Comiso and Hall*, 2014; *Meier et al.*, 2014; *Stroeve et al.*, 2012] with associated reductions in landfast ice [*Mahoney et al.*, 2014]. The recent changes in landfast ice, in combination with an increased coastal community dependence on ice-based transportation and a growing industrial presence are likely to affect ice roads [*ACIA*, 2004; *Stephenson et al.*, 2011] through shorter and more unpredictable operational seasons accompanied by increasingly hazardous and difficult travel conditions already felt across the circumpolar North [*Aporta*, 2011; *Aporta and Higgs*, 2005; *Druckenmiller et al.*, 2013; *Fienup-Riordan and Rearden*, 2010; *Ford et al.*, 2008; *Orviku et al.*, 2011].

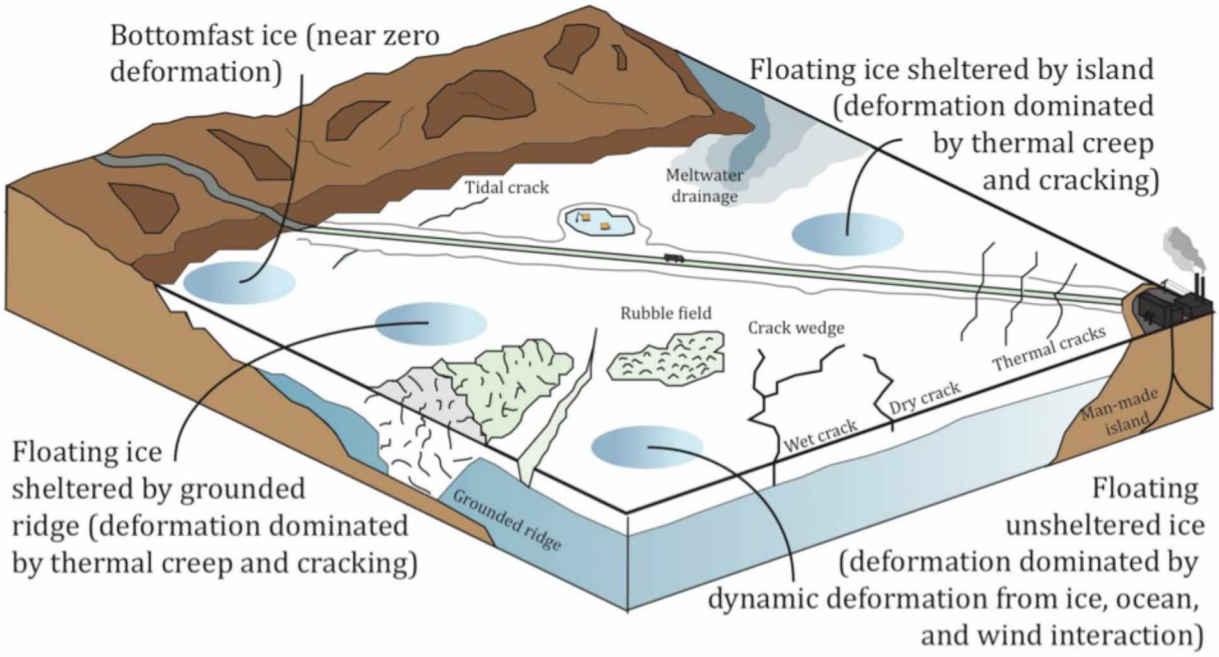

Figure 5.1 Schematic of ice road setting in coastal landfast ice, as applicable to Northstar Island and other locations. Ice features and processes that can impact trafficability, stability, and safety of the ice are also shown.

In light of recent changes, it is important to be able to quantify the changes in the ice cover that directly impact trafficability and safety of ice-based travel. So far, the majority of research on construction of ice roads has been conducted inland on fresh water ice since the vast majority of ice roads traverse lakes and rivers (review in *Fox Jr and Ott* [2000]). The research has also been limited by focusing predominately on the bearing capacity of the ice leading to specific minimum thickness requirements [*Gold*, 1971; *Squire et al.*, 1996], without identifying specific requirements pertaining to a broader trafficability context such as ice stress, stability, and structural defects.

Thinning of sea ice, particularly in dynamically constrained regions, has led to more dynamic ice [*Kwok et al.*, 2013; *Spreen et al.*, 2011] and is associated with increases in strain and fracturing [*Rampal et al.*, 2009]. Sea ice drift speeds are expected to continue to increase [*Zhang et al.*, 2012], leading to increased deformation of the landfast ice. The latter has major implications for ice users [*Druckenmiller et al.*, 2013; *Ford and Pearce*, 2012; *George et al.*,

2004; *Laidler et al.*, 2009] in part through increased density of defects and associated reductions in loadbearing capacity. However, there is little quantitative understanding of the impact of small-scale dynamic processes on on-ice operations from a safety/hazard perspective, in part due to a lack of effective assessment strategies for ice deformation over larger areas.

In regions where landfast ice is routinely used for transport and travel, the ice is typically stable enough to withstand significant stresses without complete or near-complete detachment from the coast, but may still be subject to moderate movement (mm – cm/day) and fracturing. These stresses might result from (1) thermal forcing, (2) ocean and atmospheric drag acting directly on the landfast ice and (3) stress from pack ice interaction. Previous research suggests that landfast-ice stability can be expressed in terms of the combined frictional force of relevant grounding points (e.g. islands and grounded ridges) [*Druckenmiller*, 2011; *Jones et al.*, 2016; *Mahoney et al.*, 2007], which in part determines the overall deformation rate as a result of external forcing and ultimately density of structural defects. However, substantial uncertainty exists in terms of methods to effectively detect and assess grounded ridges on a large scale. Individual ridge composition, morphology and ultimately grounding strength are also poorly assessed, making it difficult to evaluate local deformation without direct measurements of ice motion [*Mahoney et al.*, 2007].

5.2.2 Fracture Intensity Potential

To assess trafficability of landfast ice in a given region and account for local dynamic regimes and pre-existing mechanical defects in the ice, we define Fracture Intensity Potential (FIP) as the number of fracture events that can occur within a set spatial domain and timeframe, which is of critical concern for ice users [*BP*, 2013; *Eicken et al.*, 2011; *George et al.*, 2004; *Potter et al.*, 1981] mostly through reduced load-bearing capacity. Dislocation fractures can also affect trafficability by serving as drainage channels, reducing the severity of springtime flooding (but can at the same time act as strudel drains jeopardizing under-ice installations [*Dickins et al.*, 2011]). Furthermore, continued cumulative strain can potentially lead to

destabilization by reducing anchoring strength of grounded ridges [*Jones et al.*, 2016] as well as the tensile strength of the ice cover through formation of cracks.

It is recognized that in-situ assessment of relevant properties of the ice regime is required for on-ice operations [*Mesher et al.*, 2008], but this has not led to clear quantitative guidelines pertaining to ice deformation. It is therefore a timely exercise to develop methods capable of assessing FIP, which is directly related to safe operations on landfast sea ice. Recent technological advances in remote sensing have made it possible to detect continuous small-scale sea ice movements over large areas using Synthetic Aperture Radar Interferometry (InSAR) [*Dammert et al.*, 1998; *Li et al.*, 1996; *Mahoney et al.*, 2016; *Meyer et al.*, 2011; *Morris et al.*, 1999; *Vincent et al.*, 2004]. Interpretation of InSAR results is not straightforward, and is subject to ambiguities and constraints due to the one-dimensional nature of the phase information that makes up the interferograms. However, through inverse modeling constrained by plausible limits on cumulative deformation, it is possible to estimate the mode, orientation and rate of differential surface motion that may affect the smoothness and stability of landfast ice [*Dammann et al.*, 2016].

In this paper, we apply InSAR data together with an inverse model to the area surrounding Northstar Island in the Beaufort Sea – a manmade island supporting drilling and production operations in the Northstar oil and gas prospect. Facilities on the island are connected to land by a seasonal sea ice road that serves as an important logistical support route during winter and spring [*Krieger et al.*, 2003]. Economic operation of Northstar and similar installations in other Arctic locations is critically dependent on the ice road and hence also stability and properties of the surrounding ice [*Bashaw et al.*, 2013; *Potter et al.*, 1981]. We first validate InSAR and the model results using field observations (*Section 5.3*) and then assess the value of FIP as a tool for evaluating the suitability for ice road construction or long-term installments on sea ice (*Section 5.4*).

5.3 Methods and data

5.3.1 Synthetic aperture radar data and study region

This study utilizes SAR data from two sources for evaluating the FIP of landfast ice. First, we use TerraSAR-X data from the German Aerospace Center (DLR) to validate the proposed InSAR technique. TerraSAR-X is an X-band SAR sensor with high spatial resolution compared to other SAR systems favorable for validation. TerraSAR-X has been operational since 2008 with a repeat pass cycle of 11 days. For the model analysis and quantification of internal ice stress, we utilize PALSAR-1 data from the Japanese Advanced Land Observing Satellite (ALOS-1). PALSAR-1 was an L-band system, which is advantageous over sea ice compared to other wavelengths [*Meyer et al.*, 2011]. ALOS-1 operated between 2006 and 2011 with a repeat pass time period of 46 days. A summary of the data is listed in Table 5.1. The different datasets cover two areas on the Beaufort Sea coast of Alaska (Figure 5.2), both of which are located entirely within the extent of landfast sea ice at the time of acquisition.

Table 5.1 Orbit and image data for the two interferograms used

Platform	Orbit #	Frame/ cycle	Dates	Temporal baseline (d)	Location
ALOS-1 PALSAR-1	22132 22803	1410	03/21/2010 05/06/2010	46	Northstar Island
TerraSAR-X	42382	254	02/04/2015 02/15/2015	11	Elson Lagoon

5.3.2 Inverse modeling approach for InSAR-derived strain fields in sea ice

A Synthetic aperture radar (SAR) signal consists of amplitude (related to properties of the individual scatterers on the ground) and phase (related to the distance between the satellite and the individual scatterers). The phase component, ψ, of the signal equates to $2\pi n\lambda/r_0 + \psi_0$ where r_0 is the distance between a ground object and satellite, n the number

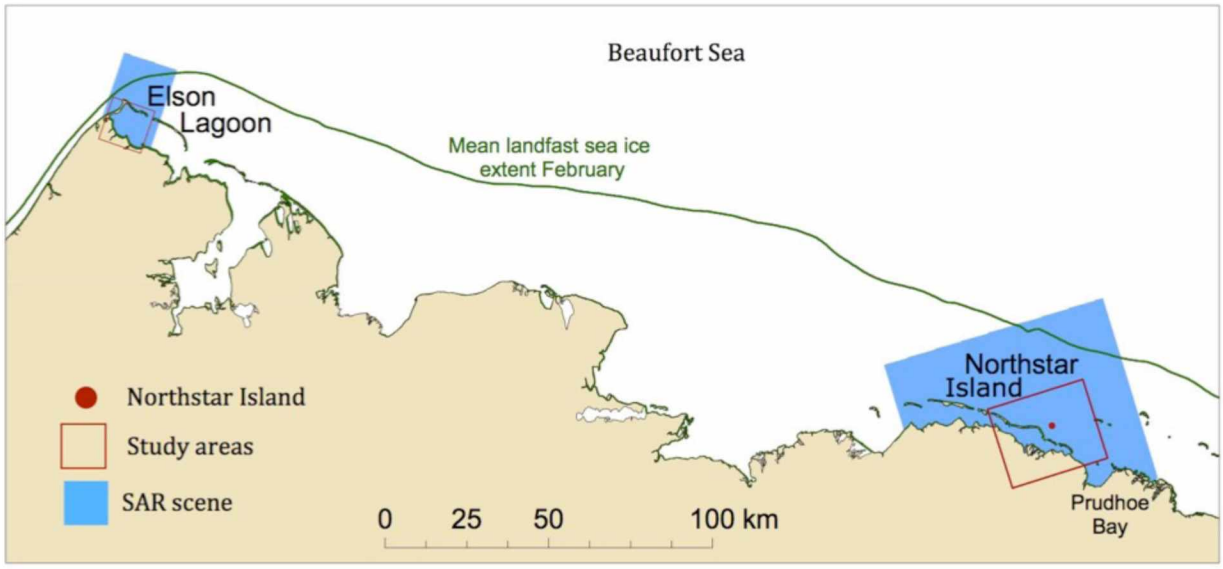

Figure 5.2 Study area of Elson Lagoon and Northstar Island with satellite scenes outlined in blue. Only subsets are used and is marked with a red rectangle. The mean landfast ice edge in February (1996-2008) is outlined in green [*Mahoney et al.*, 2014].

of whole phase cycles of 2π, and λ is the wavelength of the radar energy. As phase measurements are defined between 0 and 2π, they cannot be used to determine the absolute distance to an object on the ground. Also, due to a random phase component, ψ_0, the phase information in a single SAR image is randomized and not immediately useful. However, if acquiring two SAR scenes from coherent viewing geometries the relative difference in r_0 occurring between the acquisitions can be resolved through SAR interferometry (InSAR) [*Bamler and Hartl*, 1998; *Ferretti et al.*, 2007]. Through a standard processing workflow [*Dammann et al.*, 2016] an interferogram I is formed expressing spatial distribution of the phase difference, commonly referred to as the interferometric phase, Φ:

$$\Phi = arctan\left[\frac{Im(I)}{Re(I)}\right] \qquad (5.1)$$

In (1), I is calculated through complex conjugate multiplication of two image signals

$$I = |u_1||u_2|e^{i(\psi_1 - \psi_2)} \qquad (5.2)$$

where u_1 and u_2 represent the information in image 1 and 2 with respective phase values $\psi_1$and ψ_2. The absolute value of Φ at any point is somewhat arbitrary, due to the unknown integer number of wavelengths contributing to the difference in r_0 between the two SAR images. However, variations in Φ, which we will refer to from hereon as phase change, can be used to measure differences in r_0 with precisions of a fraction of the radar wavelength. The phase change over sea ice is typically dominated by horizontal or vertical surface deformation [*Dammann et al.*, 2016]. The surface elevation of sea ice rarely exceeds 10m [*Weeks*, 2010] and therefore rarely contributes significantly to a phase change. Other contributors such as coregistration errors, noise, and atmospheric effects can often be corrected or are minimal.

An interferogram can only be successfully created if scattering elements remain coherent (complex coherence $|\gamma| > 0$) between two co-registered SAR acquisitions u_1 and u_2. γ can be estimated from uniform patches, W, around an image pixel at location [j,k]:

$$|\hat{\gamma}[i,k]| = \frac{|\sum_W u_1[i,k] \cdot u_2{}^*[i,k]|}{\sqrt{\sum_W |u_1[i,k]|^2 \cdot |u_2{}^*[i,k]|^2}} \qquad (5.3)$$

Sea ice is often susceptible to temporal decorrelation as a result of a surface movement that displaces scatterers out of a resolution cell (i.e. pixel) and leads to complete decorrelation if the shift is larger than the cell itself (other types of decorrelation are discussed in *Dammann et al.* [2016]). It is therefore implied that interferograms can only successfully be constructed over landfast ice that experiences displacement of less than the size of one resolution cell of the SAR imagery over the timespan between acquisitions.

The contribution to the interferometric phase by surface deformation is given by:

$$\Phi_{motion} = \frac{4\pi}{\lambda} d \qquad (5.4)$$

where λ is the wavelength of the SAR system and d is the change in r_0 as a result of displacement towards or away from the satellite orbit. It is important to note that only deformation in line-of-sight direction results in a phase change since deformation components in cross-track direction do not result in change in distance from the satellite to

scatterers on the ground. Also, uniform motion across the radar footprint will result in Δd equal zero and therefore will not generate a phase change $\Delta\Phi$, known as fringes, across the interferogram. When the cumulative motion across a region of deforming ice leads to $d > \lambda/2$, the value of Φ repeats itself. Thus, the phase change over a region of consistently deforming ice will resemble a set of parallel or quasi-parallel "fringes", each representing a cumulative Δd of $\lambda/2$.

The total deformation of a particular point can therefore only be determined through phase unwrapping, but the spacing and orientation of the fringes can be used to estimate the 3-d ice deformation from the 1-d interferometric phase using an inverse approach under certain constraints. This approach was introduced in detail in *Dammann et al.* [2016] and was shown to provide a wealth of information about landfast ice deformation modes present in an area. In short, we first generate synthetic interferograms to simulate the phase change of different idealized scenarios of deformation. Each scenario is defined by a single mode of deformation (e.g., uniaxial compression, pure shear, etc.) with a specified magnitude and orientation relative to the viewing geometry. We then correlate these ideal interferograms with patches (20x20 pixels) of an observed interferogram to select the best match of mode, magnitude, and orientation angle (Equation 5.4). For more information, please refer to [Dammann et al, 2016].

Landfast sea ice can deform in several different ways, hence the model simulates five independent deformation modes (Figure 5.3). There is little evidence for rotational-type motion taking place in landfast ice and model results indicating rotation are likely a result of shear in line-of-sight direction. We therefore speculate that four of the modes may encompass the realistic ranges of differential motion that landfast ice can undergo (Table 5.2), thereby enabling a physical interpretation of the InSAR data. Due to ambiguities resulting from the translation of 1-d data into 3-d motion fields, certain deformation modes can result in synthetic interferograms that are highly correlated with each other. In these cases, additional criteria are necessary to identify the most likely mode of deformation responsible for an observed interferogram. For example, consideration of geometrical constraints may be used to rule out cases where interferograms might otherwise suggest

non-plausible solutions. Additionally, non-coherent cross correlation [*Bamler and Eineder*, 2005], or large-scale sea ice velocity products (e.g. *Fowler et al.* [2003]) can enable identification of the most likely deformation mode based on far-field ice motion patterns. Ambiguities can also occur when (1) deformation is a combination of different modes modeled, (2) there is insufficient coherence, and (3) the deformation is too slow to generate a sufficient phase change. More detailed information about the model can be found in *Dammann et al.* [2016].

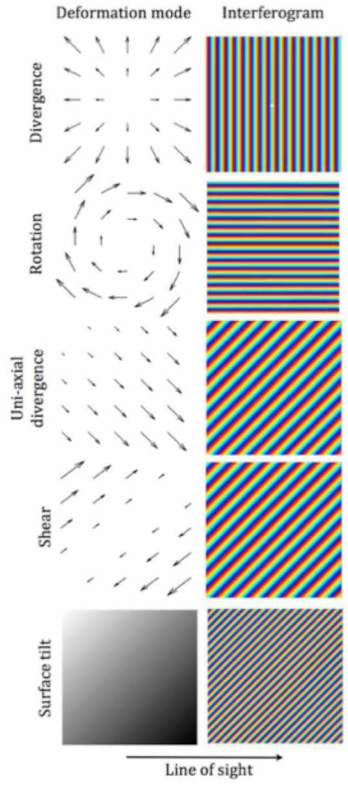

Figure 5.3 Modes and directions of deformations modeled are displayed in the top row with corresponding interferograms in the bottom row. Modes include divergence, rotation, shear, uni-axial divergence, and surface tilt. These displacements are modeled for 16 look angles varying at 22.5-degree intervals. Rotation and radial convergence are directionally independent. Uni-axial divergence is correlated with reversed directions. Shear and uni-axial divergence in cross-track direction are completely correlated with rotation and radial divergence respectively. Surface tilt is indicated by brighter (darker shading) representing higher (lower) elevation.

Table 5.2 Possible modes of ice deformation detectable by InSAR

	Deformation mode	Example mechanism
1	Radial divergence (compression/expansion)	Temperature changes
2	Uni-axial divergence	Wind stress perpendicular to coastline
3	Shear motion	Shear forcing from less stationary landfast ice or pack ice translating motion into adjacent fast ice
4	Surface tilting	Local sea-level surge, waves or large-scale buckling of the ice

5.3.3 Calculating stress fields in sea ice from InSAR-derived strain

To investigate how internal stress is distributed throughout a particular ice cover, we calculate the ice *strain* (*du/dx, dv/dy*, and *du/dy+dv/dx*) from the displacement gradients derived via the previously discussed model inversion. The strain is calculated from the best model match and by identifying the solution that is geophysically most plausible. To further derive information about the underlying *stress* state of the ice we need to make assumptions about the rheology of the landfast ice. Comprehensive studies that have explored the rheology of sea ice at the floe scale are currently lacking; here, InSAR may eventually provide substantial new insight.

Large-scale deformation fields of the Arctic ice pack have been explored using buoys [*Rampal et al.*, 2008] and the RADARSAT geophysical processor system (RGPS) [*Kwok*, 1998]. Viscous-plastic sea ice rheology approximations were shown to perform poorly at these spatial scales (10–300km) [*Kwok et al.*, 2008]. This rheology is particularly poorly suited to represent landfast ice, which lacks viscous interactions between floes. At the same time, analyzing InSAR data over Baltic sea ice, *Dammert et al.* [1998] concluded that elastic deformation alone may not be sufficient to explain the large landfast ice deformation observed with InSAR. There is growing recognition of the importance of explicit representation of fracture processes in sea ice modeling and an elasto-brittle rheology may therefore be more appropriate, where the inelastic deformation is accommodated by the differential

displacement along fracture planes from the meter- to the pan-Arctic scale [*Rampal et al.*, 2008; *Weiss et al.*, 2007]. The framework that we present in this paper considers the sea ice as a continuous elastic plate encountering accumulated damage, simulating the opening of cracks and leads, incorporates scaling laws and strain rate distributions not captured using a viscous-plastic rheology, and has shown promise as a rheology capable of accurately modeling sea ice deformation [*Girard et al.*, 2011].

To evaluate the stress distribution, we apply Hooke's law to calculate the maximum stress resulting from the observed strain (i.e., infinite yield stress):

$$\sigma_{ij} = KD\epsilon_{ij} \qquad (5.5)$$

where

$$\sigma_{ij} = \begin{bmatrix} \sigma_x \\ \sigma_y \\ \tau \end{bmatrix}, \quad D = \frac{1}{1-\nu^2}\begin{bmatrix} 1 & \nu & 0 \\ \nu & 1 & 0 \\ 0 & 0 & \frac{1-\nu}{2} \end{bmatrix}, \quad \epsilon_{ij} = \begin{bmatrix} \epsilon_x \\ \epsilon_y \\ \gamma \end{bmatrix} \qquad (5.6)$$

where σ_x/σ_y and τ are normal and shear stress, respectively. υ is Poisson's ratio and ϵ_x/ϵ_y and γ are normal and shear strain, respectively. K initially is equal to Young's modulus (E) for a flawless piece of ice. Here, we consider ice at the intersection between the lab-scale and the floe scale, with only limited field data available to guide this modeling approach. In particular, we will need to consider adapting the value of Young's modulus derived from studies at the lab-scale to the field-scale. *Girard et al.* [2011] assumed a significantly reduced E (0.35 GPa) due to the existence of pre-existing defects and fractures at larger scales. With a higher resolution and relatively stationary landfast ice in spring, our E is expected to be significantly higher, but still lower than lab-scale E. To estimate lab-scale E we use the approximation [*Langleben*, 1962]:

$$E = (10.00 - 35.1s)\ GPa \qquad (5.7)$$

Using an average sea ice bulk salinity, s, of 5‰ [*Pegau et al.*, 2016], we calculate a lab-scale E of 9.8 GPa, which is comparable to the 9.4 GPa floe-scale E estimated by using the approach of Girard et al. [2011]. We use the upper range E (9.8 GPa), which may lead to overestimated

stress and fracture since E is linearly proportional to stress. We use a typical value for Poisson's ratio, ν, of 0.33 [*Murat and Lainey*, 1982; *Schulson*, 1999].

The principal stress is approximated to assess the maximum normal stresses relevant for failure. Assuming static equilibrium, the original normal stress, σ_x and σ_y, and shear stress, τ, can be calculated in the new coordinate system (σ'_x, σ'_y, and τ') rotated by an angle θ relative to the original coordinate system:

$$\sigma'_x = \frac{\sigma_x + \sigma_y}{2} + \frac{\sigma_x - \sigma_y}{2} cos2\theta + \tau sin2\theta \qquad (5.8)$$

$$\sigma'_y = \frac{\sigma_x + \sigma_y}{2} + \frac{\sigma_x - \sigma_y}{2} sin^2\theta + \tau sin2\theta \qquad (5.9)$$

$$\tau' = \frac{\sigma_x - \sigma_y}{2} sin2\theta + \tau cos2\theta \qquad (5.10)$$

Since landfast sea ice tends to yield through fracture rather than flow in a volume conserving manner, failure will occur through tension rather than shear [*Timco and Weeks*, 2010]. Excluding shear as a mode of failure has shown promise as a way to model landfast ice on the floe-scale [*König Beatty*, 2007]. This is different from large-scale models that consider failure through Mohr-Columb failure criterion within the sea ice cover. We are interested in the maximum value of σ'_x and σ'_y regardless of rotation angle (principal stress σ_1 and σ_2). This value exists when τ' is zero:

$$\max \sigma_{1,2} = \frac{\sigma_x + \sigma_y}{2} \pm \sqrt{\left(\frac{\sigma_x - \sigma_y}{2}\right)^2 + \tau^2} \qquad (5.11)$$

leading to a rotation of:

$$\theta_0 = 2\tan^{-1}\left(\frac{2\tau}{\sigma_{22} - \sigma_{11}}\right) \qquad (5.12)$$

While cognizant of simplistic approximations of E and ν and the limitations of assuming a simple elastic rheology, we are still able to determine the likeliness of ice failure by considering yield stresses. Most sea ice models consider tensile yield stress to be zero or

near-zero since the ice is expected to include fractures of zero strength on scales that are typically used for sea ice models [*Hibler*, 1979; *König Beatty and Holland*, 2010]. However, the ubiquitous presence of pre-existing cracks may not be an appropriate assumption for landfast ice, particularly in sheltered lagoons. Such sea ice therefore possesses a significant, non-zero tensile yield stress. Since tensile yield stress is much lower than the compressive yield stress for strain rates occurring in the landfast ice, the tensile yield stress is expected to be the governing factor for failure. In this study, we therefore only consider tensional failure. Failure in tension at the floe scale typically occurs through the build up of tensional forces through wind and current action over significant fetch. At smaller scales, it can also result from compressive flow due to buckling of the ice, a process that is not as relevant in the context of this study and not considered here. In some cases and especially for small, localized regions, it may be difficult to identify the optimum model solution (see *Section 5.4.1*). In such cases, the solution that will result in the highest tensile stress is chosen, such that fracture estimates are overestimated rather than underestimated.

To evaluate the plausible tensile yield stress, it is necessary to assess strain rates (derived from InSAR data via model inversion) and ice temperatures. From laboratory experiments, tensile yield stress in sea ice is found to range between 0.2 and 0.8MPa (at strain rates mostly between 10^{-3} and 10^{-5} s^{-1}) depending primarily on porosity [*Richter-Menge and Jones*, 1993; *Timco and Weeks*, 2010]. However, the concept of a single failure envelope should be viewed with caution in relation to the ice cover since strength depends upon spatial scale and strain rate [*Schulson and Duval*, 2009]. At the floe scale, pre-existing flaws can initiate or facilitate failure and will lead to reduced tensile yield stress compared with laboratory measurements [*Schulson and Duval*, 2009]. This has been shown to reduce in-situ tensile strength by a factor of $1/\sqrt{L}$, L being the characteristic scale [*Dempsey et al.*, 1999] and in this case the pixel size.

For an elasto-brittle rheology the material fractures whenever the elastic yield stress is reached and failure occurs. If further strain takes place, the stress will again build up to a potential second failure. After each failure event the elastic stiffness, K, is recalculated:

$$K = E\varrho^{\,m} \qquad (5.13)$$

where ϱ is a scalar indicating the damage level per event, and m represents number of events. ϱ contributes to a reduction in elastic stiffness and overall stress as a result of small-scale damage, is <1, and is here set to 0.9. While E is likely overestimated (see above), this will not completely invalidate the number of damage events calculated from Equation 5.13. Instead, rather than representing the number of damage events between acquisitions, m corresponds to the total number of events experienced by an initially flawless piece of ice under the observed strain.

5.4 Validation of InSAR-based approach with in-situ data

Before we interpret stress and strain fields derived from InSAR, we first perform a validation of the individual parameters that we derived from the InSAR observations. Initially, we validate InSAR-based estimates of landfast ice deformation using GPS receivers as a reference (*Section 5.3.2*). Subsequently, we also validate the stress and strain values calculated from InSAR data via the inverse model (*Section 5.3.3*).

5.4.1 In-situ observations in Elson Lagoon

While a direct relationship between fringes and surface deformation patterns has been demonstrated in theory [*Bamler and Hartl*, 1998], the use of InSAR as a decision-support tool requires successful in-situ validation of the results from the inverse model approach outlined above. To accomplish this, a validation effort was initiated in Elson Lagoon near Barrow on the Beaufort Sea coast of Alaska. The barrier islands at the outer margin of the lagoon shelter the enclosed sea ice from dynamic interaction with the pack ice offshore, thereby largely limiting deformation to thermal contraction and expansion. This allows for a better quantitative evaluation of key assumptions underlying the InSAR-based inverse modeling approach.

GPS data was collected using four Trimble 5700 receivers and Trimble Zephyr Geodetic (TRM41249.00) antennas. These dual-frequency, survey-grade GPS receivers were operating stand-alone and recorded phase and pseudorange observations every 15 seconds; the resulting data were processed using precise-point positioning to produce daily positions in a global reference frame (ITRF2008). The receivers were positioned in a grid near the center of the lagoon approximately 3.3 km apart (colored dots in Figure 5.4a). Each receiver was powered by zinc air alkaline batteries due to air-cell batteries proven performance in cold weather conditions. Each receiver with batteries was placed in a box sealed to keep out drifting snow, but with ducted air vents attached to the antenna mast to allow sufficient airflow (0.4 m^3/day) to the batteries. Each antenna was mounted 0.5 m above the ice surface on a length of steel conduit frozen into a hole drilled into the ice. Roughly one month after deployment, site #1 stopped recording and the three remaining sensors started power cycling whenever the temperature dropped and sustained at -30˚C. Details are listed in Table 5.3.

Table 5.3 GPS operating data for the four stations in Elson Lagoon

Receiver #	**Lat**	**Lon**	**Deploy-ment**	**First power cycling**	**Loss of data**	**Retrieval**
1	71.325	-156.330	1/7/2015	-	1/29/2015	4/14/2015
2	71.325	-156.240	1/7/2015	2/11/2015 – 2/17/2015	-	4/14/2015
3	71.295	-156.240	1/7/2015	3/12/2015 – 3/19/2015	-	4/14/2015
4	71.295	-156.330	1/7/2015	2/14/2015 – 2/17/2015	-	4/14/2015

5.4.2 Groundtruth validation of InSAR-derived deformation over sea ice

The ice on Elson Lagoon consists of level first-year ice exhibiting only minor vertical relief. Accordingly, the TerraSAR-X amplitude image (4 Feb 2015) shows low backscatter,

indicating generally smooth ice, though we identify a small ridge extending across the lagoon indicated by an arrow below Station 2 (Figure 5.4a). Field observations showed that the sea ice within Elson Lagoon contains numerous refrozen cracks (e.g. Figure 5.4b), but these are often difficult to identify in SAR amplitude images due to the small vertical relief and the dependence on viewing geometry. However, one identifiable crack is indicated with an arrow near Station 1. Before the cracks refreeze they can be associated with significant lateral displacements resulting in clear discontinuities in fringes across an interferogram (indicated by the left arrow in Figure 5.4c). The phase discontinuity is therefore a potential indicator of a dislocation crack, while a continuous phase disturbance is the result of a ridge feature (indicated by the right arrow in Figure 5.4c).

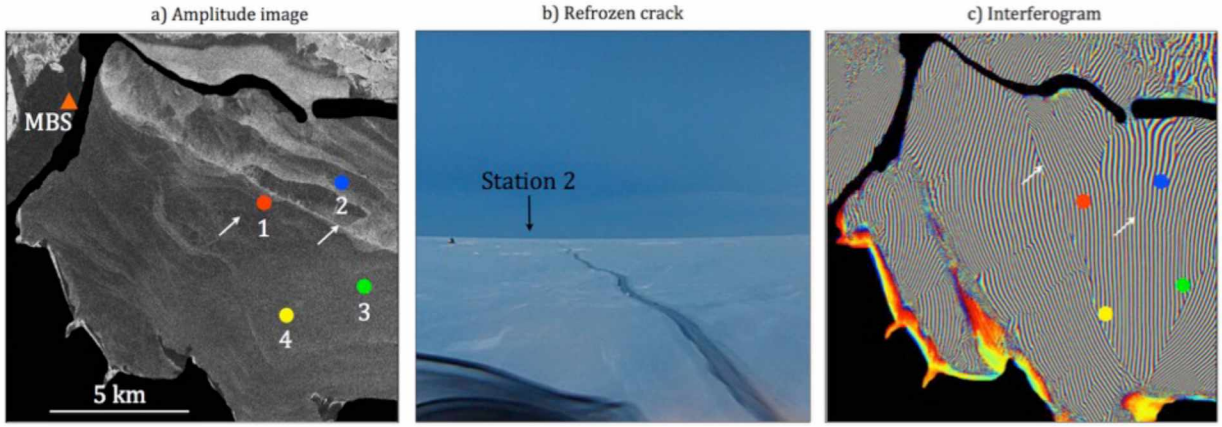

Figure 5.4 Ground validation in Elson Lagoon. (a) TerraSAR-X scene (4 Feb 2015 over Elson Lagoon. Colored dots (1-4) correspond to placement of GPS sensors tracking continuous ice displacement (7 Jan - 14 Apr, 2015). Triangle shows location of SIZONet mass balance site. The left arrow points to a visible fracture and the right arrow points to a small ridge. (b) image of a refrozen crack on the lagoon prior to GPS deployment. (c) TerraSAR-X interferogram (4 Feb 2015 - 15 Feb 2015).

Horizontal and vertical motion at the location of the four stations during the entire deployment period is plotted in Figure 5.5a-c. This dataset is compared with an interferogram (Figure 5.4c) between 4 Feb and 15 Feb 2015 (highlighted area in Figure 5.5), in which time period the ice was subjected to substantial cooling (Figure 5.5d). We compared InSAR-derived deformation (calculated from total fringe count) with DGPS-derived differential motion between all combinations of the three functioning sensors (Table 5.4). Since InSAR is only sensitive to 1-d motion, we only evaluate the DGPS- and InSAR-derived cross-track differential motion (column 2 and 3 in Table 5.4 respectively). Due to a period of rapid motion in the DGPS data between 4 and 5 February (day 35 and 36, Figure 5.5), the motion calculation is sensitive to the interpolation method used to estimate the position of the GPS stations at the precise time of the first SAR acquisition and will result in a window of strain values based on the daily DGPS solution immediately before and after the acquisitions. InSAR-derived differential motion falls well within the window of DGPS-derived strain values lending confidence to the assumption that interferometric fringes do in fact correspond predominately to lateral deformation [Dammann et al., 2016] and thus can be used to accurately quantify ice strain.

Table 5.4 Comparison between DGPS- and InSAR-derived cross-track differential motions

Station pair	**DGPS cross-track differential motion (mm)**	**InSAR cross-track differential motion (mm)**
2-3	119.6 – 199.8	175.7
4-3	372.3 – 532.2	505.3
4-2	252.7 – 332.4	329.6

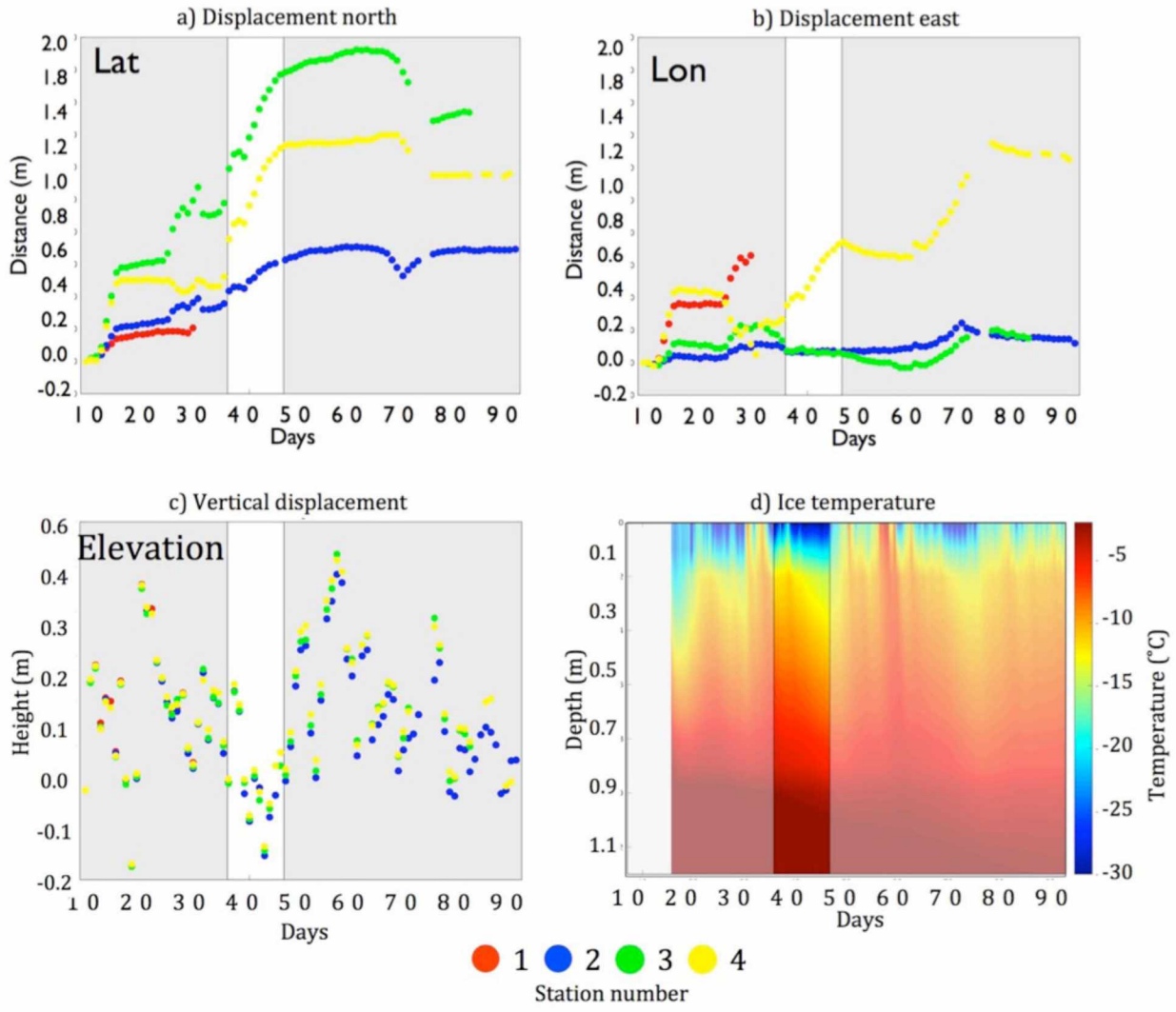

Figure 5.5 Small-scale displacement of GPS sensors (7 Jan 2015 - 14 Apr 2015) in N-S direction (a), E-W direction (b), and vertical (c). Temperature throughout the ice measured at the SIZONet mass balance site is displayed during the time of GPS acquisitions (d). The highlighted area indicates the time period between SAR acquisitions.

All four GPS stations recorded almost constant horizontal motion during the interval between SAR acquisitions (Figure 5.5 a,b). Vertical motion was more variable and resulted in a near-zero net displacement between the two acquisition dates (Figure 5.5c). The motion of the land adjacent to the lagoon (in ITRF2008) amounts to only about 5 mm over the 90-day span of the data, which is less than 1% of the observed displacements. Therefore, the

motions of the GPS sites can be interpreted as motion of the ice relative to the adjacent land, and relative motions between GPS sites provide accurate measurement of the internal deformation of the ice.

5.4.3 Groundtruth validation of the inverse interferometric model

The postulation that the lagoon ice experiences moderate deformation due to predominately thermal changes is supported by the interferogram (4 Feb – 11 Feb 2015) exhibiting parallel fringes in the along-track direction, consistent with radial convergence (Figure 5.3). Similar patterns have been observed from PALSAR-1 data between 2006 and 2010 (not shown) also linked to convergence [*Dammann et al.*, 2016]). The lagoon-wide convergence feature can be explained based on the lack of dynamic forcing and the response of the ice cover to a substantial cooling event resulting in thermal contraction of the ice (highlighted area in Figure 5.5d).

The GPS stations (colored dots in Figure 5.4) were located almost exclusively within a single region of homogenous fringes (Figure 5.4c) largely uninterrupted by discontinuities, which indicates the ice in that region underwent the same mode of deformation. It is apparent from Figure 5.5a that the southern GPS stations (3 and 4) experience faster northward motion than the northern stations (1 and 2) between acquisitions (highlighted area). Similarly, in Figure 5.5b, the western stations (1 and 4) move eastward faster than the eastern stations (2 and 3). The total motion observed by GPS between acquisitions is represented by arrows in Figure 5.6 and indicates convergence in the central part of the lagoon conforming with the inverse model results (Figure 5.6).

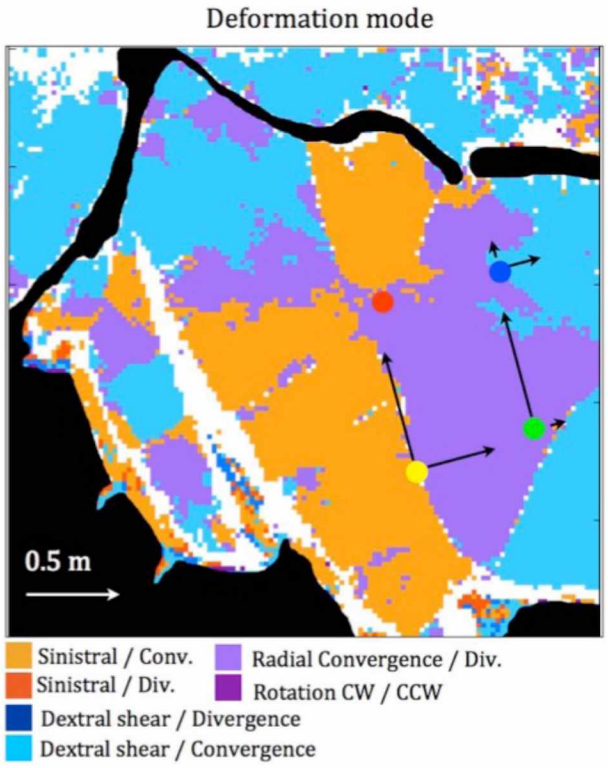

Figure 5.6 Model output indicating modes of deformation. Arrows by stations indicate lat-lon movement between acquisitions. Area encompassed by the station grid is predominately governed by radial convergence.

We evaluated the inverse model solution in the area between the sensors, which is predominately radial convergence, through quantification of normal (along-track and cross-track) strains. Normal strain is calculated in two different ways drawing upon DGPS data and inverse model results (Table 5.5):

(1) DGPS data provides 3D displacement of points, which can be used to calculate strain components in cross-track and along-track directions (column 3 in Table 5.5). Along-track DGPS strain is calculated using differential motion between station 2 and 3 and cross-track strain using station 3 and 4 (row 1 and 2 in Table 5.5 respectively). The range of strain values is due to the range of differential motion values (see Table 5.4).

(2) The inverse model, applied to the interferogram, allows us to estimate the complete 2-D strain field and thus derive both cross-track and along-track strain from the model solution (column 4 in Table 5.5).

The strain values calculated from the inverse model are slightly higher than the range estimated from the DGPS sensors. This is likely due to the resolution of the model, which only resolves magnitudes in 10-20cm intervals in each model cell. The model solution with immediately higher or lower strain would correspond to the two values listed in parenthesis (fourth column in Table 5.5) identifying a window of possible strain values. Although the model strain is not within the DGPS strain window, the model strain window overlaps. We can therefore be confident that the model captured the correct strain level. With that said, this result also indicates that the model would be improved by an increase in steps of magnitude of deformation.

Table 5.5 Normal strain calculated from both DGPS sensors and InSAR

Direction	**Station pair**	**DGPS-derived Strain (10^{-4})**	**Inverse model-derived strain (10^{-4})**
Along-track	2-3	1.18 – 1.51	1.71 (1.14 – 2.28)
Cross-track	4-3	1.16 – 1.66	1.98 (1.32 – 2.65)

Based on results obtained from Table 5.4, we are assuming that differential cross-track motion obtained by InSAR is an accurate representation of true relative motion. We therefore compared cross track inverse model-derived strain (1.98E-4 - see table 5.5) with cross-track strain derived from the interferogram (1.58E-4 - not shown in table) relying solely on deformation derived from fringe information (505.3 mm - see Table 5.3). In this particular case, the error of inverse model-derived strain is 25% and likely close to the upper range of expected error since the InSAR-derived strain (1.58E-4) is close to the mean value

of two model solutions (1.32E-4 and 1.98E-4 - see Table 5.5) hence any lower strain is expected to result in a model strain result of 1.32E-4. From here, we assume a possible inverse model-derived strain error of up to roughly 25%. The model results in Section 5.4 are directly being used to derive stress (*Section 5.4.2*) and fracture (*Section 5.4.3*). These are both linear derivations from strain (see *Section 5.2.3*) and thus result in a possible respective error of 25% as well.

It is apparent from the GPS data that the ice deformation in Elson Lagoon is not a constant process, but instead takes place in a series of episodes of relatively rapid ice motion (cm/day). These episodes coincide with periods of cooling (Figure 5.5d), as observed by a thermistor string deployed in ice of similar thickness adjacent to the lagoon (triangle in Figure 5.4a). The durations of most of the deformation episodes observed by the DGPS were shorter than the 46-day repeat pass cycle of PALSAR-1 and even the 11-day repeat pass cycle of TerraSAR-X. Therefore, InSAR-derived estimates of strain rate calculated using the temporal baseline (apparent strain rate) would typically underestimate the peak strain rate during such episodes. However, provided the ice motion is monotonic, the total motion captured in an interferogram should be an accurate measurement of the cumulative deformation over time. The ice motion observed by all four DGPS stations was largely monotonic, which is consistent with the process of opening and refreezing of cracks. With that said, the interferogram shown in Figure 5.4c (spanning 4 Feb to 15 Feb 2015) coincided almost exactly with the longest deformation episode observed by the DGPS during which time the ice motion was near constant, so we can therefore expect the interferogram to accurately capture both total deformation and deformation rate.

5.5 Results

5.5.1 Model result near Northstar Island, Alaska

The inverse model was applied to landfast ice in the vicinity of Northstar Island near Prudhoe Bay, Alaska. A PALSAR-1 amplitude image over Northstar (March 21, 2010) shows the

location of the island and the ice road that leads to the island (Figure 5.7a). Northstar Island is located in the center of the circle and the ice road can be seen as a dark line (arrow). An interferogram was constructed using imagery acquired on March 21 and May 6, 2010 (Figure 5.7b). The interferogram itself provides direct insight into key aspects of the landfast ice setting. The density of fringes depends largely on the total deformation; hence it is apparent that the ice deformation rate is significantly reduced shoreward of Northstar Island (arrow), which indicates that the presence of the island likely has significantly stabilized the shoreward ice in the area traversed by the ice road. The interferogram also indicates that the fringes significantly change orientation in the vicinity of the ice road. This implies that ice road construction or operation has altered the dynamics of the surrounding landfast ice, which will be discussed further in *Section 5.5*.

The inverse model was applied to this interferometric data set (Figure 5.7c), with the assumption that vertical deformation (i.e. surface tilt) did not contribute significantly to the phase change in the interferogram. This assumption is based on the fact that surface tilt cannot accumulate over significant distances without reversing. This would result in concentric or periodic fringe patterns [*Dammann et al.*, 2016], which we do not see in this case. The colors in Figure 5.7c correspond to the primary mode of deformation and it is apparent that a single mode of deformation uniformly describes the area north of Northstar as well as most of the area occupied by the ice road. Due to the ambiguities inherent to InSAR processing, this deformation mode is either sinistral (left handed) shear parallel to the fringes or uni-axial convergence perpendicular to the fringes. Such model-based ambiguities can be largely eliminated by considering geometrical constraints or other data sources. Here, sinistral shear parallel to the coastline is consistent with macro-scale motion derived from speckle tracking (Figure 5.7d), which uses cross correlation of the complex amplitude images to determine motion amounting to as little as 0.1 pixels [*Joughin et al.*, 2010]. The speckle tracking results indicate that northwestward ice motion increases with distance from the shoreline, in a manner consistent with interaction between the landfast ice and the westward-moving pack ice in the southern portion of the Beaufort Gyre [*Reimnitz et al.*, 1978].

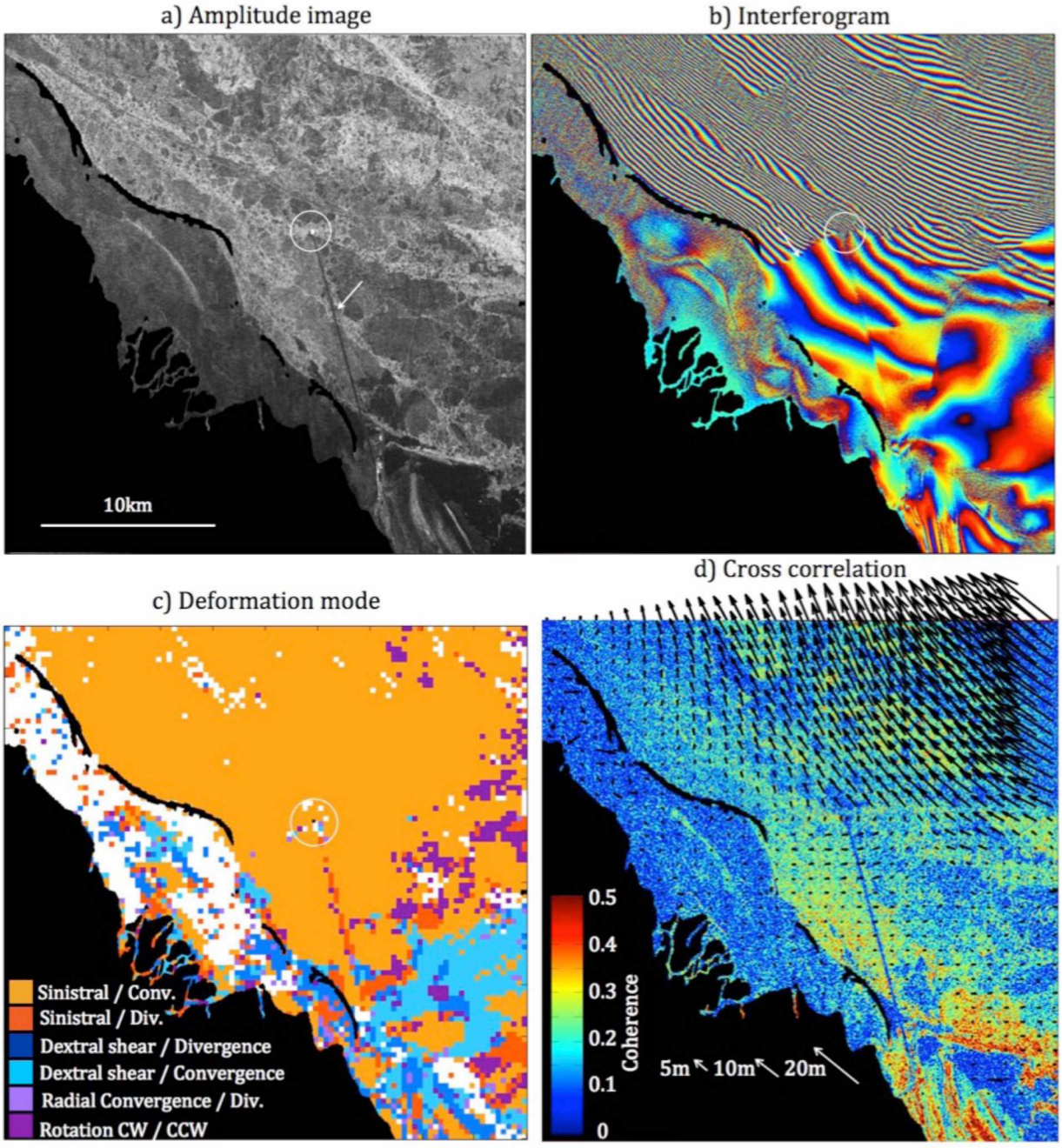

Figure 5.7 Model result over Northstar Island. (a) Amplitude image for the Northstar Island (circled) and Prudhoe Bay region, Alaska (21 Mar 2010) (arrow pointing to the ice road connecting the island to the mainland) and (b) the interferogram created from this and the following acquisition (6 May 2010) (arrow pointing to boundary between high and low fringe density by Northstar Island). (c) The model results display deformation mode with colors corresponding to the specific combination of deformation modes. (d) Incoherent cross-correlation displacement vectors superimposed on the interferogram coherence. The ice road is apparent as an area of reduced coherence due to ongoing road construction (snow

removal and thickening of the ice through pumping of water onto the ice surface). The vectors indicate a large area of uniform left-handed (sinistral) shear motion.

We identify two important issues relevant to stakeholders using the ice as a platform for operations and in particular for the construction of seasonal ice roads that this technique may help address, building on a few key assumptions regarding ice rheology. First we will estimate the internal stress distribution in the ice based on model output. Then we will assess the potential for defects, resulting in ice weakening and failure, potentially leading to the formation of cracks, buckling, and ridging.

5.5.2 Estimated strain and ice stress near Northstar Island, Alaska

To explore specific approaches to determine ice stability, we analyze the inverse model output in terms of the derived normal, ϵ_x and ϵ_y, and shear strains, γ, (Figure 5.8a-c). Subtle differences in shear orientation result in narrow linear bands of high strain magnitude parallel to barrier islands in the northwest corner of the study region. These features align with the shore-parallel ridge fields indicated by high backscatter in Figure 5.7a. Such ridges were clearly formed at an earlier time, potentially the result of similar shear deformation, and may have been weakened due to lack of consolidation.

As concluded in *Section 5.4.1* the area around Northstar Island appears to be largely governed by shear motion, which is the basis for the strain calculations. As expected, the strain decreases shoreward of Northstar and is relatively small inside of the near-coastal barrier islands. Areas of small displacement, such as stretches of landfast ice inshore of barrier islands are associated with reduced model confidence as a result of the low (20x20 pixel) resolution (not shown). The confidence of the model is reduced because fewer fringes are occupying each model patch increasing the ambiguities. The resulting low signal to noise ratio can also contribute to high errors in derived strain inside the barrier islands [*Dammann et al.*, 2016]).

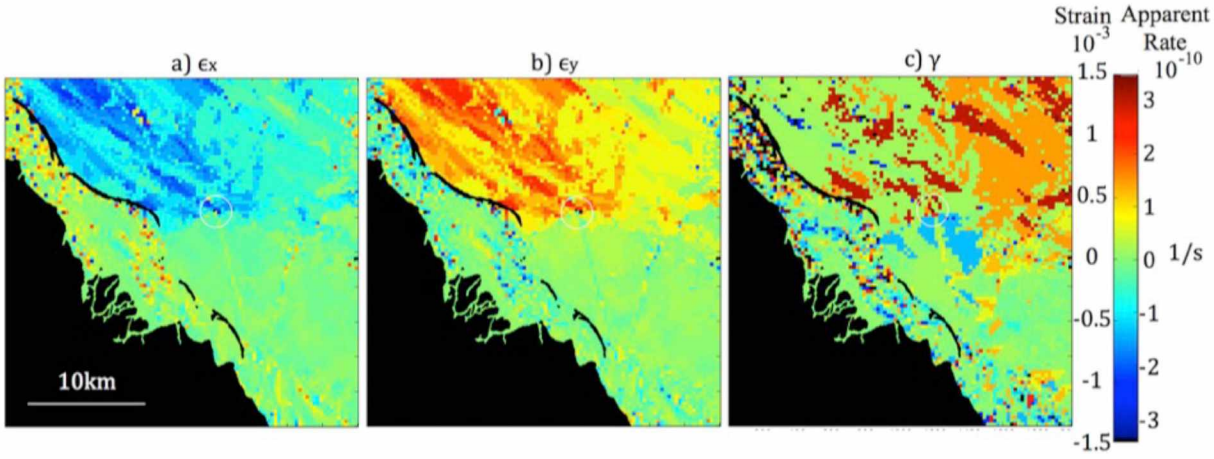

Figure 5.8 Model derived strain. (a) Range directional (left-right), (b) azimuth directional (up-down) normal strains, and (c) shear strain including apparent strain rates.

The principal maximum stress (of non-realistic elastic deformation without occurrence of damage) is calculated using Hooke's Law and is displayed in Figure 5.9. The stress is calculated assuming a fully elastic response in the absence of failure through non-elastic deformation as a first step to illustrate the stress distribution and identify areas most impacted by stress. Outside of the barrier islands, the principal stresses show linear features of higher stress parallel to features identified as ridged or deformed ice in the amplitude image (Figure 5.7a). In case this ridged ice deformed shortly prior to the interferogram, it may still be largely unconsolidated and weaker than the surrounding ice. Some of the deformed ice may also be grounded, which creates a weakened tidal crack susceptible to increased deformation through strain. The inverse model captures such dynamics well through the stress fields that originate either from actual elevated stress or a reduced Young's modulus. The stress is reduced shoreward of Northstar (Figure 5.9) clearly demonstrating the stabilizing effect of the island. Accumulation of stress through atmospheric and ocean forcing over the relatively narrow band of landfast ice can be limited, but in combination with pack ice forcing the calculated hypothetical tensile (>0) stress is far greater than the expected yield stress and hence some form of failure is expected both sea- and shoreward of Northstar.

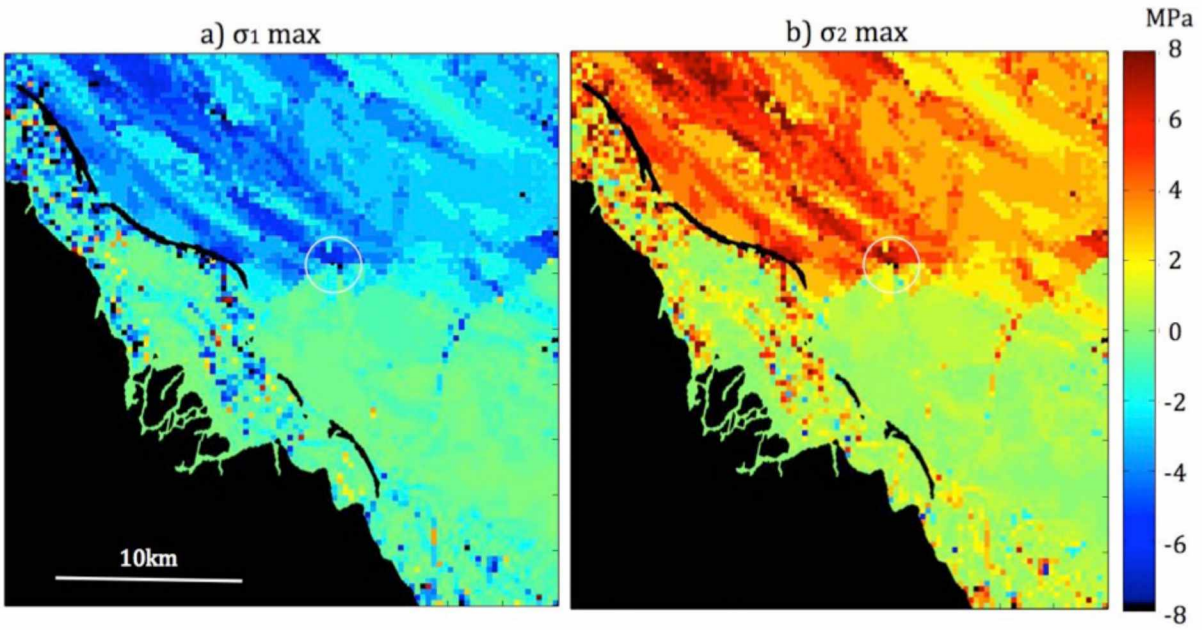

Figure 5.9 Maximum principal stresses over Northstar for the time period 21 Mar 2010 – 6 May 2010 derived from strain in (a) range (left-right), (b) azimuth (up-down) direction. The maximum stress corresponds to the stress under elastic deformation with infinite yield stress.

5.5.3 Potential for fracture based on stress estimates

In the previous subsection, we estimated the accumulated strain and stress throughout the ice cover around Northstar. So far, only the hypothetical stress has been calculated for a scenario without failure. Ice rheology and fracturing behavior depend strongly on strain rate [*Petrich and Eicken*, 2010], which can only be roughly estimated (apparent strain rate – see Figure 5.8a-c) due to the large temporal baseline of our InSAR data. During the 45 days spanning the time period of the interferogram, wind speed fluctuated around a mean of 5 m s^{-1}, but with up to roughly 13 m s^{-1} direct easterly winds over 5 days, gusting up to 17 m s^{-1} on April 30 (recorded in Deadhorse, AK). This kind of forcing variability suggests that the deformation indicated by the interferogram has likely occurred over a shorter intermediate time-scale, almost certain to be much higher than the ones estimated from the interferogram (10^{-10} s^{-1}). Similar conclusions can be drawn from work by *Jones et al.* [2016] that showed

that maximum stresses acting on landfast ice associated with failure of the ice cover persist over time periods of hours rather than days and that actual failure events play out over time scales well below one hour.

The distance across the narrow fringes in Figure 5.7b (from Northstar to the upper right corner) is roughly 20km and the maximum displacement that can be captured by interferometry is equivalent to the multi-looked resolution cell (see *Section 5.3.1*), which is roughly 15m in size. This equates to a strain of 10^{-3}, which implies that all strain observed with interferometry at this resolution will be within the ductile regime [*Petrich and Eicken*, 2010] even if all the deformation took place in a period of just one second. We are further using InSAR in combination with an elasto-brittle rheology to simulate the ductile displacement in the form of small-scale brittle failures (see *Section 5.2.3*).

Assuming a more realistic high-strain rate case where a deformation event takes place during roughly one day [*Jones et al.*, 2016] would result in a strain rate on the order of 10^{-8} s^{-1} lower than the limit used in lab experiments (10^{-5} s^{-1}) yielding a tensile yield stress of 0.8MPa (based on expected low porosity during winter – see *Section 5.2.3*). We further adjusted the lab-scale tensile yield stress (0.8MPa) to floe-scale resulting in a reduction to 46kPa due to likeliness of pre-existing cracks over the roughly 300m x 300m (20x20-pixels) model patch size (see *Section 5.2.3*). It is worth noting that the interferometric fringes across the ice in Figure 5.7b display a uniform deformation (continuous fringes) across length scales exceeding 10km and thus implies that the ice can be approximated as a quasi-continuum. This would suggest that the yield stress of this section of landfast ice might be higher than typical yield stress on the floe-scale.

The fracture intensity potential derived for an elasto-brittle rheology and a tensile yield stress of 46kPa within the timespan of the temporal baseline (B_T) is displayed in Figure 5.10. The calculation is based on the most likely inverse model solution, which in the majority of the study area is sinistral shear (Figure 5.7c). In a few small areas near shore, where the inverse model solution is ambiguous, we selected the solution with the maximum positive (tensile) stress to find the upper range as a failure estimate. σ_2 (Figure 5.9b) contains most of the positive (tensile) stress and is thus used to calculate failure in most regions, but not

all. The orientation of the tensile stress is 45 degrees clockwise relative to the direction of the shear field resulting in offshore tensile and shoreward compressional stress. In most areas, the yield stress was exceeded several times suggesting that most of the observed strain was likely accommodated by multiple small fracture events. However, the ice north of Northstar underwent significantly more failure events than the ice to the south. This is consistent with our conjecture that Northstar has a stabilizing effect on the local landfast ice.

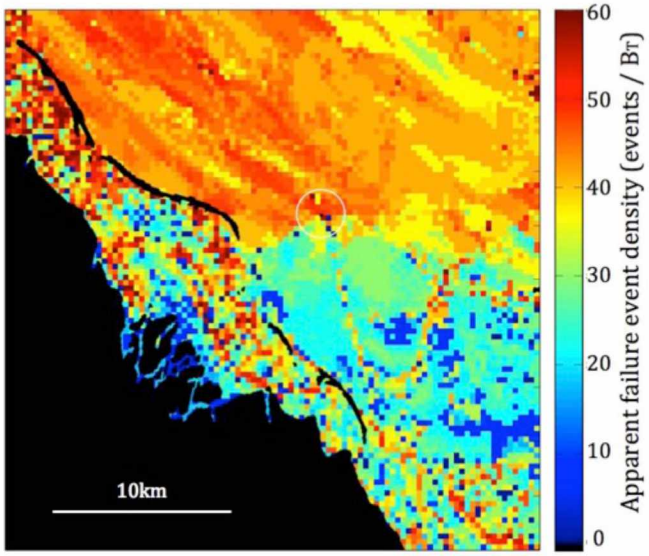

Figure 5.10 Fracture intensity potential over Northstar for the time period 21 Mar 2010 – 6 May (B_T) using an elasto-brittle rheology for the case of tensile yield stress equal to 46kPa.

5.6 Discussion

5.6.1 InSAR-derived Fracture Intensity Potential for decision support of operations on sea ice

By applying an inverse modeling approach, validated by in-situ DGPS measurements, we have estimated strain fields in a region of landfast ice subject to shear stresses likely imparted by drifting pack ice at its seaward edge. Assuming an elasto-brittle rheology, we derived maximum stresses within the ice and the resulting fracture intensity potential. We now explore how these results can be applied in the context of planning, maintenance and

operation of ice roads and other operations on landfast ice, focusing on the Northstar Island ice road as a case study.

Close examination of the landfast ice in the vicinity of the ice road (Figure 5.11) reveals that the road itself is subject to different modes of deformation and elevated stress levels compared to the surrounding ice. This finding is clearly associated with the fringe displacement identified in *Section 5.4.1* and suggests that road use or ice modification (e.g. artificial thickening of the ice) alters the localization of strain and the larger-scale stress fields. As a result, small-scale defects are concentrated into the ice road corridor, as evident from the fracture intensity potential shown in Figure 5.11c. Deformed ice featuring high backscatter exists to the east (arrows in Figure 5.11d) coinciding with areas of high stress and failure. This suggests that the increased fracture intensity around sections of the road may not be solely due to the existence and use of the road and that pre-existing defects may contribute.

The ice deformation seems to be reduced on the western side of the road where the interferogram features lower fringe densities and associated reduced strain. This likely occurs as a result of spraying seawater on the ice in an effort to artificially thicken the ice, which may impact the shoreward ice in one or more ways: (1) freezing of seawater onto the ice surface warms the ice underneath the road, raising the brine volume fraction and thereby weakening the ice, which then may act as a "crumple zone", (2) the thicker ice gets stiffer to the point where it resists deformation in such a way as to shield the shoreward ice field, or (3) the thicker ice is grounded in a few sections resulting in increased stability of the shoreward ice and reduced stress propagation.

Most of the road sections that experience defects feature about 40 failure episodes per model grid cell. Based on our observations of fractures across level first-year ice, fractures such as thermal cracks are often several cm wide (e.g. Figure 5.4b) indicating that most failure events will contribute to widen existing cracks (due to reduced strength at the location of cracks) rather than creating new ones. If we assume one crack for every grid cell, a fracture intensity potential of 40 will result in a 6-cm wide crack per model grid cell, which is plausible based on the fracture environment observed in Elson Lagoon (Figure 5.4b).

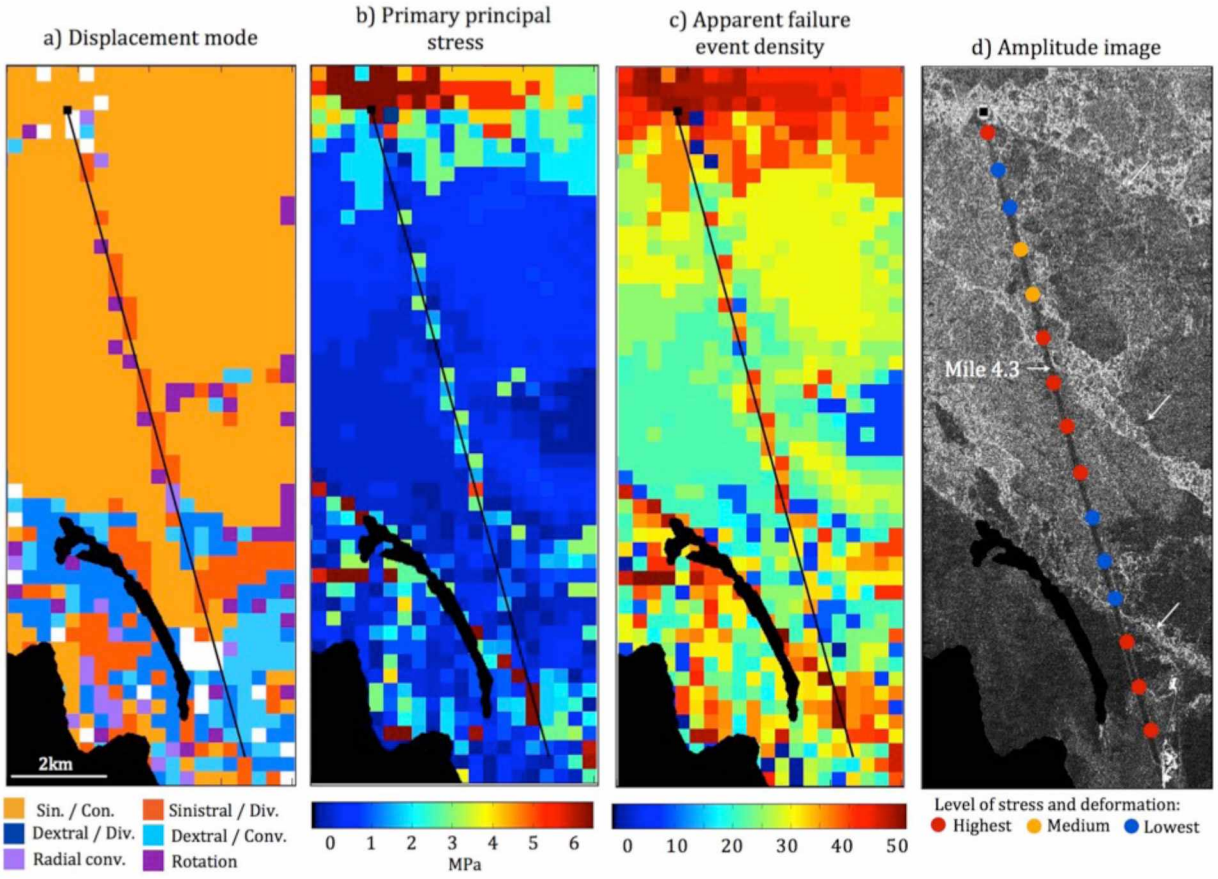

Figure 5.11 Enlarged view around the Northstar ice road for the time period 21 Mar 2010 - 6 May 2010 showing (a) displacement mode, (b) maximum tensile stress, (c) fracture intensity potential (FIP), and (d) the amplitude image with superimposed color indicating relative level of stress or FIP. Deformed ice featuring high backscatter is indicated with arrows along with mile marker 4.3 mentioned in the text. The black line in Figure a-c indicates the location of the ice road and the black square in the upper left indicates the position of Northstar Island.

The specific numbers and methods presented here are subject to uncertainty already discussed and further explored in *Section 5.5.2*. However, we are able to draw the following conclusions regarding ice characteristics and deformation processes of operational relevance in the vicinity of the ice road:

1) Deformation around the ice road is too high to be accommodated simply by elastic deformation and is therefore likely to be associated by small-scale failure and

cracking of the ice, leading to a reduced flexural strength, thereby lowering load bearing capacity.

2) The ice road construction itself changes stress patterns. Increased ice stress around the ice road may be a result of the ice serving as a barrier or crumple zone leading to increased fracturing.
3) Areas of previously deformed ice are weaker and will accommodate more of the strain (in terms of pre-existing and/or new cracks) than non-deformed areas.

Our analysis is here strictly based on a single interferogram, which limits the ability to fully evaluate seasonal fracture intensity potential (FIP) since not all forcing conditions expected during a season will be represented. Increasing the number of interferograms for a full seasonal coverage would strengthen any analysis of FIP, but is here kept to one interferogram to focus on method development and interpretation. However, even with only one interferogram, the results provide some key insights relevant to ice road planning and management and demonstrate how additional interferograms can be used accordingly.

The first stretch of road (starting from shore) is crossing the most heavily deforming ice along the whole route between the West Dock causeway and Stump Island to the west. This is a surprising result based on the location being somewhat sheltered and thus expected to be relatively stable. As the road continues past the barrier island, it appears to be less prone to external forcing (Figure 5.11b). Furthest from a grounded land point, the ice has a higher FIP before decreasing closer to Northstar Island. In close vicinity of the island there is a concentration of stress likely associated with the more dynamic, high-strain ice environment seaward of the island.

The model identifies three areas of higher FIP along the ice road, which are likely the most important sections to acquire ground assessments for road operators (Figure 5.11d). Groundtruthing indicates that Mile 4.3 of the ice road (Figure 5.11d), located in the central section identified with high FIP, is predisposed to heavy cracking and is subject to substantial repair through surface flooding (W. Crowell, personal communication, 2016) providing added validation for the technique developed here.

We have here demonstrated how maps of FIP can be used to pinpoint locations in the vicinity of an ice road, which may be subject to substantial fracturing and reduced load bearing capacity, to guide strategic observations on the ground. This is only one example of how this information can be utilized to support ice use. Other possible relevant applications of FIP maps include:

1) Routing of ice roads through stable areas less prone to ice failure.
2) Identifying areas of high fracture intensity as potential risk locations for strudel scour in the context of subsurface pipeline routing.
3) Monitoring of operations (such as ice roads or construction of artificial islands) in terms of their impact on the local ice regime from a stability and ice failure perspective.

Possible additional applications of the ice stress maps include:

1) Identifying convergence zones to locate and predict preferred ridging zones
2) Identifying zones subject to high stress under different forcing conditions, which may be used to identify areas prone to breakout events.
3) Assessment of forces acting on structures, caissons, vessels etc.

5.6.2 Method robustness and limitations

The inverse model shows promise in its ability to determine the correct mode and magnitude of deformation. In some cases, the model is unable to resolve differences between certain modes of deformation, but these ambiguities can largely be resolved by applying geometrical constraints or considering additional sea ice motion information, as discussed in *Section 5.2.2* and in more detail by *Dammann et al.* [2016].

Another important model constraint is its resolution. With a model resolution of 20x20 pixels (300 m x 300 m), modeling deformation on a spatial scale approaching the pixel size may be problematic (e.g. the case of a fringe displacement in the near vicinity of an ice road or a fringe discontinuity across a fracture). Furthermore, coherence constraints due to flooding or other modifications of the ice surface may also affect ice roads in particular (see

coherence loss across road in Figure 5.7d). Thus, higher resolution achieved in the use of X-band SAR would likely also result in reduced coherence. Interferometric fringes over sea ice are predominately caused by lateral deformation. Hence, in this analysis we have ruled out topographic effects or vertical motion, which is a valid approximation in most scenarios (see *Section 5.4.1*).

We also note that the choice of ice rheology will impact the stress derived from the modeled strain and the resulting failure densities. Here, we used a rheology that did not include creep, which can occur for strain rates of up to 10^{-8} s^{-1} [*Barnes et al.*, 1971], close to what was observed in our study region by *Weeks* [1977]. The DGPS data from Elson Lagoon show ice deformation occurring during episodes of rapid motion lasting typically < 10 days separated by longer periods of near zero motion (Figure 5.5a,b). Therefore, daily strain rates may be more than an order of magnitude higher than those inferred from interferograms spanning 10 days or more (*Section 5.3.2*).

Caution should be used when interpreting exact FIP. Excluding creep and solely considering elastic deformation likely contributes to overestimation of fractures for an elasto-brittle rheology. Also, considering consistent InSAR-derived strain rate as opposed to higher intermittent strain rates will likely contribute to underestimation of fractures. However, the main emphasis of the analysis should not be placed on exact numbers, but rather on the distribution of relative magnitudes, providing insight into the landfast sea ice dynamics and spatial patterns relevant in the context of FIP, ice stability, and features of broader relevance, in particular ice cracks.

5.7 Conclusions

At a time of continuing interest in Arctic industrial development, we stress the need for an approach to accurately evaluate and monitor ice properties and dynamics critical to ice roads and other on-ice operations, in support of planning, construction, and safe operations of over-ice transportation systems. Synthetic aperture radar interferometry has received relatively little attention in sea ice science, but is shown here to be a tool capable of providing

substantial new insight into sea ice dynamics relevant from an operational and research perspective.

Using DGPS data collected during a groundtruth campaign on sea ice in Elson Lagoon, Alaska, we performed what we believe to be the first in situ validation of InSAR-derived surface motion over sea ice. InSAR-derived ice motion was found to lie within the range of displacement values measured by DGPS. An inverse model was used in this study capable of providing detailed quantitative information about ice strain and ice deformation on the floe scale (roughly 400x400m resolution). This model was also evaluated during the groundtruth campaign where we determined the inverse model's ability to select the solution with most closely matching strain value, but at the same time overestimating strain and associated stress and fracture by up to 25% due to large steps in deformation rate inherent in the model setup. Running the model with smaller envelopes of deformation rate can most likely significantly reduce this error.

The model identified deformation mode and strain rates around Northstar Island consistent with m-scale motion derived from speckle tracking and regional-scale sea ice drift patterns in the Beaufort Gyre. This method has further proven capable of providing detailed information in support of ice use as modeled strain strikingly conforms to key coastal and ice morphological features in the vicinity of ice operations. This study has demonstrated the promise of InSAR as a tool for evaluating cm-scale sea ice displacements on spatial scales covering many square kilometers. As further evaluation, areas of high strain conform to areas of severely deformed ice identified in the amplitude images and locations identified with high fracture potential by ice road engineers, which further validates the inverse model.

Stress and FIP values have been estimated based on an elasto-brittle rheology, but are subject to caveats from constraining the model to this rheology, thereby disregarding other processes of potential relevance. However, even qualitative or relative estimates of the stress and fracture distribution are of potential use in identifying areas most prone to failure. Such estimates can offer decision-makers insights into areas possibly deviating from an assumed loading capacity and can help guide ground-based measurements and risk assessments. This approach has shown promising results evaluating the overall deformation potential of an ice

cover. However, some open questions remain regarding small-scale processes around the ice road itself due to resolution limitations and due to the inevitable coherence loss over the ice road. An example is the fringe displacement across the road and the apparent reduced ice deformation potential shoreward of the road. Here, a finite element model may provide valuable insight into possible mechanisms explaining these observations.

The InSAR data analysis and inverse modeling approach outlined above provide an opportunity to study the impact of wind, ocean, and thermodynamic forcing on stationary and near-stationary ice at a level of detail and for a spatial coverage difficult to achieve in the past. The technique provides indirect insight into the sea-ice deformation and may allow for meso-scale mapping of cm-scale surface strain as a result of such external forcing. Being able to quantitatively evaluate sea ice deformation on scales greatly exceeding the lab-scale opens up opportunities for investigating landfast sea ice from a new perspective with significant potential in evaluating and improving landfast sea ice modeling.

The techniques presented here provide an opportunity for the development of operational guidelines in terms of specific safety criteria directly related to the deformation potential of the landfast ice. To increase the value of InSAR in the context of sea ice use it will be important to further understand the rheology and yield stress at the scale of the landfast ice and the temporal resolution needed to capture failure processes. A next step will be to understand how the measured strains can result in destabilization of the ice cover and serve as precursors to substantial ice movement and detachment. Short-temporal baseline InSAR has shown great promise to be able to capture short-term processes such as wave activity [*Mahoney et al.*, 2016] and may provide substantial new insight into larger-scale failure and break-out events.

5.8 Acknowledgements

Part of this work was supported by the National Science Foundation (NSF-0856867) in the context of the Seasonal Ice Zone Observing Network. ALOS-1 PALSAR-1 data and guidance was provided by the Alaska Satellite Facility, through an ALOS data grant from the Japan

Aerospace Exploration Agency (JAXA). TerraSAR-X data was generously provided by the German Aerospace Center (DLR) through a science proposal (COA_1987).

5.9 References

ACIA (2004), *Impacts of a Warming Arctic, Arctic Climate Impact Assessment*, 144 pp., Cambridge University Press, Cambridge, UK.

Aporta, C. (2011), Shifting perspectives on shifting ice: documenting and representing Inuit use of the sea ice, *The Canadian Geographer/Le Géographe canadien*, *55*(1), 6-19, doi: 10.1111/J.1541-0064.2010.00340.X.

Aporta, C., and E. Higgs (2005), Satellite culture - Global positioning systems, inuit wayfinding, and the need for a new account of technology, *Curr Anthropol*, *46*(5), 729-753, doi: 10.1086/432651.

Bamler, R., and P. Hartl (1998), Synthetic aperture radar interferometry, *Inverse problems*, *14*(4), R1.

Bamler, R., and M. Eineder (2005), Accuracy of differential shift estimation by correlation and split-bandwidth interferometry for wideband and delta-k SAR systems, *Geoscience and Remote Sensing Letters, IEEE*, *2*(2), 151-155.

Barnes, P., D. Tabor, and J. Walker (1971), The friction and creep of polycrystalline ice, *Proceedings of the Royal Society of London. A. Mathematical and Physical Sciences*, *324*(1557), 127-155.

Bashaw, E. K., J. Drage, S. K. Lewis, and C. J. Billings (2013), Applied Ice Engineering for Exploring Arctic Natural Resources, *ISCORD 2013: Planning for Sustainable Cold Regions*, 308-319.

BP (2013), BPXA Winter Geotechnical Ancillary Activity Notification 2013, *Rep.*, 22 pp.

Comiso, J. C., and D. K. Hall (2014), Climate trends in the Arctic as observed from space, *Wiley Interdisciplinary Reviews: Climate Change*, *5*(3), 389-409.

Dammann, D. O., H. Eicken, F. Meyer, and A. Mahoney (2016), Assessing small-scale deformation and stability of landfast sea ice on seasonal timescales through L-band SAR

interferometry and inverse modeling, *Remote Sens Environ*, *187*, 492-504, doi: 10.1016/j.rse.2016.10.032.

Dammert, P. B. G., M. Lepparanta, and J. Askne (1998), SAR interferometry over Baltic Sea ice, *Int J Remote Sens*, *19*(16), 3019-3037, doi: Doi 10.1080/014311698214163.

Dempsey, J., R. Adamson, and S. Mulmule (1999), Scale effects on the in-situ tensile strength and fracture of ice. Part II: First-year sea ice at Resolute, NWT, *International journal of fracture*, *95*(1-4), 347-366.

Dickins, D., G. Hearon, K. Morris, K. Ambrosius, and W. Horowitz (2011), Mapping sea ice overflood using remote sensing: Alaskan Beaufort Sea, *Cold Reg Sci Technol*, *65*(3), 275-285.

Druckenmiller, M. L. (2011), *Alaska shorefast ice: interfacing geophysics with local sea ice knowledge and use, Doctoral thesis*, 210 pp., University of Alaska Fairbanks, Fairbanks, Alaska.

Druckenmiller, M. L., H. Eicken, J. C. George, and L. Brower (2013), Trails to the whale: reflections of change and choice on an Iñupiat icescape at Barrow, Alaska, *Polar Geography*, *36*(1-2), 5-29, doi: 10.1080/1088937X.2012.724459.

Eicken, H., A. L. Lovecraft, and M. L. Druckenmiller (2009), Sea-Ice System Services: A Framework to Help Identify and Meet Information Needs Relevant for Arctic Observing Networks, *Arctic*, *62*(2), 119-136.

Eicken, H., J. Jones, F. Meyer, A. Mahoney, M. L. Druckenmiller, M. Rohith, and C. Kambhamettu (2011), Environmental security in Arctic ice-covered seas: from strategy to tactics of hazard identification and emergency response, *Mar Technol Soc J*, *45*(3), 37-48, doi: doi.org/10.4031/MTSJ.45.3.1.

Ferretti, A., A. Monti-Guarnieri, C. Prati, F. Rocca, and D. Massonet (2007), InSAR Principles-Guidelines for SAR Interferometry Processing and Interpretation, *ESA Publications*, *TM-19*.

Fienup-Riordan, A., and A. Rearden (2010), The ice is always changing: Yup'ik understandings of sea ice, past and present, in *SIKU: knowing Our Ice: Documenting Inuit Sea Ice knowledge and Use*, Igor Krupnik, Claudio Aporta, Shari Gearheard, Gita Laidler and Lene Kielsen Holm, 295-320, Springer, New York.

Ford, J. D., and T. Pearce (2012), Climate change vulnerability and adaptation research focusing on the Inuit subsistence sector in Canada: Directions for future research, *The Canadian Geographer/Le Géographe canadien*, *56*(2), 275-287.

Ford, J. D., T. Pearce, J. Gilligan, B. Smit, and J. Oakes (2008), Climate change and hazards associated with ice use in northern Canada, *Arctic, Antarctic, and Alpine Research*, *40*(4), 647-659.

Fowler, C., W. Emery, and M. Tschudi (2003), Polar Pathfinder daily 25 km EASE-grid sea ice motion vectors, *Digital Media*.

Fox Jr, J. D., and R. A. Ott (2000), ICE THICKNESS AND ICE BRIDGES, *Region III Forest Resources & Practices Riparian Management Annotated Bibliography*, 103 pp.

George, J. C., H. P. Huntington, K. Brewster, H. Eicken, D. W. Norton, and R. Glenn (2004), Observations on shorefast ice dynamics in Arctic Alaska and the responses of the Iñupiat hunting community, *Arctic*, *57*(4), 363-374.

Girard, L., S. Bouillon, J. Weiss, D. Amitrano, T. Fichefet, and V. Legat (2011), A new modeling framework for sea-ice mechanics based on elasto-brittle rheology, *Annals of Glaciology*, *52*(57), 123-132.

Gold, L. W. (1971), Use of ice covers for transportation, *Canadian Geotechnical Journal*, *8*(2), 170-181.

Hibler, W. (1979), A dynamic thermodynamic sea ice model, *Journal of Physical Oceanography*, *9*(4), 815-846.

Jones, J. M., H. Eicken, A. R. Mahoney, M. V. Rohith, C. Kambhamettu, Y. Fukamachi, K. I. Ohshima, and J. C. George (2016), Landfast sea ice breakouts: Stabilizing ice features, oceanic and atmospheric forcing at Barrow, Alaska, *Continental Shelf Research*, *126*(50-63), doi: 10.1016/j.csr.2016.07.015.

Joughin, I., B. E. Smith, and W. Abdalati (2010), Glaciological advances made with interferometric synthetic aperture radar, *Journal of Glaciology*, *56*(200), 1026-1042.

König Beatty, C. (2007), *Arctic landfast sea ice, Ph.D. thesis*, 110 pp., New York University, New York, NY.

König Beatty, C., and D. M. Holland (2010), Modeling landfast sea ice by adding tensile strength, *Journal of Physical Oceanography*, *40*(1), 185-198.

Krieger, A. G., G. N. Kidd, and D. A. Cocking (2003), Northstar Drilling-Delivering the First Arctic Offshore Development, *SPE drilling & completion*, *18*(02), 188-193.

Kwok, R. (1998), The RADARSAT geophysical processor system, in *Analysis of SAR data of the Polar Oceans*, Tsatsoulis C and Kwok R, 235-257, Springer, Berlin.

Kwok, R., G. Spreen, and S. Pang (2013), Arctic sea ice circulation and drift speed: Decadal trends and ocean currents, *Journal of Geophysical Research: Oceans*, *118*(5), 2408-2425.

Kwok, R., E. Hunke, W. Maslowski, D. Menemenlis, and J. Zhang (2008), Variability of sea ice simulations assessed with RGPS kinematics, *Journal of Geophysical Research: Oceans (1978–2012)*, *113*(C11).

Laidler, G. J., J. D. Ford, W. A. Gough, T. Ikummaq, A. S. Gagnon, S. Kowal, K. Qrunnut, and C. Irngaut (2009), Travelling and hunting in a changing Arctic: assessing Inuit vulnerability to sea ice change in Igloolik, Nunavut, *Climatic change*, *94*(3-4), 363-397.

Langleben, M. (1962), Young's modulus for sea ice, *Canadian Journal of Physics*, *40*(1), 1-8.

Li, S., L. Shapiro, L. McNutt, and A. Feffers (1996), Application of Satellite Radar Interferometry to the Detection of Sea Ice Deformation, *Journal of the Remote Sensing Society of Japan*, *16*(2), 67-77.

Mahoney, A., H. Eicken, and L. Shapiro (2007), How fast is landfast sea ice? A study of the attachment and detachment of nearshore ice at Barrow, Alaska, *Cold Reg Sci Technol*, *47*(3), 233-255, doi: 10.1016/J.Coldregions.2006.09.005.

Mahoney, A., H. Eicken, A. G. Gaylord, and R. Gens (2014), Landfast sea ice extent in the Chukchi and Beaufort Seas: The annual cycle and decadal variability, *Cold Reg Sci Technol*, *103*, 41-56, doi: 10.1016/J.Coldregions.2014.03.003.

Mahoney, A., D. O. Dammann, M. A. Johnson, H. Eicken, and F. J. Meyer (2016), Measurement and imaging of infragravity waves in sea ice using InSAR, *Geophys Res Lett*, *43*, 6383–6392.

Masterson, D., and P. Spencer (2001), The Northstar on-ice operation, paper presented at Proceedings of the International Conference on Port and Ocean Engineering Under Arctic Conditions, Paper no. 105, Ottawa, ON, August, 2001.

Meier, W. N., G. K. Hovelsrud, B. E. Oort, J. R. Key, K. M. Kovacs, C. Michel, C. Haas, M. A. Granskog, S. Gerland, and D. K. Perovich (2014), Arctic sea ice in transformation: A

review of recent observed changes and impacts on biology and human activity, *Reviews of Geophysics*, *52*(3), 185-217.

Mesher, D., S. Proskin, and E. Madsen (2008), Ice road assessment, modeling and management, paper presented at 7th International Conference on Managing Pavement Assets, Calgary, AB, June, 2008.

Meyer, F. J., A. R. Mahoney, H. Eicken, C. L. Denny, H. C. Druckenmiller, and S. Hendricks (2011), Mapping arctic landfast ice extent using L-band synthetic aperture radar interferometry, *Remote Sens Environ*, *115*(12), 3029-3043, doi: 10.1016/J.Rse.2011.06.006.

Morris, K., S. Li, and M. Jeffries (1999), Meso-and microscale sea-ice motion in the East Siberian Sea as determined from ERS-I SAR data, *Journal of Glaciology*, *45*(150), 370-383.

Murat, J., and L. Lainey (1982), Some experimental observations on the Poisson's ratio of sea-ice, *Cold Reg Sci Technol*, *6*(2), 105-113.

NAB (2011), Northwest Arctic Borough - Ice Road Construction, edited, Commerce, Community and Economic Development, Kotzebue, Alaska.

Orviku, K., J. Jaagus, and H. Tõnisson (2011), Sea ice shaping the shores, *Journal of Coastal Research*(64), 681.

Pegau, W. S., J. Garron, and L. Zabilansky (2016), Detection of oil on-in-and-under ice. , *Rep.*, 406 pp, Arctic Response Technology.

Petrich, C., and H. Eicken (2010), Growth, structure and properties of sea ice, in *Sea Ice*, Thomas DN and Dieckmann GS, 23-77, Wiley-Blackwell, Oxford, U. K.

Potter, R., J. Walden, and R. Haspel (1981), Design and construction of sea ice roads in the Alaskan Beaufort Sea, paper presented at Offshore Technology Conference, Offshore Technology Conference, Houston, Texas.

Rampal, P., J. Weiss, and D. Marsan (2009), Positive trend in the mean speed and deformation rate of Arctic sea ice, 1979–2007, *Journal of Geophysical Research: Oceans*, *114*(C5).

Rampal, P., J. Weiss, D. Marsan, R. Lindsay, and H. Stern (2008), Scaling properties of sea ice deformation from buoy dispersion analysis, *Journal of Geophysical Research: Oceans*, *113*(C3).

Reimnitz, E., L. Toimil, and P. Barnes (1978), Arctic continental shelf morphology related to sea-ice zonation, Beaufort Sea, Alaska, *Marine Geology*, *28*(3-4), 179-185,181-210.

Richter-Menge, J., and K. Jones (1993), The tensile strength of first-year sea ice, *Journal of Glaciology*, *39*, 609-618.

Schulson, E. M. (1999), The structure and mechanical behavior of ice, *JOM*, *51*(2), 21-27.

Schulson, E. M., and P. Duval (2009), *Creep and fracture of ice*, 432 pp., Cambridge University Press Cambridge, Cambridge, UK.

Sooäär, J., and J. Jaagus (2007), Long-term changes in the sea ice regime in the Baltic Sea near the Estonian coast, *Proc Estonian Acad Sci Eng*, *13*(3), 189-200.

Spreen, G., R. Kwok, and D. Menemenlis (2011), Trends in Arctic sea ice drift and role of wind forcing: 1992–2009, *Geophys Res Lett*, *38*(19).

Squire, V., R. J. Hosking, A. D. Kerr, and P. Langhorne (1996), *Moving loads on ice plates*, Kluwer Academic Publishers, Dordrecht, The Netherlands.

Stephenson, S. R., L. C. Smith, and J. A. Agnew (2011), Divergent long-term trajectories of human access to the Arctic, *Nat Clim Change*, *1*(3), 156-160, doi: 10.1038/Nclimate1120.

Stroeve, J. C., M. C. Serreze, M. M. Holland, J. E. Kay, J. Malanik, and A. P. Barrett (2012), The Arctic's rapidly shrinking sea ice cover: a research synthesis, *Climatic Change*, *110*(3-4), 1005-1027, doi: 10.1007/S10584-011-0101-1.

Timco, G., and W. Weeks (2010), A review of the engineering properties of sea ice, *Cold Reg Sci Technol*, *60*(2), 107-129.

Vincent, F., D. Raucoules, T. Degroeve, G. Edwards, and M. Abolfazl Mostafavi (2004), Detection of river/sea ice deformation using satellite interferometry: limits and potential, *Int J Remote Sens*, *25*(18), 3555-3571.

Weeks, W. (1977), Studies of the movement of coastal sea ice near Prudhoe Bay, Alaska, USA, *Journal of Glaciology*, *19*(81), 533-546.

Weeks, W. (2010), *On sea ice*, University of Alaska Press, Fairbanks, Alaska, 664 pp.

Weiss, J., E. M. Schulson, and H. L. Stern (2007), Sea ice rheology from in-situ, satellite and laboratory observations: Fracture and friction, *Earth and Planetary Science Letters*, *255*(1), 1-8.

Zhang, J., R. Lindsay, A. Schweiger, and I. Rigor (2012), Recent changes in the dynamic properties of declining Arctic sea ice: A model study, *Geophys Res Lett*, *39*(20).

6 CONCLUSIONS

6.1 Interfacing geophysics with local and Indigenous knowledge

At the time of writing this thesis, sea ice is undergoing widespread change across the Arctic with an increasing impact on a range of ice users through reductions in trafficability [*Fienup-Riordan and Rearden*, 2010; *Laidler et al.*, 2010], increased risk of travel [*AMAP*, 2011; *Aporta*, 2011; *Aporta and Higgs*, 2005; *Druckenmiller et al.*, 2013; *Ford et al.*, 2008; *Huntington and Fox*, 2005], and increasing challenges to assess and predict ice conditions [*AMAP*, 2011; *Eicken et al.*, 2014; *Jolly et al.*, 2002]. The need for adaptation to new ice conditions by ice users is becoming increasingly apparent and in particular in terms of Indigenous coastal communities. At the same time, the role of local knowledge (LK) and Indigenous knowledge (IK) is being increasingly recognized as a key component in this adaptation process [*Ford et al.*, 2016a; *Ford et al.*, 2016b], drawing upon knowledge obtained on timescales ranging from a lifetime (LK) to many generations (IK). IK encompasses a broader worldview than what is considered in western science [*Berkes and Berkes*, 2009; *Eicken*, 2010] incorporating both the biophysical and spiritual realms and often has a strong emphasis on sustainability [*Chapin III et al.*, 2013]. It is still unclear whether combining IK systems with scientific approaches may directly increase resilience to social-ecological changes [*Bohensky and Maru*, 2011]. However, bridging knowledge systems enhances collective understanding and capacity to navigate complex environmental change [*Rathwell et al.*, 2015].

This work is one of many testimonies to the enormous potential that lies in combining local and indigenous knowledge (LIK) with state-of-the-art scientific techniques, in particular remote sensing. Prior studies have indicated that satellite-derived information can successfully be utilized in combination with LIK and interview-based information to guide ice users [*Aporta*, 2011; *Druckenmiller et al.*, 2009; *Laidler*, 2006; *Laidler et al.*, 2011; *Meier et al.*, 2006; *Norton and Gaylord*, 2004; *Riedlinger and Berkes*, 2001]. In this prior work, remote-sensing images were discussed with local residents to identify features in the imagery associated with known surface conditions or hazards. Work has also been conducted where satellite data were combined with quantitative in-situ measurements to inform ice users [*Bell et al.*, 2014; *Druckenmiller et al.*, 2013]. These approaches are valuable,

but satellite images do not always directly correspond to user needs and often lack relevant quantitative information [*Laidler et al.*, 2011] resulting in approaches that cannot easily be scaled up to cover larger areas or different regions.

In this work I applied a systematic approach to incorporate LIK into the analysis in such a way as to enable a thorough understanding of key components of landfast sea ice use and ice-based travel. This approach has allowed me to define the relevant aspects of sea ice trafficability and identify the key geophysical properties, such as ice roughness, on which it depends. This process has also helped inform our understanding of fundamental geophysical processes such as landfast ice stability. Stability has in the past been defined in terms of the grounding force of ridges [*Jones et al.*, 2016; *Mahoney et al.*, 2007], a key determinant of the position and persistence of the landfast ice edge. In this work, stability is instead viewed in terms of the dynamic deformation taking place within the ice cover, incorporating the potential for fracturing with a broad relevance to ice users. Here, a lot of uncertainty exists around how landfast ice is impacted by dynamic deformation from wind, ocean, and pack ice forcing. In part, this uncertainty is due to the difficulty in determining sea ice deformation and internal stress propagation on the km-scale. Previous studies have indicated that landfast sea ice can be susceptible to deformation from cross-shore sea level changes possibly leading to breakout events [*Kasper and Weingartner*, 2012], is responding to surface ocean waves [*Mahoney et al.*, 2016], or the loss of stability through cumulative deformation leading to reduced anchoring strength of grounded ridges [*Jones et al.*, 2016].

In this work, I relied on recent advances in remote sensing techniques that hold potential for quantifying and mapping sea ice roughness and cm-scale deformation of the landfast ice, relevant to sea ice use. These advances provided a foundation for the thesis and led to development of new methods capable of expanding information relevant to strategic and tactical decision making by ice users in a changing icescape. This process was not straightforward and involved a thorough investigation into relevant parameters through the lens of sea ice use and LIK. The result is perhaps the first major piece of work to specifically develop direct quantitative assessment strategies in support of sea ice use.

6.2 Relevance of assessment strategies beyond the study region

The applicability of this work to a wider range of ice users beyond those examined in the case studies has been addressed through the development of a general framework, enabling new assessment strategies that draw on the broader set of parameters identified in Chapter 2. Applying this approach to other study sites requires an evaluation of the set of parameters of greatest significance for a particular ice use activity and ice regime. As seen in this work, drawing on ice users' knowledge is an important aspect of such an approach, offering significant insights, helping guide research activities as well as the development of data products. However, obtaining relevant ice use information is associated with challenges.

The oil and gas industry is often mandated to carry out sustained observations and research associated with leasing and regulation of natural resources, but the mandate often lacks specificity in terms of implementation and design and therefore does not always lead to long-term assessments needed to address Arctic change [*Eicken et al.*, 2016]. Also, outside these limitations, the industry is not required to share information related to operations; hence internal reports and operational guidelines are not commonly available to scientists in part due to industrial secrecy and in part due to lack of incentives for making proprietary materials public.

During this work, I attempted to obtain relevant literature, information from industry about day-to-day operations of ice roads, and gain access to internal industry manuals related to ice road construction. Despite minor opportunistic success, this turned out to be difficult. Fortunately, I was able to obtain a critical understanding of ice road construction and maintenance from the Northwest Arctic Borough relevant to the Kotzebue-Kiana ice road. Even so, this work could have benefitted from additional information related to industry ice road management. One solution to the lack of available information pertaining to industry is for government agencies, in addition to observing requirements associated with lease agreements, require the oil and gas industry to assign a science liaison. The liaison could serve as a point of contact within the company where scientists can inquire about obtaining existing non-proprietary data and can direct specific questions to key personnel within the company. Such an approach could potentially enhance collaboration between universities

and industry, which could also substantially improve stakeholder-directed research with mutual benefits.

For coastal populations, information regarding ice use is often more readily available than from the oil and gas industry, but should be regarded as equally proprietary. Also, if such information is obtained one should ensure: (i) an open and continued dialogue and collaboration with each community and community member, (ii) direct benefit to the individual communities from the created data products [*Cochran et al.*, 2008; *Kassam*, 2009], and (iii) data products that are easily accessible and interpretable for the relevant demographic [*Laidler et al.*, 2011]. The majority of the work presented here has been supported by the Seasonal Ice Zone Observing Network (SIZONet) building on ongoing efforts to provide continued information to local ice users drawing upon scientific approaches and LIK [*Druckenmiller et al.*, 2009] in accordance with these key steps. For the regions chosen in this thesis, the population has been both eager to share information and widely interested in helpful data. However, this should not be seen as the norm as each community will have their own perspectives that need to be respected.

Availability of direct information from ice users may be limited in some areas due to lack of ice use activities in which case other information sources can often be utilized (e.g. ice maps, satellite images, in-situ observations, etc.). Although PATH is developed in a general manner based on available information from three communities, it is still necessary to reevaluate for new locations (e.g. presence of multiyear ice or icebergs do not have a separate category for the regions considered in this work). Also, ice-user needs may change over time and additional parameters not previously considered might be relevant, which further highlights the importance of sustained communication and collaboration with ice users. Being able to assess trafficability in multiple ice regimes and ice use scenarios may help extend operational seasons and increase the economic gains of ice roads and on-ice installations and further benefit:

- Local governments and agencies to assess the state of the sea ice before routing and constructing ice roads and trails.

- Small-scale community operations such as fuel delivery from ships across sea ice, transportation of heavy building materials etc.
- Local stakeholders assessing long-term prospects of subsistence and community prosperity.
- Federal and state governments to prepare for environmental change in coastal communities including change in marine mammal habitats.
- Oil and gas operators planning new prospects and ensure safe and effective operations and access through construction of ice roads.
- Federal and state regulators ensuring best practices are carried out by industrial and community operations.
- Arctic industry operators planning Escape, Evacuation, and Rescue (EER) across sea ice.

6.3 Future work

6.3.1 Expanding and standardizing methods

Through the work I present here, I have already developed assessment techniques for two widely relevant parameters governing ice use: ice roughness and fracture potential, which in addition to pre-existing tools (e.g., to detect water on ice, ice extent and duration) can be translated into a broader set of methods to obtain quantitative information pertaining to trafficability and safety. Two steps will be required to seize the full potential of these methods.

First, processing standards need to be developed for each method. This is already the case for techniques developed in Chapters 4 and 5, which are based on a specific, predetermined InSAR processing workflow. However, the technique developed in Chapter 3 derives partly from a polarimetric classification scheme where individual classes are assigned based on the localized image statistics. In such a case, the classification scheme needs to be standardized, which can be achieved by re-applying the same H/α-decomposition scheme resulting from the first Wishart classification for subsequent analysis. However, a more elegant and

potentially a more useful approach would be to identify important roughness features in a validation dataset, similar to what was obtained in this work using UAS systems. Polarimetric signals within delineated areas of distinct roughness features could then be used to assign and later recognize certain statistics of the coherence matrix to particular roughness types using Freeman-Durden decomposition [*Freeman and Durden*, 1998].

Second, with results independent of regional location and distribution of ice related parameters such as rough features, it will be possible to combine different methods. For instance, if combining approaches in Chapters 2-5 into one analysis, trafficability could then be evaluated not only in terms of efficiency (roughness), but also from the perspective of safety (fracture potential). This process would require gaining access to more information regarding ice road management to fully understand to what extent fracturing can limit operations. This is one example of how my analysis is at present limited by a lack of access to industry data and procedures. With that said, other work is further developed or continued to track ice users [*Druckenmiller et al.*, 2013; *Wilkinson et al.*, 2011], with additional data from such efforts critical in further improving the approach presented in Chapter 3 as well as developing additional trafficability analysis strategies.

With an expansion of new tools capable of now determining quantitative metrics related to sea ice use, it is becoming increasingly more important for ice users to develop thresholds for operations to guide ice use and take advantage of these new strategies. This will require additional research to further understand quantitative requirements of ice use with respect to new parameters such as fracture potential and roughness. Here, regulators may have to play a role in the development of quantitative thresholds and guidelines for ice use, in particular in terms of ice road construction for oil and gas industry that likely will face continuously changing and increasingly less safe sea ice.

6.3.2 Exploring modifications to strategies to enable operational data availability

I explored the potential for multiple products derived from interferometry in addition to the methods developed here. Preliminary work involved comparing InSAR-derived DEMs with bathymetry data to identify grounded ridges. Grounded ridges are critical for maintaining stability and ensuring safety in many ice-covered regions and hence are critical for ice use. Interferometry shows promise, but more work is needed to document the accuracy of this approach. Bottomfast ice is a region of highly stable ice and thus often favorable for sea ice travel. Preliminary work indicated once again InSAR as a promising tool to map this type of ice. SAR acquisition pairs suitable for InSAR-based deformation analysis are acquired up to multiple times along much of the Arctic coastlines enabling inter-annual comparisons of ice dynamics in key regions for ice use. Such work could reveal long-term change in fringe patterns and model based deformation mode and internal stress. Despite the potential of InSAR, the use of the technique itself can be limited due to the sometimes-complex processing steps as well as sparse data availability. The development of new open source software packages such as the Sentinel Application Platform are greatly simplifying processing making interferometry available to personnel without a background in remote sensing.

Data accessibility for products compatible with interferometry is also improving with the recent launch of ALOS-2 and Sentinel-1 in 2014 and planned launch of NISAR in 2020. These systems will substantially increase open source data availability for InSAR in terms of regional and temporal coverage. Although Sentinel and NISAR are C-band systems, which typically result in reduced coherence relative to L-band [*Meyer et al.*, 2011], the repeat pass will be on the order of days and not weeks and likely generally retain coherence over landfast ice confirmed by my unpublished InSAR modeling work using ERS-1 and 2. The expected high data availability will likely result in an acquisition roughly every week, which is sufficient for operational use such as monitoring of fracture potential.

I have shown that polarimetric information has the capacity to discriminate areas of different roughness using fully polarimetric data. However, acquisitions that capture all four combinations are rare, and hence do not easily lend themselves to operational use. The SAR

systems already mentioned frequently capture acquisitions in dual-pol as either co-pol or cross-pol. Here, more work is needed over sea ice to understand to what extent only two channels can discriminate ice roughness sufficiently for operational use. One challenge is a historically heavy focus on fully polarimetric analysis by the SAR community resulting in far more products that lend themselves to these datasets. Hence a substantial amount of work may be required to explore new dual-pol techniques that give adequate results over sea ice.

I was fortunate to get access to TanDEM-X data from the German Aerospace Center, which at the time of writing may be the only satellite-based system that can reliably be used for DEM construction over sea ice. Additional close-proximity twin constellations could greatly help ensure data availability in the future [*Dierking et al.*, 2017], but this will likely take many years. This work has demonstrated the value of single-pass interferometry to derive sea ice topography for trafficability applications, but does not exclude alternate methods. I have demonstrated that the resolution and spatial coverage of a TanDEM-X InSAR-derived DEM is sufficient for operational use. However, since the temporal coverage is not ideal, it will be necessary to explore whether other methods such as altimetry can provide an equal or more useful product for operation. ICESat-2 is scheduled to be launched next year (2018) and will have a m-scale along-track resolution, but will also be limited by incomplete coverage between beams and at scales larger than the swath width of 3km and with uncertainties reaching up to around 50cm [*Kwok and Cunningham*, 2008]. To explore whether ICESat-2 can be used for operational purposes, it will therefore be necessary to investigate the relevant topographic resolution for trafficability applications. It is for instance possible that ridge statistics collected with altimetry from different sections of landfast ice are sufficient to guide ice use and analyze trafficability. Further work is needed to investigate the critical resolution of sea ice topography, which may be explored further by using the techniques presented here, but by incrementally downgrading the DEM resolution through the trafficability analysis.

In addition to improvement in data availability through increased number of SAR systems, steps can be taken to further improve both data accessibility and use. In particular, data providers can contribute greatly to ensuring easy and prompt access to relevant data. It can

often be difficult to determine through the data portals alone what datasets can successfully be utilized for interferometry without sufficient experience with baseline requirements etc. Steps to help identify likely InSAR pairs could greatly increase data accessibility and are currently in the works for Sentinel data by the Alaska Satellite Facility. Moreover, work to identify steps to shorten processing time for data enabling as close to real-time imaging as possible will greatly expand the use of these products for operational purposes.

The work presented here has a strong focus on utilizing remote sensing products to support landfast ice use. However, some information is difficult to obtain using remote sensing, such as predicting breakout events. Here, future landfast sea ice models may provide substantial new insight. However, the ongoing model development effort [*Hopkins*, 2008; *Itkin et al.*, 2015; *König Beatty and Holland*, 2010; *Olason*, 2016] will require large-scale datasets for validation and optimization including ice stress, failure, and roughness. The techniques developed here could lend substantial support to this effort by being able to provide this information more cost-effectively than other in-situ methods.

6.3.3 Improving data availability and products for ice users

More knowledge is needed to determine how to best integrate technological advances with existing sea ice use and assessment strategies. Throughout this work, it has sometimes become clear that data products provided to community members have not been optimal at conveying information effectively. First of all, it is important to reduce the relevant information to as few products as possible. This process requires a clear identification of the relevant parameters to an individual user group. Second, it is important to realize the limitations that exist in terms of data handling and software capabilities in Arctic communities when designing completed products. For instance, in Utqiaġvik, the Search and Rescue Station predominantly handles data in Google Earth; hence providing data in appropriate format is key. Distributing data among community members can also be a challenge due to limited access to computers with sufficient bandwidth and email. However, the younger generation especially is increasingly accessing information from mobile devices

enabling distribution of data products streamlined for cell phones. This opens up opportunities to create multiple layers of trafficability information that can be utilized in combination with a phone's GPS feature in the field.

I further realized that standard scientific mapping techniques are often not optimal for effectively conveying information to the Iñupiat community. This represents one of several challenges associated with bridging two different knowledge systems. In this work, I did not have the opportunity to extensively explore best practices, but I did learn a couple of important points of what would need to be addressed in future data products and distribution. First, it will be important to study and mimic the information products that are commonly utilized among the population to portray new data in as similar way as possible to familiar products. Spatial maps are one example of information that can be easily interpreted due to the considerable use of maps by Iñupiat during traveling and hunting. However, when adding gradient colors to the same map, it can easily become difficult to understand as a stand-alone product without additional explanation.

As one example, it was often not clear to Iñupiat community members how to interpret the DEM we presented in the field (Figure 3.14). However, when showing the associated orthorectified optical image, the level of information some of the Iñupiat ice experts could extract was impressive and, I would suggest, much more intricate than what any western scientist could interpret. I would therefore recommend that future products that are developed and distributed to Indigenous communities mimic as close to what one can see with a naked eye. One idea would be to delineate information directly on an optical image identifying rough ice, deformation, fracture values etc. essentially hiding the more complex remote sensing strategies and information products used. These are just some ideas and more work is needed to fully understand how to provide information to end users and particularly Indigenous populations to maximize clarity and potential use.

6.4 Final thoughts

The work presented here is different than a typical geophysics dissertation by incorporating research conducted on the interface between geophysics and LIK. I have demonstrated the value of stakeholder-guided science by directing research not only towards important scientific questions, but also through providing important tools to ice users possibly aiding adaptation to future change. One example is our experimental work operating an Unmanned Aerial System (UAS) over areas of Indigenous subsistence activities in Utqiaġvik to explore how 3-d mapping of the ice surface can be used to guide trail construction in terms of safety and efficiency. This operation was supported by the Barrow Whaling Captains Association and was well received by community members. This work was just briefly mentioned in Chapter 3, but was still an important component of the research, exploring uncharted territory of how scientific approaches can be integrated in culturally sensitive areas. This project alone raises important questions related to how tools such as UAS may alter how ice is used and potentially impact cultural activities.

To understand the full effects of UAS and other technological advances in support of Indigenous sea ice use, it is necessary to view use not simply in terms of clear objectives, but in a broader context including a larger set of benefits and challenges. For instance, subsistence hunting is relevant well beyond mere harvest numbers and includes a range of cultural benefits. A broader context of Indigenous ice use is illustrated in Figure 6.1 as ice users separated from clear objectives by a set of relevant benefits and challenges. Here, multiple hypothetical paths are possible depending on reliance on LIK and technological advances, with two hypothetical examples (Path A and B) illustrated in the figure. Path A represents a scenario in which a community has a strong knowledge base of LIK to support sea ice travel and where there is minimal reliance on new technological equipment and data for navigation such as GPS and satellite maps. This scenario of ice use includes many cultural benefits such as educating the younger generation in ice navigation skills and preserving cultural aspects of ice use by following traditional ways. However, relying on traditional methods alone can lead to susceptibility to negative impacts of recent environmental change as described throughout this dissertation. In a different scenario (Path B in Figure 6.1) where

reliance on technological advances is large, many of these environmental challenges can potentially be mitigated, but at the same time steering away from cultural and social benefits to more goal-oriented benefits such as ease of travel. This can introduce cultural challenges such as increased reliance on technology, which may partially contribute to loss of LIK and foster increased technology dependence.

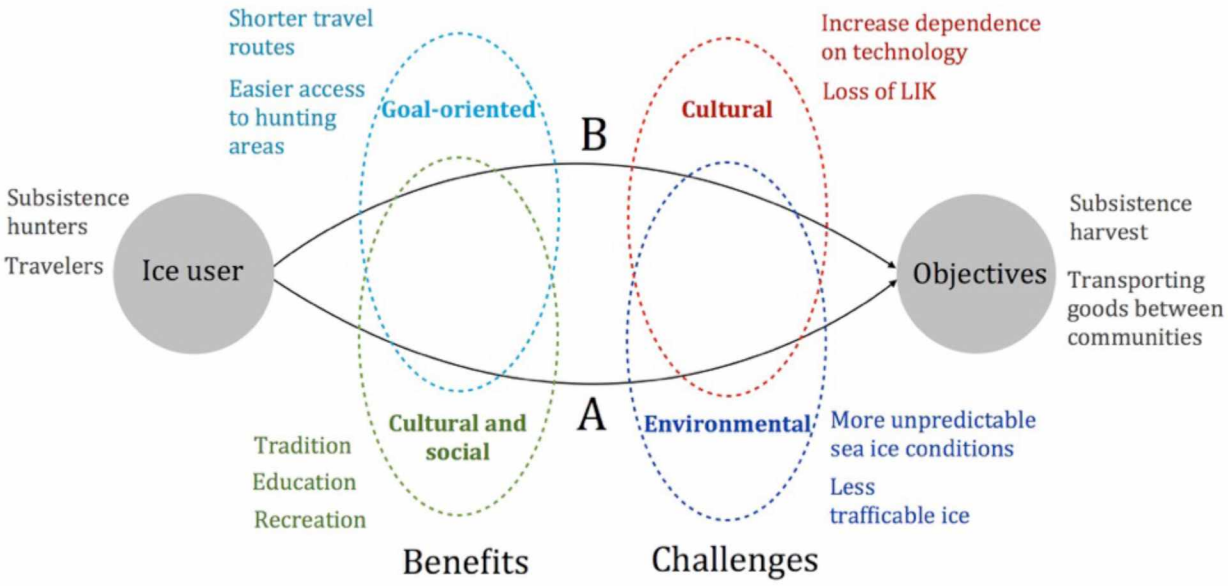

Figure 6.1: Indigenous sea ice use illustrated as ice users separated from clear objectives by a broader set of benefits and challenges. Different paths exist to navigate this ice user space depending on reliance on LIK and technological advances. Path A and B represent heavy reliance on LIK and technological advances, respectively.

The potential consequences of incorporating technological advances introduces the need for ice users to thoroughly examine the role of relevant approaches in the context of sea ice use. This would have to be done on a community level and could be addressed with input from community members similar to other local matters. Here, both geophysical and social scientists can play an important role by first of all (i) encouraging a thorough review process of different types of technological advances by the relevant communities, (ii) offering information and insights into the potential advantages and disadvantages of introducing new technology drawing upon past studies, and (iii) impartially and thoroughly weighing

potential drawbacks and being realistic about benefits to not push scientific efforts for the sake of science, without the community providing direction. In the specific case of UAS use, only limited information exists in terms of implications of use emphasizing the importance of tracking potential effects of any UAS-based study as part of the science effort to help mitigate future effects of UAS research.

Finally, I would like to acknowledge my deep respect for IK and its important role guiding the Indigenous population on sea ice over millennia. This knowledge is a key component of northern Indigenous cultures and essential for life closely tied to complex environmental patterns such as weather, animal migrations, and harvest cycles. The knowledge itself is a part of individual community members, but also the community as a whole, where knowledge and practices are continuously reevaluated based on new observations and recent experience of what works or not. Hence, IK is dynamic and is slowly altered to account for environmental change. In many communities, LIK related to sea ice is slowly disappearing from certain demographic groups due to increased reliance on modern technology such as GPS for navigation. This reliance can lead to reduced knowledge about traditional navigation (but is also used in combination with IK) and further resulting in reduced traditional observations and a reduced knowledge base from which new knowledge is gained. Also, recent rapid environmental change on timescales on the order of a generation is too short for IK to naturally adjust. Hence, in many places certain aspects of IK do not apply any longer due to recent sea ice change. Throughout this work, I have demonstrated that technological advances have the potential to supplement this knowledge. However, it is my belief that scientific approaches cannot and should not be seen as a potential replacement for LIK. Ensuring preservation of LIK should therefore be seen as an important part of maintaining sea ice use.

6.5 References

AMAP (2011), Snow, water, ice and permafrost in the Arctic (SWIPA): Climate Change and the Cryosphere, *Rep.*, xii + 538 pp, Oslo, Norway.

Aporta, C. (2011), Shifting perspectives on shifting ice: documenting and representing Inuit use of the sea ice, *The Canadian Geographer/Le Géographe canadien*, *55*(1), 6-19, doi: 10.1111/J.1541-0064.2010.00340.X.

Aporta, C., and E. Higgs (2005), Satellite culture - Global positioning systems, inuit wayfinding, and the need for a new account of technology, *Curr Anthropol*, *46*(5), 729-753, doi: 10.1086/432651.

Bell, T., R. Briggs, R. Bachmayer, and S. Li (2014), Augmenting Inuit knowledge for safe sea-ice travel—The SmartICE information system, paper presented at 2014 Oceans-St. John's, IEEE.

Berkes, F., and M. K. Berkes (2009), Ecological complexity, fuzzy logic, and holism in indigenous knowledge, *Futures*, *41*(1), 6-12.

Bohensky, E., and Y. Maru (2011), Indigenous knowledge, science, and resilience: What have we learned from a decade of international literature on "integration"?, *Ecology and Society*, *16*(4), doi: 10.5751/ES-04342-160406.

Chapin III, F. S., P. Cochran, O. H. Huntington, C. N. Knapp, T. J. Brinkman, and L. R. Gadamus (2013), Traditional knowledge and wisdom: a guide for understanding and shaping Alaskan social-ecological change, in *Linking Ecology and Ethics for a Changing World*, 49-62, Springer.

Cochran, P. A., C. A. Marshall, C. Garcia-Downing, E. Kendall, D. Cook, L. McCubbin, and R. M. S. Gover (2008), Indigenous ways of knowing: Implications for participatory research and community, *American Journal of Public Health*, *98*(1), 22-27.

Dierking, W., O. Lang, and T. Busche (2017), Sea ice local surface topography from single-pass satellite InSAR measurements: a feasibility study, *The Cryosphere Discussions*, 10.5194/tc-2017-40, doi: 10.5194/tc-2017-40.

Druckenmiller, M. L., H. Eicken, J. C. George, and L. Brower (2013), Trails to the whale: reflections of change and choice on an Iñupiat icescape at Barrow, Alaska, *Polar Geography*, *36*(1-2), 5-29, doi: 10.1080/1088937X.2012.724459.

Druckenmiller, M. L., H. Eicken, M. A. Johnson, D. J. Pringle, and C. C. Williams (2009), Toward an integrated coastal sea-ice observatory: System components and a case study at Barrow, Alaska, *Cold Reg Sci Technol*, *56*(2-3), 61-72, doi: 10.1016/J.Coldregions.2008.12.003.

Eicken, H. (2010), Indigenous knowledge and sea ice science: What can we learn from indigenous ice users?, in *SIKU: Knowing Our Ice*, 357-376, Springer.

Eicken, H., O. A. Lee, and A. L. Lovecraft (2016), Evolving roles of observing systems and data co-management in Arctic Ocean governance, paper presented at OCEANS 2016 MTS/IEEE Monterey, IEEE.

Eicken, H., M. Kaufman, I. Krupnik, P. Pulsifer, L. Apangalook, P. Apangalook, W. Weyapuk JR, and J. Leavitt (2014), A framework and database for community sea ice observations in a changing Arctic: An Alaskan prototype for multiple users, *Polar Geography*, *37*(1), 5-27, doi: 10.1080/1088937X.2013.873090.

Fienup-Riordan, A., and A. Rearden (2010), The ice is always changing: Yup'ik understandings of sea ice, past and present, in *SIKU: knowing Our Ice: Documenting Inuit Sea Ice knowledge and Use*, Igor Krupnik, Claudio Aporta, Shari Gearheard, Gita Laidler and Lene Kielsen Holm, 295-320, Springer, New York.

Ford, J. D., T. Pearce, J. Gilligan, B. Smit, and J. Oakes (2008), Climate change and hazards associated with ice use in northern Canada, *Arctic, Antarctic, and Alpine Research*, *40*(4), 647-659.

Ford, J. D., M. Maillet, V. Pouliot, T. Meredith, A. Cavanaugh, and I. R. Team (2016a), Adaptation and Indigenous peoples in the United Nations Framework Convention on Climate Change, *Climatic Change*, *139*(3-4), 429-443.

Ford, J. D., L. Cameron, J. Rubis, M. Maillet, D. Nakashima, A. C. Willox, and T. Pearce (2016b), Including indigenous knowledge and experience in IPCC assessment reports, *Nat Clim Change*, *6*(4), 349-353.

Freeman, A., and S. L. Durden (1998), A three-component scattering model for polarimetric SAR data, *IEEE Transactions on Geoscience and Remote Sensing*, *36*(3), 963-973.

Hopkins, M. A. (2008), *Simulation of Landfast Ice Along the Alaskan Coast*, 15 pp., US Army Cold Regions Research and Engineering Laboratory, US Department of the Interior, Minerals Management Service, Alaska OCS Region., Hanover, New Hampshire

Huntington, H. P., and S. Fox (2005), The changing Arctic: indigenous perspectives, in *Arctic Climate Impact Assessment*, C Symon, L Arris and B Heal, 61–98, Cambridge University Press, New York, NY.

Itkin, P., M. Losch, and R. Gerdes (2015), Landfast ice affects the stability of the Arctic halocline: Evidence from a numerical model, *Journal of Geophysical Research: Oceans*, *120*(4), 2622-2635.

Jolly, D., F. Berkes, J. Castleden, and T. Nichols (2002), We can't predict the weather like we used to: Inuvialuit observations of climate change, Sachs Harbour, Western Canadian Arctic, in *The earth is faster now: Indigenous observations of Arctic environmental change*, Igor Krupnik and Dyanna Jolly, 93-125, Arctic Research Consortium of the United States, Fairbanks, Alaska.

Jones, J. M., H. Eicken, A. R. Mahoney, M. V. Rohith, C. Kambhamettu, Y. Fukamachi, K. I. Ohshima, and J. C. George (2016), Landfast sea ice breakouts: Stabilizing ice features, oceanic and atmospheric forcing at Barrow, Alaska, *Continental Shelf Research*, *126*(50-63), doi: 10.1016/j.csr.2016.07.015.

Kasper, J. L., and T. J. Weingartner (2012), Modeling winter circulation under landfast ice: The interaction of winds with landfast ice, *Journal of Geophysical Research: Oceans*, *117*(C4), doi: 10.1029/2011JC007649.

Kassam, K.-A. S. (2009), *Biocultural diversity and indigenous ways of knowing: Human ecology in the Arctic*, University of Calgary Press.

König Beatty, C., and D. M. Holland (2010), Modeling landfast sea ice by adding tensile strength, *Journal of Physical Oceanography*, *40*(1), 185-198.

Kwok, R., and G. Cunningham (2008), ICESat over Arctic sea ice: Estimation of snow depth and ice thickness, *Journal of Geophysical Research: Oceans (1978–2012)*, *113*(C8).

Laidler, G. J. (2006), Inuit and scientific perspectives on the relationship between sea ice and climate change: The ideal complement?, *Climatic Change*, *78*(2-4), 407-444, doi: Doi 10.1007/S10584-006-9064-Z.

Laidler, G. J., P. Elee, T. Ikummaq, E. Joamie, and C. Aporta (2010), Mapping Inuit sea ice knowledge, use, and change in Nunavut, Canada (Cape Dorset, Igloolik, Pangnirtung), in *SIKU: knowing Our Ice: Documenting Inuit Sea Ice knowledge and Use*, Igor Krupnik, Claudio Aporta, Shari Gearheard, Gita Laidler and Lene Kielsen Holm, 45-80, Springer.

Laidler, G. J., T. Hirose, M. Kapfer, T. Ikummaq, E. Joamie, and P. Elee (2011), Evaluating the Floe Edge Service: how well can SAR imagery address Inuit community concerns around

sea ice change and travel safety?, *The Canadian Geographer/Le Géographe canadien*, *55*(1), 91-107.

Mahoney, A., H. Eicken, and L. Shapiro (2007), How fast is landfast sea ice? A study of the attachment and detachment of nearshore ice at Barrow, Alaska, *Cold Reg Sci Technol*, *47*(3), 233-255, doi: 10.1016/J.Coldregions.2006.09.005.

Mahoney, A., D. O. Dammann, M. A. Johnson, H. Eicken, and F. J. Meyer (2016), Measurement and imaging of infragravity waves in sea ice using InSAR, *Geophys Res Lett*, *43*, 6383–6392.

Meier, W. N., J. Stroeve, and S. Gearheard (2006), Bridging perspectives from remote sensing and Inuit communities on changing sea-ice cover in the Baffin Bay region, *Annals of Glaciology*, *44*(1), 433-438.

Meyer, F. J., A. R. Mahoney, H. Eicken, C. L. Denny, H. C. Druckenmiller, and S. Hendricks (2011), Mapping arctic landfast ice extent using L-band synthetic aperture radar interferometry, *Remote Sens Environ*, *115*(12), 3029-3043, doi: 10.1016/J.Rse.2011.06.006.

Norton, D. W., and A. G. Gaylord (2004), Drift velocities of ice floes in Alaska's northern Chukchi Sea flaw zone: Determinants of success by spring subsistence whalers in 2000 and 2001, *Arctic*, 347-362.

Olason, E. (2016), A dynamical model of Kara Sea land-fast ice, *Journal of Geophysical Research: Oceans*, *121*(5), 3141-3158.

Rathwell, K., D. Armitage, and F. Berkes (2015), Bridging knowledge systems to enhance governance of environmental commons: A typology of settings, *International Journal of the Commons*, *9*(2), 851–880, doi: 10.18352/ijc.584.

Riedlinger, D., and F. Berkes (2001), Contributions of traditional knowledge to understanding climate change in the Canadian Arctic, *Polar Record*, *37*(203), 315-328.

Wilkinson, J. P., S. Hanson, N. E. Hughes, A. James, B. Jones, R. MacKinnon, S. Rysgaard, and L. Toudal (2011), Tradition and technology: Sea ice science on Inuit sleds, *Eos, Transactions American Geophysical Union*, *92*(1), 1-4.